Controlling immunity at dendritic cell and T cell level by host, pathogens, and as therapeutics

van der Donk, L.E.H.

Publication date
2023

Document Version
Final published version

CONTROLLING IMMUNITY AT DENDRITIC CELL AND T CELL LEVEL BY HOST, PATHOGENS, AND AS THERAPEUTICS

LIEVE E.H. VAN DER DONK

CONTROLLING IMMUNITY AT DENDRITIC CELL AND T CELL LEVEL BY HOST, PATHOGENS, AND AS THERAPEUTICS

LIEVE ELISABETH HUBERTHA VAN DER DONK

This research was performed at the department of Experimental Immunology (EXIM), Amsterdam University Medical Centers, location Academic Medical Center (AMC), Amsterdam, the Netherlands. Printing of this thesis is financially supported by Amsterdam UMC.

Title: Controlling immunity at dendritic cell and T cell level by host, pathogens, and as therapeutics

Author: Lieve E.H. van der Donk

ISBN: 978-94-6419-850-8

Printing: Gildeprint, Alblasserdam
Cover design and layout: © evelienjagtman.com

CONTROLLING IMMUNITY AT DENDRITIC CELL AND T CELL LEVEL BY HOST, PATHOGENS, AND AS THERAPEUTICS

ACADEMISCH PROEFSCHRIFT

ter verkrijging van de graad van doctor
aan de Universiteit van Amsterdam
op gezag van de Rector Magnificus
prof. dr. ir. P.P.C.C. Verbeek
ten overstaan van een door het College voor Promoties ingestelde commissie,
in het openbaar te verdedigen in de Agnietenkapel
op woensdag 25 oktober 2023, te 13.00 uur

door Lieve Elisabeth Hubertha van der Donk
geboren te 's-Hertogenbosch

PROMOTIECOMMISSIE:

Promotor:	prof. dr. T.B.H. Geijtenbeek	AMC – UvA
Copromotores:	dr. L.S. Ates	BioNTech
	dr. M. Bermejo-Jambrina	AMC – UvA
Overige leden:	prof. dr. T. van der Poll	AMC – UvA
	prof. dr. R. van Ree	AMC – UvA
	prof. dr. N.M. van Sorge	AMC – UvA
	prof. dr. R.E. Mebius	Vrije Universiteit Amsterdam
	dr. C.M. van der Hoek	AMC – UvA
	dr. A. ten Brinke	Sanquin Research

Faculteit der Geneeskunde

The only constant in nature is change

Naar Heraclitus

CONTENTS

CHAPTER 1

INTRODUCTION AND THESIS OUTLINE

INTRODUCTION

The immune system is composed of multiple layers of protection, including the innate and adaptive arms of defense. The innate immune system is a network of pathogen-engulfing phagocytic cells and soluble molecules such as chemokines, cytokines and complement proteins (1). The adaptive immune system confers long-lasting immunological memory and includes T and B cells, which are responsible for antigen-specific cellular and antibody responses, respectively (2, 3).

Dendritic cells (DCs) are indispensable cells from the innate immune system that form the bridge between the innate and adaptive immune system. DCs reside in mucosal tissues where they browse the environment, looking for pathogens. Once DCs sense and recognize invading pathogens, they migrate to peripheral lymphoid organs (4), where they interact with T and B cells. Their capacity to activate T cells and instruct adaptive immune responses makes DCs an essential immune cell subset, and individuals with defective DCs suffer from varying degrees of immunodeficiency (5). But how do DCs know how and when to act?

Sensing

It is essential that immune cells sense invading pathogens. To this end, DCs express various families of pattern recognition receptors (PRRs), both on their cell surface and intracellular, which recognize conserved molecular structures expressed by pathogens, so-called pathogen-associated molecular patterns (PAMPs) (3, 6) (Figure 1A). The different families of PRRs are necessary to distinguish between the various PAMPs, including viral or bacterial surface glycoproteins, or foreign RNA or DNA molecules. Important PRR families are Toll-like receptors (TLRs), NOD-like receptors (NLRs), C type lectin receptors (CLRs), Rig-I-like receptors (RLRs), complement receptors (CRs), and cytoplasmic DNA sensor cyclic GMP-AMP synthase (cGAS) (6). Specific PRRs recognize PAMPs from a wide range of pathogens and activation of a variety of PRRs induces a tailored immune response against a specific pathogen. To illustrate this, a bacterium is not only composed of membrane proteins and lipids, but also contains bacterial DNA. Together, these PAMPs trigger different PRRs, resulting in crosstalk. This crosstalk programs DCs for a custom-made immune response against the bacterium. In this thesis, we highlight multiple PRR family members, each of which is responsible for the recognition of different types of PAMPs and induces expression of a specific array of cytokines to combat infection.

Type I interferons are not only essential for defense against viruses but also against other pathogens and cancers

DCs are potent producers of cytokines, including the type I interferon (IFN)-β. IFN-β is induced by different pathogens and via different PRR signaling, as described in detail below. The cytokine IFN-β is an important source for antiviral immunity, and has recently also been attributed antibacterial and antifungal functions (7, 8). Notably, IFN-β has also gained interest in the field of oncology, where its expression was found to be strongly correlated to an efficient anti-tumor response (9). In a first wave of IFN-β production, IFN-β is secreted and subsequently binds to the IFNα/β receptor (IFNAR) in an autocrine and paracrine manner, thereby inducing the transcription of hundreds of IFN-stimulated genes (ISGs) with antiviral and/or antibacterial properties (7, 10). Whilst some ISGs exert direct effects on pathogens, other ISGs possess immune-modulatory capacity and affect the immune responses against pathogens. These type I IFN responses enhance DC maturation (11), improve cytotoxic T cell function and T helper cell polarization (12-15), and are therefore important in shaping the adaptive immune responses against bacteria, fungi, viruses, and tumors.

TLR activation is crucial in immunity

The TLRs are an important family of PRRs. Some TLRs are expressed on the cell membrane where they recognize extracellular structures, whilst other TLRs are expressed in endosomes where they sense foreign RNA or DNA (16). TLR4 is an extracellular PRR abundantly expressed on DCs, and is key in the recognition of the bacterial component lipopolysaccharide (LPS) (17, 18) (Figure 1A). TLR4 triggering induces DC maturation as well as production of IFN-β and proinflammatory cytokines (19, 20). These inflammatory mediators are important to fight off bacterial infections. Notably, as new pathogens emerge, new PAMPs are being discovered. These PAMPs can potentially bind existing PRRs, or lead to the discovery of new PRRs. A relevant example is severe acute respiratory syndrome coronavirus 2 (SARS-CoV-2). SARS-CoV-2 is an enveloped positive-sense single-stranded RNA (ssRNA) virus. The SARS-CoV-2 envelope comprises Spike (S) glycoproteins, which facilitate cell entry by binding to the angiotensin converting enzyme 2 (ACE2) receptor (21, 22). The S protein consists of two functional subunits: the S1 subunit, which is responsible for binding the host cell receptor, and the S2 subunit, which plays a role in the fusion of the viral and host cell membranes (23). During the SARS-CoV-2 pandemic, various reports published that the S protein could trigger TLR4 to induce an immune response against the virus (24, 25), and this has also been investigated in this thesis.

RLR activation by viral RNA

PRRs from the RLR family, such as retinoic acid-inducible gene I (RIG-I) or melanoma-differentiation-associated protein 5 (MDA5) are located in the cytoplasm, where they detect 5'-PPP single-stranded (ss)RNA or double-stranded (ds)RNA, respectively (26-29). Triggering RIG-I or MDA5 induces multimerization, leading to engagement of the downstream adaptor protein mitochondrial antiviral signaling (MAVS). Further downstream signaling ultimately results in the production of type I IFN, ISGs and cytokines, which are required for an adequate antiviral response (30).

cGAS/STING activation induces type I IFN responses

The cGAS/stimulator of IFN genes (STING) pathway is responsible for eliciting a type I IFN response against cytosolic dsDNA (31, 32). Under normal circumstances, there is no dsDNA present in the cytosol of healthy mammalian cells; however, this can be introduced by cellular damage, or by pathogens. The dsDNA sensor cGAS is located in the cytosol, and upon recognition of dsDNA, cGAS synthesizes second messengers called 2'3'- cyclic GMP-AMP (cGAMP) (33, 34) (Figure 1A). cGAMPs in turn activate the adaptor protein STING, leading to a signaling cascade that produces IFN-β responses (32, 35). The cGAS/STING pathway is important in the immune defense against various viral and bacterial species including human immunodeficiency virus 1 (HIV-1), SARS-CoV-2, *Streptococcus pneumonia*, *Burkholderia pseudomallei* and *Mycobacterium (M.) tuberculosis* (36-39). Notably, there are studies investigating the use of cGAMPs or STING agonists in anti-tumor therapy, especially for solid tumors (40-42). However, these treatments are limited in their application because of the necessity to administer the treatments locally into the tumor. Therefore, out-of-the-box activation of the cGAS/STING pathway is an important advance in anti-tumor therapy. In this thesis we have investigated how ectopic expression of cGAS in *Salmonella enterica* serovar *typhimurium* (*S. typhimurium*) could harness DCs to kill off tumor cells.

DC-SIGN crosstalk modulates immunity

The CLR DC-SIGN is expressed by DCs and recognizes high-mannose-containing glycoproteins on the surface of pathogens (43, 44) (Figure 1A). DC-SIGN functions as an adhesion receptor that interacts with intercellular adhesion molecule 2 (ICAM-2) on endothelial cells to induce DC migration, and mediates contact with naïve T cells through binding of ICAM-3 (43, 45). Moreover, although DC-SIGN does not induce immune responses by itself (46), it operates as a PRR that – in combination with other PRRs – induces specific immune responses upon pathogen interaction (44, 47). Notably, previous research has shown that certain pathogens, including *M. tuberculosis*, measles virus and HIV-1 are able to modulate TLR and RLR signaling

via DC-SIGN signaling. ManLAM, a cell wall component of *M. tuberculosis*, interacts with DC-SIGN and affects TLR-mediated signaling (48). Binding of ManLAM to DC-SIGN modulates TLR signaling through the phosphorylation and acetylation of NFκB, resulting in enhanced induction of IL-10, IL-12 and IL-6 (48, 49). Moreover, binding of measles virus to DC-SIGN prevents RIG-I and MDA5 activation and recognition of HIV-1 by DC-SIGN was found to block MAVS, both resulting in suppressed type I IFN signaling and obstruction of host defense (50-52). These results suggest that crosstalk between distinct PRRs is essential to induce tailored immune responses. However, these results also show that some pathogens have evolved and developed strategies to modulate the immune response in their favor, thereby weakening the antibacterial or antiviral defense.

The complement system: a non-specific first line of defense

Despite the idea that the expression of a plethora of PRRs for different pathogens seems a watertight defense mechanism, pathogens are not always directly sensed by PRRs. Some pathogens have developed ways to evade sensing and prevent immune activation. However, the immune system is not solely dependent on recognition of PAMPs, but has multiple mechanisms to sense pathogens. The proteins of the complement system are an example of an alternative and complementary line of defense. Complement proteins are not antigen-specific but will interact with pathogens, marking them for recognition by immune cells (53). Complement-opsonized pathogens bind DCs using complement receptor (CR)3 and CR4 and when triggered, CR signaling leads to immune activation (54). The complement system is an incredibly extensive and intricate system that possesses three main pathways: the classical, the lectin and the alternative pathway. In brief, although each pathway starts differently, they all converge in the same central step of complement activation (55). In particular, the complement convertase C3 is cleaved into the highly reactive C3b fragment that opsonizes the pathogen, and the soluble anaphylatoxin C3a fragment that has proinflammatory properties. The fragment C3b can in turn be cleaved to create iC3b opsonins. The iC3b opsonins bind and activate DCs via CR3 and CR4. HIV-1 is an example of a virus that has evolved ways to escape DC-mediated antiviral immunity. Although DCs become infected by HIV-1, the virus escapes direct immune sensing by circumventing or aborting PRR signaling (56). Interestingly, complement-opsonized HIV-1 pseudovirus more efficiently infects DCs leading to immune detection and antiviral responses (57, 58). However, in turn, HIV-1 has developed ways to also escape complement-dependent lysis and promote viral infectivity and transmission (54, 59). Therefore, complement-opsonization of viruses might act as a double-edged sword, balancing between virus detection and immune activation, or infection and viral spread.

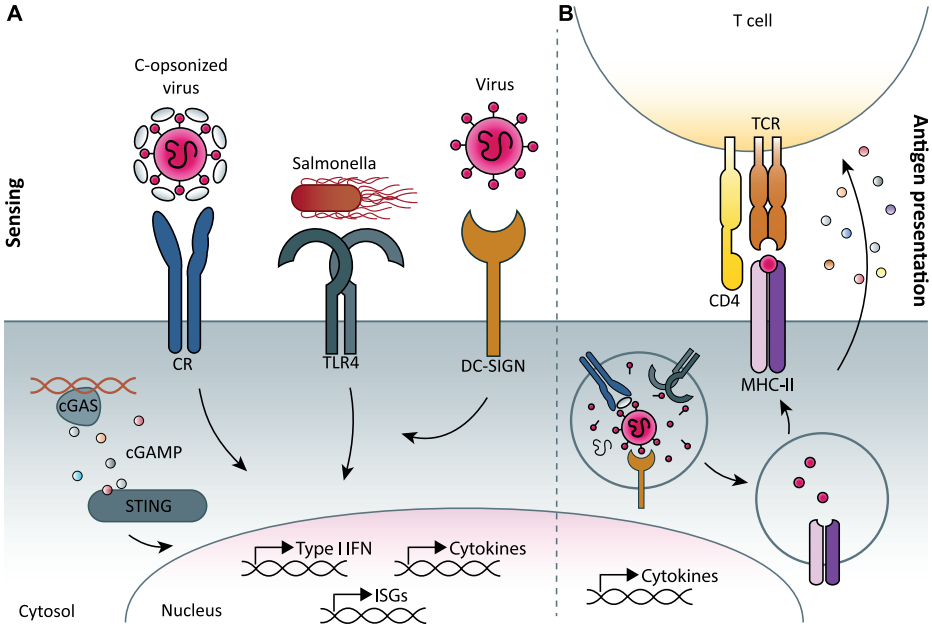

Figure 1: Dendritic cells (DCs) sense pathogens and present antigens to T cells.

(A) DCs express PRRs that recognize viral or bacterial PAMPs. Sensing various PAMPs with various PRRs induces a tailored immune response against a specific pathogen. (B) DCs take up and process the pathogens and present processed antigens to T cells in a MHC-specific fashion to instigate proper adaptive immune responses against the invading pathogens. C-opsonized = complement-opsonized.

Antigen presentation

Apart from their role as pathogen sensors, DCs are also antigen presenting cells (APCs) that engulf and process pathogens for antigen-presentation (Figure 1B).

Naïve T cells are not directly activated by pathogens, but they need instruction and programming by APCs like DCs (60). DCs continuously sample their local environment, until they sense pathogens. Upon encounter, DCs not only sense the pathogens as discussed above, but also internalize pathogens via phagocytosis or receptor-mediated endocytosis (61, 62), and migrate to the nearest lymph node where T cells reside (60). There, DCs process antigens, which are presented on the cell surface in major histocompatibility complex (MHC) molecules (63). T cells express a T cell receptor (TCR) on their surface, which detects and identifies antigen:MHC molecules (64). This interaction is very specific: T cells scan various antigen:MHC molecules until they have found their specific cognate counterpart as first step in T cell activation. DCs also provide co-stimulatory signaling required to properly activate

T cells. Importantly, as discussed above, DCs secrete a distinct array of cytokines in response to a pathogen to induce differentiation of the naïve T cells into a specific T helper cell subset (63).

The TCR thus recognizes antigens presented in MHC molecules by APCs. This specific recognition, supported by co-stimulatory molecule interactions, induces signaling pathways that lead to T cell differentiation, effector functions, and survival (64). Engagement of the TCR leads to rapid activation of the Src family kinase members Lck and Fyn (65-69), and the subsequent activation of the kinase ZAP70, which is recruited to the TCR (70, 71). ZAP70, in turn, phosphorylates downstream molecules eventually leading to T cell activation (72). T cell activation is tightly regulated to induce specific responses, while preventing hyper-reactivity that could lead to tissue damage or autoimmunity.

T cell activation manifests in various phenotypic changes, including upregulation of activation markers (e.g. CD69), cytokine production such as IFN-γ and IL-2, but also in TCR downregulation (73-78). During TCR downregulation the TCR is rapidly internalized and degraded in a controlled fashion that prevents T cell overactivation. Besides the quick and transient ligand-induced TCR downregulation, clonally expanded T cells also display programmed TCR downregulation (79). After a secondary antigen encounter, these T cells with decreased TCR expression exhibit an increased threshold for cytokine production and proliferation, and are therefore presumably better equipped to maintain a balanced immune response. Although a lot of research has been performed on TCR downregulation, and the importance of TCR downregulation is well underscored, it remains unclear which mechanisms underlie TCR downregulation. In this thesis we have investigated the individual importance of the kinases Lck, Fyn, and ZAP70 for T cell activation and TCR downregulation.

In conclusion, DCs are versatile cells with multiple essential tasks to induce appropriate immune responses against pathogens. It is fundamental to continue research on DCs since all aspects of an uncontrolled or flawed immune response likely start and end with incorrect DC triggering, subsequently affecting adaptive immune responses. In this thesis I aim to underscore the importance of fruitful DC and T cell activation in the combat against pathogens or cancer, and explore how the activation is controlled by pathogens or by the host.

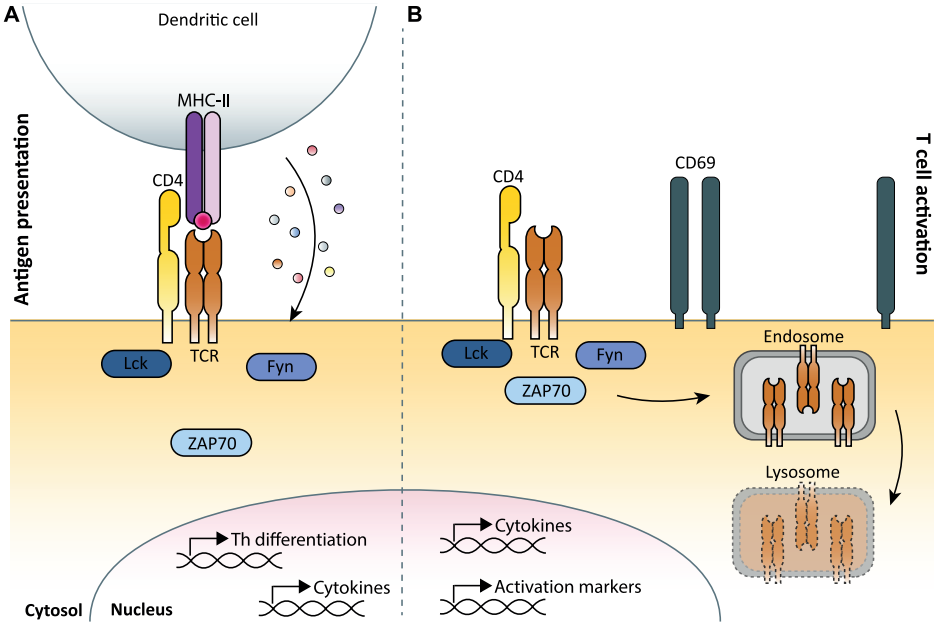

Figure 2: T cell receptor (TCR) triggering induces T cell activation and TCR downregulation.
(A) T cells become activated when their TCR is triggered by cognate antigen:MHC molecules presented by DCs. Co-stimulation and cytokine secretion by DCs is required for adequate T cell activation. (B) TCR triggering leads to the activation of kinases Lck, Fyn and ZAP70, ultimately resulting in internalization of the TCR and subsequent degradation in lysosomes. TCR downregulation is paired with upregulation of T cell activation markers, including CD69.

THESIS OUTLINE

In this thesis, we have investigated how various pathogens are sensed by DCs and influence subsequent T cell responses, and which pathways underlie these processes.

Part I describes the activation of the innate immune system by viruses and bacteria, specifically focusing on SARS-CoV-2. In COVID-19 patients, it is not the viral infection alone wreaking havoc in the body, but especially the overactive and uncontrolled immune responses against the virus causing harm, sometimes very severely. Therefore, we studied how DCs respond to SARS-CoV-2 infection in **chapter 2**. Notably, DCs were neither infected nor became activated by SARS-CoV-2. After ectopic expression of ACE2 on the cell membrane, DCs were infected by SARS-CoV-2, resulting in appropriate antiviral immune responses. These results present a possible explanation for the uncontrolled immune response against SARS-

CoV-2 observed in COVID-19 patients, since lack of activation or infection of DCs might induce inadequate T cell responses. Moreover, we showed that DCs were activated indirectly by SARS-CoV-2-infected epithelial cells, suggesting that indirect activation might induce and dictate anti-SARS-CoV-2 immunity. Nevertheless, it remains unclear whether these indirectly-induced immune responses are sufficient to eliminate the virus. Therefore, in **chapter 3** we examined whether the complement system is involved in direct DC activation by SARS-CoV-2. Complement-opsonized SARS-CoV-2 induced DC activation through CR3 and CR4 signaling. Strikingly, complement-mediated DC activation was suppressed by antibodies against SARS-CoV-2 present in serum of convalescent COVID-19 patients. These data suggest that the antibody response is essential in the control of complement-mediated DC activation, underscoring the importance of vaccination in the current and future pandemics. In **chapter 4** we continued to investigate the interaction of SARS-CoV-2 with DCs. Our data strongly suggest that SARS-CoV-2 actively suppresses DC activation. Notably, SARS-CoV-2-mediated DC-SIGN signaling blocked TLR4-induced DC activation. These results suggest that SARS-CoV-2 targets DC-SIGN to suppress the immune response against additional stimuli, thereby paralyzing DCs during infection.

Besides their essential role during infection, we also investigated how DC functions can be harnessed to induce effective adaptive immune responses against solid tumors. In **chapter 5** we employed genetically engineered *S. typhimurium* bacteria to induce strong type I IFN responses by DCs via the cGAS/STING pathway. Ectopic expression of cGAS in *S. typhimurium* resulted in the production and transport of cGAMPs into DCs, where the cGAMPs triggered STING to induce type I IFN responses. The type I IFN responses by DCs were essential for the induction of $CD8^+$ T cell responses, which are required to fight off cancer. Furthermore, T cells that were instructed by *Salmonella*-infected DCs were better equipped to kill tumor cells. These engineered bacteria therefore could ultimately be used as a cancer treatment for solid tumors in humans.

In **Part II** we focus on the molecular mechanisms behind TCR downregulation and T cell activation, using a toolbox for overexpression and genetic perturbation of primary lymphocytes. In **chapter 6** we describe the design and extensive optimization of this toolbox for overexpression and genetic perturbation of primary murine and human lymphocytes. Subsequently, in **chapter 7**, we utilized this toolbox to genetically modify primary human T cells to study the pathways underlying TCR downregulation. Because T cell activation and TCR downregulation are tightly linked, we suggested that the upstream pathways of T cell activation

and TCR downregulation might overlap. With the use of our gene-editing toolbox, we were able to knockdown important kinases known to be essential in T cell activation, and investigate their involvement in TCR downregulation. Our research suggests that the kinases Lck, Fyn, and ZAP70 are essential for T cell activation; however, they are individually redundant for TCR downregulation. Further research on TCR downregulation is warranted, as it has direct clinical implications for the understanding of autoimmune disorders and immune therapies against cancer by increasing the activity and reactivity of T cells. The results and implications of our investigations are discussed in **chapter 8**.

REFERENCES

1. Delves PJ, Roitt IM. The immune system. First of two parts. N Engl J Med. 2000;343(1):37-49.
2. Delves PJ, Roitt IM. The immune system. Second of two parts. N Engl J Med. 2000;343(2):108-17.
3. Janeway CA, Jr., Medzhitov R. Innate immune recognition. Annu Rev Immunol. 2002;20:197-216.
4. Banchereau J, Steinman RM. Dendritic cells and the control of immunity. Nature. 1998;392(6673):245-52.
5. Bigley V, Barge D, Collin M. Dendritic cell analysis in primary immunodeficiency. Curr Opin Allergy Clin Immunol. 2016;16(6):530-40.
6. Akira S, Uematsu S, Takeuchi O. Pathogen recognition and innate immunity. Cell. 2006;124(4):783-801.
7. McNab F, Mayer-Barber K, Sher A, Wack A, O'Garra A. Type I interferons in infectious disease. Nat Rev Immunol. 2015;15(2):87-103.
8. Pekmezovic M, Dietschmann A, Gresnigt MS. Type I interferons during host-fungus interactions: Is antifungal immunity going viral? PLoS Pathog. 2022;18(8):e1010740.
9. Borden EC. Interferons alpha and beta in cancer: therapeutic opportunities from new insights. Nat Rev Drug Discov. 2019;18(3):219-34.
10. Platanias LC. Mechanisms of type-I- and type-II-interferon-mediated signalling. Nat Rev Immunol. 2005;5(5):375-86.
11. Simmons DP, Wearsch PA, Canaday DH, Meyerson HJ, Liu YC, Wang Y, et al. Type I IFN Drives a Distinctive Dendritic Cell Maturation Phenotype That Allows Continued Class II MHC Synthesis and Antigen Processing. Journal of Immunology. 2012;188(7):3116-26.
12. Gonzalez-Navajas JM, Lee J, David M, Raz E. Immunomodulatory functions of type I interferons. Nat Rev Immunol. 2012;12(2):125-35.
13. Curtsinger JM, Valenzuela JO, Agarwal P, Lins D, Mescher MF. Type I IFNs provide a third signal to CD8 T cells to stimulate clonal expansion and differentiation. J Immunol. 2005;174(8):4465-9.
14. Mescher MF, Curtsinger JM, Agarwal P, Casey KA, Gerner M, Hammerbeck CD, et al. Signals required for programming effector and memory development by CD8+ T cells. Immunol Rev. 2006;211:81-92.
15. Gringhuis SI, Kaptein TM, Remmerswaal EBM, Drewniak A, Wevers BA, Theelen B, et al. Fungal sensing by dectin-1 directs the non-pathogenic polarization of T(H)17 cells through balanced type I IFN responses in human DCs. Nat Immunol. 2022.
16. Medzhitov R. Toll-like receptors and innate immunity. Nat Rev Immunol. 2001;1(2):135-45.
17. Chow JC, Young DW, Golenbock DT, Christ WJ, Gusovsky F. Toll-like receptor-4 mediates lipopolysaccharide-induced signal transduction. J Biol Chem. 1999;274(16):10689-92.
18. Visintin A, Mazzoni A, Spitzer JH, Wyllie DH, Dower SK, Segal DM. Regulation of Toll-like receptors in human monocytes and dendritic cells. J Immunol. 2001;166(1):249-55.
19. Ouaaz F, Arron J, Zheng Y, Choi Y, Beg AA. Dendritic cell development and survival require distinct NF-kappaB subunits. Immunity. 2002;16(2):257-70.
20. Hofer S, Rescigno M, Granucci F, Citterio S, Francolini M, Ricciardi-Castagnoli P. Differential activation of NF-kappa B subunits in dendritic cells in response to Gram-negative bacteria and to lipopolysaccharide. Microbes Infect. 2001;3(4):259-65.
21. Hoffmann M, Kleine-Weber H, Schroeder S, Kruger N, Herrler T, Erichsen S, et al. SARS-CoV-2 Cell Entry Depends on ACE2 and TMPRSS2 and Is Blocked by a Clinically Proven Protease Inhibitor. Cell. 2020;181(2):271-80 e8.

22. Letko M, Marzi A, Munster V. Functional assessment of cell entry and receptor usage for SARS-CoV-2 and other lineage B betacoronaviruses. Nat Microbiol. 2020;5(4):562-9.
23. Walls AC, Park YJ, Tortorici MA, Wall A, McGuire AT, Veesler D. Structure, Function, and Antigenicity of the SARS-CoV-2 Spike Glycoprotein. Cell. 2020;183(6):1735.
24. Bhattacharya M, Sharma AR, Mallick B, Sharma G, Lee SS, Chakraborty C. Immunoinformatics approach to understand molecular interaction between multi-epitopic regions of SARS-CoV-2 spike-protein with TLR4/MD-2 complex. Infect Genet Evol. 2020;85:104587.
25. Choudhury A, Mukherjee S. In silico studies on the comparative characterization of the interactions of SARS-CoV-2 spike glycoprotein with ACE-2 receptor homologs and human TLRs. J Med Virol. 2020;92(10):2105-13.
26. Chen N, Xia P, Li S, Zhang T, Wang TT, Zhu J. RNA sensors of the innate immune system and their detection of pathogens. IUBMB Life. 2017;69(5):297-304.
27. Loo YM, Gale M, Jr. Immune signaling by RIG-I-like receptors. Immunity. 2011;34(5):680-92.
28. Kato H, Takeuchi O, Sato S, Yoneyama M, Yamamoto M, Matsui K, et al. Differential roles of MDA5 and RIG-I helicases in the recognition of RNA viruses. Nature. 2006;441(7089):101-5.
29. Hornung V, Ellegast J, Kim S, Brzozka K, Jung A, Kato H, et al. 5'-Triphosphate RNA is the ligand for RIG-I. Science. 2006;314(5801):994-7.
30. Goubau D, Deddouche S, Reis e Sousa C. Cytosolic sensing of viruses. Immunity. 2013;38(5):855-69.
31. Luecke S, Holleufer A, Christensen MH, Jonsson KL, Boni GA, Sorensen LK, et al. cGAS is activated by DNA in a length-dependent manner. EMBO Rep. 2017;18(10):1707-15.
32. Sun L, Wu J, Du F, Chen X, Chen ZJ. Cyclic GMP-AMP synthase is a cytosolic DNA sensor that activates the type I interferon pathway. Science. 2013;339(6121):786-91.
33. Ablasser A, Goldeck M, Cavlar T, Deimling T, Witte G, Rohl I, et al. cGAS produces a 2'-5'-linked cyclic dinucleotide second messenger that activates STING. Nature. 2013;498(7454):380-4.
34. Diner EJ, Burdette DL, Wilson SC, Monroe KM, Kellenberger CA, Hyodo M, et al. The innate immune DNA sensor cGAS produces a noncanonical cyclic dinucleotide that activates human STING. Cell Rep. 2013;3(5):1355-61.
35. Ouyang S, Song X, Wang Y, Ru H, Shaw N, Jiang Y, et al. Structural analysis of the STING adaptor protein reveals a hydrophobic dimer interface and mode of cyclic di-GMP binding. Immunity. 2012;36(6):1073-86.
36. Watson RO, Bell SL, MacDuff DA, Kimmey JM, Diner EJ, Olivas J, et al. The Cytosolic Sensor cGAS Detects Mycobacterium tuberculosis DNA to Induce Type I Interferons and Activate Autophagy. Cell Host Microbe. 2015;17(6):811-9.
37. Liu N, Pang X, Zhang H, Ji P. The cGAS-STING Pathway in Bacterial Infection and Bacterial Immunity. Front Immunol. 2021;12:814709.
38. Domizio JD, Gulen MF, Saidoune F, Thacker VV, Yatim A, Sharma K, et al. The cGAS-STING pathway drives type I IFN immunopathology in COVID-19. Nature. 2022;603(7899):145-51.
39. Gao D, Wu J, Wu YT, Du F, Aroh C, Yan N, et al. Cyclic GMP-AMP synthase is an innate immune sensor of HIV and other retroviruses. Science. 2013;341(6148):903-6.
40. Carozza JA, Bohnert V, Nguyen KC, Skariah G, Shaw KE, Brown JA, et al. Extracellular cGAMP is a cancer cell-produced immunotransmitter involved in radiation-induced anti-cancer immunity. Nat Cancer. 2020;1(2):184-96.
41. Corrales L, Glickman LH, McWhirter SM, Kanne DB, Sivick KE, Katibah GE, et al. Direct Activation of STING in the Tumor Microenvironment Leads to Potent and Systemic Tumor Regression and Immunity. Cell Rep. 2015;11(7):1018-30.

42. Li T, Cheng H, Yuan H, Xu Q, Shu C, Zhang Y, et al. Antitumor Activity of cGAMP via Stimulation of cGAS-cGAMP-STING-IRF3 Mediated Innate Immune Response. Sci Rep. 2016;6:19049.
43. Geijtenbeek TB, Torensma R, van Vliet SJ, van Duijnhoven GC, Adema GJ, van Kooyk Y, et al. Identification of DC-SIGN, a novel dendritic cell-specific ICAM-3 receptor that supports primary immune responses. Cell. 2000;100(5):575-85.
44. van Kooyk Y, Geijtenbeek TB. DC-SIGN: escape mechanism for pathogens. Nat Rev Immunol. 2003;3(9):697-709.
45. Geijtenbeek TB, Krooshoop DJ, Bleijs DA, van Vliet SJ, van Duijnhoven GC, Grabovsky V, et al. DC-SIGN-ICAM-2 interaction mediates dendritic cell trafficking. Nat Immunol. 2000;1(4):353-7.
46. Gringhuis SI, Kaptein TM, Wevers BA, Mesman AW, Geijtenbeek TB. Fucose-specific DC-SIGN signalling directs T helper cell type-2 responses via IKKepsilon- and CYLD-dependent Bcl3 activation. Nat Commun. 2014;5:3898.
47. den Dunnen J, Gringhuis SI, Geijtenbeek TB. Innate signaling by the C-type lectin DC-SIGN dictates immune responses. Cancer Immunol Immunother. 2009;58(7):1149-57.
48. Geijtenbeek TB, Van Vliet SJ, Koppel EA, Sanchez-Hernandez M, Vandenbroucke-Grauls CM, Appelmelk B, et al. Mycobacteria target DC-SIGN to suppress dendritic cell function. J Exp Med. 2003;197(1):7-17.
49. Gringhuis SI, den Dunnen J, Litjens M, van Het Hof B, van Kooyk Y, Geijtenbeek TB. C-type lectin DC-SIGN modulates Toll-like receptor signaling via Raf-1 kinase-dependent acetylation of transcription factor NF-kappaB. Immunity. 2007;26(5):605-16.
50. Gringhuis SI, Hertoghs N, Kaptein TM, Zijlstra-Willems EM, Sarrami-Fooroshani R, Sprokholt JK, et al. Erratum: HIV-1 blocks the signaling adaptor MAVS to evade antiviral host defense after sensing of abortive HIV-1 RNA by the host helicase DDX3. Nat Immunol. 2017;18(4):474.
51. Gringhuis SI, Hertoghs N, Kaptein TM, Zijlstra-Willems EM, Sarrami-Forooshani R, Sprokholt JK, et al. HIV-1 blocks the signaling adaptor MAVS to evade antiviral host defense after sensing of abortive HIV-1 RNA by the host helicase DDX3. Nat Immunol. 2017;18(2):225-35.
52. Mesman AW, Zijlstra-Willems EM, Kaptein TM, de Swart RL, Davis ME, Ludlow M, et al. Measles virus suppresses RIG-I-like receptor activation in dendritic cells via DC-SIGN-mediated inhibition of PP1 phosphatases. Cell Host Microbe. 2014;16(1):31-42.
53. Merle NS, Church SE, Fremeaux-Bacchi V, Roumenina LT. Complement System Part I - Molecular Mechanisms of Activation and Regulation. Front Immunol. 2015;6:262.
54. Posch W, Bermejo-Jambrina M, Lass-Florl C, Wilflingseder D. Role of Complement Receptors (CRs) on DCs in Anti-HIV-1 Immunity. Front Immunol. 2020;11:572114.
55. Noris M, Remuzzi G. Overview of complement activation and regulation. Semin Nephrol. 2013;33(6):479-92.
56. Manel N, Littman DR. Hiding in plain sight: how HIV evades innate immune responses. Cell. 2011;147(2):271-4.
57. Posch W, Bermejo-Jambrina M, Steger M, Witting C, Diem G, Hortnagl P, et al. Complement Potentiates Immune Sensing of HIV-1 and Early Type I Interferon Responses. mBio. 2021;12(5):e0240821.
58. Posch W, Steger M, Knackmuss U, Blatzer M, Baldauf HM, Doppler W, et al. Complement-Opsonized HIV-1 Overcomes Restriction in Dendritic Cells. PLoS Pathog. 2015;11(6):e1005005.
59. Yu Q, Yu R, Qin X. The good and evil of complement activation in HIV-1 infection. Cell Mol Immunol. 2010;7(5):334-40.
60. Guermonprez P, Valladeau J, Zitvogel L, Thery C, Amigorena S. Antigen presentation and T cell stimulation by dendritic cells. Annu Rev Immunol. 2002;20:621-67.

61. Hoffmann E, Kotsias F, Visentin G, Bruhns P, Savina A, Amigorena S. Autonomous phagosomal degradation and antigen presentation in dendritic cells. Proc Natl Acad Sci U S A. 2012;109(36):14556-61.
62. Platt CD, Ma JK, Chalouni C, Ebersold M, Bou-Reslan H, Carano RA, et al. Mature dendritic cells use endocytic receptors to capture and present antigens. Proc Natl Acad Sci U S A. 2010;107(9):4287-92.
63. Hilligan KL, Ronchese F. Antigen presentation by dendritic cells and their instruction of CD4+ T helper cell responses. Cell Mol Immunol. 2020;17(6):587-99.
64. Alcover A, Alarcon B, Di Bartolo V. Cell Biology of T Cell Receptor Expression and Regulation. Annu Rev Immunol. 2018;36:103-25.
65. Chakraborty AK, Weiss A. Insights into the initiation of TCR signaling. Nat Immunol. 2014;15(9):798-807.
66. Denny MF, Patai B, Straus DB. Differential T-cell antigen receptor signaling mediated by the Src family kinases Lck and Fyn. Mol Cell Biol. 2000;20(4):1426-35.
67. James JR, Vale RD. Biophysical mechanism of T-cell receptor triggering in a reconstituted system. Nature. 2012;487(7405):64-9.
68. Palacios EH, Weiss A. Function of the Src-family kinases, Lck and Fyn, in T-cell development and activation. Oncogene. 2004;23(48):7990-8000.
69. Su X, Ditlev JA, Hui E, Xing W, Banjade S, Okrut J, et al. Phase separation of signaling molecules promotes T cell receptor signal transduction. Science. 2016;352(6285):595-9.
70. Thill PA, Weiss A, Chakraborty AK. Phosphorylation of a Tyrosine Residue on Zap70 by Lck and Its Subsequent Binding via an SH2 Domain May Be a Key Gatekeeper of T Cell Receptor Signaling In Vivo. Mol Cell Biol. 2016;36(18):2396-402.
71. van Oers NS, Killeen N, Weiss A. Lck regulates the tyrosine phosphorylation of the T cell receptor subunits and ZAP-70 in murine thymocytes. J Exp Med. 1996;183(3):1053-62.
72. Wang H, Kadlecek TA, Au-Yeung BB, Goodfellow HE, Hsu LY, Freedman TS, et al. ZAP-70: an essential kinase in T-cell signaling. Cold Spring Harb Perspect Biol. 2010;2(5):a002279.
73. Cenciarelli C, Hou D, Hsu KC, Rellahan BL, Wiest DL, Smith HT, et al. Activation-induced ubiquitination of the T cell antigen receptor. Science. 1992;257(5071):795-7.
74. D'Oro U, Vacchio MS, Weissman AM, Ashwell JD. Activation of the Lck tyrosine kinase targets cell surface T cell antigen receptors for lysosomal degradation. Immunity. 1997;7(5):619-28.
75. Liu H, Rhodes M, Wiest DL, Vignali DA. On the dynamics of TCR:CD3 complex cell surface expression and downmodulation. Immunity. 2000;13(5):665-75.
76. Rubin B, Llobera R, Gouaillard C, Alcover A, Arnaud J. Dissection of the role of CD3gamma chains in profound but reversible T-cell receptor down-regulation. Scand J Immunol. 2000;52(2):173-83.
77. Smith-Garvin JE, Koretzky GA, Jordan MS. T cell activation. Annu Rev Immunol. 2009;27:591-619.
78. Wucherpfennig KW, Gagnon E, Call MJ, Huseby ES, Call ME. Structural biology of the T-cell receptor: insights into receptor assembly, ligand recognition, and initiation of signaling. Cold Spring Harb Perspect Biol. 2010;2(4):a005140.
79. Gallegos AM, Xiong H, Leiner IM, Susac B, Glickman MS, Pamer EG, et al. Control of T cell antigen reactivity via programmed TCR downregulation. Nat Immunol. 2016;17(4):379-86.

PART 1

INNATE IMMUNITY: CONTROLLING SENSING AND IMMUNE ACTIVATION

CHAPTER 2

SARS-COV-2 INFECTION ACTIVATES DENDRITIC CELLS VIA CYTOSOLIC RECEPTORS RATHER THAN EXTRACELLULAR TLRS

Lieve E.H. van der Donk[1], Julia Eder[1], John L. van Hamme[1], Philip J.M. Brouwer[2], Mitch Brinkkemper[2], Ad C. van Nuenen[1], Marit J. van Gils[2], Rogier W. Sanders[2,3], Neeltje A. Kootstra[1], Marta Bermejo-Jambrina[1#], Teunis B.H. Geijtenbeek[1#*]

[1] Department of Experimental Immunology, Amsterdam institute for Infection and Immunity, Amsterdam University Medical Centers, University of Amsterdam, Meibergdreef 9, Amsterdam, The Netherlands.

[2] Department of Medical Microbiology, Amsterdam institute for Infection and Immunity, Amsterdam University Medical Centers, University of Amsterdam, Meibergdreef 9, Amsterdam, The Netherlands.

[3] Department of Microbiology and Immunology, Weill Medical College of Cornell University, New York, NY 10021, USA.

\# These authors contributed equally to this work.

* Address correspondence and reprint requests to T.B.H. Geijtenbeek, Amsterdam UMC, Meibergdreef 9, 1105 AZ, Amsterdam.

European Journal of Immunology 2022, 52(4): 646-655.

ABSTRACT

Severe acute respiratory syndrome coronavirus 2 (SARS-CoV-2) causes coronavirus disease 2019 (COVID-19), an infectious disease characterized by strong induction of inflammatory cytokines, progressive lung inflammation and potentially multi-organ dysfunction. It remains unclear how SARS-CoV-2 infection leads to immune activation. The Spike (S) protein of SARS-CoV-2 has been suggested to trigger Toll-like receptor 4 (TLR4) and thereby activate immunity. Here, we have investigated the role of TLR4 in SARS-CoV-2 infection and immunity. Neither exposure of isolated S protein, SARS-CoV-2 pseudovirus nor primary SARS-CoV-2 isolate induced TLR4 activation in a TLR4-expressing cell line. Human monocyte-derived dendritic cells (DCs) express TLR4 but not angiotensin converting enzyme 2 (ACE2), and DCs were not infected by SARS-CoV-2. Notably, neither S protein nor SARS-CoV-2 induced DC maturation or cytokines, indicating that both S protein and SARS-CoV-2 virus particles do not trigger extracellular TLRs including TLR4. Ectopic expression of ACE2 in DCs led to efficient infection by SARS-CoV-2 and, strikingly, efficient type I interferon (IFN) and cytokine responses. These data strongly suggest that not extracellular TLRs but intracellular viral sensors are key players in sensing SARS-CoV-2. These data imply that SARS-CoV-2 escapes direct sensing by TLRs, which might underlie the lack of efficient immunity to SARS-CoV-2 early during infection.

Keywords: SARS-CoV-2, dendritic cells, Toll-like receptor 4, innate immune response, intracellular viral sensors

INTRODUCTION

Severe acute respiratory syndrome coronavirus 2 (SARS-CoV-2) is a novel coronavirus that causes coronavirus disease 2019 (COVID-19) (1). COVID-19 emerged in 2019 in Wuhan, China (2), and has since spread globally causing a pandemic. The symptoms of COVID-19 vary amongst individuals, ranging from mild respiratory symptoms to severe lung injury, multi-organ dysfunction and death (3-6). Increasing evidence suggests that disease severity depends not solely on viral infection, but also on an excessive host proinflammatory response, whereby high concentrations of proinflammatory cytokines result in an unfavorable immune response and induce tissue damage (7, 8). The events leading to excessive proinflammatory responses are not completely understood. Therefore, it is necessary to elucidate the mechanisms that are triggered by SARS-CoV-2 to induce innate and adaptive immune responses.

Innate immune cells express pattern recognition receptors (PRRs) that recognize pathogen-associated molecular patterns (PAMPs) and subsequently orchestrate an immune response against pathogens (9). Dendritic cells (DCs) are essential immune cells that function as a bridge between innate and adaptive immunity. DCs express various PRR families such as Toll-like receptors (TLRs) and cytosolic RIG-I-like receptors (RLRs) that are triggered upon virus interaction or infection (10). DCs are therefore essential during SARS-CoV-2 infection to sense infection and instruct T and B cells for efficient antiviral immune responses. However, it is unclear whether and how SARS-CoV-2 is sensed by DCs.

SARS-CoV-2 Spike (S) protein uses angiotensin converting enzyme 2 (ACE2) (11, 12) as receptor for infection. However, besides interacting with ACE2, recent *in silico* analyses suggest that the S protein could also potentially interact with members of the TLR family, in particular TLR4 (13, 14). TLR4 is abundantly expressed on DCs (15, 16), and therefore TLR4 signaling could be involved in induction of proinflammatory mediators. Other studies using cell lines and SARS-CoV-2 S protein support a potential interaction of TLR4 with the S protein (17-19). However, it remains unclear whether infectious SARS-CoV-2 virus is sensed by TLR4 and whether this interaction induces DC activation and initiation of immunity.

Here, we have investigated how SARS-CoV-2 is sensed by human DCs. Neither recombinant S protein, SARS-CoV-2 pseudovirus nor a primary SARS-CoV-2 isolate induced immunity in TLR4-expressing cell lines or DCs, indicating that TLR4 or other extracellular TLRs are not involved in SARS-CoV-2 infection. However,

ectopic expression of ACE2 on DCs led to infection by SARS-CoV-2 and induction of type I interferon (IFN) and cytokines. These data imply that intracellular PRRs rather than transmembrane TLRs are involved in instigating an immune response against SARS-CoV-2.

MATERIALS AND METHODS

Cell lines

The Simian kidney cell line VeroE6 (ATCC® CRL-1586™) was maintained in CO_2 independent medium (Gibco Life Technologies, Gaithersburg, Md.) supplemented with 10% fetal calf serum (FCS), 2mM L-glutamine and penicillin/streptomycin. Culture was maintained at 37°C without CO_2.

Human embryonic kidney cells (HEK293) were maintained in IMDM (Gibco) supplemented with 10% FCS and 1% penicillin/streptomycin (Invitrogen). HEK293 cells stably transfected with TLR4 cDNA (HEK/TLR4) were a kind gift from D. T. Golenbock (15). HEK293 and HEK/TLR4 cells were transiently transfected with pcDNA3.1(-)hACE2 (Addgene plasmid #1786) to generate HEK/ACE2 or HEK/TLR4/ACE2 cell lines. Transfection was performed using Lipofectamine LTX and PLUS reagent (Invitrogen) according to the manufacturer's protocol. After 24 hours, cells were split and seeded into flat-bottom 96-well plates (Corning) and left to attach for 24 hours, before performing further experiments. Cultures were maintained at 37°C and 5% CO_2. Before infection with the SARS-CoV-2 isolate (described below), media was exchanged for CO_2-independent media, since infection with a SARS-CoV-2 primary isolate occurs under CO_2 negative conditions. Human ACE2-expressing cell lines were analyzed for ACE2 expression via quantitative real-time PCR.

Primary cells

This study was performed in accordance with the ethical principles set out in the declaration of Helsinki and was approved by the institutional review board of the Amsterdam University Medical Centers, location AMC Medical Ethics Committee and the Ethics Advisory Body of Sanquin Blood Supply Foundation (Amsterdam, Netherlands). Human $CD14^+$ monocytes were isolated from the blood from healthy volunteer donors (Sanquin blood bank) and subsequently differentiated into monocyte-derived dendritic cells (DCs). The isolation from buffy coats was done by density gradient centrifugation on Lymphoprep (Nycomed) and Percoll (Pharmacia). After separation by Percoll, the isolated monocytes were cultured in RPMI 1640 (Gibco) supplemented with 10% FCS, 2mM L-glutamin (Invitrogen) and 10 U/mL penicillin and 100 µg/mL streptomycin, containing the cytokines IL-4 (500 U/mL) and GM-CSF (800

U/mL) (both Gibco) for differentiation into DCs. After 4 days of differentiation, DCs were seeded at $1x10^6$ /mL in a 96-well plate (Greiner), and after 2 days of recovery, DCs were stimulated or infected as described below.
Alternatively, monocyte-derived DCs that were transfected with hACE2 were seeded at $0.5x10^6$ cells/mL in a 6-well plate and transfection was performed with Lipofectamine LTX and PLUS reagents (Invitrogen) according to the manufacturer's instructions for primary cells. After 24 hours, cells were seeded at $1x10^6$/mL in a 96-well plate and after 24 hours of recovery, they were infected with primary SARS-CoV-2 isolate.

SARS-CoV-2 pseudovirus production

For production of single-round infection viruses, human embryonic kidney 293T/17 cells (ATCC, CRL-11268) were co-transfected with an adjusted HIV-1 backbone plasmid (pNL4-3.Luc.R-S-) containing previously described stabilizing mutations in the capsid protein (PMID: 12547912) and firefly luciferase in the *nef* open reading frame (1.35 µg) and pSARS-CoV-2 expressing SARS-CoV-2 S protein (0.6 µg) (GenBank; MN908947.3) (22). Transfection was performed in 293T/17 cells using genejuice (Novagen, USA) transfection kit according to manufacturer's protocol. At day 3 or day 4, pseudotyped SARS-CoV-2 virus particles were harvested and filtered over a 0.45 µm nitrocellulose membrane (SartoriusStedim, Gottingen, Germany). SARS-CoV-2 pseudovirus productions were quantified by p24 ELISA (Perkin Elmer Life Sciences).

SARS-CoV-2 (primary isolate) virus production

The following reagent was obtained from Dr. Maria R. Capobianchi through BEI Resources, NIAID, NIH: SARS-Related Coronavirus 2, Isolate Italy-INMI1, NR-52284, originally isolated January 2020 in Rome, Italy. VeroE6 cells (ATCC® CRL-1586™) were inoculated with the SARS-CoV-2 isolate and used for reproduction of virus stocks. Cytopathic effect formation was closely monitored and virus supernatant was harvested after 48 hours. Tissue culture infectious dose (TCID50) was determined on VeroE6 cells by MTT assay 48 hours after infection. Loss of MTT staining as determined by spectrometer is indicative of cell death. The virus titer was determined as TCID50/mL and calculated based on the Reed Muench method (35), as described before (23).

Stimulation and infection

HEK293 and transfected derivatives were left unstimulated or stimulated for 24 hours with 10 ng/mL lipopolysaccharide (LPS) from Salmonella (Sigma), 10 µg/mL isolated S protein, 10 µg/mL S nanoparticles, or with pseudotyped or authentic SARS-CoV-2, as specified below. DCs were left unstimulated, or stimulated with 10 µg/ml Pam3CSK4 (Invivogen), 10 ng/mL LPS from *Salmonella typhosa* (Sigma), 10

µg/mL flagellin from *Salmonella typhimurium* (Invivogen), 10 µg/mL lipoteichoic acid (LTA) from *Staphylococcus aureus* (Invivogen), pseudotyped virus or SARS-CoV-2. Blocking of ACE2 or TLR4 was performed with 8 µg/mL anti-ACE2 (R&D systems) or 10 µg/mL anti-TLR4 (clone 7E3, Hycult) for 30 minutes at 37°C before adding stimuli. Monocyte-derived DCs do not express ACE2 and are therefore not infected. Therefore, pseudovirus stimulation was performed for 6 hours, after which the cells were lysed for mRNA analysis of cytokine production. DCs ectopically expressing ACE2 were stimulated for 24 hours with virus before the cells were lysed for mRNA analysis of cytokine production. Also, cells were stimulated for 24 hours and fixed for 30 minutes with 4% paraformaldehyde, after which the expression of maturation markers was assessed with flow cytometry.
For the pseudovirus infection assays, HEK293 or 293/TLR4 cell lines and DCs were exposed to 95 ng/mL and 191.05 ng/mL of SARS-CoV-2 pseudovirus, respectively. Viral protein production was quantified after 3 days at 37°C by measuring luciferase reporter activity. Luciferase activity was measured using the Luciferase assay system (Promega, USA) according to manufacturer's instructions.
For the primary SARS-CoV-2 infection assays, HEK293 or HEK/TLR4 cell lines and DCs were exposed to the SARS-CoV-2 isolate (hCoV-19/Italy) at different TCIDs (100 and 1000; MOI 0.0028-0.028) for 24 hours at 37°C. After 24 hours, cell supernatant was taken and DCs were lysed for isolation of viral RNA. Also, the HEK293/ACE2 and HEK/TLR4/ACE2 cell lines were exposed to the SARS-CoV-2 isolate (hCoV-19/Italy) at TCID 100 (MOI 0.0028) for 24 hours at 37°C. After 24 hours, the cells were washed 3 times and new media was added. After 48 hours, cell supernatant was harvested and the cells were lysed to investigate productive infection.

RNA isolation and quantitative real-time PCR

Cells exposed to SARS-CoV-2 pseudovirus were lysed and mRNA was isolated with the mRNA Catcher™ PLUS Purification Kit (ThermoFisher). Subsequently, cDNA was synthesized with a reverse-transcriptase kit (Promega). RNA of cells exposed to SARS-CoV-2 WT was isolated with the QIAamp Viral RNA Mini Kit (Qiagen) according to the manufacturer's protocol. cDNA was synthesized with the M-MLV reverse-transcriptase kit (Promega) and diluted 1 in 5 in DNase/RNase-free water before further application. PCR amplification was performed in the presence of SYBR green (ThermoFisher) in a 7500 Fast Realtime PCR System (ABI). Specific primers were designed with Primer Express 2.0 (Applied Biosystems). The ORF1b primers used were as described before (36). The normalized amount of target mRNA was calculated from the Ct values obtained for both target and household mRNA with the equation $Nt = 2^{Ct(GAPDH)-Ct(target)}$. The following primers were used:

GAPDH: F_CCATGTTCGTCATGGGTGTG; R_GGTGCTAAGCAGTTGGTGGTG;
TLR4: F_CTGCAATGGATCAAGGACCAG; R_CCATTCGTTCAACTTCCACCA;
ACE2: F_GGACCCAGGAAATGTTCAGA; R_ GGCTGCAGAAAGTGACATGA;
ORF1b: F_TGGGGTTTTACAGGTAACCT; R_AACACGCTTAACAAAGCACTC;
IL-8: F_TGAGAGTGGACCACACTGCG; R_TCTCCACAACCCTCTGCACC;
IFNB: F_ACAGACTTACAGGTTACCTCCGAAAC; R_CATCTGCTGGTTGAAGAATGCTT;
APOBEC3G: F_TTGAGCCTTGGAATAATCTGCC; R_TCGAGTGTCTGAGAATCTCCCC;
IL-6: F_TGCAATAACCACCCCTGACC; R_TGCGCAGAATGAGATGAGTTG;
IL-10: F_GAGGCTACGGCGCTGTCAT; R_CCACGGCCTTGCTCTTGTT.

ELISA

Cell supernatants were harvested after 24 hours of stimulation and secretion of IL-8 was measured by ELISA (eBiosciences) according to the manufacturer's instructions. OD450 nm values were measured using a BioTek Synergy HT. Supernatant containing SARS-CoV-2 pseudovirus was inactivated with 0.1% triton and supernatant containing SARS-CoV-2 was inactivated with 1% triton before performing ELISA.

Flow cytometry

For cell surface staining, cells were incubated in 0.5% PBS-BSA (phosphate-buffered saline containing 0.5% bovine serum albumin (BSA; Sigma-Aldrich)) containing antibodies for 30 minutes at 4°C. Single-cell measurements were performed on a FACS Canto flow cytometer (BD Biosciences) and FlowJo V10 software (TreeStar) was used to analyze the data. The antibody clones used are: CD86 (2331 (FUN-1), BD Pharmingen), CD80 (L307.4, BD Pharmingen), CD83 (HB15e, BD Pharmingen), ACE2 (AF933, R&D systems), goat-IgG (AB-2535864, ThermoFisher Scientific), donkey-anti-goat (A-21447, ThermoFisher Scientific). For each experiment, live cells were gated on FSC and SSC and analyzed further with the markers mentioned (Supplemental Figure 1). The authors adhered to the guidelines for the use of flow cytometry and cell sorting in immunological studies (37).

Statistics

Graphpad Prism v8 (GraphPad Software) was used to generate all graphs and for statistical analyses. Statistics were performed using a Student's *t* test for pairwise comparisons. Multiple comparisons within groups were performed using an RM one-way analysis of variance (ANOVA) with a Tukey's multiple comparisons test, or two-way ANOVA with a Tukey's or Šidák's multiple comparisons test where indicated. $p < 0.05$ were considered statistically significant.

RESULTS

SARS-CoV-2 S protein does not trigger TLR4

To assess whether TLR4 acts as a sensor of S protein of SARS-CoV-2, we treated a TLR4-expressing HEK293 cell line (293/TLR4) with SARS-CoV-2 recombinant S protein or S nanoparticles (20) and determined activation by measuring interleukin (IL)-8. Neither S protein nor S nanoparticles induced IL-8 secretion by 293/TLR4 cells, in contrast to the positive control lipopolysaccharide (LPS) (Figure 1A). The parental 293 cells did not induce IL-8 upon treatment with S protein or S nanoparticles and LPS. These data suggest that S protein of SARS-CoV-2 does not trigger TLR4.

Primary monocyte-derived DCs express TLR4 but also other TLRs (21). We therefore exposed primary human DCs to SARS-CoV-2 S nanoparticles and assessed cytokine production by qPCR. Treatment of DCs with S nanoparticles did neither induce type I interferon (IFN) nor cytokines (Figure 1B-E). The positive control LPS induced IFN-β (Figure 1B) and the interferon-stimulated gene (ISG) APOBEC3G (A3G) (Figure 1C) as well as cytokines IL-6 and IL-10 (Figure 1D, E). These data strongly suggest that S protein from SARS-CoV-2 does not trigger extracellular TLRs on DCs.

SARS-CoV-2 virus particles do not trigger TLR4

To assess whether TLR4 plays a role in SARS-CoV-2 entry and replication, we ectopically expressed ACE2 on 293 and 293/TLR4 cell lines and infected the cells with SARS-CoV-2 pseudovirus that expresses the full-length S glycoprotein from SARS-CoV-2 and contains a luciferase reporter gene (22). Infection was determined by measuring luciferase activity. SARS-CoV-2 pseudovirus infected ACE2-positive 293 and 293/TLR4 cells but not the parental 293 and 293/TLR4 cells (Figure 2A). TLR4 expression did not affect infection, as infection was comparable between 293/ACE2 and 293/TLR4/ACE2 cells.

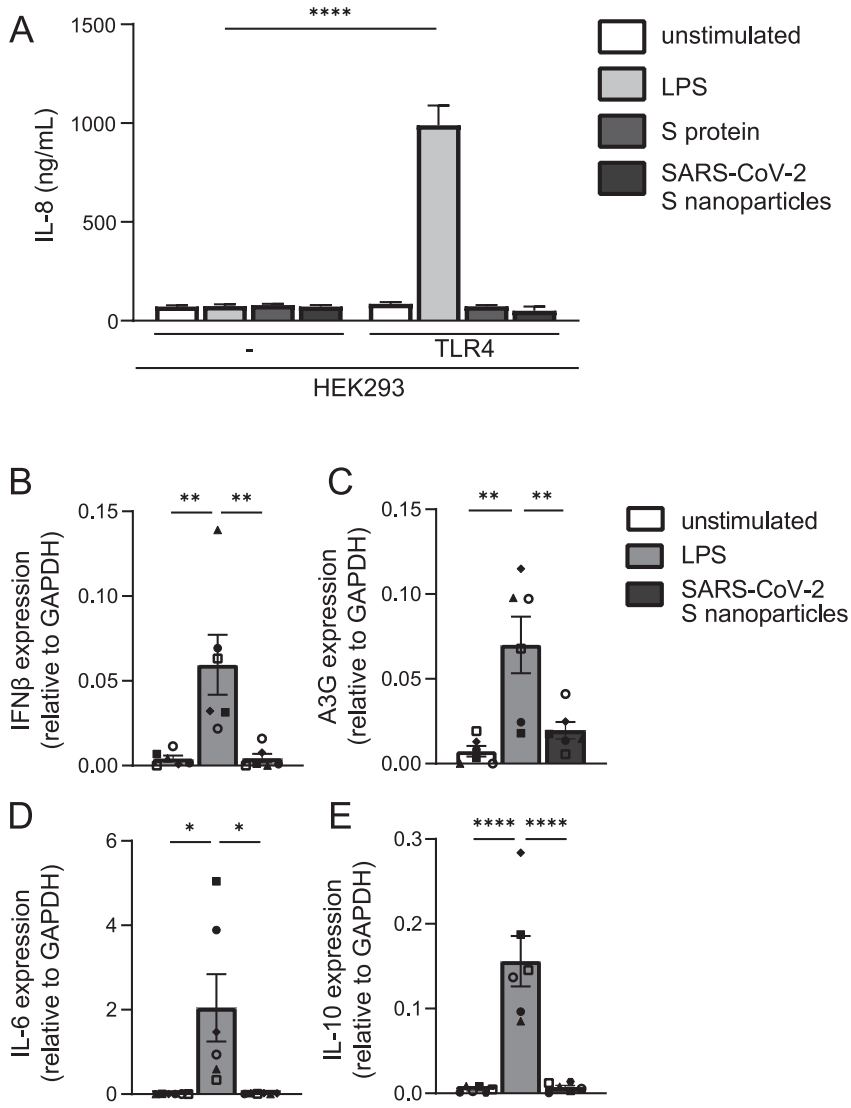

Figure 1: S protein and SARS-CoV-2 S nanoparticles do not trigger TLR4.

(A) 293 cells or 293/TLR4 cells were exposed to LPS, SARS-CoV-2 S protein or S nanoparticles for 24 hours. IL-8 production was determined by ELISA. (B-E) Primary dendritic cells were exposed to LPS or SARS-CoV-2 S nanoparticles for 8 hours. Expression of IFN-β (B), A3G (C), IL-6 (D) and IL-10 (E) was determined with qPCR. Data show the mean values and SEM. Statistical analysis was performed using (A) two-way ANOVA with Šidák's multiple comparisons test, or (B-E) one-way ANOVA with Tukey's multiple comparisons test. Data represent six replicates obtained in three separate experiments (A), or experiments performed with six donors in three independent experiments, with each symbol representing a different donor (B-E). ****p<0.0001, ***p<0.001; **p<0.01; *p<0.05.

Next we investigated whether SARS-CoV-2 pseudovirus activates TLR4. SARS-CoV-2 pseudovirus neither induced IL-8 in parental 293 nor in 293/TLR4 cells (Figure 2B). Moreover, ACE2 expression did not induce activation as exposure of ACE2-positive 293 and 293/TLR4 cells to SARS-CoV-2 pseudovirus did not lead to IL-8 production (Figure 2B). These data further support the findings that S protein from SARS-CoV-2 does not trigger TLR4 and also show that ACE2 does not affect TLR4 signaling.
Next, we performed a serial dilution with a primary SARS-CoV-2 isolate (hCoV-19/Italy) on 293 and 293/TLR4 cells to determine whether high virus concentrations are able to induce TLR4. Neither 293 nor 293/TLR4 cells expressed IL-8 upon exposure to the primary SARS-CoV-2 isolate, suggesting that high virus concentrations do not trigger TLR4 (Figure 2C). Next, we treated either ACE2-positive or -negative 293 and 293/TLR4 cells with the primary SARS-CoV-2 isolate and determined infection and activation. Infection was determined by measuring virus particles in the supernatant by qPCR. As expected, both 293/ACE2 and 293/TLR4/ACE2 cells were productively infected at similar levels by SARS-CoV-2, in contrast to ACE2-negative 293 and 293/TLR4 cells (cutoff Ct values >30), (Figure 2D). Neither ACE2-positive nor -negative 293 and 293/TLR4 cells expressed any IL-8 upon exposure to the primary SARS-CoV-2 isolate (Figure 2E). These data strongly suggest that TLR4 does not sense infectious SARS-CoV-2 virus particles.

Infectious SARS-CoV-2 does not activate DCs

Subsequently, we examined whether SARS-CoV-2 pseudovirus induces DC maturation and cytokine production. DCs do not express ACE2 and we have previously shown that SARS-CoV-2 pseudovirus does not infect DCs (23, 24). We investigated the maturation and cytokine production by DCs stimulated with SARS-CoV-2 pseudovirus. Exposure of DCs to SARS-CoV-2 pseudovirus did neither induce expression of co-stimulatory markers CD80 and CD86 nor maturation marker CD83, in contrast to LPS (Figure 3A-D, Supplemental Figure 1). Moreover, SARS-CoV-2 pseudovirus did not induce any cytokines, in contrast to LPS (Figure 3E-H). These data indicate that the S protein expressed by SARS-CoV-2 pseudovirus does not activate DCs.
Next, we exposed DCs to a primary SARS-CoV-2 isolate and determined DC maturation and cytokine production. We have previously shown that DCs do not become infected by primary SARS-CoV-2 (23). Exposure of DCs to the primary SARS-CoV-2 isolate did neither induce expression of CD80 CD86, nor CD83, whereas LPS induced expression of CD83 and CD86 (Figure 4A-C).

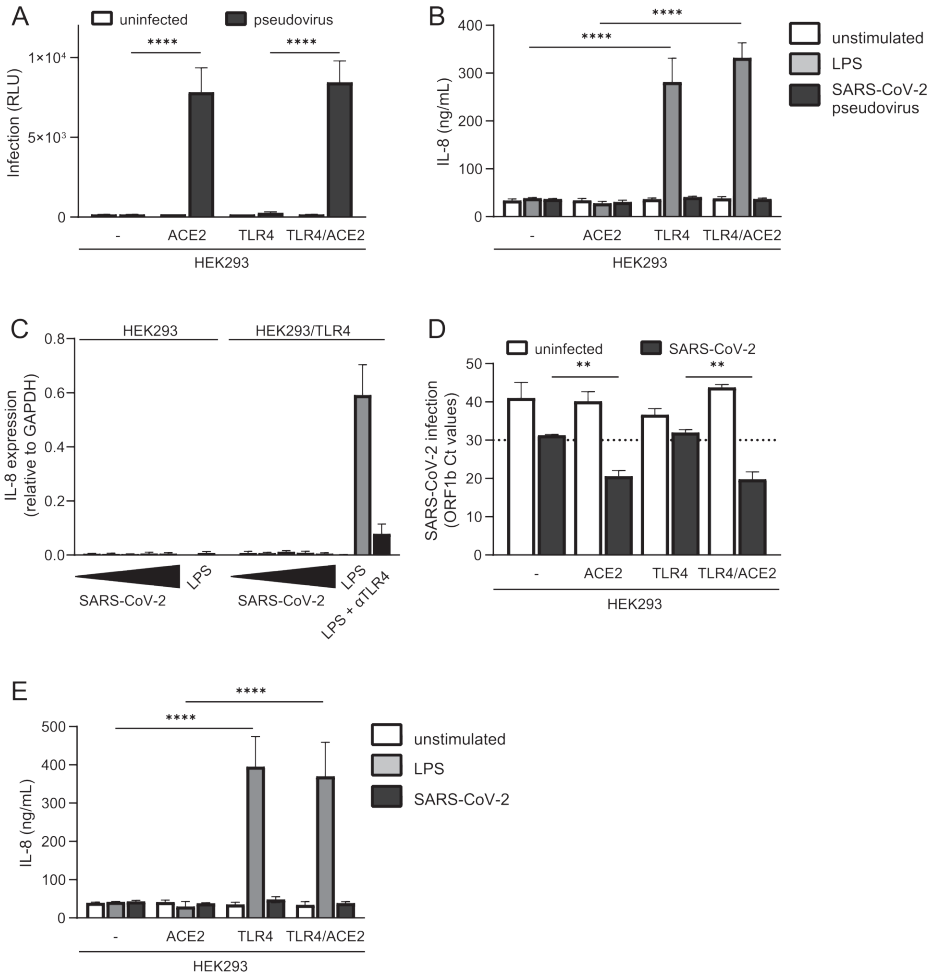

Figure 2: SARS-CoV-2 virus particles do not trigger TLR4.

(A-B) ACE2-positive and -negative 293 and 293/TLR4 cells were exposed to SARS-CoV-2 pseudovirus and infection was determined after 3 days by measuring luciferase activity (A), and IL-8 production was measured after 24 hours by ELISA (B). (C) 293 and 293/TLR4 cells were exposed to increasing titers of SARS-CoV-2, or LPS in the absence or presence of anti-TLR4 antibodies, and IL-8 production was determined after 24 hours by qPCR. Increasing titers are indicated by a bar, ranging from TCID100 (narrow) to TCID100.000 (wide). (D-E) ACE2-positive and -negative 293 and 293/TLR4 cells were exposed to a primary SARS-CoV-2 isolate and infection was determined after 24 hours by measuring the viral gene ORFb1 expression in supernatant by qPCR (D) and IL-8 production was measured after 24 hours by ELISA (E). Data show the mean values and SEM. Statistical analysis was performed using two-way ANOVA with Šidák's (A) or Tukey's (B, D-E) multiple comparisons test. Data represent nine replicates obtained in three separate experiments (A-B), or three separate experiments (C-E). ****p<0.0001; **p<0.01. RLU = relative light units.

Next we investigated cytokine induction by DCs after exposure to primary SARS-CoV-2 isolate or agonists for extracellular TLRs (TLR1/2, TLR2/6, TLR4, and TLR5). LPS, flagellin and LTA induced type I IFN responses as well as cytokines, whereas Pam3CSK4 only induced cytokines (Figure 4D-G). However, exposure of DCs to the primary SARS-CoV-2 isolate did not lead to induction of type I IFN responses nor cytokines (Figure 4D-G). Therefore, these data strongly indicate that primary SARS-CoV-2 virus particles are not sensed by any extracellular PRRs on DCs such as TLR2, TLR4, and TLR5.

Although SARS-CoV-2 did not directly activate DCs, we investigated whether DCs become activated indirectly by SARS-CoV-2-infected cells. Therefore, DCs were co-cultured with SARS-CoV-2 infected VeroE6 cells and DC activation was determined. Strikingly, co-culture of DCs with SARS-CoV-2-infected, but not uninfected VeroE6 cells induced expression of co-stimulatory molecules CD80 and CD86 (Figure 4H-K). These data support a role for indirect activation of DCs by infected cells during SARS-CoV-2 infection.

Ectopic ACE2 expression on DCs results in SARS-CoV-2 infection and immune activation

Next, we investigated whether infection of DCs after ectopic expression of ACE2 with primary SARS-CoV-2 isolate would induce immune responses. DCs do not express ACE2, but transfection with ACE2 plasmid resulted in ACE2 mRNA and surface expression (Figure 5A-C). Next, both DCs and ACE2-expressing DCs were exposed to the primary SARS-CoV-2 isolate for 24 hours in presence or absence of blocking antibodies against ACE2. ACE2-expressing DCs were infected by SARS-CoV-2 and infection was blocked by antibodies against ACE2 (Figure 5D). Notably, infection of DCs with SARS-CoV-2 induced transcription of IFN-β (Figure 5E) as well as the ISG A3G (Figure 5F). Infection also induced proinflammatory cytokine IL-6 (Figure 5G). Both type I IFN responses and IL-6 were abrogated by blocking infection using ACE2 antibodies. Although the transfection procedure itself slightly activates DCs, SARS-CoV-2 infection significantly increased DC activation, which was abrogated by blocking ACE2. These data strongly suggest that DC activation of ACE2-expressing DCs is due to SARS-CoV-2 infection.

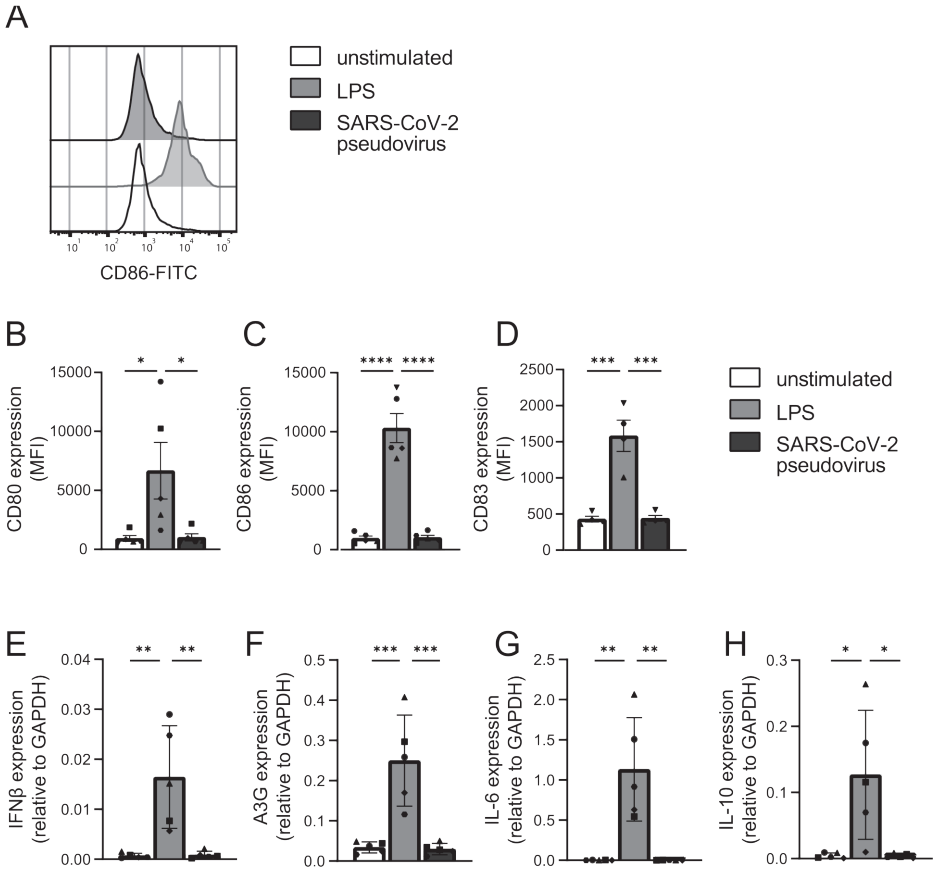

Figure 3: SARS-CoV-2 pseudovirus does not activate dendritic cells.

(A-D) Primary DCs were exposed to LPS or SARS-CoV-2 pseudovirus and maturation and cytokine production was determined after 24 hours and 6 hours respectively. (A) Representative histogram of CD86 expression. (B-D) Cumulative flow cytometry data of CD80 (B), CD86 (C), and CD83 (D) expression. (E-H) mRNA levels of IFN-β (E), A3G (F), IL-6 (G) and IL-10 (H) were determined with qPCR. Data show the mean values and SEM. Statistical analysis was performed using one-way ANOVA with Tukey's multiple comparisons test. Data represent five donors analyzed in three separate experiments (B-C, E-H), or four donors analyzed in two separate experiments (D), with each symbol representing a different donor. ****p<0.0001; ***p<0.001; **p<0.01; *p<0.05. MFI = mean fluorescence intensity.

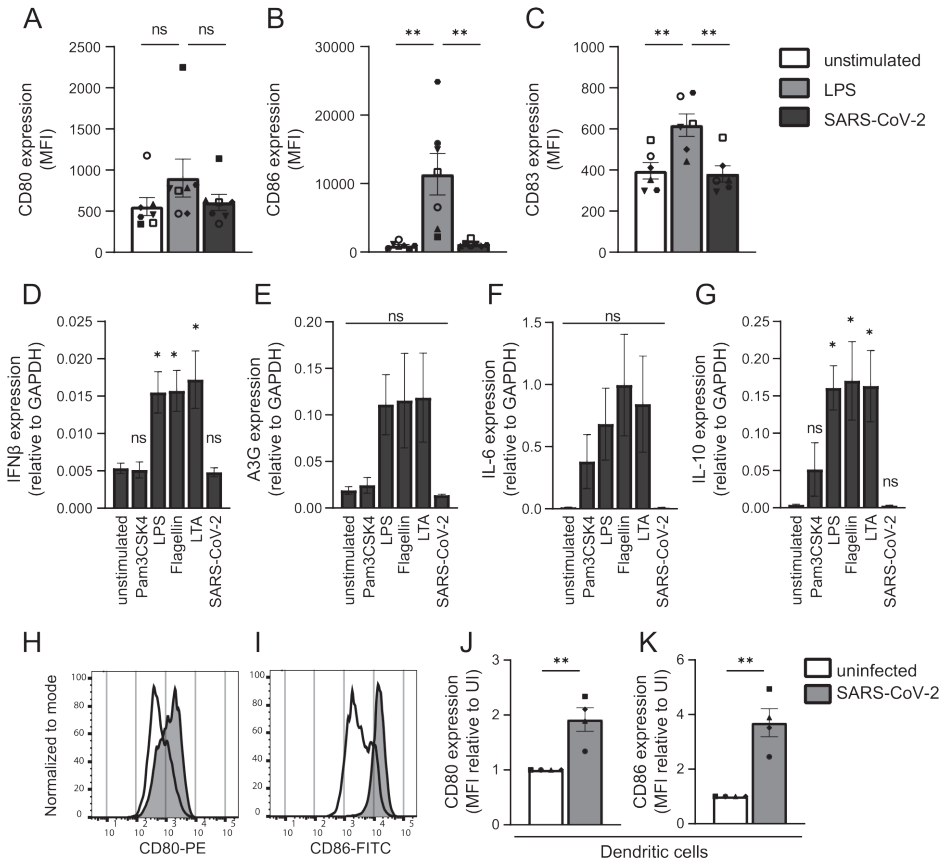

Figure 4: Primary SARS-CoV-2 isolate does not activate dendritic cells.

(A-C) Primary DCs were exposed to LPS or primary SARS-CoV-2 isolate and DC maturation was measured after 24 hours by flow cytometry. Cumulative flow cytometry data of CD80 (A), CD86 (B), and CD83 (C) expression. (D-G) Primary DCs were exposed to different TLR agonists or primary SARS-CoV-2 isolate and mRNA levels of IFN-β (D), A3G (E), IL-6 (F) and IL-10 (G) were determined with qPCR. (D-G) Data are compared to the unstimulated condition. (H-K) Primary DCs were co-cultured with VeroE6 cells infected by SARS-CoV-2 and DC maturation was determined after 24 hours by measuring expression of CD80 and CD86. (H-I) Representative histograms of CD80 (H) and CD86 (I) expression. (J-K) Cumulative flow cytometry data of CD80 (J) and CD86 (K) expression. Data is relative to the uninfected condition (UI). Data show the mean values and SEM. Statistical analysis was performed using one-way ANOVA with Tukey's multiple comparisons test (A-G), or using an unpaired student's *t*-test (J-K). Data represent seven donors (A-B) or six donors (C) analyzed in four experiments; or five donors analyzed in three separate experiments (D-G); or four donors analyzed in two separate experiments (J-K), with each symbol representing a different donor. **p<0.01; *p<0.05; ns = non-significant. MFI = mean fluorescence intensity; UI = uninfected.

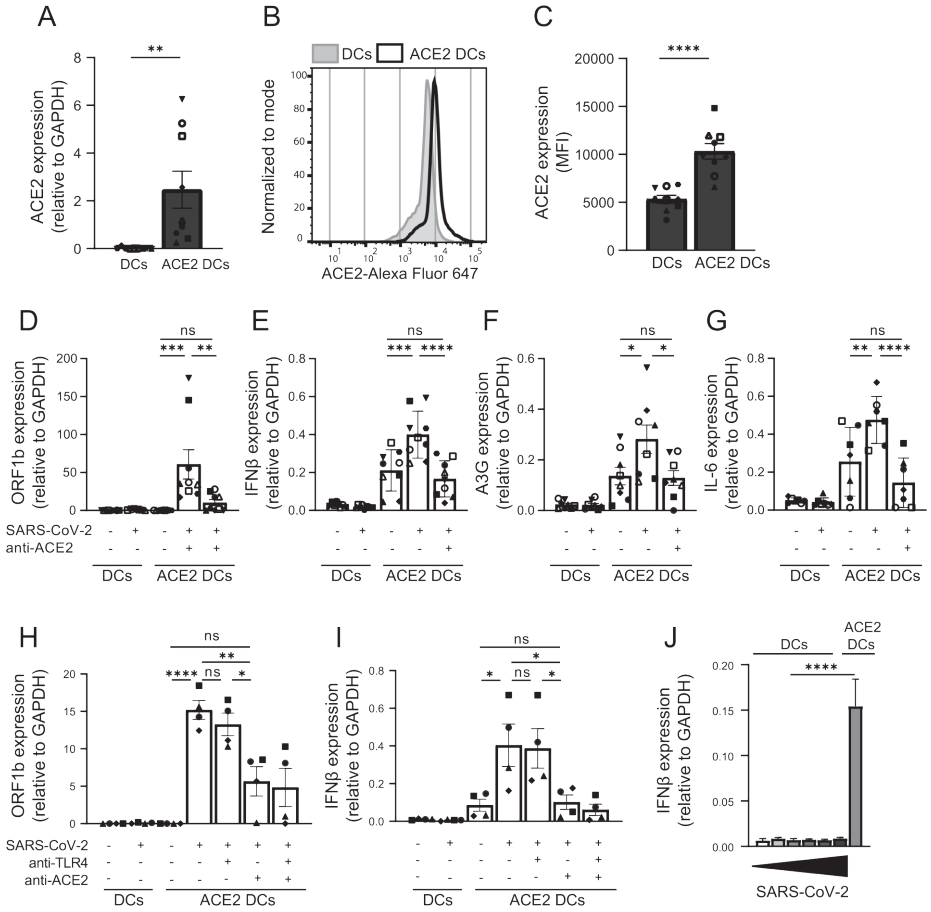

Figure 5: Ectopic expression of ACE2 on DCs results in infection and induction of immune responses.

(A-C) Ectopic expression of ACE2 on primary DCs was determined by qPCR and flow cytometry. (A) Cumulative qPCR data of ACE2 expression on DCs. (B) Representative histogram of ACE2 expression on DCs. (C) Cumulative flow cytometry data of ACE2 expression. (D-G) ACE2-positive and -negative DCs were exposed to primary SARS-CoV-2 isolate in presence or absence of blocking antibodies against ACE2. Infection (D) and mRNA levels of IFN-β (E), A3G (F), and IL-6 (G) were determined with qPCR. (H-I) ACE2-positive and -negative DCs were exposed to primary SARS-CoV-2 isolate in presence of blocking antibodies against TLR4 and ACE2. Infection (H) and mRNA levels of IFN-β (I) were determined with qPCR. (J) ACE2- negative DCs were exposed to increasing titers of primary SARS-CoV-2 isolate for 24 hours and compared to ACE2-positive DCs infected with TCID1000, and mRNA levels of IFN-β were determined by qPCR. Increasing titers are indicated by a bar, ranging from TCID100 (narrow) to TCID100.000 (wide). Data show the mean values and SEM. Statistical analysis was performed using (A, C) unpaired student's *t*-test or (D-I) one-way ANOVA with Tukey's multiple comparisons test. Data represent nine donors (A, C-F) or seven donors (G) obtained in five separate experiments, or four donors (H-J) obtained in two separate experiments, with each symbol representing a different donor. ****p<0.0001; ***p<0.001; **p<0.01; *p<0.05; ns = non-significant. MFI = mean fluorescence intensity.

It has been described that TLR4 not only induces signaling pathways from the plasma membrane, but could also be internalized to the endosomal pathway to induce alternative signaling (25). To investigate whether ACE2-mediated internalization of SARS-CoV-2 triggers endosomal TLR4, we blocked TLR4 upon infection. Both DCs and ACE2-expressing DCs were exposed to the primary SARS-CoV-2 isolate in presence or absence of blocking antibodies against TLR4 and ACE2. ACE2-expressing DCs were infected by SARS-CoV-2 and both infection and IFN-β production was blocked by antibodies against ACE2, but not by antibodies against TLR4 (Figure 5H-I), suggesting that endosomal TLR4 triggering is not involved in the observed SARS-CoV-2-induced immune activation. Moreover, higher concentrations of the primary SARS-CoV-2 isolate did not induce type I IFN responses in DCs compared to ACE2-expressing DCs (Figure 5J). Taken together, these data strongly indicate that infection is required to induce cytokine responses by DCs and suggest that intracellular PRRs rather than extracellular TLRs are involved in sensing SARS-CoV-2 and instigating immune responses against SARS-CoV-2.

DISCUSSION

SARS-CoV-2 has established itself as a contagious human respiratory pathogen, which can trigger a robust inflammatory cytokine response (8). However, it remains largely unknown whether innate immune receptors are involved in the onset of immune responses against SARS-CoV-2. TLR4 has been suggested to play a role in sensing SARS-CoV-2 and inducing a strong immune response (13, 14). Here, our data suggest that SARS-CoV-2 by itself is not recognized by TLR4, as neither a TLR4-expressing 293 cell line nor primary DCs were activated by exposure to recombinant S protein, SARS-CoV-2 pseudovirus or primary SARS-CoV-2 virus particles. Ectopic expression of ACE2 on primary DCs allowed infection with primary SARS-CoV-2. Notably, productive infection of ACE2-positive DCs induced type I IFN and cytokine responses, which were abrogated by blocking ACE2. Our data therefore suggest that SARS-CoV-2 virus particles are not sensed by extracellular TLRs, including TLR4, but that infection via ACE2 is required.

Other studies have reported that SARS-CoV-2 S protein triggers TLR4, and also TLR2 and TLR6 are suggested to interact with the S protein (13, 14, 17-19, 26). However, neither a TLR4-expressing 293 cell line nor primary DCs were activated by recombinant S proteins. It is possible that contamination during the purification process of recombinant proteins might induce activation and explain the differences. Therefore, we have also investigated immune activation by SARS-CoV-2 pseudovirus

and infectious primary SARS-CoV-2 isolates. However, neither TLR4-expressing 293 cells nor primary DCs were activated by pseudovirus or a primary isolate of SARS-CoV-2, even at high virus concentrations. Therefore, our data strongly suggest that S protein expressed by SARS-CoV-2 does not trigger TLR4. Differences between our findings and those published might be due to different S protein preparations, purity of recombinant proteins or cell models. Most studies have used cell lines whereas we have used primary monocyte-derived DCs, which express high levels of TLR4, and are sensitive to TLR4 agonists. Monocyte-derived DCs are present in human lung (27, 28) and monocytes infiltrating the lungs can differentiate into monocyte-derived DCs after pathogen exposure (29, 30), which further supports the relevance of monocyte-derived DCs to study TLR4 function in SARS-CoV-2 infection.

Monocyte-derived DCs do not express ACE2 (24) and did not become infected by SARS-CoV-2, suggesting that the inability of primary SARS-CoV-2 to activate DCs strongly implies that SARS-CoV-2 is not sensed by TLR4 or other extracellular PRRs. Notably, ectopically expressing ACE2 on DCs led to infection and the production of cytokines, indicating that replication of SARS-CoV-2 triggers cytosolic sensors. Indeed, studies suggest that intracellular viral sensors such as RIG-I or MDA5 are involved in SARS-CoV-2 infection (31-33). Our data therefore support an important role for infection by SARS-CoV-2 in inducing immune activation and imply that infection of immune cells, such as antigen presenting cells (APCs), is essential to induction of immunity. Therefore, it is important to identify ACE2-positive DC subsets and macrophages, since these APCs could be sensitive to infection and thereby orchestrate adaptive immunity. However, in the absence of DC infection, epithelial cell infection and subsequent inflammation and tissue damage might account for initial immune activation as release of PAMPs and DAMPs by these infected cells might activate ACE2-negative DCs (34). Notably, co-culture of DCs with SARS-CoV-2-infected cells led to activation of DCs, supporting a role for indirect activation of DCs by infected cells. It remains unclear whether these secondary signals are able to correctly instruct DCs and this might underlie the strong inflammatory responses observed during COVID-19. Our finding that SARS-CoV-2 is not recognized by TLR4 might therefore be an escape mechanism leading to inefficient DC activation and subsequent aberrant inflammatory responses.

It has been suggested that worsening of disease in COVID-19 patients coincides with the activation of the adaptive immune response, 1-2 weeks after infection (8). Since DCs have a bridging function to activate the adaptive immune response, it is important to study DCs in the context of COVID-19. Our research suggests that ACE2-negative DCs are not properly activated by infectious SARS-CoV-2. Moreover,

our data suggest that SARS-CoV-2 is able to escape from extracellular TLRs that are one of the most important PRR families crucial for induction of innate and adaptive immunity, and further research will show whether the lack of TLR activation underlies observed inflammation during COVID-19.

Author Contribution:
LEHvdD and MBJ designed experiments; LEHvdD, MBJ, JE, and JLvH performed the experiments; PJMB, MB, ACvN, NAK, MJvG and RWS contributed essential research materials and scientific input. LEHvdD, MBJ and TBHG analyzed and interpreted data; LEHvdD, MBJ and TBHG wrote the manuscript with input from all listed authors. TBHG supervised all aspects of this study.

Funding:
This research was funded by the Netherlands Organisation for Health Research and Development together with the Stichting Proefdiervrij (ZonMW MKMD COVID-19 grant nr. 114025008 to TBHG) and European Research Council (Advanced grant 670424 to TBHG), and two COVID-19 grants from the Amsterdam institute for Infection & Immunity (to TBHG, RWS, and MJvG). LEHvdD was supported by the Netherlands Organization for Scientific Research (NWO) (Grant number: 91717305). This study was also supported by NWO through a Vici grant (to RWS), and by the Bill & Melinda Gates Foundation through the Collaboration for AIDS Vaccine Discovery (CAVD), grant INV-002022 (to RWS).

Conflicts of interest statement:
All authors declare no commercial or financial conflicts of interest.

Ethics approval statement:
This study was performed in accordance with the ethical principles set out in the Declaration of Helsinki and was approved by the institutional review board of the Amsterdam University Medical Centers, location AMC Medical Ethics Committee and the Ethics Advisory Body of Sanquin Blood Supply Foundation (Amsterdam, the Netherlands).

Data availability:
The data that support the findings of this study are available from the corresponding author upon reasonable request.

REFERENCES

1. Zhu N, Zhang D, Wang W, Li X, Yang B, Song J, et al. A Novel Coronavirus from Patients with Pneumonia in China, 2019. N Engl J Med. 2020;382(8):727-33.
2. Li Q, Guan X, Wu P, Wang X, Zhou L, Tong Y, et al. Early Transmission Dynamics in Wuhan, China, of Novel Coronavirus-Infected Pneumonia. N Engl J Med. 2020;382(13):1199-207.
3. Harrison AG, Lin T, Wang P. Mechanisms of SARS-CoV-2 Transmission and Pathogenesis. Trends Immunol. 2020;41(12):1100-15.
4. Wang D, Hu B, Hu C, Zhu F, Liu X, Zhang J, et al. Clinical Characteristics of 138 Hospitalized Patients With 2019 Novel Coronavirus-Infected Pneumonia in Wuhan, China. JAMA. 2020;323(11):1061-9.
5. Wiersinga WJ, Rhodes A, Cheng AC, Peacock SJ, Prescott HC. Pathophysiology, Transmission, Diagnosis, and Treatment of Coronavirus Disease 2019 (COVID-19): A Review. JAMA. 2020;324(8):782-93.
6. Yuki K, Fujiogi M, Koutsogiannaki S. COVID-19 pathophysiology: A review. Clin Immunol. 2020;215:108427.
7. Mangalmurti N, Hunter CA. Cytokine Storms: Understanding COVID-19. Immunity. 2020;53(1):19-25.
8. Tay MZ, Poh CM, Renia L, MacAry PA, Ng LFP. The trinity of COVID-19: immunity, inflammation and intervention. Nat Rev Immunol. 2020;20(6):363-74.
9. Akira S, Uematsu S, Takeuchi O. Pathogen recognition and innate immunity. Cell. 2006;124(4):783-801.
10. Freer G, Matteucci D. Influence of dendritic cells on viral pathogenicity. PLoS Pathog. 2009;5(7):e1000384.
11. Hoffmann M, Kleine-Weber H, Schroeder S, Kruger N, Herrler T, Erichsen S, et al. SARS-CoV-2 Cell Entry Depends on ACE2 and TMPRSS2 and Is Blocked by a Clinically Proven Protease Inhibitor. Cell. 2020;181(2):271-80 e8.
12. Letko M, Marzi A, Munster V. Functional assessment of cell entry and receptor usage for SARS-CoV-2 and other lineage B betacoronaviruses. Nat Microbiol. 2020;5(4):562-9.
13. Bhattacharya M, Sharma AR, Mallick B, Sharma G, Lee SS, Chakraborty C. Immunoinformatics approach to understand molecular interaction between multi-epitopic regions of SARS-CoV-2 spike-protein with TLR4/MD-2 complex. Infect Genet Evol. 2020;85:104587.
14. Choudhury A, Mukherjee S. In silico studies on the comparative characterization of the interactions of SARS-CoV-2 spike glycoprotein with ACE-2 receptor homologs and human TLRs. J Med Virol. 2020;92(10):2105-13.
15. Chow JC, Young DW, Golenbock DT, Christ WJ, Gusovsky F. Toll-like receptor-4 mediates lipopolysaccharide-induced signal transduction. J Biol Chem. 1999;274(16):10689-92.
16. Visintin A, Mazzoni A, Spitzer JH, Wyllie DH, Dower SK, Segal DM. Regulation of Toll-like receptors in human monocytes and dendritic cells. J Immunol. 2001;166(1):249-55.
17. Aboudounya MM, Holt MR, Heads RJ. SARS-CoV-2 Spike S1 glycoprotein is a TLR4 agonist, upregulates ACE2 expression and induces pro-inflammatory M₁ macrophage polarisation. bioRxiv. 2021:2021.08.11.455921.
18. Shirato K, Kizaki T. SARS-CoV-2 spike protein S1 subunit induces pro-inflammatory responses via toll-like receptor 4 signaling in murine and human macrophages. Heliyon. 2021;7(2):e06187.
19. Zhao Y, Kuang M, Li J, Zhu L, Jia Z, Guo X, et al. SARS-CoV-2 spike protein interacts with and activates TLR41. Cell Res. 2021;31(7):818-20.

20. Brouwer PJM, Brinkkemper M, Maisonnasse P, Dereuddre-Bosquet N, Grobben M, Claireaux M, et al. Two-component spike nanoparticle vaccine protects macaques from SARS-CoV-2 infection. Cell. 2021;184(5):1188-200 e19.
21. Kawai T, Akira S. Toll-like receptors and their crosstalk with other innate receptors in infection and immunity. Immunity. 2011;34(5):637-50.
22. Brouwer PJM, Caniels TG, van der Straten K, Snitselaar JL, Aldon Y, Bangaru S, et al. Potent neutralizing antibodies from COVID-19 patients define multiple targets of vulnerability. Science. 2020;369(6504):643-50.
23. Bermejo-Jambrina M, Eder J, Kaptein TM, van Hamme JL, Helgers LC, Vlaming KE, et al. Infection and transmission of SARS-CoV-2 depends on heparan sulfate proteoglycans. bioRxiv. 2021:2020.08.18.255810.
24. Song X, Hu W, Yu H, Zhao L, Zhao Y, Zhao X, et al. Little to no expression of angiotensin-converting enzyme-2 on most human peripheral blood immune cells but highly expressed on tissue macrophages. Cytometry A. 2020.
25. Kagan JC, Su T, Horng T, Chow A, Akira S, Medzhitov R. TRAM couples endocytosis of Toll-like receptor 4 to the induction of interferon-beta. Nat Immunol. 2008;9(4):361-8.
26. Zheng M, Karki R, Williams EP, Yang D, Fitzpatrick E, Vogel P, et al. TLR2 senses the SARS-CoV-2 envelope protein to produce inflammatory cytokines. Nat Immunol. 2021;22(7):829-38.
27. Baharom F, Thomas S, Rankin G, Lepzien R, Pourazar J, Behndig AF, et al. Dendritic Cells and Monocytes with Distinct Inflammatory Responses Reside in Lung Mucosa of Healthy Humans. J Immunol. 2016;196(11):4498-509.
28. Baharom F, Rankin G, Blomberg A, Smed-Sorensen A. Human Lung Mononuclear Phagocytes in Health and Disease. Front Immunol. 2017;8:499.
29. Landsman L, Varol C, Jung S. Distinct differentiation potential of blood monocyte subsets in the lung. J Immunol. 2007;178(4):2000-7.
30. Osterholzer JJ, Chen GH, Olszewski MA, Curtis JL, Huffnagle GB, Toews GB. Accumulation of CD11b+ lung dendritic cells in response to fungal infection results from the CCR2-mediated recruitment and differentiation of Ly-6Chigh monocytes. J Immunol. 2009;183(12):8044-53.
31. Thorne LG, Reuschl AK, Zuliani-Alvarez L, Whelan MVX, Turner J, Noursadeghi M, et al. SARS-CoV-2 sensing by RIG-I and MDA5 links epithelial infection to macrophage inflammation. EMBO J. 2021:e107826.
32. Yang D, Geng T, Harrison AG, Wang P. Differential roles of RIG-I-like receptors in SARS-CoV-2 infection. bioRxiv. 2021.
33. Yin X, Riva L, Pu Y, Martin-Sancho L, Kanamune J, Yamamoto Y, et al. MDA5 Governs the Innate Immune Response to SARS-CoV-2 in Lung Epithelial Cells. Cell Rep. 2021;34(2):108628.
34. Campana P, Parisi V, Leosco D, Bencivenga D, Della Ragione F, Borriello A. Dendritic Cells and SARS-CoV-2 Infection: Still an Unclarified Connection. Cells. 2020;9(9).
35. Reed LJ, Muench H. A simple method of estimating fifty per cent endpoints. American journal of epidemiology. 1938;27(3):493-7.
36. Chu DKW, Pan Y, Cheng SMS, Hui KPY, Krishnan P, Liu Y, et al. Molecular Diagnosis of a Novel Coronavirus (2019-nCoV) Causing an Outbreak of Pneumonia. Clin Chem. 2020;66(4):549-55.
37. Cossarizza A, Chang HD, Radbruch A, Abrignani S, Addo R, Akdis M, et al. Guidelines for the use of flow cytometry and cell sorting in immunological studies (third edition). Eur J Immunol. 2021;51(12):2708-3145.

SUPPLEMENTAL INFORMATION

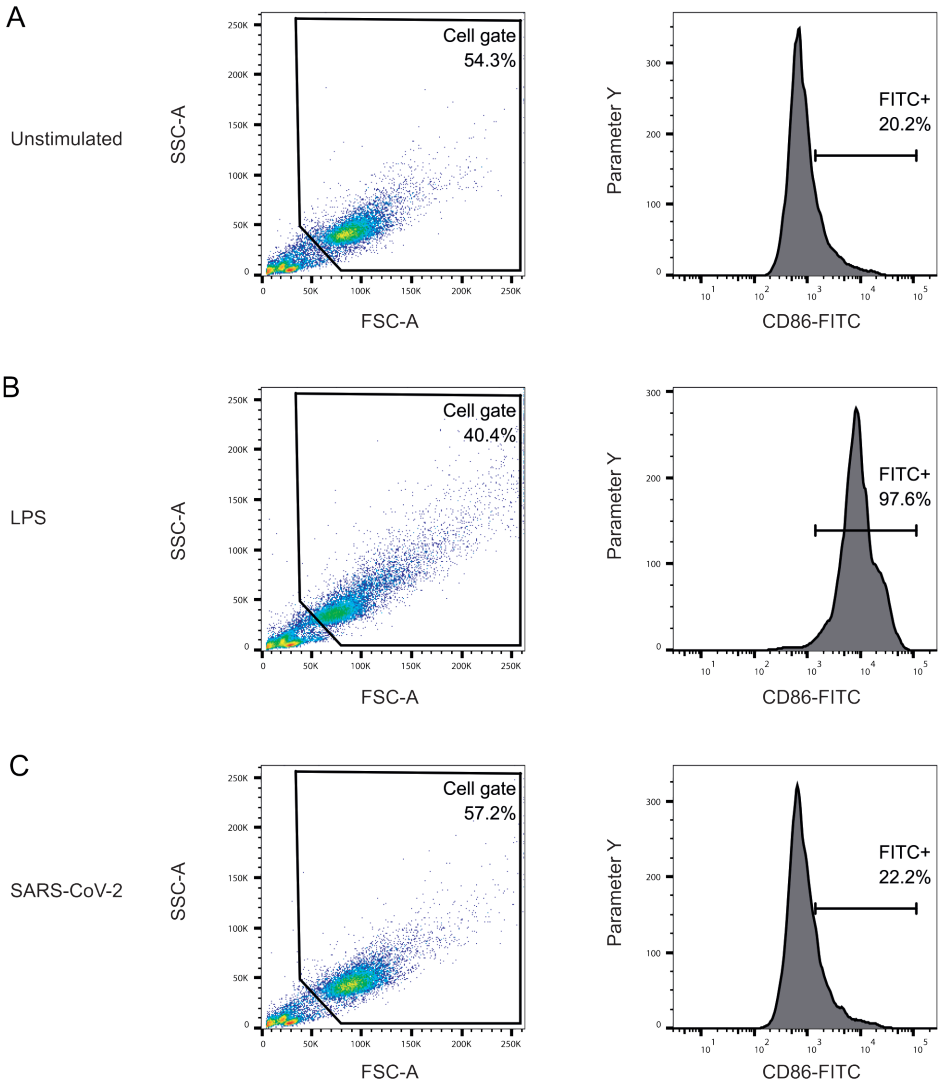

Supplemental Figure 1: Dendritic cell gating strategy.

After exposure to different stimuli, dendritic cells were harvested, fixed, and stained with antibodies against various markers and analyzed by flow cytometry. (A-C) Representative flow cytometry plots of one donor stimulated with medium (A), LPS (B), or SARS-CoV-2 (C). The percentage of selected cells is depicted in the upper right corner of the dot plot, and the expression of CD86 was plotted in a histogram. Histograms show the percentages of CD86-FITC-positive cells.

CHAPTER 3

ANTIBODIES AGAINST SARS-COV-2 CONTROL COMPLEMENT-INDUCED INFLAMMATORY RESPONSES TO SARS-COV-2

Marta Bermejo-Jambrina[1,2,3], Lieve E.H. van der Donk[1,2], John L. van Hamme[1,2], Doris Wilflingseder[3], Godelieve de Bree[5,2], Maria Prins[5,6] Menno de Jong[4], Pythia Nieuwkerk[7,6,2], Marit J. van Gils[4], Neeltje A. Kootstra[1,2], Teunis B.H. Geijtenbeek[1,2]*

[1] Amsterdam UMC location University of Amsterdam, Department of Experimental Immunology, Meibergdreef 9, Amsterdam, The Netherlands.
[2] Amsterdam institute for Infection and Immunity, Amsterdam, The Netherlands.
[3] Institute of Hygiene and Medical Microbiology, Medical University of Innsbruck, Innsbruck, Austria
[4] Amsterdam UMC location University of Amsterdam, Department of Medical Microbiology and Infection Prevention, Meibergdreef 9, Amsterdam, The Netherlands
[5] Department of Internal Medicine, Amsterdam UMC location AMC, University of Amsterdam, Amsterdam, The Netherlands.
[6] Department of Infectious Diseases, Public Health Service of Amsterdam, GGD, Amsterdam, the Netherlands.
[7] Department of Medical Psychology (J3-2019-1), Amsterdam UMC location AMC University of Amsterdam, Amsterdam, The Netherlands.

* Address correspondence and reprint requests to T.B.H. Geijtenbeek, Amsterdam UMC, Meibergdreef 9, 1105 AZ, Amsterdam.

Manuscript submitted

ABSTRACT

Dysregulated immune responses contribute to pathogenesis of COVID-19 leading to uncontrolled and exaggerated inflammation observed during severe COVID-19. However, it remains unclear how immunity to SARS-CoV-2 is induced and subsequently controlled. Notably, here we have uncovered an important role for complement in the induction of innate and adaptive immunity to SARS-CoV-2. Complement rapidly opsonized SARS-CoV-2 via the lectin pathway. Complement-opsonized SARS-CoV-2 efficiently interacted with dendritic cells (DCs), inducing type I IFN and proinflammatory cytokine responses, which were inhibited by antibodies against the complement receptors (CR)3 and CR4. These data suggest that complement is important in inducing immunity via DCs in the acute phase against SARS-CoV-2. Strikingly, serum from COVID-19 patients as well as monoclonal antibodies against SARS-CoV-2 attenuated innate and adaptive immunity induced by complement-opsonized SARS-CoV-2. Blocking the FcγRII, CD32, restored complement-induced immunity. These data strongly suggest that complement opsonization of SARS-CoV-2 is important for inducing innate and adaptive immunity to SARS-CoV-2. Subsequent induction of antibody responses is important to limit the immune responses and restore immune homeostasis. These data suggest that dysregulation in complement and FcγRII signaling might underlie mechanisms causing severe COVID-19.

Keywords: SARS-CoV-2, dendritic cells, complement, antibodies

INTRODUCTION

Since severe acute respiratory syndrome coronavirus 2 (SARS-CoV-2) was first identified in Wuhan, China, in December of 2019 (1, 2) the virus has spread all over the world, causing a respiratory disease, termed coronavirus disease 2019 (COVID-19) (3). To date COVID-19 pathogenesis is still unclear. Asymptomatic patients and patients with mild COVID-19 gain control of infection within a couple of days most likely via innate immune responses as effective adaptive immune responses are expected to be elicited after 2 weeks in naïve individuals (4, 5). Failure of antiviral innate responses to control infection might lead to uncontrolled viral replication in the airways eliciting an inflammatory cascade observed in severe COVID-19 cases (6, 7). Severe to fatal outcomes in COVID-19 patients have been attributed to the dysfunction of innate and adaptive immune responses against SARS-CoV-2 (8). These aberrant or uncontrolled innate and/or adaptive immune responses lead to delayed viral clearance, inflammation and tissue damage, affecting organs (8-10). It remains however unclear how the interplay of innate immune responses with adaptive immunity controls infection and how homeostasis is achieved after infection to prevent aberrant systemic inflammatory responses observed in severe COVID-19 disease.

The complement system constitutes an important innate immune response and acts as a first line of defense against viruses and might have a critical role in COVID-19 pathogenesis (11-14). Complement activation limits SARS-CoV-2 infection but uncontrolled activity can lead to aberrant inflammatory responses observed during severe COVID-19 (11, 15, 16). SARS-CoV-2 infection can activate complement by direct interaction of Spike (S) proteins with the lectin pathway via mannose-binding lectin (MBL) (17-20). Interestingly, SARS-CoV-2-specific antibodies binding to S protein also activate complement by the classical pathway through C1q (21, 22). Moreover, the alternative pathway is triggered by SARS-CoV-2 S protein by binding to cell surface heparan sulfates (23, 24). Severe COVID-19 patients have high circulating C5a in their blood as well as high levels of processed C3 (16, 25), suggesting that uncontrolled complement activation might be involved in severity of COVID-19 (11, 26). These studies suggest that although the complement system is vital in limiting SARS-CoV-2 infection, dysregulation or lack of control of complement activation leads to severe pathogenesis (14, 26-28). Mechanisms underlying complement-induced immunity and subsequent return to homeostasis after complement activation remain unclear.

Activation of mucosal dendritic cells (DCs) is a crucial step in the induction of effective innate and adaptive immune responses against invading viruses (29). Notably, SARS-CoV-2 infection does not lead to strong DC activation (30-32). Exposure of DCs to

SARS-CoV-2 neither leads to infection nor production of type I IFN and cytokine responses (33). Although infection of bystander cells with SARS-CoV-2 can lead to DC activation (30, 34, 35), it is unclear whether complement deposition on SARS-CoV-2 can induce DC activation.

Here we investigated the role of complement in induction of immunity and how the inflammatory responses are controlled to prevent aberrant inflammation. Complement-opsonized SARS-CoV-2 induced DC maturation and efficient type-I IFN responses via complement receptors CR3/CD11b and CR4/CD11c. Moreover, complement-opsonized SARS-CoV-2 induced proinflammatory cytokines as well as IL-1b by caspase-1 inflammasome activation. Notably, serum from COVID-19 patients or anti-SARS-CoV-2 antibodies abrogated complement-induced DC activation and subsequent type I IFN and cytokine responses via CD32 activation. These data strongly suggest that complement is important in induction of innate and adaptive immunity but that antibody responses either elicited after infection or vaccination suppress complement-induced immunity and restore homeostasis. These data strongly suggest that antibodies against SARS-CoV-2 might be important in switching off complement-induced immunity and could be used to treat patients suffering from severe COVID-19 (36-39).

MATERIALS AND METHODS

Ethics statement

This study was performed according to the Amsterdam University Medical Centers, location Academic Medical Center (AMC) and human material was obtained in accordance with the AMC Medical Ethics Review Committee (Institutional Review Committee) following the Medical Ethics Committee guidelines. This study, including the tissue harvesting procedures, was consent by all donors and conducted in accordance with the ethical principles set out in the declaration of Helsinki and was approved by the institutional review board of the Amsterdam University Medical Centers and the Ethics Advisory Body of the Sanquin Blood Supply Foundation (Amsterdam, Netherlands). All research was performed in accordance with appropriate guidelines and regulations.

Patient consent

To enable comparison between complement and antibody response following infection, we included serum collected in the RECoVERED cohort (40). In total 10 RECoVERED serum samples from participants who experienced mild (5x) or severe

(5x) COVID-19 were included. Written informed consent was obtained from each study participant. The study design was approved by the local ethics committee of the Amsterdam UMC (Medisch Ethische Toetsingscommissie [METC]; NL73759.018.20). All samples were handled anonymously.

Patient serum

We have used three different types of sera. Firstly, pre-COVID-19 pandemic normal human serum (NHS) was generated from a pool of 10 healthy individuals and was stored at -80˚C until use. This serum contains complement components, but does not contain anti-SARS-CoV-2 antibodies. This serum was used to generate the C-opsonized SARS-CoV-2 condition. Secondly, pooled serum from at least 20 random individuals (mild/moderate disease) all infected in 2020 (Wuhan variant, no vaccination), collected 19 days post-symptom onset with high neutralizing antibody content, was heat inactivated (1 hour at 56˚C) to destroy complement activity and obtain antibody serum. In brief, SARS-CoV-2 isolate (hCoV-19/Italy-WT, 1000TCID/mL) was incubated for 1 hour at 37˚C with high neutralizing antibody pooled serum in a 1:10 ratio, to generate antibody(Ab)-opsonized SARS-CoV-2. This serum was used for Figure 4 in combination with pre-COVID-19 pandemic NHS to generate the Ab/C-opsonized SARS-CoV-2 condition. To generate Ab/C-opsonized SARS-CoV-2, both pre-COVID-19 pandemic NHS and antibody sera were added simultaneously to mimic physiological circumstances. Lastly, serum from 10 COVID-19 patients after natural infection with either mild (5x) or severe (5x) disease outcome, collected approximately 3 months post-infection, was used in a 1:10 ratio as antibody mediated-complement opsonization source to generate complement- and antibody-opsonized SARS-CoV-2. These sera were not heat-inactivated to maintain the original complement and antibody composition of the sera. These sera were used separately for Figure 6A, and pooled for Figure 6B-D. When used alone, this condition was labeled sera-opsonized SARS-CoV-2; when supplemented with pre-COVID-19 pandemic NHS this condition was labeled Ab/C-opsonized SARS-CoV-2. As mentioned above, in the conditions where patient serum was supplemented with pre-COVID-19 pandemic NHS, this was done simultaneously (so not sequential) and incubated together with virus. The ability to opsonize the virions was assessed by ELISA, as previously described (48, 49).

Reagents and antibodies

The following antibodies were used (all anti-human): CD86 (2331 (FUN-1), BD Pharmingen), CD80 (L307.4, BD Pharmingen), PE-conjugated mouse IgG1 CR3/CD11b (101208, Biolegend), LEAF purified CR3/CD11b mouse IgG1, LEAF purified CR4/CD11c mouse IgG1, CR3/CD11b (M1/70), CR4/CD11c (S-HCL-3), CD32 (FUN-2), DC-SIGN (FAB161F, R&D systems), CD16, CD32, CD64 (all BD Pharmingen) and, viability dye

(Ghost DyeTM Violet 510, Tonbo Biosciences, San Diego, USA). For extracellular staining, cells were incubated in 0.5% PBS-BSA (Sigma-Aldrich) containing antibodies for 30 minutes at 4˚C. Single cell measurements were performed on a Canto flow cytometer II (BD Biosciences) and data was analyzed using FlowJo V10.8.1 (Software by TreeStar).
Neutralizing COVA1-18 and non-neutralizing COVA1-27 antibodies were isolated from participants in the "COVID-19 Specific Antibodies" (COSCA) study and were generated by Karlijn van der Straten as described previously (41). These isolated antibodies were used at 10 µg/mL and were supplemented with pre-COVID-19 pandemic NHS (1:10) and simultaneously incubated with SARS-CoV-2 (hCoV-19/Italy-WT, 1000TCID/mL) to generate the Ab/C-opsonized SARS-CoV-2 condition for Figure 5.

Cell lines

The simian kidney cell line VeroE6 (ATCC® CRL-1586™) were cultured in CO_2 independent medium (Gibco life Technologies, Gaithersburg, Md.) supplemented with 10% fetal calf serum (FCS), L-glutamine and penicillin/streptomycin (10µg/mL). Cultures were maintained at 37˚C without CO_2. The human embryonic kidney 293T/17cells (ATCC, CRL-11268) were maintained in Dulbecco's modified Eagle's medium (Gibco Life Technologies) containing 10%FCS, L-glutamine, and penicillin/streptomycin (10µg/mL).

DC generation

Human $CD14^+$ monocytes were isolated from the blood of healthy volunteer donors (Sanquin blood bank) and subsequently differentiated into monocyte-derived DCs. In short, the isolation from buffy coats was performed by density gradient centrifugation on Lymphoprep (Nycomed) and Percoll (Pharmacia). After Percoll separation, the isolated $CD14^+$ monocytes were differentiated into monocyte-derived DCs within 5 days and cultured in RPMI 1640 medium (Gibco Life Technologies, Gaithersburg, Md.) containing 10% FCS, penicillin/streptomycin (10 µg/mL) and supplemented with the cytokines IL-4 (500 U/mL) and GMCSF (800 U/mL) (both Gibco) (42). After 4 days of differentiation, DCs were seeded at 1×10^6/mL in a 96-well plate (Greiner), and after 2 days of recovery, DCs were stimulated or infected as described below. This study was performed in accordance with the ethical principles set out in the Declaration of Helsinki and was approved by the institutional review board of the Amsterdam University Medical Centers, location AMC Medical Ethics Committee and the Ethics Advisory Body of Sanquin Blood Supply Foundation (Amsterdam, Netherlands).

SARS-CoV-2 pseudovirus production

For production of single-round infection viruses, human embryonic kidney 293T/17 cells (ATCC, CRL-11268) were co-transfected with an adjusted HIV backbone plasmid (pNL4-3.Luc.R-S-) containing previously described stabilizing mutations in the capsid protein (PMID: 12547912) (43) and firefly luciferase in the *nef* open reading frame (1.35ug) and pSARS-CoV-2 expressing SARS-CoV-2 S protein (0.6ug) (GenBank; MN908947.3), a gift from Paul Bieniasz (41, 44). Transfection was performed in 293T/17 cells using genejuice (Novagen, USA) transfection kit according to manufacturer's protocol. At day 3 or day 4, pseudotyped SARS-CoV-2 virus particles were harvested and filtered over a 0.45 µm nitrocellulose membrane (Sartorius Stedim, Gottingen, Germany). SARS-CoV-2 pseudovirus productions were quantified by RETRO-TEK HIV-1 p24 ELISA according to manufacturer instructions (ZeptoMetrix Corporation).

SARS-CoV-2 isolate (hCoV-19/Italy-WT)

The wild-type (WT) authentic SARS-CoV-2 virus hCoV-19/WT (D614G variant) was obtained from Dr. Maria R. Capobianchi through BEI Resources, NIAID, NIH: SARS-Related Coronavirus 2, Isolate Italy-INMI1, NR-52284, originally isolated on January 2020 in Rome, Italy. SARS-CoV-2 authentic virus stocks from primary isolates were generated in VeroE6 cells. Cytopathic effect (CPE) formation was monitored and after 48 hours the virus supernatant was harvested. Viral titers were determined by tissue cultured infectious dose (TCID50) on VeroE6 cells. Briefly, VeroE6 cells were seeded in a 96 well-plate at a cell density of 10000 cells/well. The following day, cells were inoculated with a 5-fold serial dilution of SARS-CoV-2 isolate in quadruplicate. Cell cytotoxicity was measured by using an MTT assay 48 hours post infection. Loss of MTT staining, analyzed by spectrometer (OD_{580nm}) was indicative of SARS-CoV-2 induced CPE. Viral titer was determined as TCID50/mL and calculated based on the method first proposed by Reed & Muench (45). All experiments with the WT SARS-CoV-2 isolate (hCoV-19/Italy-WT) were performed in a BSL-3 laboratory, following appropriate safety and security protocols approved by the Amsterdam UMC BioSafetyGroup and performed under the environmental license obtained from the municipality of Amsterdam.

SARS-CoV-2 (hCoV-19/Italy-WT) neutralization assay

Antibody neutralization activity of SARS-CoV-2 infection was tested as previously described (46), including some modifications. In brief, VeroE6 cells were seeded at a density of 10,000 cells/well in a 96-well plate one day prior to the start of the neutralization assay. Heat-inactivated serum samples were serially diluted in CO_2-independent cell culture medium (Gibco life Technologies, Gaithersburg, Md.) supplemented with 10% fetal calf serum (FCS), L-glutamine and penicillin/

streptomycin (10µg/mL), mixed 1:1 ratio with authentic SARS-CoV-2 and incubated for 1 hour at 37˚C. Subsequently, these mixtures were added to the cells in a 1:1 ratio and incubated for 48 hours at 37˚C without CO_2, followed by an MTT assay. Loss of MTT staining, analyzed by spectrometer (OD_{580nm}) was indicative of SARS-CoV-2 induced CPE. The neutralization titers (IC50) were determined as the serum dilution or antibody concentration at which infectivity was inhibited by 50%, respectively, using a non-linear regression curve fit (GraphPad Prism software version 8.3) and serum dilutions were converted into international units per mL (IU/mL) using the WHO International Standard for anti-SARS-CoV-2 immunoglobulin (NIBSC 20/136).

Opsonization assay of SARS-CoV-2 pseudovirus and hCoV-19/Italy-WT

Incubation of SARS-CoV-2 with pre-COVID-19 pandemic NHS mediated covalent deposition of C3 fragments (C3b, iC3b,C3d, C3c) and specific IgGs on the viral surfaces. To mimic the *in vivo* situation (22), where SARS-CoV-2 is opsonized with complement or IgGs, SARS-CoV-2 pseudovirus (191.05 ng/mL of SARS-CoV-2 pseudovirus) and authentic SARS-CoV-2 (hCoV-19/Italy-WT, 1000TCID/mL) were incubated for 1 hour at 37˚C with pre-COVID-19 pandemic NHS (1:10 ratio), as complement source to obtain complement-opsonized SARS-CoV-2 (C-opsonized SARS-CoV-2); or with sera from mild/severe COVID-19 patients (containing complement and specific IgGs) in a 1:10 ratio, similar as done previously (47). As negative control, the virus was incubated under the same conditions with plain RPMI1640. The presence of C3 fragments and IgGs on the viral surface was detected by opsonization ELISA assay, also called Viral Capture Assay (VCA) as previously described (48-50). Briefly, 96-well plates were coated with rabbit anti-mouse IgG (DAKO) at 4ºC overnight. ELISA plates were coated with anti-human C3c and C3d as well as human IgG and incubated overnight with differentially opsonized virus preparations (1ng/p24 per well) at 4˚C and extensively washed with RPMI1640 medium to remove unbound virus. Mouse IgG antibodies were used as control for background binding. For the SARS-CoV-2 pseudovirus, viral samples were lysed (1% Triton) and binding was quantified by p24 ELISA to confirm the opsonization pattern (51). The opsonization pattern of SARS-CoV-2 isolate (hCoV-19/Italy-WT) was determined by qPCR. The viral samples were lysed, and SARS-CoV-2 RNA was extracted using FavorPrep Viral RNA Minikit (FAVORGEN, Ping-Tung, Taiwan), according to the manufacturer's instructions. Sequences specific to region N1 of the Nucleocapsid gene published on the CDC website (https://www.cdc.gov/coronavirus/2019-ncov/lab/rt-pcr-panel-primer-probes.html) were used. Luna Universal Probe One-Step RT-PCR kit (New England BioLabs, Ipswich, Mass) was used for target amplification, and runs were performed on the CFX96 real-time detection system (Bio-Rad). For absolute quantification using the standard curve method, SARS-CoV-2 RNA was obtained as a PCR standard control from the National Institute for Biological Standards and Control UK (Ridge, UK).

Virus binding and internalization

In order to determine SARS-CoV-2 binding and internalization, target cells were seeded in a 96-well plate at a density of 100,000 cells in 100µl. Cells were exposed to SARS-CoV-2 isolate (hCoV-19/Italy-WT, 1000TCID/mL) for 4 hours at 4˚C for binding as well as 4 hours at 37˚C for internalization. After 4 hour incubation, cells were washed extensively to remove the unbound virus. Cells were lysed with AVL buffer and RNA was isolated with the QIAmp Viral RNA Mini Kit (Qiagen) according to the manufacturer's protocol.

DC stimulation and infection

DCs were left unstimulated or stimulated with 10ng/mL LPS from *Salmonella typhosa* (Sigma) and SARS-CoV-2 isolate (hCoV-19/Italy-WT) with different opsonization patterns, including SARS-CoV-2, C-opsonized SARS-CoV-2, Ab-opsonized SARS-CoV-2 and Ab/C-opsonized SARS-CoV-2 at 1000TCID/mL. Blocking of CR3/CD11b (LEAF-purified CR3/CD11b) and CR4/CD11c (LEAF-purified CR4/CD11c) was performed with 10µg/mL for 30 minutes at 37˚C before adding the virus preparations. Similarly, for blocking of FcγRII, DCs were treated with anti-CD32 antibody 1µg/mL for 1 hour at 37˚C. DCs do not express ACE2 and are therefore not infected by SARS-CoV-2 (33). Therefore, viral stimulation SARS-CoV-2 isolate (hCoV-19/Italy-WT) at 1000TCID/mL (MOI 0.028) was performed for 2, 6, and 8 hours (not shown) after which the cells were lysed for RNA isolation and cytokine production analysis. In addition, cells were stimulated for 24 hours and fixed for 30 minutes with 4% paraformaldehyde to assess the maturation phenotype with flow cytometry.

Caspase-1 activity

Active caspase-1 was detected using the FAM-FLICA Caspase-1 Assay kit (Immunochemistry Technologies) according to manufacturer's instructions. In brief, DCs were washed in IMDM medium lacking phenol red (Gibco), supplemented with 10% FCS, penicillin and streptomycin (100 U/mL and 100 µg/mL, respectively, ThermoFisher) prior to stimulations. After 14 hours, DCs were treated with FAM FLICA reagent and incubated at 37ºC, 5% CO_2 for 1 hour. Cells were washed three times in apoptotic wash buffer (Immunochemistry Technologies), immediately followed by flow cytometry analysis using the FACS Canto II (BD Bioscience) and FlowJo software version 10.7 and guidelines for the use of flow cytometry and cell sorting in immunological studies were followed. Live cells were gated based on FSC/SSC and the caspase-1$^+$ (FAM-FLICA) population within this live cell population was assessed.

RNA isolation and quantitative real-time PCR

Cells incubated with SARS-CoV-2 isolate (hCoV-19/Italy-WT) were lysed with AVL buffer and RNA was isolated with QIAmp Viral RNA Mini Kit (Qiagen) according to the manufacturer's protocol. cDNA was synthesized with M-MLV reverse transcriptase Kit (Promega) and diluted 1/5 before further application. PCR amplification was performed by using RT-PCR in the presence of SYBR green in a 7500 Fast Realtime PCR System (ABI). Specific primers were designed with Primer Express 2.0 (Applied Biosystems). The following primer sequences were used:

GAPDH: F-primer 5′-CCATGTTCGTCATGGGTGTG-3′, R-primer 5′-GGTGCTAA GCAGTTG-GTGGTG-3′; SARS-CoV-2 ORF1b: F-primer 5′-TGGGGTTTTACAGGTAACCT-3′, R-primer 5′-AACACGCTTAACAAAGCACTC-3′; IFNB: F-primer 5′-ACAGACTTACAGGTTACCTC-CGAAAC-3′, R-primer 5′-CATCTGCTGGTTGAAGAATGCTT-3′; CXCL10: F-primer 5′-CGCTGTACCTGCATCAGCAT-3′; R-primer 5′-CATCTCTTCTCACCCTTCTTTTTCA-3′ ; IL-6: F-primer 5′-TGCAATAACCACCCCTGACC-3′, R-primer 5′-TGCGCAGAATGAGAT-GAGTTG-3′; IL-10: F-primer 5′-GAGGCTACGGCGCTGTCAT-3′, R-primer 5′-CCACGG-CCTTGCTCTTGTT-3′; IL-12p35: F-primer 5′-TGGACCACCTCAGTTTGGC-3′; R-primer 5′-TTCCTGGGTCTGGAGTGGC-3′.

The normalized amount of target mRNA was calculated from the Ct values obtained for both target and household mRNA with the equation $Nt = {}^{2Ct\ (GAPDH)\ -\ Ct(target)}$.

ELISA

Cell supernatants were harvested after 24 hours of stimulation and secretion of IL-1β was measured by ELISA (eBiosciences) according to the manufacturer's instructions. Supernatant containing SARS-CoV-2 was inactivated with 1% triton before performing the ELISA. OD_{450nm} values were measured using BioTek Synergy HT.

Statistics

All results are presented as mean ± SEM and were analyzed by GraphPad Prism 9 software (GraphPad Software Inc.). A two-tailed, parametric Student's *t*-test for paired observations (differences within the same donor) or unpaired observation, Mann-Whitney tests (differences between different donors that were not normally distributed) was performed. For unpaired, non-parametric observations a one-way ANOVA or two-way ANOVA test with post hoc analysis (Tukey's or Dunnett's) were performed. Statistical significance was set at *P< 0.05, **P<0.01***P<0.001****P<0.0001.

RESULTS

Complement-opsonized SARS-CoV-2 (hCoV-19/Italy-WT) activates dendritic cells via CR3/CD11b and CR4/CD11c

DCs neither become infected nor activated by SARS-CoV-2 (hCoV-19/Italy-WT) (33, 52). Here we investigated whether complement-opsonized SARS-CoV-2 interacts with DCs. Incubation of pseudotyped SARS-CoV-2 and SARS-CoV-2 isolate (hCoV-19/Italy-WT) with pre-COVID-19 pandemic normal human serum (NHS), which contains complement but no virus-specific antibodies, led to efficient opsonization of SARS-CoV-2 as observed by detection of C3c and C3d, but as expected IgGs were not found on the virus surface. This was determined by ELISA for complement proteins and antibodies (49, 51) and qPCR (Figure 1A, Supplemental Figure 1A). Notably, complement-opsonized SARS-CoV-2 isolate (hCoV-19/Italy-WT) bound more strongly to DCs than non-opsonized SARS-CoV-2 (Figure 1B). Blocking antibodies against the α-chain of complement receptors CR3/CD11b and CR4/CD11c abrogated complement-opsonized SARS-CoV-2 binding to DCs.
We next investigated induction of DC maturation by complement-opsonized SARS-CoV-2 isolate (hCoV-19/Italy-WT) by analyzing expression of co-stimulatory molecules CD80 and CD86, DC-SIGN, and complement receptors CR3/CD11b and CR4/CD11c. In contrast to SARS-CoV-2, complement-opsonized SARS-CoV-2 induced significant expression of CD80 (Figure 1C, F) and CD86 (Figure 1D, G) to similar levels as observed for LPS. Upregulation of CD80 and CD86 was abrogated by blocking antibodies against CR3/CD11b and CR4/CD11c alone or in combination (Figure 1C, D). DC-SIGN expression was reduced by complement-opsonized SARS-CoV-2 (Figure 1E, H), similar as observed for LPS, and expression was restored in presence of blocking antibodies against CR3/CD11b and/or CR4/CD11c (Figure 1E). These results strongly suggest that complement-opsonization enhances SARS-CoV-2 capture by DCs and induces DC maturation via CR3 and CR4 in contrast to non-opsonized SARS-CoV-2.

Complement-opsonized SARS-CoV-2 (hCoV-19/Italy-WT) induces type I IFN and cytokine responses

Next, we investigated whether complement-opsonized SARS-CoV-2 isolate (hCoV-19/Italy-WT) induces antiviral type I interferon (IFN) as well as cytokine responses. Notably, in contrast to non-opsonized SARS-CoV-2, complement-opsonized SARS-CoV-2 isolate (hCoV-19/Italy-WT) induced significantly higher mRNA levels of IFN-β as well as IFN-stimulated genes (ISGs) APOBEC3G, IRF7 and CXCL10 (Figure 2A-D). Blocking antibodies against CR3/CD11b and CR4/CD11c abrogated the induction of IFN-β and ISGs to similar levels as observed with SARS-CoV-2 alone (Figure 2A-D). These data strongly suggest that, in contrast to its non-opsonized counterpart, complement-opsonized SARS-CoV-2 induces antiviral type I IFN responses via CR3 and CR4.

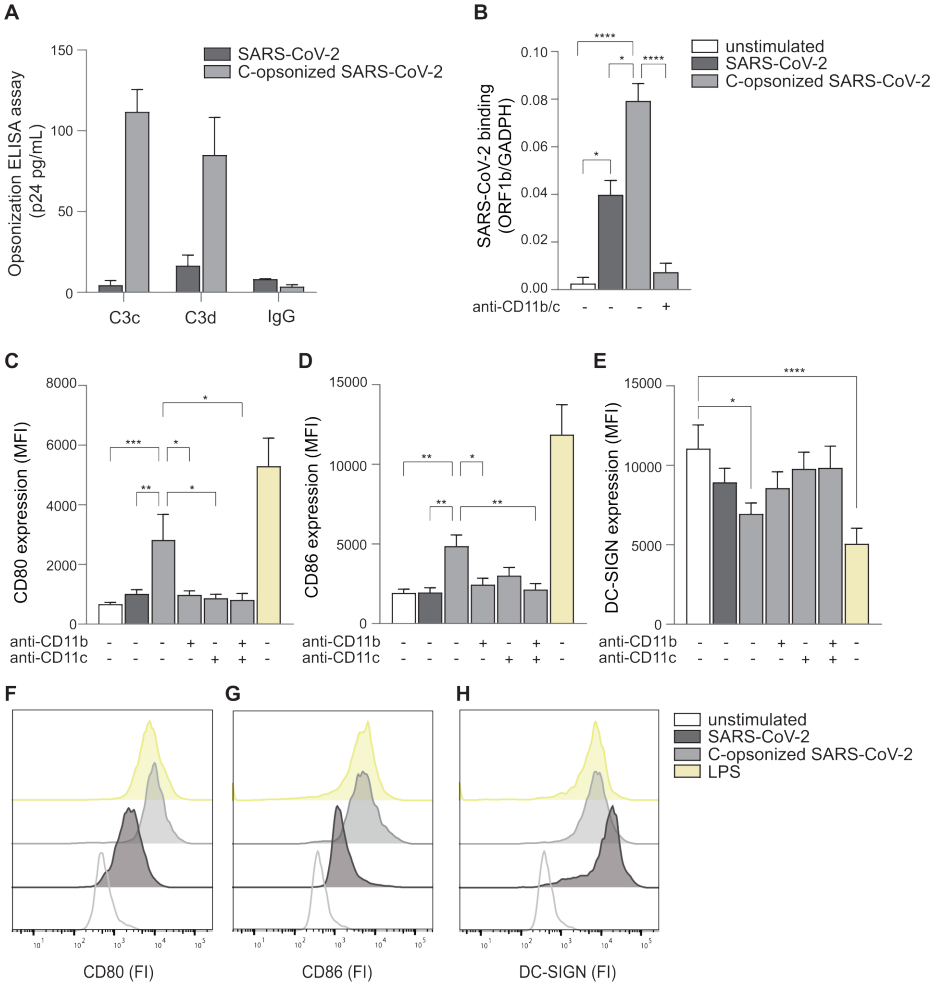

Figure 1: Complement-opsonized SARS-CoV-2 activates DCs via CD11b and CD11c.

(A) SARS-CoV-2 pseudovirus was incubated with pre-COVID-19 pandemic NHS and opsonization by C3c and C3d was determined by ELISA (p24 pg/mL) (n=3). (B) Human monocyte-derived DCs were exposed to SARS-CoV-2 isolate (hCoV-19/Italy-WT, 1000TCID/mL) and C-opsonized SARS-CoV-2 (hCoV-19/Italy-WT, 1000TCID/mL; opsonized with pre-COVID-19 pandemic NHS) for 4 hours in presence or absence of antibodies against CD11b and CD11c. Virus binding was determined by quantitative real-time PCR (n=6 donors). (C-E) DCs were exposed to SARS-CoV-2 or C-opsonized SARS-CoV-2 for 24 hours and expression of CD80, CD86 and DC-SIGN was determined by flow cytometry (n=12 donors). LPS stimulation was used as positive control. (F-H) Representative histograms of CD80 (F), CD86 (G) and DC-SIGN (H) expression. Data show the mean values and error bars are the SEM. Statistical analysis was performed using (B) ordinary one-way ANOVA with Tukey multiple-comparison test; *p ≤ 0.05, ****p ≤ 0.0001(n=6 donors); (C-E) 2-way ANOVA with Tukey multiple-comparison test; *p ≤ 0.05, **p ≤ 0.01, ***p ≤ 0.001, ****p ≤ 0.0001 (n=12 donors). C-opsonized = complement-opsonized.

Moreover, complement-opsonized SARS-CoV-2 induced transcription of cytokines IL-6, IL-10 and IL-12p35, and expression was abrogated by blocking CR3/CD11b and CR4/CD11c (Figure 2E-G). Secretion of biologically active IL-1β is tightly regulated and depends on induction of pro-IL1β and caspase-dependent processing into IL-1β, which is subsequently secreted by DCs (53-55). Notably, complement-opsonized SARS-CoV-2 induced secretion of IL-1β protein in contrast to non-opsonized SARS-CoV-2, and IL-1β production was inhibited by antibodies against CR3/CD11b and CR4/CD11c (Figure 3A). As caspase-1 is an important caspase involved in pro-IL-1β processing, we investigated whether complement-opsonized SARS-CoV-2 activates caspase-1 using the FAM FLICA assay. Complement-opsonized SARS-CoV-2 significantly increased active caspase-1 in DCs, similar as observed for LPS- and ATP-stimulated DCs (Figure 3B; Supplemental Figure 1D). Caspase-1 activation by complement-opsonized SARS-CoV-2 was blocked by antibodies against CR3/CD11b and CR4/CD11c. Non-opsonized SARS-CoV-2 did not induce caspase-1 activation.

Next, we investigated whether the lectin pathway was involved in complement activation by SARS-CoV-2. Pre-treatment of pre-COVID-19 pandemic NHS with mannan, which acts as an inhibitor of the lectin pathway via MBL (56), significantly decreased DC-induced type I IFN and IL-6 responses (Figure 3C-E), indicating that SARS-CoV-2 activates complement by the lectin pathway through the carbohydrate-recognition domain. Together these data strongly suggest that complement-opsonization of SARS-CoV-2 by MBL induces a potent proinflammatory as well as an antiviral type I IFN response in DCs via CR3 and CR4.

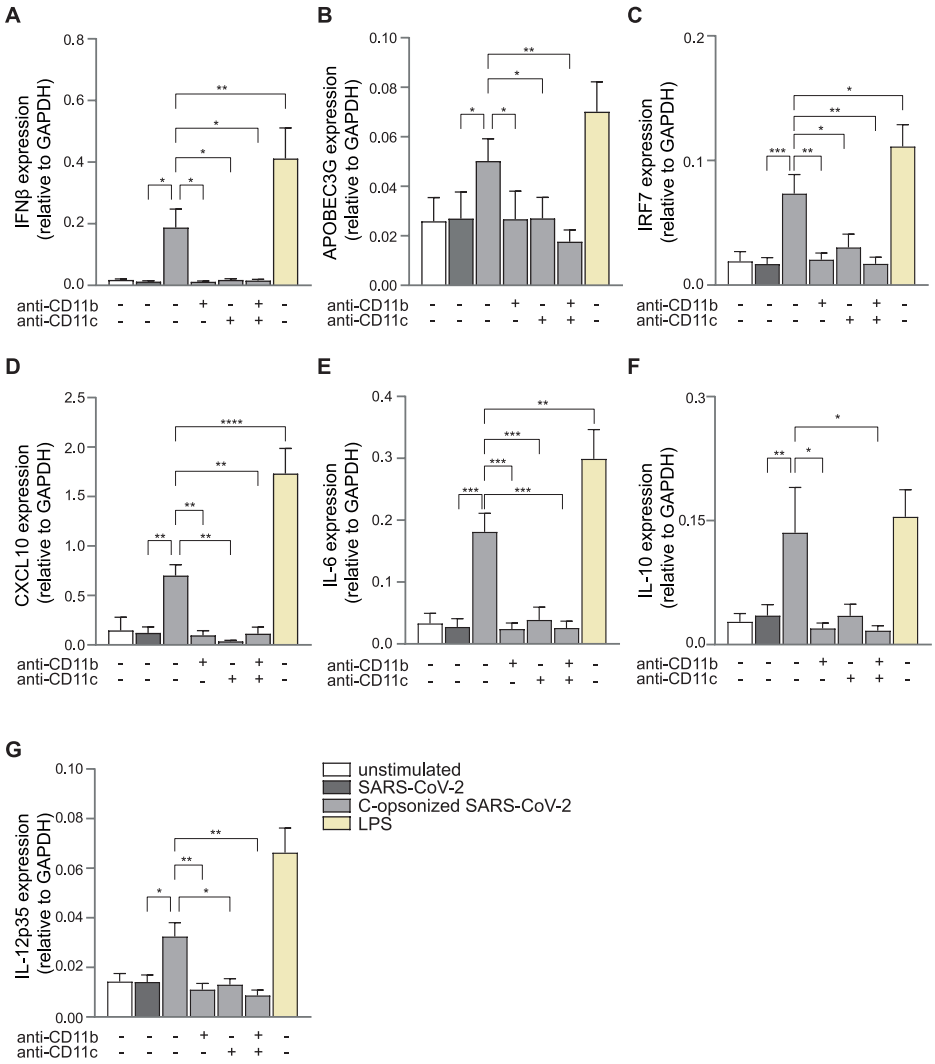

Figure 2: Complement-opsonized SARS-CoV-2 induces type I IFN and cytokine responses.

(A-G) Human monocyte-derived DCs were exposed to SARS-CoV-2 isolate (hCoV-19/Italy-WT, 1000TCID/mL), C-opsonized SARS-CoV-2 (hCoV-19/Italy-WT, 1000TCID/mL; opsonized with pre-COVID-19 pandemic NHS) and LPS (10 ng/mL) in presence or absence of antibodies against CD11b and CD11c for 2 and 6 hours. mRNA levels of IFN-β (A), APOBEC3G (B), IRF7 (C), CXCL10 (D), IL-6 (E), IL-10 (F) and IL-12p35 (G) were determined with qPCR after 2 hours (A) and after 6 hours (B-G) (n=14 donors). Data show the mean values and error bars are the SEM. Statistical analysis was performed using (A-F) 2-way ANOVA with Dunnett's multiple-comparison test; *p ≤ 0.05, **p ≤ 0.01, ***p ≤ 0.001, ****p ≤ 0.0001 (n=14 donors). C-opsonized = complement opsonized.

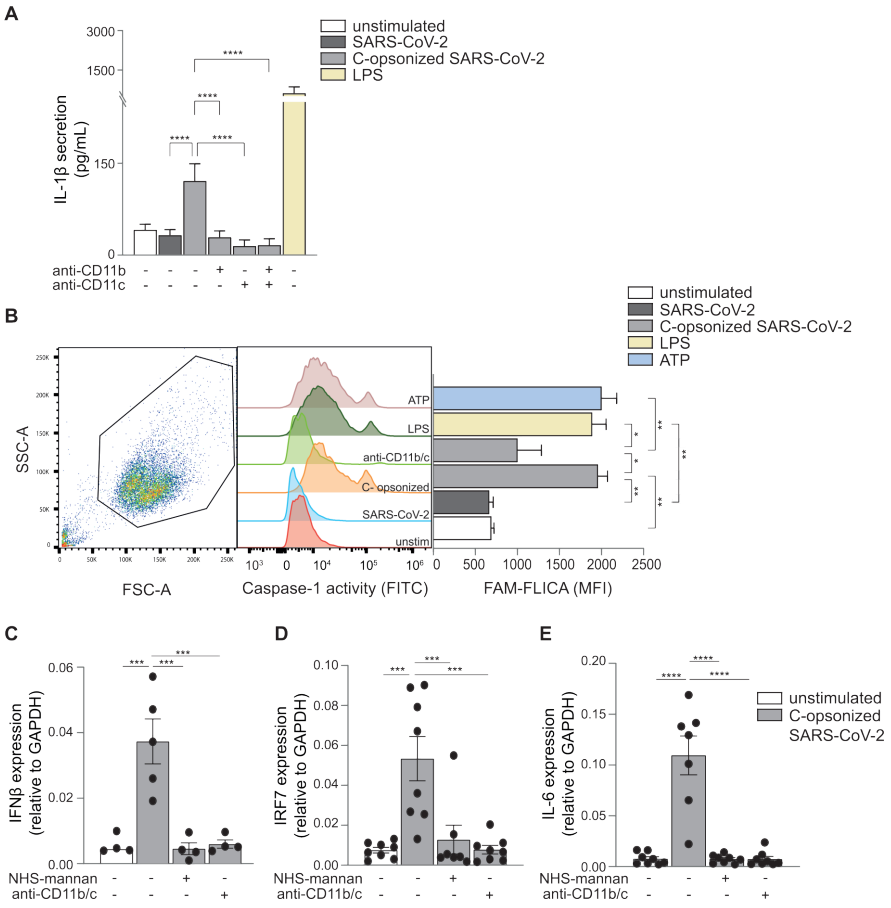

Figure 3: Caspase-1 activity is enhanced by activated DCs by complement-opsonized SARS-CoV-2.

(A) Human monocyte-derived DCs were exposed to SARS-CoV-2 isolate (hCoV-19/Italy-WT, 1000TCID/mL), C-opsonized SARS-CoV-2 (hCoV-19/Italy-WT, 1000TCID/mL; opsonized with pre-COVID-19 pandemic NHS) and LPS (10 ng/mL) in presence or absence of antibodies against CD11b and CD11c and IL-1β secretion (pg/mL) in the supernatant was measured after 24 hours by ELISA (n=8). (B) DCs were left unstimulated or treated with anti-CD11b/c prior exposure to non- and C-opsonized SARS-CoV-2, LPS and ATP. DCs with active caspase-1 were detected after 14 hours by flow cytometry using the FAM-FLICA assay (n=3). (C-E) Pre-COVID-19 pandemic NHS was incubated with mannan, prior to SARS-CoV-2 opsonization. DCs were exposed to non-opsonized SARS-CoV-2, C-opsonized SARS-CoV-2 and C-mannan opsonized SARS-CoV-2 in presence or absence of anti-CD11b/c, and mRNA levels of IFN-β (C), IRF7 (D) and IL-6 (E) were determined by qPCR (n=8 donors). Data show the mean values and error bars are the SEM. Statistical analysis was performed using (A) 2-way ANOVA with Tukey multiple-comparison test; ****p ≤ 0.0001 (n=8 donors); (B) Ordinary one-way with Tukey's multiple-comparison test; *p ≤ 0.05, **p ≤ 0.01 (n=3 donors); (C-E) 2-way ANOVA with Tukey multiple-comparison test; ***p ≤ 0.001, ****p ≤ 0.0001 (n=8 donors). C-opsonized = complement-opsonized.

Convalescent serum from COVID-19 patients blocks immune responses induced by complement-opsonized SARS-CoV-2 isolate (hCoV-19/Italy-WT) via CD32

Antibodies are important in induction of complement activation and subsequent deposition (57, 58). Here we investigated whether antibodies against SARS-CoV-2 affect complement-induced immunity by DCs. Serum from 20 (mild/moderate disease) recovered COVID-19 patients neutralized SARS-CoV-2 infection (Supplemental Figure 2A), indicating that serum contains neutralizing antibodies against SARS-CoV-2 (41, 46, 59). The serum was heat-inactivated to eliminate complement activity and donor-dependent complement differences. It was subsequently supplemented with pre-COVID-19 pandemic NHS to generate Ab/C-opsonized SARS-CoV-2 to make the complement contents similar, enabling us to focus on the antibody-mediated effects. Complement-opsonized SARS-CoV-2 (hCoV-19/Italy-WT; opsonized with pre-COVID-19 pandemic NHS) induced ISGs APOBEC3G, IRF7 and CXCL10 as well as cytokines IL-6, IL-10 and IL-12p35 (Figure 4A-F). Notably, co-incubation of SARS-CoV-2 with pre-COVID-19 NHS and COVID-19 convalescent serum (Ab/C-opsonized SARS-CoV-2) abrogated type I IFN as well as cytokine responses by DCs. The complement-induced responses were restored by blocking FcγRII (CD32) using an inhibitory CD32 antibody (Figure 4A-F). These data strongly suggest that antibodies against SARS-CoV-2 suppress immune responses induced by complement-opsonized SARS-CoV-2 via CD32.

Monoclonal antibodies against SARS-CoV-2 block complement-induced immunity to SARS-CoV-2

We investigated whether monoclonal antibodies against SARS-CoV-2 suppress the inflammation induced by complement-opsonized SARS-CoV-2 and how this is affected by the neutralizing capacity. We compared the effect of neutralizing antibodies (COVA1-18) and non-neutralizing antibodies (COVA1-27) against SARS-CoV-2, isolated from COVID-19 patients (41). Complement-opsonized SARS-CoV-2 induced IFN-β transcription and, notably, co-incubation of SARS-CoV-2 with pre-COVID-19 pandemic NHS and either neutralizing antibodies (Ab(COVA1-18)/C-opsonized SARS-CoV-2), or non-neutralizing antibodies (Ab(COVA1-27)/C-opsonized SARS-CoV-2) against SARS-CoV-2, abrogated IFN-β transcription (Figure 5A). The COVA1-27-mediated suppression was abrogated by CD32 inhibition thereby restoring IFN-β transcription to levels observed with complement-opsonized SARS-CoV-2 (Figure 5A). CD32 inhibition had less effect on COVA1-18-mediated suppression (Figure 5A). Similarly, both COVA1-18 and COVA1-27 suppressed induction of ISGs APOBEC3G, IRF7 and CXCL10 as well as cytokines IL-6 and IL-10 (Figure 5B-F). CD32 inhibition restored induction of CXCL10 and partially for APOBEC3G and IRF7. In contrast to IL-6, IL-10 induction was restored by CD32 inhibition. Moreover,

induction of CD86 was also suppressed by COVA1-18 and COVA1-27, which was restored by CD32 inhibition (Supplemental Figure 2B). These data strongly suggest that antibodies against SARS-CoV-2 present in serum inhibit complement-induced immune responses via CD32 and this is independent of neutralization capacity.

Serum samples from mild and severe COVID-19 patients block complement-induced immunity to SARS-CoV-2

Circulating immune complexes have been correlated with complement activation in severe/critical COVID-19 patients (59-62). To analyze the impact of antibody status and complement function in parallel, we screened serum from 5 individuals with mild *versus* 5 individuals with severe COVID-19. Serum from both groups was incubated with SARS-CoV-2 isolate (hCoV-19/Italy-WT) and the presence of C3c/C3d and IgGs was determined by ELISA (Figure 6A). Opsonization of SARS-CoV-2 with serum from either mild or severe COVID-19 patients led to the deposition of C3c and C3d fragments as well as IgG on SARS-CoV-2. Serum from mild COVID-19 patients caused inferior opsonization by C3c/d compared to IgG, whereas serum from severe COVID-19 patients induced more C3c/d opsonization compared to IgG. These results suggest that in severe COVID-19 patients, complement is fully activated. DCs from healthy donors were stimulated with opsonized-SARS-CoV-2 with serum from either mild or severe COVID-19 patients and induction of IFN-β, ISGs, such as IRF7, and IL-6 was measured. (Figure 6B-D). SARS-CoV-2 opsonized with serum from either mild or severe COVID-19 patients did not induce IFN-β, IRF7 nor IL-6 (Figure 6B-D). Notably, CD32 inhibition showed a trend to induction of IFN-β, IRF7 and IL-6 expression in response to virus opsonized with serum from severe patients in contrast to those observed with virus opsonized with serum from mild patients. Interestingly, when SARS-CoV-2 was opsonized with serum of mild or severe COVID-19 patients supplemented with pre-COVID-19 pandemic NHS, CD32 inhibition enhanced IFN-β, IRF7 and IL-6 responses compared to sera-opsonized SARS-CoV-2 and even compared to complement-opsonized SARS-CoV-2 alone. These data suggest that induction of antibodies during COVID-19 disease is important to resolve inflammation.

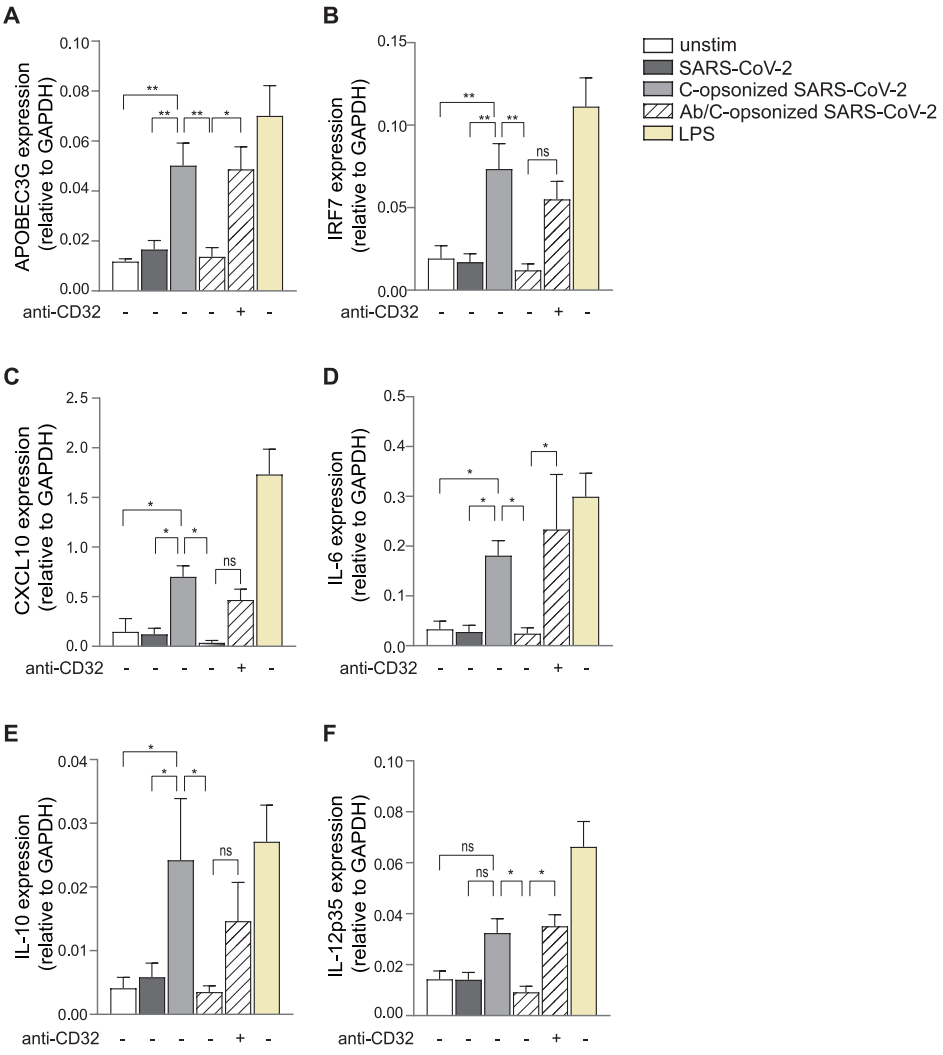

Figure 4: Anti-SARS-CoV-2 antibodies present in sera suppress complement activation mediated immune activation via CD32.

(A-F) Human monocyte-derived DCs were exposed to SARS-CoV-2 isolate (hCoV-19/Italy-WT, 1000TCID/mL), C-opsonized SARS-CoV-2 (hCoV-19/Italy-WT, 1000TCID/mL; opsonized with pre-COVID-19 pandemic NHS), Ab/C-opsonized SARS-CoV-2 (hCoV-19/Italy-WT, 1000TCID/mL; opsonized with heat-inactivated patient sera supplemented with pre-COVID-19 pandemic NHS) and LPS (10 ng/mL) in presence or absence of anti-CD32 for 6 hours. mRNA levels of APOBEC3G (A), IRF7 (B), CXCL10 (C), IL-6 (D), IL-10 (E) and IL-12p35 (F) were determined with qPCR (n=14 donors). Data show the mean values and error bars are the SEM. Statistical analysis was performed using (A-F) 2-way ANOVA with Dunnett's multiple-comparison test; *p ≤ 0.05, **p ≤ 0.01, ***p ≤ 0.001, ****p ≤ 0.0001 (n=14 donors). C-opsonized = complement opsonized; Ab/C-opsonized = antibody- and complement-opsonized.

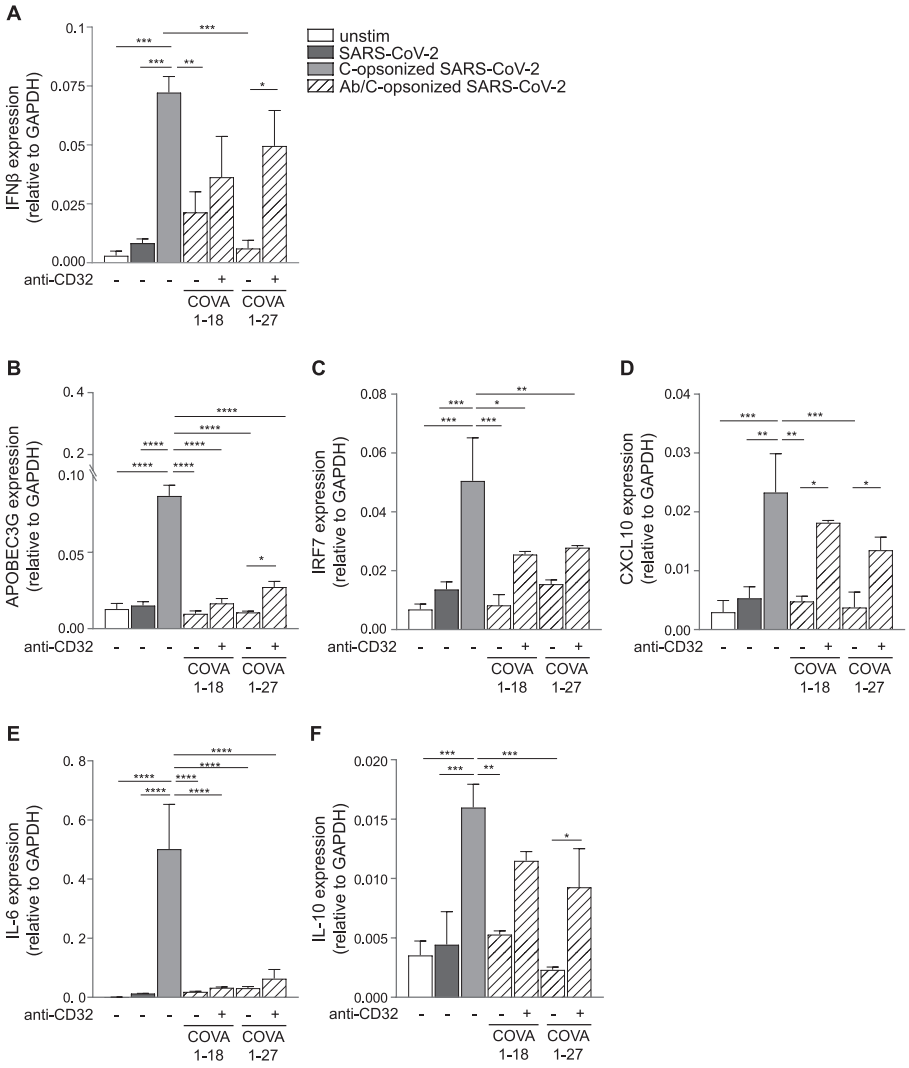

Figure 5: Non- and neutralizing anti-SARS-CoV-2 antibodies suppress complement activation mediated immune activation via CD32.

(A-F) SARS-CoV-2 was co-incubated with pre-COVID-19 pandemic NHS and COVID-19 patient isolated mAb COVA1-18 and COVA1-27 (10µg/mL) for 30 minutes at 37˚C. Human monocyte-derived DCs were exposed to SARS-CoV-2 isolate (hCoV-19/Italy-WT, 1000TCID/mL), C-opsonized SARS-CoV-2 (hCoV-19/Italy-WT, 1000TCID/mL; opsonized with pre-COVID-19 pandemic NHS), Ab/C-opsonized SARS-CoV-2 (hCoV-19/Italy-WT, 1000TCID/mL; opsonized with COVA antibodies supplemented with pre-COVID-19 pandemic NHS) and LPS (10 ng/mL) in presence or absence of anti-CD32 for 2 and 6 hours. mRNA levels of IFN-β (A), APOBEC3G (B), IRF7 (C), CXCL10 (D), IL-6 (E) and IL-10 (F) were determined by qPCR (n=6 donors (A) and (n=4 donors) (B-F). Data show the mean values and error bars are the SEM. Statistical analysis was performed using (A-F) 2-way ANOVA with Tukey's multiple-comparison test; *p ≤ 0.05, **p ≤ 0.01, ***p ≤ 0.001, ****p ≤ 0.0001, (A) (n=6 donors) and (B-F) (n=4 donors).

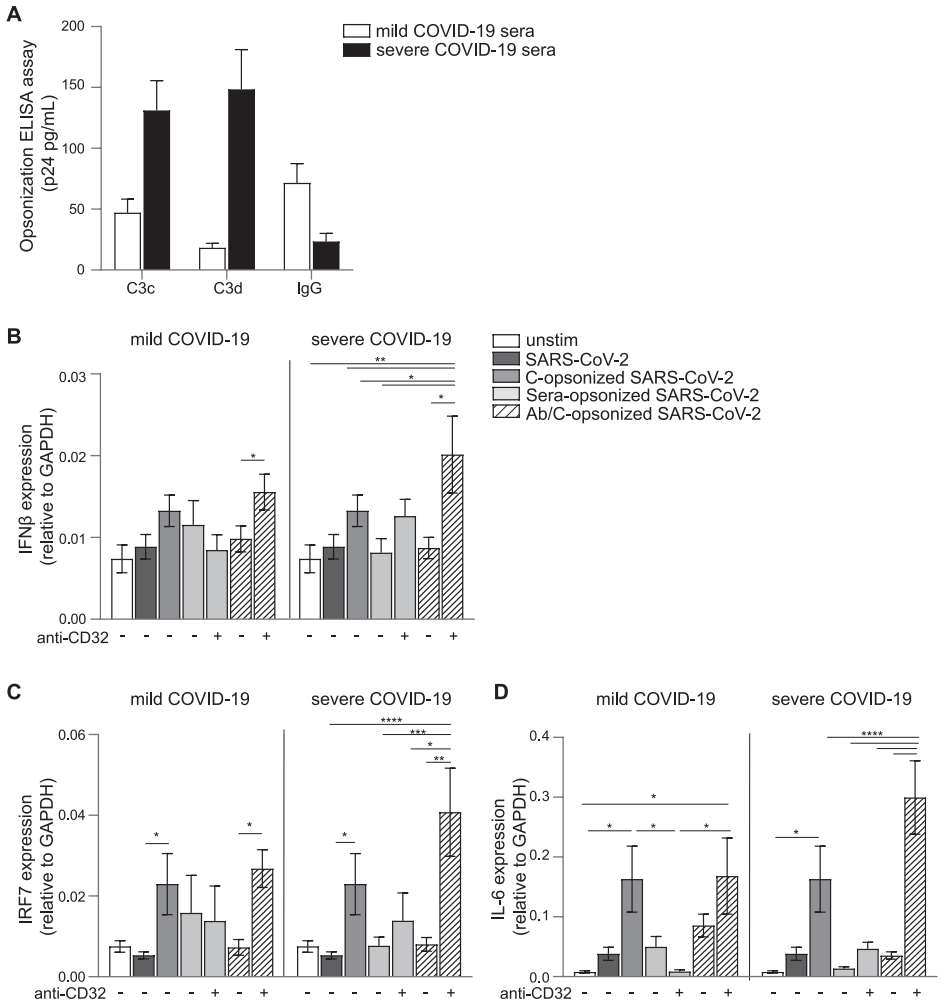
A
mild COVID-19 sera
severe COVID-19 sera
Opsonization ELISA assay (p24 pg/mL)
200
150
100
50
0
C3c
C3d
IgG
B
mild COVID-19
severe COVID-19
unstim
SARS-CoV-2
C-opsonized SARS-CoV-2
Sera-opsonized SARS-CoV-2
Ab/C-opsonized SARS-CoV-2
IFNβ expression (relative to GAPDH)
0.03
0.02
0.01
0.00
anti-CD32 - - - - + - +
C
mild COVID-19
severe COVID-19
IRF7 expression (relative to GAPDH)
0.06
0.04
0.02
0.00
anti-CD32 - - - - + - +
D
mild COVID-19
severe COVID-19
IL-6 expression (relative to GAPDH)
0.4
0.3
0.2
0.1
0.0
anti-CD32 - - - - + - +

◂ Figure 6: Disease severity dictates SARS-CoV-2 complement activation and antibody response.
(A) SARS-CoV-2 pseudovirus opsonization patterns with mild and severe COVID-19 patient sera was determined by ELISA (p24 pg/mL) using anti-human C3c and C3d for iC3b recognition, and anti-human IgG for immunoglobulins detection. (B) Human monocyte-derived DCs were exposed to SARS-CoV-2 isolate (hCoV-19/Italy-WT, 1000TCID/mL), C-opsonized SARS-CoV-2 (hCoV-19/Italy-WT, 1000TCID/mL; opsonized with pre-COVID-19 pandemic NHS), sera-opsonized SARS-CoV-2 (hCoV-19/Italy-WT, 1000TCID/mL; serum from mild or severe COVID-19 patients) and Ab/C-opsonized SARS-CoV-2 (hCoV-19/Italy-WT, 1000TCID/mL; serum from mild or severe COVID-19 patients supplemented with pre-COVID-19 pandemic NHS) in presence or absence of anti-CD32 for 2 and 6 hours. mRNA levels for IFN-β (B) were determined after 2 hours and mRNA levels of IRF7 (C) and IL-6) (D) after 6 hours by qPCR (n=6 donors) (B) and (n=8 donors) (C-D). Data show the mean values and error bars are the SEM. Statistical analysis was performed using (B-D) ordinary one-way ANOVA with Tukey's multiple-comparison test; *$p \leq 0.05$, **$p \leq 0.01$ (B) (n=6 donors) and (C-D) (n=8 donors). C-opsonized = complement-opsonized; Ab/C-opsonized = antibody- and complement-opsonized.

DISCUSSION

Complement is crucial for the induction of inflammatory responses to pathogens leading to an effective adaptive immune response. A hallmark of severe COVID-19 disease is excessive inflammation associated with enhanced morbidity and mortality. Accumulating evidence suggests that overactivation of the complement system contributes to pathophysiology of severe COVID-19 disease. Previously, we have shown that authentic SARS-CoV-2 isolate (hCoV-19/Italy-WT) (1000TCID/mL or MOI 0.028) does not activate DCs, which suggests immune escape. Here we show that SARS-CoV-2 isolate viruses are well opsonized by complement C3b/c fragments and complement-opsonized SARS-CoV-2 efficiently induced DC activation, type I IFN and cytokine responses via complement receptors CR3/CD11b and CR4/CD11c. Notably, we identified antibody responses against SARS-CoV-2 as a negative feedback mechanism in limiting complement-induced inflammation via CD32 signaling, as previously illustrated for HIV-1 (95). Our data therefore suggest that complement is crucial in the induction of antiviral innate and adaptive immune responses to SARS-CoV-2 and subsequently elicited antibodies against SARS-CoV-2 downregulate complement-induced immunity thereby preventing aberrant inflammation. This study highlights an important role for antibodies against SARS-CoV-2 to control immune homeostasis and suggests that dysregulation in this control might underlie aberrant inflammatory responses observed in severe COVID-19.

SARS-CoV-2 itself can activate the complement system directly through the lectin pathway (17, 19, 63-65) and the alternative pathway (23). Specifically, SARS-CoV-2 Spike and nucleocapsid proteins are directly recognized by the lectin pathway components,

leading to complement activation and the subsequent complement deposition (C3b) on virions (17). We observed that inoculation of SARS-CoV-2 isolate (hCoV-19/Italy-WT) with human pre-COVID-19 pandemic NHS led to efficient opsonization of SARS-CoV-2 by C3c and C3d fragments. Opsonization was inhibited by carbohydrate mannan, strongly supporting a role for MBL and the lectin pathway in activating complement. The use of pre-COVID-19 pandemic serum excluded a potential role for antibodies against SARS-CoV-2 in complement activation as has been shown by others (22, 28, 66, 67).

SARS-CoV-2 (hCoV-19/Italy-WT) binds to human DCs via heparan sulfate proteoglycans and C-type lectin receptor DC-SIGN (52, 68-70). SARS-CoV-2 binding to DCs is important for viral transmission to epithelial cells but does not cause immune activation (30, 52, 71). The lack of immune activation by SARS-CoV-2 is at least partially due to finding that human DCs do not become infected by SARS-CoV-2 as these immune cells do not express ACE2 (30, 72). Complement-opsonized SARS-CoV-2 was more efficiently bound by DCs than non-opsonized SARS-CoV-2, and binding was inhibited by antibodies against complement receptors CR3/CD11b and CR4/CD11c. In contrast to SARS-CoV-2 alone, complement-opsonized SARS-CoV-2 strongly induced DC maturation as determined by upregulation of co-stimulatory molecules CD80 and CD86. Moreover, complement-opsonized SARS-CoV-2 induced expression of IFN-β and ISGs IRF7, APOBEC3G and CXCL10 as well as cytokines IL-6, IL-10 and IL-1β. Type I IFN responses are pivotal to antiviral immunity by induction of innate resistance to virus replication but also activating cytotoxic T cell and T helper cell responses to viruses (73-75). In particular, IL-1β is a very potent proinflammatory cytokine activating both innate and adaptive immune responses (76, 77). Our data suggest that complement-opsonized SARS-CoV-2 binding to DCs via CR3 and CR4 leads to pro-IL-1β expression and subsequent activation of Caspase-1 inflammasome and processing of pro-IL-1β into bioactive IL-1β. Although IL-1β induction is important to induce innate and adaptive immunity, unrestrained expression of IL-1β leads to severe inflammation in different diseases (78-81). Several studies suggest that IL-1β production is an important factor in inflammatory responses during COVID-19 (80, 82-84) but mechanisms that control IL-1β production or type I IFN responses upon SARS-CoV-2 infection remain unidentified.

Antibodies against SARS-CoV-2 have been suggested to activate complement during infection (22, 85-87). We neither observed induction of complement opsonization of SARS-CoV-2 isolate (hCoV-19/Italy-WT) by serum from COVID-19 patients nor monoclonal human non- or neutralizing antibodies against SARS-CoV-2. In contrast, we observed that serum from COVID-19 patients as well as monoclonal human

antibodies against SARS-CoV-2 attenuated complement-opsonized SARS-CoV-2-induced immune inflammatory response. The observed DC maturation as well as type I IFN and cytokine responses induced by complement-opsonized SARS-CoV-2 was inhibited to levels observed for SARS-CoV-2 by serum from mild and severe COVID-19 patients. Similarly, both neutralizing and non-neutralizing antibodies against SARS-CoV-2 blocked these immune responses induced by complement-opsonized SARS-CoV-2.

Human monocyte-derived DCs express the low affinity immunoglobulin FcγRIIa CD32 which is a receptor for IgG and is involved in DC activation (88, 89). Notably, our data strongly suggest that antibodies against SARS-CoV-2 suppress complement induced immunity by CD32 as blocking antibodies against CD32 restored immune activation induced by complement-opsonized SARS-CoV-2. We also examined the composition of serum from mild and severe COVID-19 patients. We observed that serum from severe COVID-19 patients enhanced C3c and C3d deposition on SARS-CoV-2 compared to virus opsonized by serum from mild COVID-19 patients, whereas antibody deposition was increased with serum from mild COVID-19 patients. Interestingly, we observed that non-heat inactivated serum from mild and severe COVID-19 patients did not induce IFN-β, ISG IRF7 and cytokine IL-6, as opposed to complement-opsonized SARS-CoV-2. Although neither serum from mild nor severe patients induced immune responses, we observed that blocking CD32 led to a trend of enhanced inflammatory responses in presence of serum from severe patients, which could be explained by the higher complement opsonization of SARS-CoV-2 by serum from severe COVID-19 patients. However, these levels of immune activation hardly reached the levels of activation induced by complement-opsonized SARS-CoV-2. Notably, CD32 inhibition significantly induced inflammatory responses when serum of both mild and severe COVID-19 patients was supplemented with pre-COVID-19 NHS, similar to or surpassing complement-opsonized SARS-CoV-2, suggesting that the complement of severe COVID-19 patients might be less functional, despite high opsonization of SARS-CoV-2. Importantly, these data strongly suggest that antibodies in serum from mild and severe patients suppress immune responses to complement-opsonized SARS-CoV-2.

Our data suggest that complement activation by the MBL pathway is important for the induction of innate and adaptive antiviral immunity to SARS-CoV-2 via CR3 and/or CR4 on human DCs. Complement is present in mucosal tissues and this will lead to rapid activation of immunity upon SARS-CoV-2 infection. Our data have uncovered a striking role for antibodies against SARS-CoV-2 in attenuating the complement-induced inflammatory responses and thereby might be required in resolving inflammation. Our findings support a role for antibodies against SARS-CoV-2 induced by vaccinations

and after natural infection, not only in limiting infection but importantly in attenuating inflammation upon SARS-CoV-2 infection. Genetic polymorphisms in CD32 signaling pathways involved in attenuating complement-induced immunity might be responsible for unresolved inflammatory responses observed in severe COVID-19. Polymorphisms in MBL and FcγRII have been associated with susceptibility to or severity of some infectious diseases, such as SARS-CoV or influenza (90-92) as well as COVID-19 (18, 63, 93, 94), but whether these affect the complement activation and negative feedback mechanism remains to be investigated. We here provide novel immunologic and mechanistic insights into SARS-CoV-2 infection, where the host can cope with the virus due to efficient cellular and humoral immune response. These findings might be exploited for future therapeutic options to improve antiviral immune responses via triggering not yet considered host mechanisms, i.e. complement receptors expressed on immune cells.

Acknowledgements:
We thank Jonne Snitselaar, Yoann Aldon and Judith Burger for help with production of antibodies and pseudovirus reagents. In addition, we thank Elke Wynberg and Hugo D.G. van Willigen for their contribution to the *RECoVERED* study. This research was funded by the Netherlands Organisation for Health Research and Development (ZonMw) together with the Stichting Proefdiervrij (ZonMw MKMD COVID-19 grant nr.114025008to TBHG), and European Research Council (Advanced grant 670424 to TBHG), Amsterdam UMC PhD grant and two COVID-19 grants from the Amsterdam institute for Infection & Immunity (to TBHG, RWS, and MJG). This research was supported by a Work Visit Grant of the Amsterdam institute for Infection and Immunity and by an APART-MINT Fellowship of the Austrian Academy of Sciences at the Institute of Hygiene and medical Microbiology of the University of Innsbruck.

Author contribution:
MB-J conceived and designed experiments. MB-J and LEHvdD performed the experiments, MB-J, LEHvdD and JvH acquired data and analyzed data. MB-J, LEHvdD, JvH and TBHG interpreted data and contributed to scientific discussion. DW, GJdB, MJG, NAK and RWS contributed essential research materials and scientific input. MB-J and TBHG wrote the manuscript with input from all listed authors. TBHG perceived of the original study idea and was involved in all aspects of the study. All authors had access to all the data in this study and approved the final version of the manuscript. The corresponding author vouches for the completeness and accuracy of the data.

Funding:
This research was further funded through a ZonMW-NWO grant (Dutch Research Council/ Nederlandse organisatie voor Wetenschappelijk Onderzoek) together with the Stichting Proefdiervrij (ZonMW MKMD COVID-19 grant with project number 114025008) as well as the European Research Council (Advanced grant 670424). LEHvdD was supported by the Netherlands Organization for Scientific Research (NWO) (Grant No. 91717305) and MB-J by the ÖAW- APART MINT (Grant No. 11978).

Conflict of interest statement:
The authors have declared that no conflict of interest exists.

Ethics approval statement:
This study was performed in accordance with the ethical principles set out in the Declaration of Helsinki and was approved by the institutional review board of the Amsterdam University Medical Centers, location AMC Medical Ethics Committee and Ethics Advisory Body of Sanquin Blood Supply Foundation (Amsterdam, The Netherlands). The RECoVERED study was approved by the medical ethical review board of the Amsterdam University Medical Centers (NL73759.018.20). All participants provided written informed consent.

Data availability:
The data that support the findings of this study are available from the corresponding author upon reasonable request.

REFERENCES

1. Zhou, P., et al., *A pneumonia outbreak associated with a new coronavirus of probable bat origin*. Nature, 2020. 579(7798): p. 270-273.
2. *The species Severe acute respiratory syndrome-related coronavirus: classifying 2019-nCoV and naming it SARS-CoV-2*. Nat Microbiol, 2020. 5(4): p. 536-544.
3. Organization, W.H., *COVID-19 weekly epidemiological update, edition 119, 23 November 2022*. 2022.
4. Weitz, J.S., et al., *Modeling shield immunity to reduce COVID-19 epidemic spread*. Nature Medicine, 2020. 26(6): p. 849-854.
5. Thevarajan, I., et al., *Breadth of concomitant immune responses prior to patient recovery: a case report of non-severe COVID-19*. Nature Medicine, 2020. 26(4): p. 453-455.
6. Zhang, S., L. Wang, and G. Cheng, *The battle between host and SARS-CoV-2: Innate immunity and viral evasion strategies*. Mol Ther, 2022. 30(5): p. 1869-1884.
7. Boechat, J.L., et al., *The immune response to SARS-CoV-2 and COVID-19 immunopathology – Current perspectives*. Pulmonology, 2021. 27(5): p. 423-437.
8. Arish, M., et al., *COVID-19 immunopathology: From acute diseases to chronic sequelae*. Journal of Medical Virology, 2023. 95(1): p. e28122.
9. Yang, L., et al., *COVID-19: immunopathogenesis and Immunotherapeutics*. Signal Transduction and Targeted Therapy, 2020. 5(1): p. 128.
10. Lopes-Pacheco, M., et al., *Pathogenesis of Multiple Organ Injury in COVID-19 and Potential Therapeutic Strategies*. Front Physiol, 2021. 12: p. 593223.
11. Afzali, B., et al., *The state of complement in COVID-19*. Nature Reviews Immunology, 2022. 22(2): p. 77-84.
12. Tierney, A.L., et al., *Levels of soluble complement regulators predict severity of COVID-19 symptoms*. Front Immunol, 2022. 13: p. 1032331.
13. Lim, E.H.T., et al., *Complement activation in COVID-19 and targeted therapeutic options: A scoping review*. Blood Rev, 2023. 57: p. 100995.
14. Yu, J., et al., *Complement dysregulation is associated with severe COVID-19 illness*. Haematologica, 2022. 107(5): p. 1095-1105.
15. Ma, L., et al., *Increased complement activation is a distinctive feature of severe SARS-CoV-2 infection*. Science Immunology, 2021. 6(59): p. eabh2259.
16. Mastellos, D.C., et al., *Complement C3 vs C5 inhibition in severe COVID-19: Early clinical findings reveal differential biological efficacy*. Clin Immunol, 2020. 220: p. 108598.
17. Ali, Y.M., et al., *Lectin Pathway Mediates Complement Activation by SARS-CoV-2 Proteins*. Front Immunol, 2021. 12: p. 714511.
18. Stravalaci, M., et al., *Recognition and inhibition of SARS-CoV-2 by humoral innate immunity pattern recognition molecules*. Nature Immunology, 2022. 23(2): p. 275-286.
19. Gao, T., et al., *Highly pathogenic coronavirus N protein aggravates inflammation by MASP-2-mediated lectin complement pathway overactivation*. Signal Transduction and Targeted Therapy, 2022. 7(1): p. 318.
20. Satyam, A., et al., *Activation of classical and alternative complement pathways in the pathogenesis of lung injury in COVID-19*. Clin Immunol, 2021. 226: p. 108716.

21. Lamerton, R.E., et al., *SARS-CoV-2 Spike- and Nucleoprotein-Specific Antibodies Induced After Vaccination or Infection Promote Classical Complement Activation*. Frontiers in Immunology, 2022. 13.
22. Jarlhelt, I., et al., *SARS-CoV-2 Antibodies Mediate Complement and Cellular Driven Inflammation*. Frontiers in Immunology, 2021. 12.
23. Yu, J., et al., *Direct activation of the alternative complement pathway by SARS-CoV-2 spike proteins is blocked by factor D inhibition*. Blood, 2020. 136(18): p. 2080-2089.
24. Lo, M.W., et al., *SARS-CoV-2 triggers complement activation through interactions with heparan sulfate*. Clinical & Translational Immunology, 2022. 11(8): p. e1413.
25. Skendros, P., et al., *Complement C3 inhibition in severe COVID-19 using compstatin AMY-101*. Sci Adv, 2022. 8(33): p. eabo2341.
26. Posch, W., et al., *C5aR inhibition of nonimmune cells suppresses inflammation and maintains epithelial integrity in SARS-CoV-2-infected primary human airway epithelia*. J Allergy Clin Immunol, 2021. 147(6): p. 2083-2097.e6.
27. Java, A., et al., *The complement system in COVID-19: friend and foe?* JCI Insight, 2020. 5(15).
28. Holter, J.C., et al., *Systemic complement activation is associated with respiratory failure in COVID-19 hospitalized patients*. Proc Natl Acad Sci U S A, 2020. 117(40): p. 25018-25025.
29. Soloff, A.C. and S.M. Barratt-Boyes, *Enemy at the gates: dendritic cells and immunity to mucosal pathogens*. Cell Research, 2010. 20(8): p. 872-885.
30. van der Donk, L.E.H., et al., *SARS-CoV-2 infection activates dendritic cells via cytosolic receptors rather than extracellular TLRs*. Eur J Immunol, 2022. 52(4): p. 646-655.
31. Pérez-Gómez, A., et al., *Dendritic cell deficiencies persist seven months after SARS-CoV-2 infection*. Cellular & Molecular Immunology, 2021. 18(9): p. 2128-2139.
32. Zhou, R., et al., *Acute SARS-CoV-2 Infection Impairs Dendritic Cell and T Cell Responses*. Immunity, 2020. 53(4): p. 864-877.e5.
33. van der Donk, L.E.H., et al., *SARS-CoV-2 infection activates dendritic cells via cytosolic receptors rather than extracellular TLRs*. European Journal of Immunology, 2022. 52(4): p. 646-655.
34. Jamal, M., et al., *Immune dysregulation and system pathology in COVID-19*. Virulence, 2021. 12(1): p. 918-936.
35. Sanche, S., et al., *A simple model of COVID-19 explains disease severity and the effect of treatments*. Scientific Reports, 2022. 12(1): p. 14210.
36. Casadevall, A., L.A. Pirofski, and M.J. Joyner, *The Principles of Antibody Therapy for Infectious Diseases with Relevance for COVID-19*. mBio, 2021. 12(2).
37. Casadevall, A., M.J. Joyner, and L.A. Pirofski, *A Randomized Trial of Convalescent Plasma for COVID-19-Potentially Hopeful Signals*. Jama, 2020. 324(5): p. 455-457.
38. Janssen, M., et al., *A Randomized Open label Phase-II Clinical Trial with or without Infusion of Plasma from Subjects after Convalescence of SARS-CoV-2 Infection in High-Risk Patients with Confirmed Severe SARS-CoV-2 Disease (RECOVER): A structured summary of a study protocol for a randomised controlled trial*. Trials, 2020. 21(1): p. 828.
39. Herman, J.D., et al., *Functional convalescent plasma antibodies and pre-infusion titers shape the early severe COVID-19 immune response*. Nature Communications, 2021. 12(1): p. 6853.
40. van Gils, M.J., et al., *A single mRNA vaccine dose in COVID-19 patients boosts neutralizing antibodies against SARS-CoV-2 and variants of concern*. Cell Rep Med, 2022. 3(1): p. 100486.
41. Brouwer, P.J.M., et al., *Potent neutralizing antibodies from COVID-19 patients define multiple targets of vulnerability*. Science, 2020. 369(6504): p. 643-650.

42. Mesman, Annelies W., et al., *Measles Virus Suppresses RIG-I-like Receptor Activation in Dendritic Cells via DC-SIGN-Mediated Inhibition of PP1 Phosphatases.* Cell Host & Microbe, 2014. 16(1): p. 31-42.
43. Kootstra, N.A., et al., *Abrogation of postentry restriction of HIV-1-based lentiviral vector transduction in simian cells.* Proc Natl Acad Sci U S A, 2003. 100(3): p. 1298-303.
44. Schmidt, F., et al., *Measuring SARS-CoV-2 neutralizing antibody activity using pseudotyped and chimeric virusesSARS-CoV-2 neutralizing antibody activity.* Journal of Experimental Medicine, 2020. 217(11).
45. REED, L.J. and H. MUENCH, *A SIMPLE METHOD OF ESTIMATING FIFTY PER CENT ENDPOINTS12.* American Journal of Epidemiology, 1938. 27(3): p. 493-497.
46. Caniels, T.G., et al., *Emerging SARS-CoV-2 variants of concern evade humoral immune responses from infection and vaccination.* Sci Adv, 2021. 7(36): p. eabj5365.
47. Sullivan, B.L., et al., *Susceptibility of HIV-1 plasma virus to complement-mediated lysis. Evidence for a role in clearance of virus in vivo.* The Journal of Immunology, 1996. 157(4): p. 1791-1798.
48. Frank, I., et al., *Acquisition of host cell-surface-derived molecules by HIV-1.* Aids, 1996. 10(14): p. 1611-20.
49. Nijmeijer, B.M., et al., *HIV-1 subverts the complement system in semen to enhance viral transmission.* Mucosal Immunol, 2021. 14(3): p. 743-750.
50. Wilflingseder, D., et al., *IgG opsonization of HIV impedes provirus formation in and infection of dendritic cells and subsequent long-term transfer to T cells.* J Immunol, 2007. 178(12): p. 7840-8.
51. Purtscher, M., et al., *A broadly neutralizing human monoclonal antibody against gp41 of human immunodeficiency virus type 1.* AIDS Res Hum Retroviruses, 1994. 10(12): p. 1651-8.
52. Bermejo-Jambrina, M., et al., *Infection and transmission of SARS-CoV-2 depend on heparan sulfate proteoglycans.* The EMBO Journal, 2021. 40(20): p. e106765.
53. Schroder, K. and J. Tschopp, *The Inflammasomes.* Cell, 2010. 140(6): p. 821-832.
54. Franchi, L., R. Muñoz-Planillo, and G. Núñez, *Sensing and reacting to microbes through the inflammasomes.* Nat Immunol, 2012. 13(4): p. 325-32.
55. Martinon, F., A. Mayor, and J. Tschopp, *The inflammasomes: guardians of the body.* Annu Rev Immunol, 2009. 27: p. 229-65.
56. Héja, D., et al., *Revised mechanism of complement lectin-pathway activation revealing the role of serine protease MASP-1 as the exclusive activator of MASP-2.* Proceedings of the National Academy of Sciences, 2012. 109(26): p. 10498-10503.
57. Goldberg, B.S. and M.E. Ackerman, *Antibody-mediated complement activation in pathology and protection.* Immunology & Cell Biology, 2020. 98(4): p. 305-317.
58. Sörman, A., et al., *How antibodies use complement to regulate antibody responses.* Molecular Immunology, 2014. 61(2): p. 79-88.
59. van Gils, M.J., et al., *Antibody responses against SARS-CoV-2 variants induced by four different SARS-CoV-2 vaccines in health care workers in the Netherlands: A prospective cohort study.* PLOS Medicine, 2022. 19(5): p. e1003991.
60. Caniels, T.G., et al., *Emerging SARS-CoV-2 variants of concern evade humoral immune responses from infection and vaccination.* Science Advances, 2021. 7(36): p. eabj5365.
61. Wynberg, E., et al., *Evolution of Coronavirus Disease 2019 (COVID-19) Symptoms During the First 12 Months After Illness Onset.* Clin Infect Dis, 2022. 75(1): p. e482-e490.
62. Verveen, A., et al., *Severe Fatigue in the First Year Following SARS-CoV-2 Infection: A Prospective Cohort Study.* Open Forum Infect Dis, 2022. 9(5): p. ofac127.

63. Malaquias, M.A.S., et al., *The role of the lectin pathway of the complement system in SARS-CoV-2 lung injury.* Transl Res, 2021. 231: p. 55-63.
64. Magro, C., et al., *Complement associated microvascular injury and thrombosis in the pathogenesis of severe COVID-19 infection: A report of five cases.* Transl Res, 2020. 220: p. 1-13.
65. Hurler, L., et al., *Complement lectin pathway activation is associated with COVID-19 disease severity, independent of MBL2 genotype subgroups.* Frontiers in Immunology, 2023. 14.
66. Poston, D., et al., *Absence of Severe Acute Respiratory Syndrome Coronavirus 2 Neutralizing Activity in Prepandemic Sera From Individuals With Recent Seasonal Coronavirus Infection.* Clin Infect Dis, 2021. 73(5): p. e1208-e1211.
67. Gaikwad, H., et al., *Antibody-Dependent Complement Responses toward SARS-CoV-2 Receptor-Binding Domain Immobilized on "Pseudovirus-like" Nanoparticles.* ACS Nano, 2022.
68. Clausen, T.M., et al., *SARS-CoV-2 Infection Depends on Cellular Heparan Sulfate and ACE2.* Cell, 2020. 183(4): p. 1043-1057.e15.
69. Lempp, F.A., et al., *Lectins enhance SARS-CoV-2 infection and influence neutralizing antibodies.* Nature, 2021. 598(7880): p. 342-347.
70. Thépaut, M., et al., *DC/L-SIGN recognition of spike glycoprotein promotes SARS-CoV-2 trans-infection and can be inhibited by a glycomimetic antagonist.* PLoS Pathog, 2021. 17(5): p. e1009576.
71. Singh, K., et al., *SARS-CoV-2 spike and nucleocapsid proteins fail to activate human dendritic cells or γδ T cells.* PLOS ONE, 2022. 17(7): p. e0271463.
72. Song, X., et al., *Little to no expression of angiotensin-converting enzyme-2 on most human peripheral blood immune cells but highly expressed on tissue macrophages.* Cytometry A, 2023. 103(2): p. 136-145.
73. McNab, F., et al., *Type I interferons in infectious disease.* Nature Reviews Immunology, 2015. 15(2): p. 87-103.
74. Park, A. and A. Iwasaki, *Type I and Type III Interferons - Induction, Signaling, Evasion, and Application to Combat COVID-19.* Cell Host Microbe, 2020. 27(6): p. 870-878.
75. Crouse, J., U. Kalinke, and A. Oxenius, *Regulation of antiviral T cell responses by type I interferons.* Nature Reviews Immunology, 2015. 15(4): p. 231-242.
76. Mantovani, A., et al., *Interleukin-1 and Related Cytokines in the Regulation of Inflammation and Immunity.* Immunity, 2019. 50(4): p. 778-795.
77. Van Den Eeckhout, B., J. Tavernier, and S. Gerlo, *Interleukin-1 as Innate Mediator of T Cell Immunity.* Frontiers in Immunology, 2021. 11.
78. Carta, S., et al., *Dysregulated IL-1β Secretion in Autoinflammatory Diseases: A Matter of Stress?* Frontiers in Immunology, 2017. 8.
79. Hoffman, H.M. and A.A. Wanderer, *Inflammasome and IL-1β-Mediated Disorders.* Current Allergy and Asthma Reports, 2010. 10(4): p. 229-235.
80. Potere, N., et al., *Interleukin-1 and the NLRP3 inflammasome in COVID-19: Pathogenetic and therapeutic implications.* eBioMedicine, 2022. 85.
81. Kaneko, N., et al., *The role of interleukin-1 in general pathology.* Inflammation and Regeneration, 2019. 39(1): p. 12.
82. Makaremi, S., et al., *The role of IL-1 family of cytokines and receptors in pathogenesis of COVID-19.* Inflamm Res, 2022. 71(7-8): p. 923-947.
83. Yudhawati, R., S. Sakina, and M. Fitriah, *Interleukin-1β and Interleukin-10 Profiles and Ratio in Serum of COVID-19 Patients and Correlation with COVID-19 Severity: A Time Series Study.* Int J Gen Med, 2022. 15: p. 8043-8054.

84. Del Valle, D.M., et al., *An inflammatory cytokine signature predicts COVID-19 severity and survival.* Nature Medicine, 2020. 26(10): p. 1636-1643.
85. Farkash, I., et al., *Anti-SARS-CoV-2 antibodies elicited by COVID-19 mRNA vaccine exhibit a unique glycosylation pattern.* Cell Rep, 2021. 37(11): p. 110114.
86. Castanha, P.M.S., et al., *Contribution of Coronavirus-Specific Immunoglobulin G Responses to Complement Overactivation in Patients with Severe Coronavirus Disease 2019* The Journal of Infectious Diseases, 2022. 226(5): p. 766-777.
87. Dufloo, J., et al., *Asymptomatic and symptomatic SARS-CoV-2 infections elicit polyfunctional antibodies.* Cell Rep Med, 2021. 2(5): p. 100275.
88. Boruchov, A.M., et al., *Activating and inhibitory IgG Fc receptors on human DCs mediate opposing functions.* J Clin Invest, 2005. 115(10): p. 2914-23.
89. Vogelpoel, L.T., et al., *Control of cytokine production by human fc gamma receptors: implications for pathogen defense and autoimmunity.* Front Immunol, 2015. 6: p. 79.
90. Yuan, F.F., et al., *Influence of FcγRIIA and MBL polymorphisms on severe acute respiratory syndrome.* Tissue Antigens, 2005. 66(4): p. 291-296.
91. Mehrbod, P., et al., *Association of the host genetic factors, hypercholesterolemia and diabetes with mild influenza in an Iranian population.* Virology Journal, 2021. 18(1): p. 64.
92. Fricke-Galindo, I. and R. Falfán-Valencia, *Genetics Insight for COVID-19 Susceptibility and Severity: A Review.* Front Immunol, 2021. 12: p. 622176.
93. Medetalibeyoglu, A., et al., *Mannose binding lectin gene 2 (rs1800450) missense variant may contribute to development and severity of COVID-19 infection.* Infect Genet Evol, 2021. 89: p. 104717.
94. López-Martínez, R., et al., *The FCGR2A rs1801274 polymorphism was associated with the risk of death among COVID-19 patients.* Clin Immunol, 2022. 236: p. 108954.
95. Posch W., et al., *Antibodies attenuate the capacity of dendritic cells to stimulate HIV-specific cytotoxic T lymphocytes.* Journal of allergy and clinical immunology, 2012. 130(6): p.1368-1374.

SUPPLEMENTAL INFORMATION

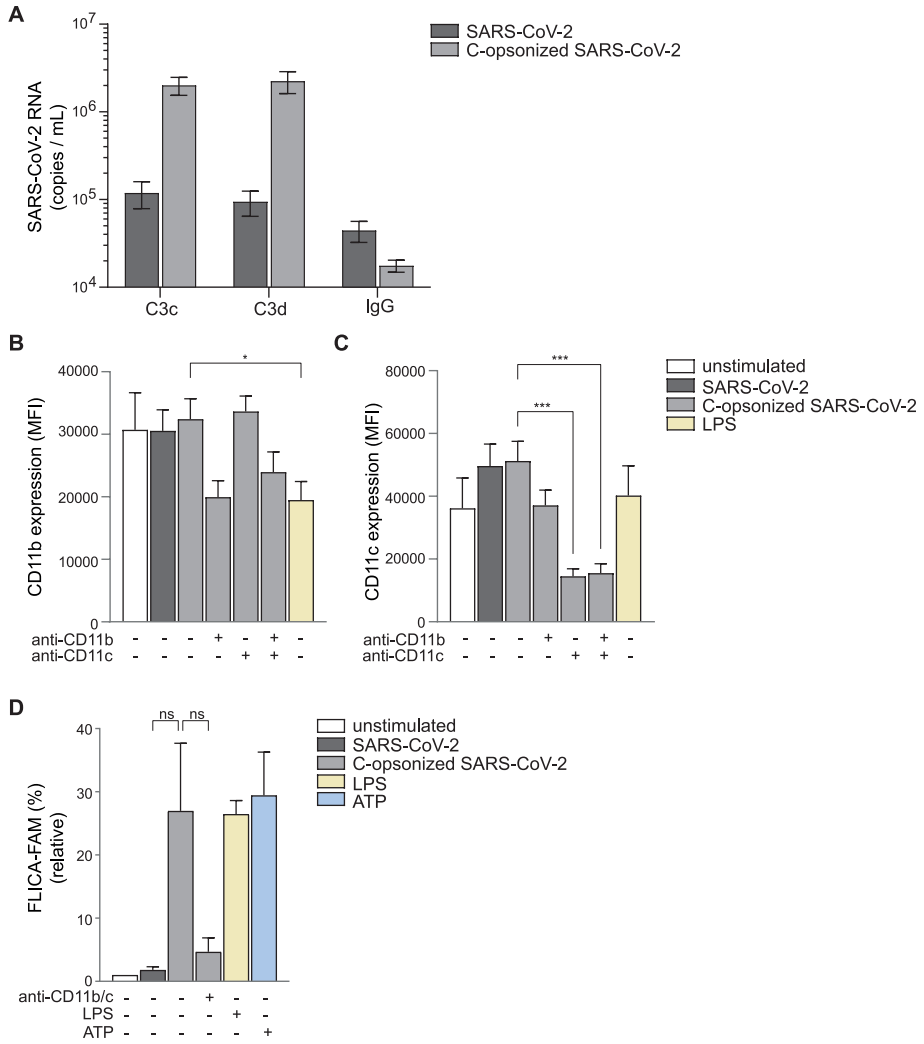

Supplementary Figure 1:

(A) SARS-CoV-2 RNA copy numbers/mL in pre-coated C3c, C3d and human IgG wells, were detected through qPCR (n=10 donors). (B-C) Human monocyte-derived DCs were exposed to SARS-CoV-2 isolate (hCoV-19/Italy-WT, 1000TCID/mL) and complement-opsonized SARS-CoV-2 (hCoV-19/Italy-WT, 1000TCID/mL) in presence or absence of anti-CD11b and anti-CD11c. LPS stimulation was used as positive control for DC maturation, which was measured after 24 hours by flow cytometry. Cumulative flow cytometry data of CD11b and CD11c (n=12 donors). (D) Percentages of FLICA+ cells from different stimulated DCs (n=3 donors). Data show the mean values and error bars are the SEM. Statistical analysis was performed using (B-C) 2-way ANOVA with Tukey multiple-comparison test; *$p \leq 0.05$, **$p \leq 0.01$, ***$p \leq 0.001$ (n=12 donors); (D) ordinary one-way with Tukey's multiple-comparison test (n=3 donors).

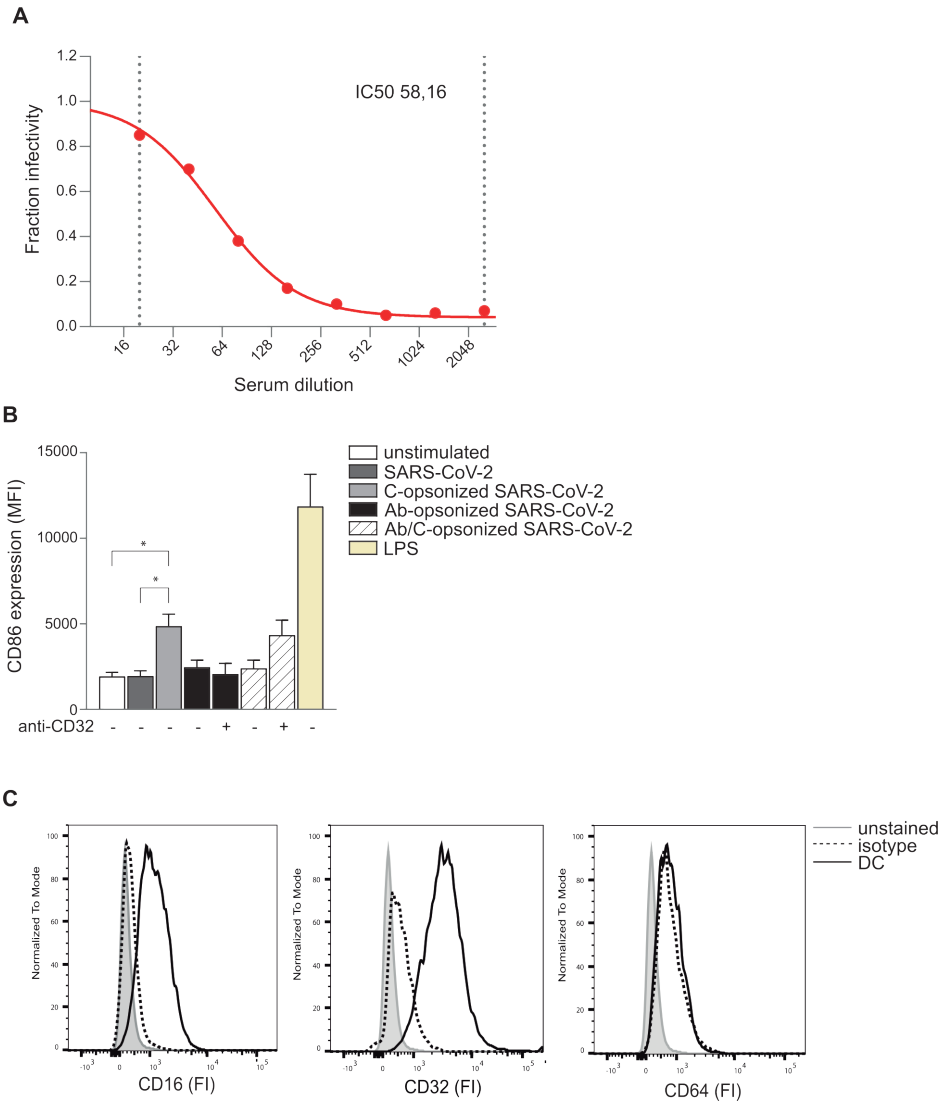
A
IC50 58,16
Fraction infectivity
Serum dilution
B
CD86 expression (MFI)
unstimulated
SARS-CoV-2
C-opsonized SARS-CoV-2
Ab-opsonized SARS-CoV-2
Ab/C-opsonized SARS-CoV-2
LPS
anti-CD32
C
Normalized To Mode
CD16 (FI)
CD32 (FI)
CD64 (FI)
unstained
isotype
DC

◂ Supplementary Figure 2:

(A) Neutralization assay using serum collected from 20 confirmed SARS-CoV-2-infected patients at 19 days post-symptom onset ("p.s.o."). The IC50 for this serum was 58,16 for the Spike-protein. (B) Human monocyte-derived DCs were exposed to SARS-CoV-2 isolate (hCoV-19/Italy-WT, 1000TCID/mL), to complement-opsonized SARS-CoV-2 (hCoV-19/Italy-WT, 1000TCID/mL), to antibody opsonized SARS-CoV-2 (hCoV-19/Italy-WT, 1000TCID/mL) and to antibody/complement-opsonized SARS-CoV-2 (hCoV-19/Italy-WT, 1000TCID/mL) in presence or absence of anti-CD32 for 24 hours. LPS stimulation was used as positive control for DC maturation, which was measured after 24 hours by flow cytometry. Cumulative flow cytometry data of CD86 (n=12 donors). (C) DCs were stained with antibodies against the surface markers CD16, CD32 and CD64 and analyzed by flow cytometry. Representative histograms for an experiment repeated more than three times with similar results (n=3 donors). Data show the mean values and error bars are the SEM. Statistical analysis was performed using (B) ordinary one-way ANOVA with Tukey multiple-comparison test; *$p \leq 0.05$ (n=6 donors).

CHAPTER 4

SARS-COV-2 SUPPRESSES TLR4-INDUCED IMMUNITY BY DENDRITIC CELLS VIA C-TYPE LECTIN RECEPTOR DC-SIGN

Lieve E.H. van der Donk[1,2], Marta Bermejo-Jambrina[1,2,3], John L. van Hamme[1,2], Mette M.W. Volkers[1,2], Ad C. van Nuenen[1,2], Neeltje A. Kootstra[1,2], Teunis B.H. Geijtenbeek[1,2]*

[1] Department of Experimental Immunology, Amsterdam UMC location University of Amsterdam, Amsterdam, The Netherlands.
[2] Amsterdam institute for Infection and Immunity, Infectious Diseases, Amsterdam, The Netherlands.
[3] Institute of Hygiene and Medical Microbiology, Medical University of Innsbruck, Innsbruck, Austria.

* Address correspondence and reprint requests to T.B.H. Geijtenbeek, Amsterdam UMC, Meibergdreef 9, 1105 AZ, Amsterdam.

Manuscript submitted

ABSTRACT

SARS-CoV-2 causes COVID-19, an infectious disease with symptoms ranging from a mild cold to severe pneumonia, inflammation, and even death. Although strong inflammatory responses are a major factor in causing morbidity and mortality, superinfections with bacteria during severe COVID-19 often cause pneumonia, bacteremia and sepsis. Aberrant immune responses might underlie increased sensitivity to bacteria during COVID-19 but the mechanisms remain unclear. Here we investigated whether SARS-CoV-2 directly suppresses immune responses to bacteria. We studied the functionality of human dendritic cells (DCs) towards a variety of bacterial triggers after exposure to SARS-CoV-2 Spike (S) protein and SARS-CoV-2 primary isolate (hCoV-19/Italy). Notably, pre-exposure of DCs to either SARS-CoV-2 S protein or a SARS-CoV-2 isolate led to reduced type I interferon (IFN) and cytokine responses in response to Toll-like receptor (TLR)4 agonist lipopolysaccharide (LPS), whereas other TLR agonists were not affected. SARS-CoV-2 S protein interacted with the C-type lectin receptor DC-SIGN and, notably, blocking DC-SIGN with antibodies restored type I IFN and cytokine responses to LPS. Moreover, blocking the kinase Raf-1 by a small molecule inhibitor restored immune responses to LPS. These results suggest that SARS-CoV-2 modulates DC function upon TLR4 triggering via the DC-SIGN-induced Raf-1 pathway. These data imply that SARS-CoV-2 actively suppresses DC function via DC-SIGN, which might account for the higher mortality rates observed in patients with COVID-19 and bacterial superinfections.

Keywords: SARS-CoV-2, dendritic cells, innate immunity, immunomodulation, superinfection

INTRODUCTION

SARS-CoV-2 causes coronavirus disease 2019 (COVID-19), which is an infectious disease characterized by strong induction of inflammatory cytokines, progressive lung inflammation and potentially multi-organ dysfunction (1-3). SARS-CoV-2 infects epithelial cells of the airways using the receptor angiotensin-converting enzyme 2 (ACE2) for infection (4, 5). Notably, it has been reported that COVID-19 patients, in particular severely ill patients, are vulnerable to viral, fungal or bacterial superinfections (6-10). Superinfections arise when a primary infection is followed by a secondary infection (11). Many of the superinfections in COVID-19 patients are caused by bacteria, for instance through hospital-acquired pneumonia or ventilator-acquired pneumonia with different virulent bacterial species such as *Pseudomonas (P.) aeruginosa* and *Klebsiella (K.) pneumoniae* (6-10, 12). Severe COVID-19 with superinfections is therefore associated with significantly worse prognosis (10, 12). However, it is currently unclear whether increased susceptibility of COVID-19 patients to bacterial superinfections is due to systemic inflammation or SARS-CoV-2 specifically affecting defense against bacterial infections.

Dendritic cells (DCs) are located throughout the mucosal barrier tissues such as the airways and lungs, and are essential for defense against infections by microbes including bacteria and viruses. DCs sense foreign microbes with pattern recognition receptors (PRRs), leading to antigen presentation to T cells and potent adaptive immune responses (13). Toll-like receptors (TLR) are important PRRs for sensing bacteria and TLR triggering induces type I Interferon (IFN) and proinflammatory cytokine responses, required for adaptive immunity (14). The TLR family member TLR4 is highly expressed by DCs and senses the bacterial component lipopolysaccharide (LPS) (15). Notably, whereas recent research has focused on TLR4-mediated immune activation by SARS-CoV-2 (16-19), the suppressive effects of SARS-CoV-2 on the immune response are not yet investigated.

Here, we investigated whether SARS-CoV-2 affects DC-induced immunity to bacteria using both SARS-CoV-2 S protein and SARS-CoV-2 primary isolate (hCoV-19/Italy). Notably, our data strongly suggest that SARS-CoV-2 suppresses DC-induced immune responses by TLR4, whilst signaling through other TLRs was not affected. Our data suggest that SARS-CoV-2 S protein as well as SARS-CoV-2 virus particles bind DC-SIGN, which induces signaling via kinase Raf-1 suppressing TLR4 signaling. Thus, we have identified a novel mechanism of immunosuppression by SARS-CoV-2 that might underlie the increased susceptibility to Gram-negative bacteria and targeting this pathway might attenuate bacterial infections during COVID-19.

MATERIALS AND METHODS

Cell lines

The Simian kidney cell line VeroE6 (ATCC® CRL-1586™) was maintained in CO_2-independent medium (Gibco Life Technologies, Gaithersburg, Md.) supplemented with 10% fetal calf serum (FCS), 2mM L-glutamine and penicillin/streptomycin (Invitrogen). Cultures were maintained at 37°C without CO_2. The human embryonic kidney (HEK) 293 cells (ATCC CRL-11268) were maintained in Iscove's modified Dulbecco's medium (IMDM) (Gibco Life Technologies) containing 10% FCS, L-glutamine, and 1% penicillin/streptomycin. Cultures were maintained at 37°C and 5% CO_2. HEK293 cells stably transfected with TLR4 cDNA (HEK/TLR4) were a kind gift from Dr. T. Golenbock (15). Cells were split and seeded into flat-bottom 96-well plates (Corning) and left to attach for 24 hours, before performing further experiments.

Primary cells

This study was performed in accordance with the ethical principles set out in the declaration of Helsinki and was approved by the institutional review board of the Amsterdam University Medical Centers, location AMC Medical Ethics Committee and the Ethics Advisory Body of Sanquin Blood Supply Foundation (Amsterdam, Netherlands). Human $CD14^+$ monocytes were isolated from the blood of healthy volunteer donors and subsequently differentiated into monocyte-derived dendritic cells (DCs) as described before (20). In short, the isolation of monocytes from buffy coats was performed by density centrifugation on Lymphoprep (Nycomed) and Percoll (Pharmacia). Monocytes were cultured in Roswell Park Memorial Institute (RPMI) 1640 (Gibco), supplemented with 10% FCS, 2mM L-glutamin (Invitrogen), and 1% penicillin/streptomycin. Differentiation into DCs was performed by the addition of cytokines IL-4 (500U/mL) and GM-CSF (800U/mL) (both Gibco). After 4 days of differentiation, DCs were seeded at 1 x 10^6/mL in a round-bottom 96-well plate (Corning). After 2 days of recovery, DCs were stimulated as described below.

SARS-CoV-2 (hCoV-19/Italy) virus production

The wild-type SARS-CoV-2 primary isolate was obtained from Dr. Maria R. Capobianchi through BEI Resources, NIAID, NIH:SARS-related coronavirus 2, Isolate Italy-INMI1, NR-52284, originally isolated in January 2020 in Rome, Italy. SARS-CoV-2 virus productions were performed as described before (19, 21) In brief, VeroE6 cells were inoculated with the SARS-CoV-2 primary isolate and incubated for 48 hours, after which virus supernatant was harvested. Tissue culture infectious dose (TCID50) was determined on VeroE6 cells by MTT assay. MTT

staining is indicative of cell viability and can be measured using a spectrometer. The virus titer was determined as TCID50/mL and calculated based on the Reed Muench method (22) as described before (21).

Reagents and stimulations

DCs were left unstimulated or exposed to 10 µg/mL SARS-CoV-2 S protein (Biotechne) for 1 hour, after which DCs were exposed to the following TLR stimuli: 10µg/mL Pam3CSK4 (Invivogen), 10 µg/mL Poly(I:C) (Invivogen), 10 ng/mL LPS from *Salmonella typhi* (Sigma), 10 µg/mL flagellin from *Bacillus subtilis* (Invivogen), 10 µg/mL lipoteichoic acid from *Staphylococcus aureus* (Invivogen). To investigate the contribution of DC-SIGN and Raf-1, cells were pre-incubated with 20µg/mL anti-DC-SIGN blocking antibody AZN-D1 for 30 minutes, or with 1µM GW5074 (Calbiochem) for 2 hours, respectively, before adding S protein. For exposure to SARS-CoV-2 (hCoV-19/Italy), DCs were incubated with inhibitors prior to exposure to SARS-CoV-2 TCID1000 for 1 hour, and then to LPS for 2 or 6 hours, after which cells were lysed.
Similarly, HEK293 and HEK/TLR4 cells were incubated for 2 hours with SARS-CoV-2 S protein or SARS-CoV-2 (hCoV-19/Italy), after which LPS was added. Cells were lysed after 24 hours for qPCR analysis.

RNA isolation and quantitative real-time PCR

Cells exposed to SARS-CoV-2 primary isolate (hCoV-19/Italy) were lysed and RNA was isolated with the QIAamp Viral RNA Mini Kit (Qiagen) according to the manufacturer's protocol. cDNA was synthesized using the M-MLV reverse-transcriptase kit (Promega). Before further application, cDNA was diluted 1 in 5 in depc. Cells exposed to SARS-CoV-2 S protein were lysed and RNA was isolated with the RNA Catcher™ PLUS kit (Invivogen) according to the manufacturer's instructions. Subsequently, cDNA was synthesized with a reverse-transcriptase kit (Promega). PCR amplification was performed in the presence of SYBR green (ThermoFisher) in a 7500 Fast Realtime PCR system (ABI). Specific primers were designed using Primer Express 2.0 (Applied Biosystems). The comparative delta Ct method was used to normalize the amount of target mRNA to the expression of household gene GAPDH. The following primers were used:

GAPDH: F_CCATGTTCGTCATGGGTGTG; R_GGTGCTAAGCAGTTGGTGGTG;
IFNB: F_ACAGACTTACAGGTTACCTCCGAAAC; R_CATCTGCTGGTTGAAGAATGCTT;
ISG15: F_ TTTGCCAGTACAGGAGCTTGTG; R_ GGGTGATCTGCGCCTTCA;
CXCL10 (IP10): F_ CGCTGTACCTGCATCAGCAT; R_ CATCTCTTCTCACCCTTCTTTTTCA;
IL-6: F_TGCAATAACCACCCCTGACC; R_TGCGCAGAATGAGATGAGTTG;

IL-10: F_GAGGCTACGGCGCTGTCAT; R_CCACGGCCTTGCTCTTGTT;
ORF1b: F_TGGGGTTTTACAGGTAACCT; R_AACACGCTTAACAAAGCACT.

Bead binding and SARS-CoV-2 isolate (hCoV-19/Italy) binding assays

To investigate ligand-receptor interactions, we used a fluorescent bead binding assay as described before (23). PerCP fluorescent streptavidin beads were coated with biotinylated S protein (Bio-techne). DCs were seeded at a density of 50.000 cell/well in a 96-well V-bottom plate in TSA (TSA: 0.5% bovine serum albumin (BSA) in TSM (200mM Tris, 1500mM NaCl, 10mM $CaCl_2$, 20mM $MgCl_2$) pH 7.4). Subsequently, cells were incubated with TSA, 20µg/mL anti-DC-SIGN antibody AZN-D1, or 100µg/mL mannan for 30 minutes at 37°C. Beads were added to each corresponding well in a 1:20 dilution and incubated at 37°C for 45 minutes. After washing once with TSA, cells were resuspended in TSA and adhesion was measured on a FACS Canto flow cytometer (BD Biosciences). The data was analyzed using FlowJo V10 software (Treestar).

To assess virus binding, DCs were exposed to 20µg/mL anti-DC-SIGN blocking antibody AZN-D1 or 50µg/mL mannan for 30 minutes at 37°C prior to incubation with SARS-CoV-2 isolate (hCoV-19/Italy) for 2 hours at 4°C. After 2 hours, cells were washed extensively with phosphate-buffered saline (PBS) to remove unbound virus and subsequently lysed with AVL buffer (Qiagen). RNA and cDNA were prepared as described above, and the amount of virus bound was determined with qPCR using ORF1b primers (24).

Statistics

Graphpad Prism version 8 (GraphPad Software) was used to generate all graphs and to perform statistical analyses. For pairwise comparisons, a Student's *t*-test was used. Multiple comparisons within groups were performed using a one-way ANOVA with a Tukey's multiple comparisons test, or two-way ANOVA with a Tukey's multiple comparisons test, where indicated. $p<0.05$ were considered statistically significant.

RESULTS

SARS-CoV-2 S protein specifically suppresses TLR4 activation

To investigate whether SARS-CoV-2 affects DC function towards other external stimuli, we exposed DCs to recombinant SARS-CoV-2 S protein before adding different TLR agonists, and screened for immune responses by measuring induction of interferon (IFN)-stimulated gene (ISG) IP10. As we have previously shown, S protein alone did not induce DC activation (19), whereas TLR agonists against TLR2/6, TLR3 and TLR4 induced IP10 (Figure 1). TLR1/2 and TLR5 agonists induced no IP10. Notably, pre-incubation with S

protein decreased induction of IP10 to TLR4 agonist, but not for the other TLR agonists. These data suggest that SARS-CoV-2 specifically modulates TLR4 signaling.

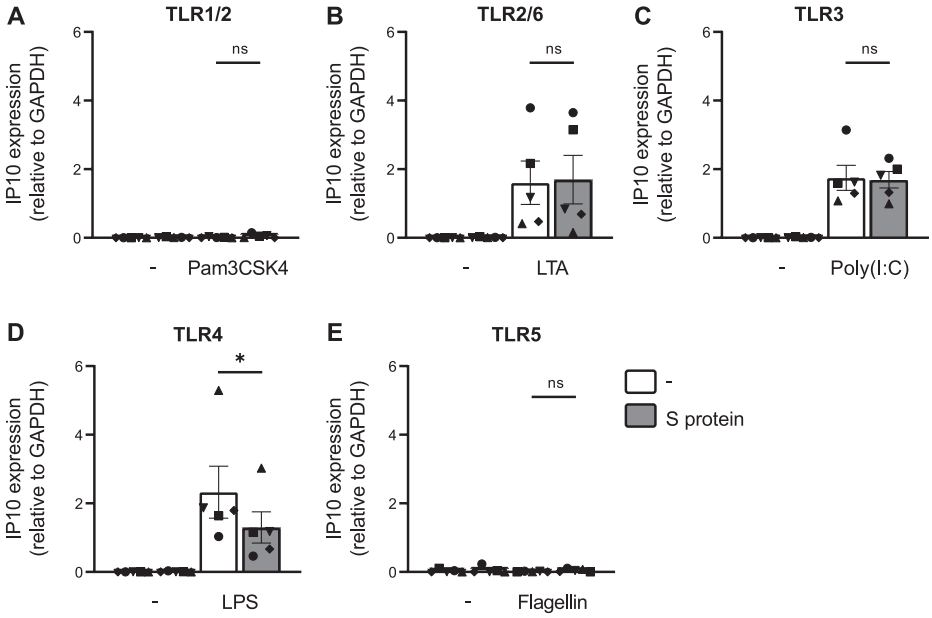

Figure 1: S protein modulates TLR4 signaling.

(A-E) DCs were pre-incubated with S protein before exposure to a plethora of bacterial TLR stimuli. After 6 hours incubation, cells were lysed and mRNA levels of IP10 were determined by qPCR. Data show the mean values and SEM. Statistical analysis was performed using student's *t*-test. Data represent n=5 DC donors obtained in three separate experiments with each symbol representing a different donor. *p<0.05; ns = non-significant.

SARS-CoV-2 S protein is involved in the suppression of immune responses by DCs

We next determined the effect of SARS-CoV-2 on TLR4-induced immune responses. DCs from 10-12 healthy donors were exposed to recombinant S protein before adding TLR4 agonist lipopolysaccharide (LPS) and type I IFN and cytokine responses were determined. LPS alone induced mRNA levels of IFN-β and ISGs IP10 and ISG15, and cytokines interleukin (IL)-6 and IL-10 (Figure 2A-E). Notably, pre-exposure to recombinant S protein significantly reduced mRNA levels of IFN-β, IP10 and ISG15 as well as IL-6 and IL-10. As published before, S protein alone did not induce any type I IFN or cytokine responses (data not shown; (19)). Our data therefore strongly suggest that SARS-CoV-2 S protein suppresses both TLR4-induced type I IFN and cytokine responses.

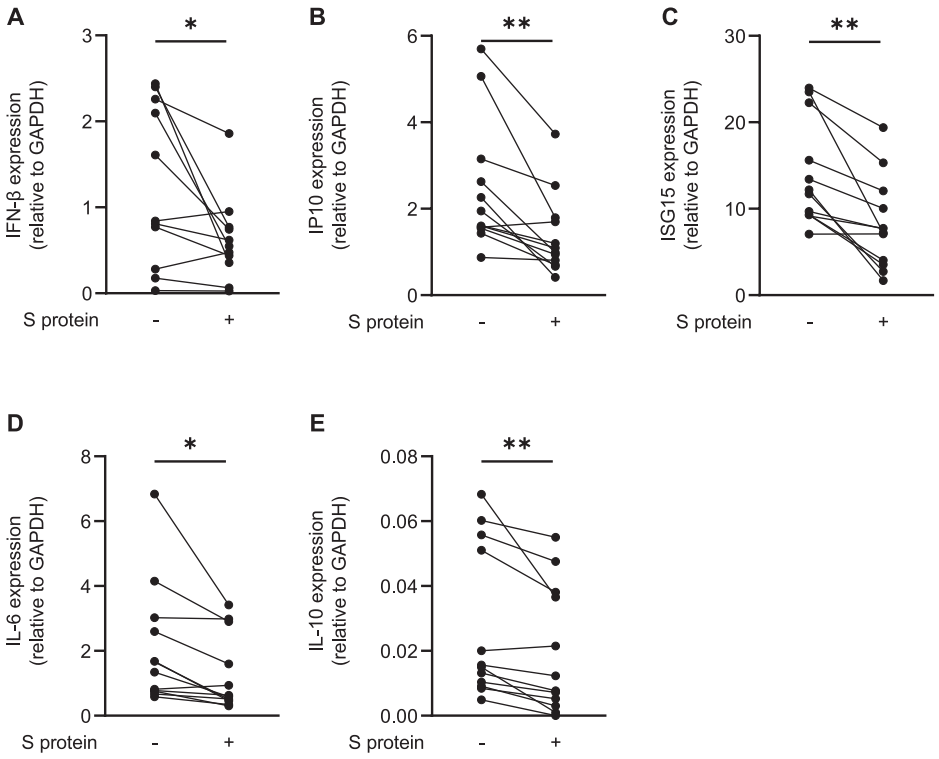

Figure 2: S protein modulates TLR4-mediated immune responses by DCs.

(A-E) DCs were exposed to S protein prior to addition of TLR4 agonist LPS. After 2 or 6 hours incubation, cells were lysed and mRNA levels of IFN-β (A) were determined after 2 hours, and mRNA expression levels of IP10 (B), ISG15 (C) and cytokines IL-6 (D) and IL-10 (E) were determined by qPCR. Data show expression for n=10-12 donors obtained in 5-6 separate experiments. Statistical analysis was performed using student's *t*-test. **p<0.01; *p<0.05.

SARS-CoV-2 S protein does not directly affect TLR4 signaling

SARS-CoV-2 has been suggested to interact with TLR4 (17, 25, 26) and therefore we investigated whether S protein could sterically hinder the binding of LPS using a TLR4-expressing HEK293 cell line (HEK293/TLR4). In contrast to parental HEK293 cells, incubation of HEK293/TLR4 cells with LPS induced IL-8 production (Figure 3A, B; HEK293 data not shown). Pre-incubation with a low and high concentration of recombinant S protein did not affect LPS-induced IL-8 production by the HEK293/TLR4 cells (Figure 3A, B). Additionally, pre-incubation of HEK293/TLR4 cells with SARS-CoV-2 primary isolate (hCoV-19/Italy) prior to exposure to LPS did also not affect IL-8 production (Figure 3C). Taken together, these results suggest that neither S protein nor SARS-CoV-2 primary isolate directly suppress TLR4 signaling either by sterically hindering binding of LPS to TLR4 or direct modulation of TLR4 signaling.

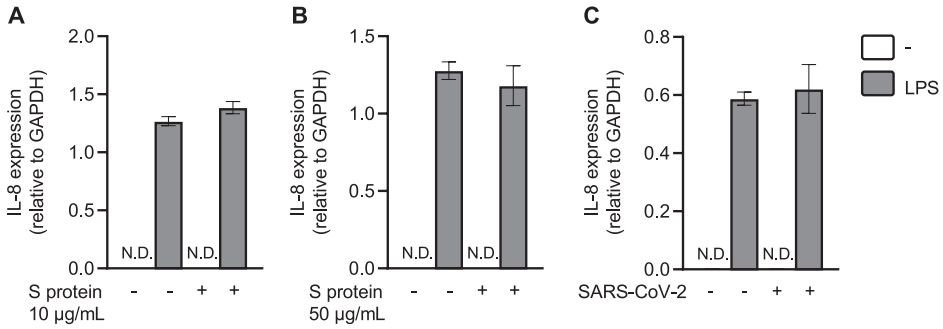

Figure 3: S protein or SARS-CoV-2 primary isolate does not sterically hinder binding of LPS to TLR4.

(A-C) HEK293/TLR4 cells were pre-incubated for 2 hours with a low (A) or high (B) concentration of S protein or SARS-CoV-2 primary isolate (C) before exposure to TLR4 agonist LPS. After 24 hours incubation, cells were lysed and mRNA levels of IL-8 (A-C) were determined by qPCR. Data show the mean values and SEM obtained in three separate experiments. N.D. = not detected.

SARS-CoV-2 S protein binds DC-SIGN expressed by DCs

Next we investigated whether crosstalk with the C-type lectin receptor (CLR) DC-SIGN is involved in the modulation of TLR4 signaling. Previous reports with different pathogens have shown that DC-SIGN signaling modulates immune responses by DCs (20, 27-29) and SARS-CoV-2 S protein has been shown to interact with DC-SIGN (30, 31). However, whilst these reports show SARS-CoV-2 S protein binding on DC-SIGN-overexpressing cell lines, the direct binding of S protein to DC-SIGN expressed by primary DCs has not yet been investigated. Therefore we investigated whether human DCs interact with SARS-CoV-2 S protein via DC-SIGN using an S-protein-labeled fluorescent bead binding assay (23). Notably, S protein strongly bound to DCs and binding was abrogated by the CLR inhibitor mannan and blocking antibodies against DC-SIGN (Figure 4A). Moreover, DCs efficiently captured SARS-CoV-2 virus particles and binding was blocked by mannan as well as anti-DC-SIGN antibodies (Figure 4B). These data strongly suggest that SARS-CoV-2 binds DC-SIGN on primary DCs via envelope glycoprotein S.

SARS-CoV-2 suppresses TLR4-mediated DC activation via DC-SIGN

Next we investigated whether SARS-CoV-2 suppresses TLR4 functionality via DC-SIGN. DCs from 9-12 donors were treated with recombinant SARS-CoV-2 S protein prior to LPS stimulation in presence or absence of antibodies against DC-SIGN, and type I IFN and cytokine responses were determined. Exposure to S protein induced a trend of decreased mRNA levels of IFN-β, and significantly decreased mRNA levels of IP10 and ISG15 induced by LPS (Figure 5A-C). Antibodies against

DC-SIGN significantly restored IP10 and ISG15 levels to levels observed with LPS alone (Figure 5A-C). IFN-β production was not affected by antibodies against DC-SIGN. Similarly, exposure to S protein showed a trend of decreased mRNA levels of IL-6, and significantly reduced IL-10 mRNA induced by LPS (Figure 5D-E). S protein-mediated suppression of IL-6 and IL-10 was restored by blocking DC-SIGN, albeit not significantly due to high donor variation (Figure 5D-E). These data suggest that DC-SIGN binding by S protein suppresses TLR4 signaling.

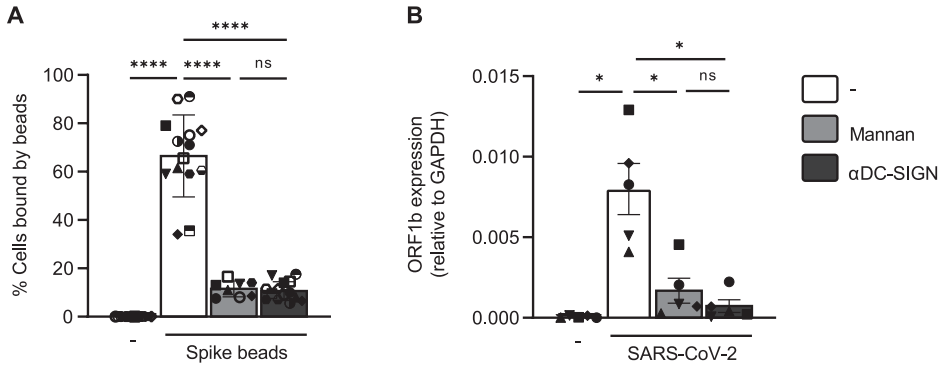

Figure 4: S protein binds DC-SIGN expressed by DCs.

(A) DCs were exposed to S-protein-coated fluorescent beads in the absence or presence of CLR block mannan, or DC-SIGN blocking antibodies, after which S protein binding to DCs was determined by flow cytometry. (B) DCs were exposed to SARS-CoV-2 primary isolate in the absence or presence of CLR block mannan, or DC-SIGN blocking antibodies, after which virus binding to DCs was determined by qPCR. Data show the mean values and SEM. Statistical analysis was performed using one-way ANOVA. Data represent n=8-14 donors obtained in 6 separate experiments (A) or n=5 donors obtained in 3 separate experiments (B) with each symbol representing a different donor. ****p<0.0001; *p<0.05; ns = non-significant.

Next we investigated whether SARS-CoV-2 primary isolate suppresses LPS-induced immune responses by DCs. Previously we have shown that SARS-CoV-2 primary isolate does not induce type I IFN and cytokine responses by DCs (19). Strikingly, pre-incubation of DCs with SARS-CoV-2 primary isolate prior to exposure to LPS suppressed mRNA levels of IFN-β, ISGs IP10 and ISG15, as well as cytokines IL-6 and IL-10 (Figure 6A-E). Moreover, anti-DC-SIGN antibodies restored expression of type I IFN and cytokine responses to levels observed with LPS alone (Figure 6A-E). DC-SIGN signaling via mannose-expressing pathogens triggers Raf-1 activation leading to immune modulation (32). We therefore investigated whether a small molecule inhibitor of Raf-1 affects SARS-CoV-2-suppression of LPS signaling. Although Raf-1 inhibition did not affect SARS-CoV-2 suppression of IFN-β, the

expression of ISGs IP10 and ISG15 as well as cytokines IL-6 and IL-10 were restored by inhibiting Raf-1 to levels observed for LPS alone (Figure 6A-E). We observed a high donor variation, which affected the reproducibility. These results suggest that SARS-CoV-2 modulates DC activation through DC-SIGN, thereby disabling DCs to respond to bacterial superinfections during COVID-19.

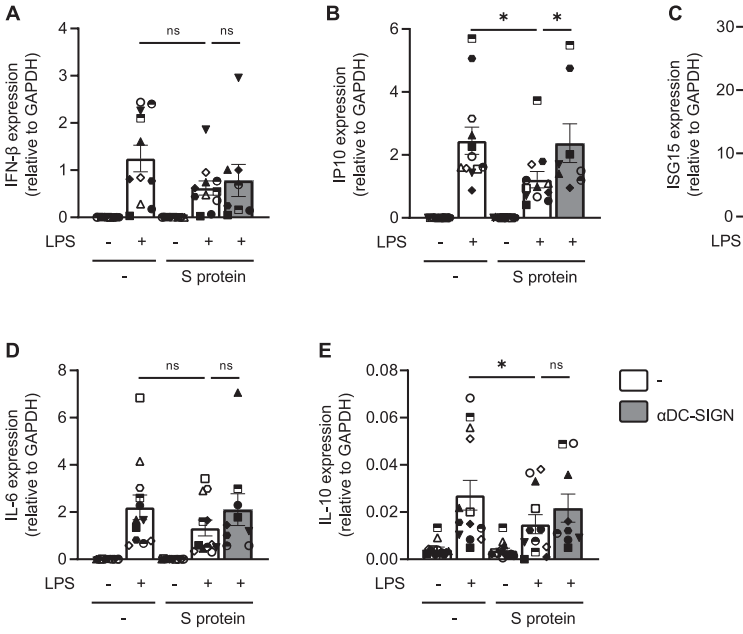

Figure 5: S protein suppresses TLR4-induced immunity via DC-SIGN.

(A-B) DCs were incubated with S protein in the absence or presence of anti-DC-SIGN blocking antibodies before exposure to LPS. After 2 or 6 hours incubation, DCs were lysed and mRNA transcription of IFN-β (A), IP10 (B), ISG15 (C), IL-6 (D) and IL-10 (E) was determined by qPCR. Data show the mean values and SEM. Statistical analysis was performed using one-way ANOVA with Tukey's multiple comparison's test for mixed-effects analysis. Data represent n=8-12 donors obtained in 6 separate experiments with each symbol representing a different donor. **p<0.01; *p<0.05; ns = non-significant.

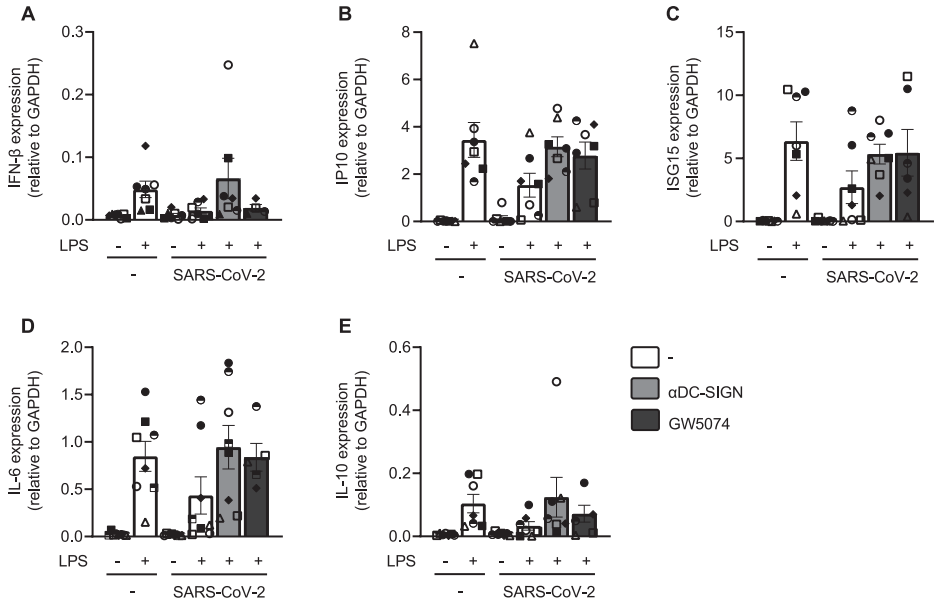

Figure 6: SARS-CoV-2 primary isolate suppresses DC immunity via DC-SIGN.

(A-B) DCs were incubated with SARS-CoV-2 primary isolate in the absence or presence of anti-DC-SIGN blocking antibodies before exposure to LPS. After 2 or 6 hours incubation, DCs were lysed and mRNA transcription of IFN-β (A), IP10 (B), ISG15 (C), IL-6 (D) and IL-10 (E) was determined by qPCR. Data show the mean values and SEM of n=4-8 donors obtained in 4 separate experiments with each symbol representing a different donor. Statistical analysis was performed using one-way ANOVA with Tukey's multiple comparison's test. Differences were not significant.

DISCUSSION

The SARS-CoV-2 pandemic has made an enormous impact all over the world. The high morbidity and mortality rates are not merely due to SARS-CoV-2 infection and aberrant immune responses against the virus, but are also due to superinfections (6-12). Hospitalized patients with severe COVID-19 are susceptible to superinfections with other viruses, fungi or bacteria. Often these superinfections are caused by bacteria leading to pneumonia, bacteremia and sepsis (33, 34). Damage inflicted on lung tissue by SARS-CoV-2, and mechanical stress caused by intubations are major reasons for the spread of various bacteria in the lungs and throughout the body (9, 33, 34). However, other mechanisms might underlie increased susceptibility to bacterial superinfections, such as decreased function of DCs during COVID-19 (35). Here we have identified a novel pathway activated by SARS-CoV-2 that suppresses TLR4, the major bacterial TLR on human DCs. Our data strongly suggest that SARS-

CoV-2 interacts with the C-type lectin receptor DC-SIGN leading to Raf-1-mediated suppression of TLR4 signaling. We observed suppression of both type I IFN and cytokine responses and these inflammatory mediators are crucial in the defense against bacterial infections (36, 37).

Bacterial superinfections are caused by both Gram-positive bacteria, including *Streptococcus pneumoniae* and Gram-negative bacteria including *P. aeruginosa* and *K. pneumoniae* (12). Notably, DCs responded similarly to stimulation with Gram-positive stimuli Pam3CSK4 and LTA, irrespective of pre-exposure to recombinant SARS-CoV-2 S protein. Moreover, DCs in presence or absence of S protein also reacted similarly to the Gram-negative stimulus flagellin, whereas DCs were significantly less responsive towards LPS in the presence of S protein. These findings led us to investigate how TLR4 binding or signaling was affected. Another study reported decreased functioning of DCs from COVID-19 patients towards TLR triggers during acute SARS-CoV-2 infection as DC activation upon TLR3, TLR4, TLR7 and TLR8 triggering was suppressed (38). Here we observed that SARS-CoV-2 specifically affected TLR4 signaling. As we have used DCs from healthy donors, our data suggest that SARS-CoV-2 as well as S protein directly affects TLR4 signaling.

Some pathogens are known to mimic pathogen or host structures to remain hidden from immune detection or become more pathogenic by inducing alternative signaling (39-43). Previous research suggests that S protein binds TLR4 to trigger immune activation (17, 25, 26, 44). We have shown that S protein does not activate DCs through TLR4 triggering (19); however, S protein might still bind TLR4 and thereby inhibit TLR4 signaling. TLR4 activation in HEK293 cells ectopically expressing TLR4 was neither affected by recombinant SARS-CoV-2 S protein nor SARS-CoV-2 infectious virus. These data strongly suggest that SARS-CoV-2 does neither sterically block binding of LPS to TLR4 nor directly inhibit TLR4 signaling. Besides TLRs, DCs express many different PRRs involved in virus binding. An important PRR family are the CLRs that interact with pathogens via carbohydrates and have been shown to induce signaling that directs or modulates immune responses (45, 46). In particular, the CLR DC-SIGN is expressed by DCs and macrophages, and recognizes high-mannose-containing glycoproteins on the surface of pathogens (47, 48). Previous research has shown that DC-SIGN modulates immune activation towards various pathogens (29, 48, 49). ManLAM, a highly mannosylated cell-wall component of *Mycobacterium (M.) tuberculosis*, interacts with DC-SIGN resulting in an altered immune response through crosstalk between DC-SIGN and TLR4 (27, 29). Interaction between ManLAM and DC-SIGN modulates TLR4 signaling via Raf-1 resulting in phosphorylation and acetylation of NFκB, which enhances induction of IL-10, IL-12 and IL-6 (27, 29). Similarly, envelope

glycoprotein of HIV-1 enhances LPS-induced IL-10, IL-12 and IL-6 responses via DC-SIGN (32). However, our data strongly suggest that SARS-CoV-2 interaction with DC-SIGN suppresses TLR4 signaling via Raf-1. Thus, DC-SIGN modulation of immunity is strongly dependent on the PRR triggered as well as the pathogen that is recognized by DC-SIGN. Further research on the effect of DC-SIGN triggering during SARS-CoV-2 infection is required to elucidate underlying mechanisms. In addition, it is important to note that also coinfections or superinfections with other viruses and fungi were reported (6, 12, 50-52). It would be interesting to further investigate how superinfections with different bacteria, viruses or fungi might affect DC function during COVID-19. In conclusion, our data suggest that SARS-CoV-2 S protein-mediated DC-SIGN crosstalk affects TLR4-induced immunity, which might underlie bacterial superinfections during COVID-19.

Author contribution:
LEHvdD and MBJ designed experiments; LEHvdD, MBJ, MMWV and JLvH performed the experiments; ACvN and NAK contributed essential research materials and scientific input. LEHvdD, MBJ and TBHG analyzed and interpreted data; LEHvdD and TBHG wrote the manuscript with input from all listed authors. TBHG supervised all aspects of this study.

Funding:
This research was funded by the Netherlands Organisation for Health Research and Development together with the Stichting Proefdiervrij (ZonMW MKMD COVID-19 grant nr. 114025008 to TBHG) and European Research Council (Advanced grant 670424 to TBHG). LEHvdD was supported by the Netherlands Organization for Scientific Research (NWO) (Grant number: 91717305). MBJ was supported by a Work Visit Grant of the Amsterdam institute for Infection and Immunity and by an APART-MINT Fellowship of the Austrian Academy of Sciences at the Institute of Hygiene and Medical Microbiology of the University of Innsbruck (Grant number 11978).

Conflict of interest statement:
All authors declare no commercial or financial conflicts of interest.

Ethics approval statement:
This study was performed in accordance with the ethical principles set out in the declaration of Helsinki and was approved by the institutional review board of the Amsterdam University Medical Centers, location AMC Medical Ethics Committee and the Ethics Advisory Body of Sanquin Blood Supply Foundation (Amsterdam, Netherlands).

Data availability:
The data that support the findings of this study are available from the corresponding author upon reasonable request.

REFERENCES

1. Harrison AG, Lin T, Wang P. Mechanisms of SARS-CoV-2 Transmission and Pathogenesis. Trends Immunol. 2020;41(12):1100-15.
2. Wang D, Hu B, Hu C, Zhu F, Liu X, Zhang J, et al. Clinical Characteristics of 138 Hospitalized Patients With 2019 Novel Coronavirus-Infected Pneumonia in Wuhan, China. JAMA. 2020;323(11):1061-9.
3. Wiersinga WJ, Rhodes A, Cheng AC, Peacock SJ, Prescott HC. Pathophysiology, Transmission, Diagnosis, and Treatment of Coronavirus Disease 2019 (COVID-19): A Review. JAMA. 2020;324(8):782-93.
4. Hoffmann M, Kleine-Weber H, Schroeder S, Kruger N, Herrler T, Erichsen S, et al. SARS-CoV-2 Cell Entry Depends on ACE2 and TMPRSS2 and Is Blocked by a Clinically Proven Protease Inhibitor. Cell. 2020;181(2):271-80 e8.
5. Letko M, Marzi A, Munster V. Functional assessment of cell entry and receptor usage for SARS-CoV-2 and other lineage B betacoronaviruses. Nat Microbiol. 2020;5(4):562-9.
6. Garcia-Vidal C, Sanjuan G, Moreno-Garcia E, Puerta-Alcalde P, Garcia-Pouton N, Chumbita M, et al. Incidence of co-infections and superinfections in hospitalized patients with COVID-19: a retrospective cohort study. Clin Microbiol Infect. 2021;27(1):83-8.
7. Langford BJ, So M, Raybardhan S, Leung V, Westwood D, MacFadden DR, et al. Bacterial co-infection and secondary infection in patients with COVID-19: a living rapid review and meta-analysis. Clin Microbiol Infect. 2020;26(12):1622-9.
8. Omoush SA, Alzyoud JAM. The Prevalence and Impact of Coinfection and Superinfection on the Severity and Outcome of COVID-19 Infection: An Updated Literature Review. Pathogens. 2022;11(4).
9. Pickens CO, Gao CA, Cuttica MJ, Smith SB, Pesce LL, Grant RA, et al. Bacterial Superinfection Pneumonia in Patients Mechanically Ventilated for COVID-19 Pneumonia. Am J Respir Crit Care Med. 2021;204(8):921-32.
10. Catano-Correa JC, Cardona-Arias JA, Porras Mancilla JP, Garcia MT. Bacterial superinfection in adults with COVID-19 hospitalized in two clinics in Medellin-Colombia, 2020. PLoS One. 2021;16(7):e0254671.
11. Feldman C, Anderson R. The role of co-infections and secondary infections in patients with COVID-19. Pneumonia (Nathan). 2021;13(1):5.
12. Musuuza JS, Watson L, Parmasad V, Putman-Buehler N, Christensen L, Safdar N. Prevalence and outcomes of co-infection and superinfection with SARS-CoV-2 and other pathogens: A systematic review and meta-analysis. PLoS One. 2021;16(5):e0251170.
13. Janeway CA, Jr., Medzhitov R. Innate immune recognition. Annu Rev Immunol. 2002;20:197-216.
14. Medzhitov R. Toll-like receptors and innate immunity. Nat Rev Immunol. 2001;1(2):135-45.
15. Chow JC, Young DW, Golenbock DT, Christ WJ, Gusovsky F. Toll-like receptor-4 mediates lipopolysaccharide-induced signal transduction. J Biol Chem. 1999;274(16):10689-92.
16. Shirato K, Kizaki T. SARS-CoV-2 spike protein S1 subunit induces pro-inflammatory responses via toll-like receptor 4 signaling in murine and human macrophages. Heliyon. 2021;7(2):e06187.
17. Zhao Y, Kuang M, Li J, Zhu L, Jia Z, Guo X, et al. SARS-CoV-2 spike protein interacts with and activates TLR41. Cell Res. 2021;31(7):818-20.
18. Petruk G, Puthia M, Petrlova J, Samsudin F, Stromdahl AC, Cerps S, et al. SARS-CoV-2 spike protein binds to bacterial lipopolysaccharide and boosts proinflammatory activity. J Mol Cell Biol. 2020;12(12):916-32.

19. van der Donk LEH, Eder J, van Hamme JL, Brouwer PJM, Brinkkemper M, van Nuenen AC, et al. SARS-CoV-2 infection activates dendritic cells via cytosolic receptors rather than extracellular TLRs. Eur J Immunol. 2022;52(4):646-55.
20. Mesman AW, Zijlstra-Willems EM, Kaptein TM, de Swart RL, Davis ME, Ludlow M, et al. Measles virus suppresses RIG-I-like receptor activation in dendritic cells via DC-SIGN-mediated inhibition of PP1 phosphatases. Cell Host Microbe. 2014;16(1):31-42.
21. Bermejo-Jambrina M, Eder J, Kaptein TM, van Hamme JL, Helgers LC, Vlaming KE, et al. Infection and transmission of SARS-CoV-2 depend on heparan sulfate proteoglycans. EMBO J. 2021;40(20):e106765.
22. Reed LJ, Muench H. A simple method of estimating fifty per cent endpoints. American journal of epidemiology. 1938;27(3):493-7.
23. Sprokholt JK, Hertoghs N, Geijtenbeek TB. Flow Cytometry-Based Bead-Binding Assay for Measuring Receptor Ligand Specificity. Methods Mol Biol. 2016;1390:121-9.
24. Chu DKW, Pan Y, Cheng SMS, Hui KPY, Krishnan P, Liu Y, et al. Molecular Diagnosis of a Novel Coronavirus (2019-nCoV) Causing an Outbreak of Pneumonia. Clin Chem. 2020;66(4):549-55.
25. Aboudounya MM, Heads RJ. COVID-19 and Toll-Like Receptor 4 (TLR4): SARS-CoV-2 May Bind and Activate TLR4 to Increase ACE2 Expression, Facilitating Entry and Causing Hyperinflammation. Mediators Inflamm. 2021;2021:8874339.
26. Choudhury A, Mukherjee S. In silico studies on the comparative characterization of the interactions of SARS-CoV-2 spike glycoprotein with ACE-2 receptor homologs and human TLRs. J Med Virol. 2020;92(10):2105-13.
27. Geijtenbeek TB, Van Vliet SJ, Koppel EA, Sanchez-Hernandez M, Vandenbroucke-Grauls CM, Appelmelk B, et al. Mycobacteria target DC-SIGN to suppress dendritic cell function. J Exp Med. 2003;197(1):7-17.
28. Gringhuis SI, Hertoghs N, Kaptein TM, Zijlstra-Willems EM, Sarrami-Forooshani R, Sprokholt JK, et al. HIV-1 blocks the signaling adaptor MAVS to evade antiviral host defense after sensing of abortive HIV-1 RNA by the host helicase DDX3. Nat Immunol. 2017;18(2):225-35.
29. Gringhuis SI, den Dunnen J, Litjens M, van Het Hof B, van Kooyk Y, Geijtenbeek TB. C-type lectin DC-SIGN modulates Toll-like receptor signaling via Raf-1 kinase-dependent acetylation of transcription factor NF-kappaB. Immunity. 2007;26(5):605-16.
30. Amraei R, Yin W, Napoleon MA, Suder EL, Berrigan J, Zhao Q, et al. CD209L/L-SIGN and CD209/DC-SIGN Act as Receptors for SARS-CoV-2. ACS Cent Sci. 2021;7(7):1156-65.
31. Thepaut M, Luczkowiak J, Vives C, Labiod N, Bally I, Lasala F, et al. DC/L-SIGN recognition of spike glycoprotein promotes SARS-CoV-2 trans-infection and can be inhibited by a glycomimetic antagonist. PLoS Pathog. 2021;17(5):e1009576.
32. Gringhuis SI, den Dunnen J, Litjens M, van der Vlist M, Geijtenbeek TB. Carbohydrate-specific signaling through the DC-SIGN signalosome tailors immunity to Mycobacterium tuberculosis, HIV-1 and Helicobacter pylori. Nat Immunol. 2009;10(10):1081-8.
33. Maslove DM, Sibley S, Boyd JG, Goligher EC, Munshi L, Bogoch, II, et al. Complications of Critical COVID-19: Diagnostic and Therapeutic Considerations for the Mechanically Ventilated Patient. Chest. 2022;161(4):989-98.
34. Wicky PH, Niedermann MS, Timsit JF. Ventilator-associated pneumonia in the era of COVID-19 pandemic: How common and what is the impact? Crit Care. 2021;25(1):153.
35. Winheim E, Rinke L, Lutz K, Reischer A, Leutbecher A, Wolfram L, et al. Impaired function and delayed regeneration of dendritic cells in COVID-19. PLoS Pathog. 2021;17(10):e1009742.

36. Boxx GM, Cheng G. The Roles of Type I Interferon in Bacterial Infection. Cell Host Microbe. 2016;19(6):760-9.
37. Giamarellos-Bourboulis EJ, Raftogiannis M. The immune response to severe bacterial infections: consequences for therapy. Expert Rev Anti Infect Ther. 2012;10(3):369-80.
38. Zhou R, To KK, Wong YC, Liu L, Zhou B, Li X, et al. Acute SARS-CoV-2 Infection Impairs Dendritic Cell and T Cell Responses. Immunity. 2020;53(4):864-77 e5.
39. Gowthaman U, Eswarakumar VP. Molecular mimicry: good artists copy, great artists steal. Virulence. 2013;4(6):433-4.
40. Rahman MM, McFadden G. Modulation of NF-kappaB signalling by microbial pathogens. Nat Rev Microbiol. 2011;9(4):291-306.
41. Rojas JM, Alejo A, Martin V, Sevilla N. Viral pathogen-induced mechanisms to antagonize mammalian interferon (IFN) signaling pathway. Cell Mol Life Sci. 2021;78(4):1423-44.
42. Chathuranga K, Weerawardhana A, Dodantenna N, Lee JS. Regulation of antiviral innate immune signaling and viral evasion following viral genome sensing. Exp Mol Med. 2021;53(11):1647-68.
43. Reddick LE, Alto NM. Bacteria fighting back: how pathogens target and subvert the host innate immune system. Mol Cell. 2014;54(2):321-8.
44. Aboudounya MM, Holt MR, Heads RJ. SARS-CoV-2 Spike S1 glycoprotein is a TLR4 agonist, upregulates ACE2 expression and induces pro-inflammatory M₁ macrophage polarisation. bioRxiv. 2021:2021.08.11.455921.
45. Li D, Wu M. Pattern recognition receptors in health and diseases. Signal Transduct Target Ther. 2021;6(1):291.
46. Geijtenbeek TB, Gringhuis SI. Signalling through C-type lectin receptors: shaping immune responses. Nat Rev Immunol. 2009;9(7):465-79.
47. Geijtenbeek TB, Torensma R, van Vliet SJ, van Duijnhoven GC, Adema GJ, van Kooyk Y, et al. Identification of DC-SIGN, a novel dendritic cell-specific ICAM-3 receptor that supports primary immune responses. Cell. 2000;100(5):575-85.
48. van Kooyk Y, Geijtenbeek TB. DC-SIGN: escape mechanism for pathogens. Nat Rev Immunol. 2003;3(9):697-709.
49. Gringhuis SI, Kaptein TM, Wevers BA, Mesman AW, Geijtenbeek TB. Fucose-specific DC-SIGN signalling directs T helper cell type-2 responses via IKKepsilon- and CYLD-dependent Bcl3 activation. Nat Commun. 2014;5:3898.
50. Nowak MD, Sordillo EM, Gitman MR, Paniz Mondolfi AE. Coinfection in SARS-CoV-2 infected patients: Where are influenza virus and rhinovirus/enterovirus? J Med Virol. 2020;92(10):1699-700.
51. Chen N, Zhou M, Dong X, Qu J, Gong F, Han Y, et al. Epidemiological and clinical characteristics of 99 cases of 2019 novel coronavirus pneumonia in Wuhan, China: a descriptive study. Lancet. 2020;395(10223):507-13.
52. Rawson TM, Moore LSP, Zhu N, Ranganathan N, Skolimowska K, Gilchrist M, et al. Bacterial and Fungal Coinfection in Individuals With Coronavirus: A Rapid Review To Support COVID-19 Antimicrobial Prescribing. Clin Infect Dis. 2020;71(9):2459-68.

CHAPTER 5

ECTOPIC EXPRESSION OF CGAS IN SALMONELLA TYPHIMURIUM ENHANCES STING-MEDIATED IFN-β RESPONSE IN HUMAN MACROPHAGES AND DENDRITIC CELLS

Lieve E.H. van der Donk[2,3¶], Lisette Waanders[1,3,4¶], Louis S. Ates, Janneke Maaskant[1], John L. van Hamme[2,3], Eric Eldering[2,3,4,5,6], Jaco A.C. van Bruggen[2,3,4,5], Joanne M. Rietveld[2,3,4,5], Wilbert Bitter[1,3,7], Teunis B.H. Geijtenbeek[2,3#], Coenraad P. Kuijl[1,3,4#*]

[1] Amsterdam UMC location VUmc, Department of Medical Microbiology and Infection Control, De Boelelaan 1117, Amsterdam, The Netherlands;
[2] Amsterdam UMC location AMC, Department of Experimental Immunology, Meibergdreef 9, Amsterdam, The Netherlands;
[3] Amsterdam institute for Infection and Immunity, Infectious diseases, Amsterdam, The Netherlands;
[4] Cancer Center Amsterdam, Cancer Immunology, Amsterdam, The Netherlands;
[5] Amsterdam institute for Infection and Immunity, Cancer Immunology, Amsterdam, The Netherlands;
[6] The Lymphoma and Myeloma Center Amsterdam, LYMMCARE;
[7] Amsterdam Institute for Life and Environment, Vrije Universiteit, Amsterdam, The Netherlands

¶ LEHvdD and LW contributed equally
# TBHG and CPK contributed equally
* Address correspondence and reprint requests to C.P. Kuijl, Amsterdam UMC, De Boelelaan 1117, 1081 HV, Amsterdam.

Journal for ImmunoTherapy of Cancer 2023, 11(4).

ABSTRACT

Background: Interferon-β (IFN-β) induction via activation of the Stimulator of Interferon Genes (STING) pathway has shown promising results in tumor models. STING is activated by cyclic dinucleotides, such as cGAMPs, that are produced by cyclic GMP-AMP synthetase (cGAS). However, delivery of STING pathway agonists to the tumor site is a challenge. Bacterial vaccine strains have the ability to specifically colonize hypoxic tumor tissues and could therefore be modified to overcome this challenge. Combining high STING-mediated IFN-β levels with the immunostimulatory properties of *Salmonella typhimurium*, could have potential to overcome the immune suppressive tumor microenvironment.

Methods: We have engineered *S. typhimurium* to produce cGAMP by expression of cGAS. The ability of cGAMP to induce IFN-β and its interferon-stimulating genes was addressed in infection assays of THP-I macrophages and human primary dendritic cells (DCs). Expression of catalytically inactive cGAS is used as a control. DC maturation and cytotoxic T cell cytokine and cytotoxicity assays were conducted to assess the potential anti-tumor response *in vitro*. Finally, by making use of different *S. typhimurium* type III secretion (T3S) mutants, the mode of cGAMP transport was elucidated.

Results: Expression of cGAS in *S. typhimurium* results in a 87-fold stronger IFN-β response in THP-I macrophages. This effect was mediated by cGAMP production and is STING dependent. Interestingly, the needle-like structure of the T3S system was necessary for IFN-β induction in epithelial cells. DC activation included upregulation of maturation markers and induction of type I IFN response. Co-culture of challenged DCs with cytotoxic T cells revealed an improved cGAMP mediated Interferon-γ (IFN-γ) response. In addition, co-culture of cytotoxic T cells with challenged DCs led to improved immune-mediated tumor B cell killing.

Conclusion: *S. typhimurium* can be engineered to produce cGAMPs that activate the STING pathway *in vitro*. Furthermore, they enhanced the cytotoxic T cell response by improving IFN-γ release and tumor cell killing. Thus, the immune response triggered by *S. typhimurium* can be enhanced by ectopic cGAS expression. This data shows the potential of *S. typhimurium*-cGAS *in vitro* and provides rationale for further research *in vivo*.

Keywords: Immunotherapy, *Salmonella typhimurium*, cGAS, STING, IFN-β, THP-I, dendritic cells, cytotoxic T cells

INTRODUCTION

In the last decade, various successful cancer therapies have been developed that are based on reactivation of the immune system. Many of these novel cancer immunotherapies aim to improve the capacity of T cells to kill tumor cells (1). Nevertheless, 13-87% of patients show poor tumor sensitivity to such treatments depending on the type of cancer (2, 3). One of the reasons is that malignant, solid tumors promote an immune-suppressive microenvironment and are often characterized by an abnormal vascularization that restricts entry of therapeutics to the tumor site (4). To target and disrupt this poorly accessible immune-suppressive microenvironment is one of the greatest challenges in immunotherapy of solid tumors.

Bacterial immune therapies hold great potential in the treatment of solid tumors because of their natural properties (5). The immune-modulatory and metabolic characteristics of bacterial species, such as *Salmonella (S.) typhimurium*, allow them to penetrate deeply into tumor tissues and even preferentially replicate in this hypoxic environment (6). In addition, bacteria are recognized by the immune system as foreign and are therefore strong immune activators. Despite pre-clinical success, phase I clinical trial with *S. typhimurium* pointed out that the vaccine strain alone is not sufficient to cure the patient and requires optimization (7). Here, we investigated whether the immune-stimulating properties of *Salmonella* can be improved by ectopic expression of cyclic GMP-AMP synthetase (cGAS).

The enzyme cGAS is a cytosolic surveillance protein that detects double-stranded DNA (dsDNA) (8, 9). Normally, there is no dsDNA present in the cytosol of healthy mammalian cells, but this can be introduced by viruses, bacteria or dead cells. Upon recognition, mammalian cytosolic cGAS synthesizes cyclic GMP-AMP dinucleotides with phosphodiester linkages 2′-5′ and 3′-5′ (cGAMPs) (10-14). These dinucleotides function as second messengers to activate stimulator of interferon genes (STING), which in turn leads to a signaling cascade that induces interferon-β (IFN-β) (8, 15). IFN-β is part of the large type I IFN family and binds to the IFNα/β receptor (IFNAR) in an autocrine manner, thereby inducing hundreds of IFN-stimulated genes (ISGs).

Notably, IFN-β and ISGs have become of great interest in the field of oncology as their expression is strongly correlated to an anti-tumor immune response (16). IFN-β has shown to enhance antigen-presenting capacity of dendritic cells (DCs) and macrophages as well as cross-priming of cytotoxic $CD8^+$ T cells (CTLs) (17-19). In addition, IFN-β and ISGs are also associated with improved natural killer (NK) cytotoxicity and have a synergistic tumor-suppressive effect in combination with other

therapies such as radiotherapy (16, 20-22). STING agonist 5,6-Dimethylxanthenone-4-acetic-acid (DMXAA) was successfully used to treat tumor-harboring mice in pre-clinical models (23-26). However, it was found that, due to structural differences between murine STING and human STING, DMXAA showed poor results in phase III trials (22, 27-29). Since then, various human-specific STING agonists have been discovered and potentiated for the clinic. Unfortunately, the use of STING agonists in patients is limited by the need to locally administer these medications directly into tumor tissues. There is an urgent need to develop innovative targeting strategies.

Here, we investigated whether *S. typhimurium* can be engineered to activate the STING pathway, thereby combining its hypoxic colonization with its inherent immune-stimulatory capacity as well as the induction of type I IFN required for anti-tumor responses. We engineered *S. typhimurium* to ectopically express murine cGAS, which led to the production of the natural STING agonist cGAMP. A functional needle of the type III secretion (T3S) system was required to inject cGAMPs into host cells. Notably, infection of THP-I macrophages with the cGAS-engineered bacteria induced a strong type I IFN response in a STING dependent manner. Moreover, infection of human primary dendritic cells (DCs) with cGAS-engineered *S. typhimurium* induced DC maturation a well as cytotoxic $CD8^+$ T cell (CTL) responses. These data strongly suggest that ectopic expression of cGAS in *S. typhimurium* could be an effective way to induce intratumor type I IFN responses leading to effective immune activation and subsequent elimination of the tumor.

MATERIALS AND METHODS

Cell lines

All THP-I cell lines were cultured in Rosewell Park Memorial Institute-1640 medium, glutaMAX (RPMI-1640, ThermoFisher), supplemented with 10% fetal bovine serum (FBS, Gibco Life Technologies) and 1% penicillin/streptomycin (Gibco Life Technologies). THP-I, harboring an IFN-β promoter-GFP-Firefly-Luciferase reporter, was obtained from Jan Rehwinkel (University of Oxford) and THP-I single clone $SLC19A1^{-/-}$ cells were a kind gift from David Raulet (University of California) (30). HeLa cells, kindly provided by David Holden (Imperial College London), were cultured in Dulbecco's Modified Eagle's, Medium glutaMAX (DMEM, Lonza), supplemented with 10% FBS and 1% penicillin/streptomycin. JeKo-1 B cells were cultured in RPMI-1640 supplemented with 10% fetal calf serum (FCS, Trinity Tek) and 1% penicillin/streptomycin. All cell lines were kept at 37°C 5.0% CO_2.

Primary cells

This study was approved by the institutional review board of the Amsterdam University Medical Centers, location University of Amsterdam Medical Ethics Committee and the Ethics Advisory Body of Sanquin Blood Supply Foundation (Amsterdam, Netherlands). We used buffy coats donated by healthy volunteer donors, obtained in accordance with the ethical principles set out in the declaration of Helsinki. Human $CD14^+$ monocytes were isolated from buffy coats and subsequently differentiated into monocyte-derived DCs as described before (31). In brief, the isolation from buffy coats was performed by density gradient centrifugation on Lymphoprep (Nycomed) and Percoll (Pharmacia). After separation by Percoll, the isolated monocytes were cultured in RPMI-1640 (Gibco) supplemented with 10% FCS, 2mM L-glutamin (Invitrogen) and 1% penicillin/streptomycin, containing the cytokines IL-4 (500 U/mL) and GM-CSF (800 U/mL) (both Gibco) for differentiation into DCs. The peripheral blood lymphocyte (PBL) fraction was processed and stored at -80°C. After 4 days of differentiation, DCs were seeded at $1x10^6$/mL in antibiotic-free RPMI-1640 in a 96-well plate (Greiner), and after 2 days of recovery, DCs were stimulated or infected as described below.

Bacteria

All *S. typhimurium* wildtype and mutant strains were cultivated in Lucia Broth growth medium (LB) at 37°C and kept shaking at 200rpm (32). *S. typhimurium* SL1344 Salmonella wildtype SB300, SL1344 Δ*invG* SB161 (referred in manuscript as SL1344 $SPI\text{-}1_{KO}$), SL1344 Δ*sseD::aphT* M556 (referred as SL1344 $SPI\text{-}2_{KO}$) and SL1344 Δ*sseD::aphT sopBEE2* M716 (referred as SL1344 $SPI\text{-}2_{NEEDLE}$) were kindly provided by Wolf-Dietrich Hardt (ETH Zürich) (33). All *S. typhimurium* strains were transformed via electroporation using gene pulser cuvettes (BioRad) and Eporator (Eppendorf) at 1700V. *S. typhimurium* 1344 and SL3261 were transformed with pAbcon Flag-hcGAS-mCherry, pMW215 HA-cGAS-mScarlet or pMW215 HA-$cGAS_{AA}$ and were grown in LB under continuous antibiotic selection with 0.03µg/mL Chloramphenicol (Sigma) for pABCON constructs or 0.1µg/mL ampicillin sodium salt (Sigma) for pMW215 constructs.

Immunoblot analysis

Expression of proteins was verified by loading bacterial lysates resuspended in sample buffer (50 mM Tris-HCl, 100 mM dithiothreitol (DTT), 2% sodium dodecyl sulphate (SDS), 5 mM ehtylenediaminetetraacetic acid (EDTA), 10% glycerol) on 10% SDS page gel (figure 1A) or 12.5% SDS page gel (supplement 3+4). Western blot was used to visualize proteins by using α-Ha.11 Monoclonal Mouse IgG1 clone 16B12 (Biolegend) or Monoclonal Mouse α-Flag clone M2 (Sigma) and the loading control Polyclonal Rabbit

α-TatB (a kind gift from Matthias Müller, Albert-Ludwigs-Universität Freiburg). Goat-anti-mouse or goat-anti-rabbit IgG peroxidase-labelled antibodies (American Qualex Antibodies, San Clemente, USA) were used as secondary antibodies and detected with electro-chemi-luminescence Western Blotting Detection Reagent (Amersham Bioscience, Amersham, UK).

Gentamycin protection assay

Gentamycin protection assay was conducted and analyzed according to protocol Hapfelmeier *et al*. (33). In short, HeLa cells were exposed to bacteria for 10 minutes at 37°C 5% CO_2. Infection stocks were plated to determine input colony forming units (CFU). After infection, cells were washed 3 times with HBSS ($CaCl_2$ 0.14g/L, KCl 0.4g/L, KH_2PO_4 0.06g/L, $MgSO_4$ 0.098 g/L, NaCl 8g/L, Na_2HPO_4 0.048g/L, $NaHCO_3$ 0.35g/L and glucose 1g/L). DMEM supplemented with 10% FBS was added to cells for 20 minutes. Afterwards the medium was replaced with DMEM supplemented with 10% FBS and 100µg/mL gentamycin (Gibco) and incubated for 30 minutes. After one wash (PBS, CaCl2 0.1g/L, MgCl2 x $6H_2O$ pH7.4 0.1g/L), cells were lysed with 0.2g sodium deoxycholate in water. Output CFU plates were made and invasiveness was calculated normalized to wildtype of 2 independent experiments, conducted in duplicate.

Macrophage and DC infections

THP-I cells were seeded and differentiated for 24 hours with 25ng/mL Phorbol 12-myristate 13-acetate (PMA, Sigma). After 24 hours, medium was replaced with RPMI-1640 with 10% FBS and kept for 48 hours in incubator prior to infection. *S. typhimurium* infection stocks were prepared from overnight cultures in LB of which 1:33 was added to RPMI supplemented with 10% FBS the following day. Strains were kept at 37°C 200 rpm until they reached the exponential phase. Macrophages and DCs were infected with a multiplicity of infection (MOI) 30 and incubated for 30 minutes at 37°C 5.0% CO_2. Extracellular bacteria were removed from THP-I macrophages by a single wash with PBS, followed by 1 hour incubation in RPMI-1640 supplemented with 10% FBS and 100µg/mL gentamycin (Gibco). Afterwards, medium was replaced with RPMI-1640 supplemented with 10% FBS and 10µg/mL gentamycin and kept in incubator at 37°C 5.0% CO_2 until the time of measurement or processing. Extracellular bacteria were removed from DC cultures by a single wash with PBS followed by addition of RPMI-1640 10% FCS and 10µg/mL gentamycin and kept in incubator at 37°C 5.0% CO_2. A lipopolysaccharide (LPS)-only control was included to help distinguish between TLR4-induced IFN-β production and cGAS/STING-induced IFN-β production. For this, THP-I macrophages and DCs were stimulated with 10ng/mL LPS from *S. typhimurium* (Sigma). Bacterial input was determined by spotting bacterial suspension and counting of CFU on LB agar plates.

Cytotoxic T lymphocyte responses – cytokine production

DCs were infected with SL3261 mcGAS or SL3261 mcGAS$_{AA}$ for 30 minutes, spun down and medium was replaced with RPMI-1640 supplemented with 10% FCS and 100µg/mL gentamycin. Next, the stimuli LPS or cGAMP (10µg/mL, Invitrogen) were added to the corresponding wells. The cGAMPs were incubated with transfection reagent Lyovec (Invivogen) according to manufacturer's instructions to ensure intracellular delivery of the cGAMPs prior to adding to DCs. After 16 hours incubation, DCs were co-cultured with allogeneic PBLs in Iscove's Modified Dulbecco's Media (IMDM, Gibco) supplemented with 10% FCS and 1% penicillin/streptomycin, using a 1:8 ratio. As a positive control, T cells were stimulated with plate-bound anti-CD3 and anti-CD28 (Biolegend). After 3 days, IL-2 (20 U/mL, Chiron) was added to the co-cultures. After 6 days, PBLs were harvested, plated in 96-well plates, and incubated for 4 hours with Brefeldin A (10 µg/mL, Sigma), after which they were analyzed for cytokine production by flow cytometry as described below.

Cytotoxic T cell killing assay

Co-cultures of DCs and PBLs were performed as described above. After 6 days of co-culture, CD19-expressing JeKo-1 B cells were labelled with Cell Trace Violet (CTV) (ThermoFisher Scientific) according to the manufacturer's instructions. Stimulated PBLs were harvested, counted, and subsequently co-cultured for 16 hours with CTV$^+$ JeKo-1 B cells in an effector to target ratio of 4:1. The CD19-targeting bispecific T-cell engager Blinatumomab (34) (a kind gift from Eric Eldering) was added in concentrations ranging from 0-100 pg/mL where indicated. Viability of the JeKo-1 B cells was assessed using TO-PRO-3 and Mito-Tracker Orange (Invitrogen) using flow cytometry. Specific cell death of the JeKo-1 B cells was assessed by gating the live cells (TO-PRO-3 negative and Mito-Tracker Orange positive) within the CTV$^+$ population, and the percentage of specific target cell killing was subsequently calculated as 100 - the percentage of viable JeKo-1 B cells.

Real-time quantitative PCR analysis

THP-I and HeLa cells were harvested at 2.5 or 5 hours post infection. Isolation of mRNA was conducted with NucleoSpin kit (Machery-Nagel) or mRNA Catcher PLUS Purification kit (ThermoFisher) according to protocol of manufacturer. Reverse transcriptase of mRNA to cDNA was conducted with RevertAid First Strand cDNA Synthesis kit (ThermoScientific) or with a reverse-transcriptase kit (Promega) according to protocol of manufacturer. An input of 30ng cDNA and total primer concentration of 0.06µM was used per reaction. SYBR Green Master Mix (BioRad) and white 96-well PCR plates, semi-skirted (Applied Biosystems) were used in StepOne Real-Time PCR System (Applied Biosystems). Alternatively for data in figure 2 and 4, PCR amplification was performed in the presence of SYBR green (ThermoFisher), primers and cDNA in a 7500 Fast Realtime PCR System (ABI). Comparative delta Ct method was used to determine relative expression levels.

Flow cytometry

To measure DC activation markers, cells were fixated for 30 minutes with 4% paraformaldehyde (PFA, Electron Microscopy Sciences). For cell surface staining, cells were incubated in 0.5% PBS-BSA (Sigma-Aldrich) containing antibodies for 30 minutes at 4°C. To measure CTL responses, PBLs were harvested and stained for viability using Fixable Viability Dye eFluor™ 780 (eBioscience) for 5 minutes at 4°C, and subsequently fixated for 10 minutes with 2% PFA. After fixation, cells were permeabilized using Perm/Wash solution (BD Biosciences) for 5 minutes at 4°C and incubated with antibodies diluted in Perm/Wash solution for 10 minutes at 4°C. Single cell measurements were performed with a FACS Canto flow cytometer (BD Biosciences). FlowJo V10 software was used to analyze the data. Antibody clones used to analyze DC activation are: CD86 (2331 (FUN-1)), CD80 (L307.4), CD83 (HB15e) (all BD Pharmingen). For each experiment, live cells were gated on FSC and SCC and analyzed further with the markers mentioned. Antibody clones used for cytotoxic T cell responses are: CD3 (UCHT1), CD8 (RPA-T8), IFNγ (B27) (all Biolegend), Perforin (dG9, eBioscience) and Granzyme B (GB11, BD Pharmingen). For each experiment, live cells were selected, and gated on CD3 and CD8 expression. In this $CD3^+CD8^+$ population, cytokine expression was analyzed.

ELISA

Overnight cultures of SL1344 mcGAS and SL1344mcGAS$_{AA}$ were continued by taking 1 optical density (OD) and added to 10mL MgM-MES pH7.4 (170mM MES, 5mM KCl, 7.5mM $(NH_4)_2SO_4$, 0.5mM K_2SO_4, 1mM KH_2PO_4, 8μM $MgCl_2(6xH_2O)$, 38mM Glycerol, 0.1% Casamino acids) supplemented with antibiotics until cultures reached again ~OD 1. Bacteria were pelleted for 10 minutes at 5000 rpm and supernatant was taken for cGAMP measurement according to 2'3'-cGAMP ELISA Kit manufacturer (Cayman chemical). THP-I and DC supernatants were harvested 18-24 hours after stimulation and secretion of IFN-β was measured by a Human IFN-beta DuoSet ELISA (R&D Systems) according to the manufacturer's instructions.

Growth curves

Bacterial OD600nm was measured by using a BioTek Synergy. A bacterial suspension of $OD600_{nm}$ 0.05 in LB with appropriate antibiotics was used as input. Bacteria were incubated at 37°C, linear shaking. LB background was subtracted from $OD600_{nm}$ values.

Constructs and oligo's

Supplement 1.

RESULTS

Murine cGAS in *S. typhimurium* induces IFN-β production in macrophages

The cytoplasmic dsDNA sensor cGAS synthesizes cGAMPs (8, 10, 12-15). Although both human and murine cGAS produce cGAMPs, they differ in dsDNA recognition. Human cGAS (hcGAS) is more selective as it is only activated by long dsDNA, while murine cGAS (mcGAS) is more sensitive (35). To investigate which mammalian cGAS is most efficient in inducing IFN-β in the host, both were introduced in *S. typhimurium* strain SL1344. Human Flag-cGAS and murine HA-cGAS were cloned in pAbcon and pMW215, respectively. Both cGAS proteins were efficiently expressed in *S. typhimurium* SL1344 (Figure 1A). Expression of neither hcGAS nor mcGAS affected bacterial growth as growth curves of transformed SL1344 were similar to SL1344-wildtype (Figure 1B). Interestingly, whereas expression of hcGAS did not show a significant effect, infection of the human macrophage cell line THP-I with SL1344-mcGAS induced on average 87-fold more IFN-β than SL1344-wildtype (Figure 1C). Next, we determined the amount of cGAMPs produced by SL1344-mcGAS (Figure 1D, supplemental 2). We used a double point mutation in the catalytic site of mcGAS (mcGAS$_{AA}$) as negative cGAMP control (Supplemental 3) (8). Notably, SL1344-mcGAS shows a 39-fold higher increase in cGAMP production than SL1344-mcGAS$_{AA}$. Collectively, these data strongly suggest that mcGAS expressed in *S. typhimurium* is well tolerated, produces high amounts of cGAMPs and induces an IFN-β response in infected macrophages.

mcGAS-mediated IFN-β expression is STING dependent

As SL1344-mcGAS produce cGAMPs and induce strong IFN-β expression, we investigated the role of STING by infecting THP-I wildtype and THP-I STING$^{-/-}$ macrophages. Macrophages were infected with either SL1344-mcGAS or SL1344-mcGAS$_{AA}$ and type I IFN responses were measured by RT-qPCR (Figure 2A,B) and ELISA (Figure 2C). Stimulation of THP-I with LPS showed no significant effect on IFN-β mRNA levels as compared to uninfected control, indicating that LPS alone does not induce a strong IFN-β response in THP-I macrophages. In contrast, SL1344-mcGAS showed a 100-fold increase of IFN-β mRNA expression compared to mcGAS$_{AA}$ at both time points. Therefore, we conclude that the enzymatic activity of mcGAS is responsible for IFN-β induction in SL1344-mcGAS. IFN-β production was fully abrogated in the THP-I STING$^{-/-}$ macrophages. These results were confirmed on protein level in an IFN-β ELISA (Figure 2C). Although IFN-β protein levels were not statistically different, THP-I infected macrophages with SL1344-mcGAS induced an average 6.1-fold increase compared to SL1344-mcGAS$_{AA}$. Again, THP-I STING$^{-/-}$ infected macrophages did not show a difference between SL1344-mcGAS and SL1344-mcGAS$_{AA}$. Next, we investigated the induction of ISG Interferon Regulatory Factor (IRF7) and ISG15 to verify that a functional IFN-β

response was induced (Figure 2D, E). SL1344-mcGAS infection of wildtype, but not THP-I STING$^{-/-}$ macrophages, led to a significant induction of both IRF7 (average 3-fold) and ISG15 (average 12.7-fold) in contrast to infection with SL1344-mcGAS$_{AA}$. These data strongly suggest that cGAMP produced by SL1344-mcGAS induces STING-dependent type I IFN responses in THP-I macrophages.

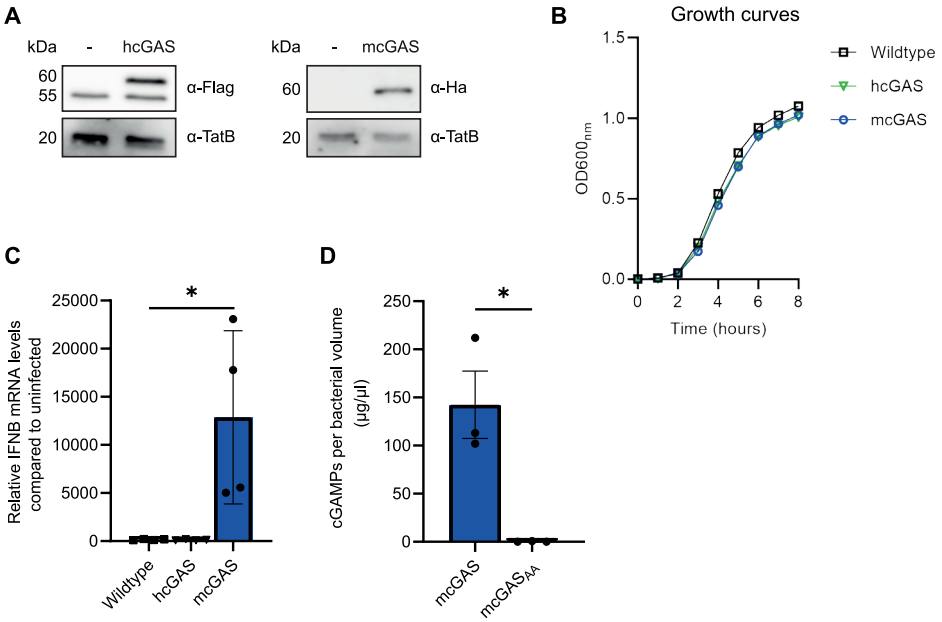

Figure 1: Expression of mcGAS in SL1344 induces IFN-β expression in a human macrophage cell line. (A) Protein expression of SL1344 transformed with pABCON Flag-hcGAS (60.2kDa) or pMW215 Ha-mcGAS (59.6 kDa) verified with Western blot. Equal loading was detected with α-TatB. (B) SL1344 wildtype, SL1344 hcGAS and SL1344 mcGAS growth curves in LB. (C) THP-I cells were infected with SL1344 wildtype, SL1344 hcGAS and SL1344 mcGAS. IFN-β mRNA levels are determined by qRT-PCR 2.5 hours after infection. IFN-β Levels are relative to uninfected THP-I. IFN-β levels: SL1344-wildtype mean 147.7 SEM 28.3; SL1344-mcGAS mean 12859, SEM 4499. Statistics: One-way ANOVA, corrected for multiple comparisons, error bars: SEM *p≤0.05. (D) Production of cGAMPs by SL1344 mcGAS and SL1344 mcGAS$_{AA}$ quantified. Concentration cGAMPs in bacterial pellets are corrected for OD unit input and bacterial volume. cGAMP levels: SL1344-mcGAS mean 142.3, SEM 35.0; SL1344-mcGAS$_{AA}$ mean 0.29, SEM 0.23. Statistics: unpaired *t*-test, error bars: SEM. p=0.12.

cGAMPs are transported through SPI-1 needle

In order to induce the STING pathway, cGAMPs should be in the cytosol of the host cell. We therefore set out to determine the molecular mechanism of cytosolic cGAMP delivery by SL1344-mcGAS. Several cyclic dinucleotide transporters have been identified of which mammalian folate carrier SLC19A1 has been shown to be important

in extracellular cGAMP uptake by THP-I cells (30, 36). To determine if SLC19A1 is involved in cGAMP uptake, we infected THP-I wildtype and THP-I SLC19A1$^{-/-}$ single clones with SL1344-mcGAS and SL1344-mcGAS$_{AA}$. No statistical differences in IFN-β mRNA levels were observed between the THP-I SLC19A1$^{-/-}$ and wildtype macrophages after 5 hours of infection, indicating that SLC19A1 is not the principal transporter responsible for cGAMP transport into the cytoplasm (Figure 3A).

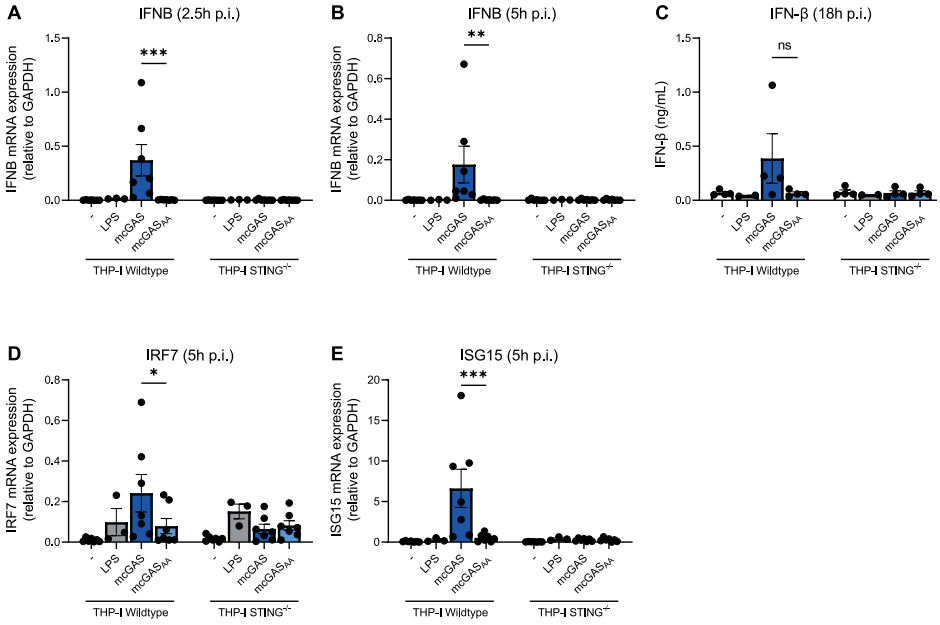

Figure 2: IFN-β induction by mcGAS is mediated via cGAMPs and STING.

(A-B) THP-I wildtype or THP-I STING$^{-/-}$ were exposed to LPS, SL1344 mcGAS and SL1344 mcGAS$_{AA}$. Samples were analyzed 2.5 hours and 5 hours post infection (p.i.) with qRT-PCR. 2.5 hours: SL1344-mcGAS mean 0.37, SEM 0.15; SL1344-mcGAS$_{AA}$ mean 0.0037, SEM 0.00094; 5 hours: SL1344-mcGAS mean 0.18, SEM 0.09; SL1344-mcGAS$_{AA}$ mean 0.0017, SEM 0.0009. (C) IFN-β protein expression in the supernatant of different conditions is determined 18 hours post infection: SL1344-mcGAS mean 0.39, SEM 0.23; SL1344-mcGAS$_{AA}$ mean 0.063, SEM 0.015. (D) IRF7 mRNA expression 5 hours post infection: SL1344-mcGAS mean 0.24, SEM 0.09; SL1344-mcGAS$_{AA}$ mean 0.08, SEM 0.04. (E) ISG15 mRNA expression in THP-I 5 hours post infection: SL1344-mcGAS mean 6.63, SEM 2.36; SL1344-mcGAS$_{AA}$ mean 0.52, SEM 0.18. Statistics: 2-way ANOVA, Tukey's multiple comparison test, error bars: SEM *p≤0.05, **p≤0.005, ***p≤0.0005.

To test whether bacterial transporters are important for STING activation, we used mcGAS expressing T3S *Salmonella* mutants to infect HeLa cells (33). Unlike macrophages, HeLa cells can only be invaded by *S. typhimurium* using the T3S

systems encoded by the Salmonella pathogenicity island 1 (SPI-1). The T3S systems form a needle-like structure that inject bacterial effectors in host cells (37). A second T3S system encoded by SPI-2 is important for intracellular survival by maintaining the Salmonella containing vacuole (SCV) (37). To study the role of the T3S systems on IFN-β induction, we made use of four strains: wildtype Salmonella (SL1344), a SPI-1 mutant (SL1344 *SPI-1*$_{KO}$), a SPI-2 mutant (SL1344 *SPI-2*$_{KO}$), and a SPI-1 mutant lacking secreted effectors required for invasion, yet having a functional needle (SL1344 *SPI-1*$_{NEEDLE}$) (33) (Figure 3B). We verified bacterial invasion of these T3S system mutants. As expected, SL1344 *SPI-1*$_{KO}$ and SL1344 *SPI-1*$_{NEEDLE}$ CFU counts were strongly reduced by the gentamycin treatment, whereas both wildtype and the *SPI-2*$_{KO}$ where protected due to their intracellular localization (Figure 3C). In parallel, the IFN-β expression was determined in infected HeLa cells (Figure 3D). SL1344 *SPI-2*$_{KO}$ mcGAS induced similar IFN-β levels to wildtype mcGAS, indicating that SPI-2 T3S machinery is not necessary for IFN-β induction. However, SL1344 *SPI-1*$_{KO}$ showed reduced IFN-β expression, demonstrating that SPI-1 is required for STING-pathway activation. Notably, SL1344 *SPI-1*$_{NEEDLE}$ showed similar IFN-β induction as wildtype mcGAS, strongly suggesting that the SPI-1 T3S needle facilitates cGAMP transport from the bacterium to the host.

Expression of mcGAS in auxotrophic *S. typhimurium* SL3261 strengthens IFN-β production by primary human dendritic cells

S. typhimurium SL1344 is a virulent strain and is therefore not applicable in a clinical setting. Therefore, we further investigated the potential of mcGAS in the live-attenuated vaccine strain SL3261. SL3261 is derived from SL1344 but is a histidine auxotroph due to a mutation in the *AroA* gene (32), making it a safe, self-limiting organism. Similar as to SL1344, SL3261 growth is unaffected by ectopic mcGAS expression (Supplemental 4). We compared the IFN-β response upon challenge with SL1344-mcGAS and SL3261-mcGAS in primary monocyte-derived DCs from healthy donors (Figure 4A). DCs were exposed to LPS, SL1344-mcGAS, SL1344-mcGAS$_{AA}$, SL3261-mcGAS and SL3261-mcGAS$_{AA}$. After 5 hours incubation, the cells were lysed and the expression of IFN-β was determined by qRT-PCR. Both SL1344 and SL3261 strains expressing mcGAS, showed a significant increase in IFN-β expression in DCs as compared to their respective catalytically inactive mcGAS$_{AA}$ controls. These data indicate that both the virulent and non-virulent *Salmonella* strains with mcGAS expression, induce IFN-β expression in human primary DCs.

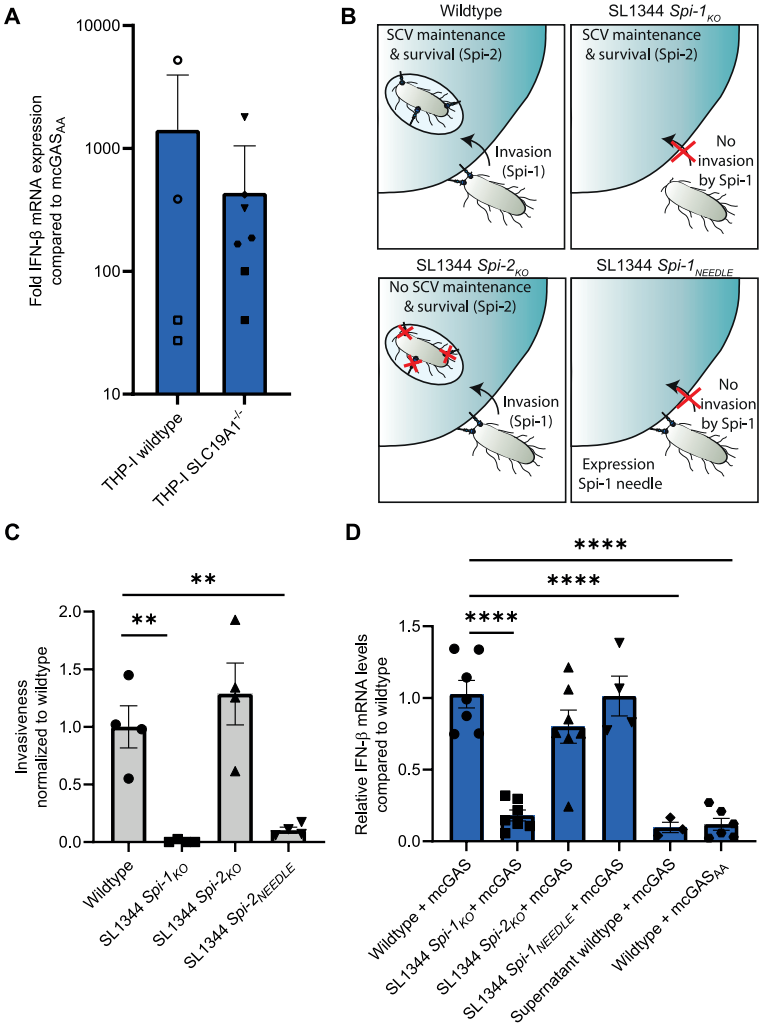

Figure 3: *Salmonella* produces cGAMPs that are injected into host cells by SPI-1.

(A) IFNB expression levels of THP-I SLC19A1$^{-/-}$ single clones compared to THP-I wildtype 2.5 hours p.i. with SL1344 mcGAS or SL1344 mcGAS$_{AA}$. Results of each THP-I control or SLC19A1$^{-/-}$ single cell clone is indicated with a similar symbol. (B) Overview of SL1344 SPI-1 or SPI-2 mutants. SL1344 wildtype has functional SPI-1 and SPI-2 T3S which enables the bacterium to invade the host and to survive within the Salmonella containing vacuole (SCV). SL1344 *SPI-1$_{KO}$* is a functional SPI-1 knock out and cannot invade host cells. SL1344 *SPI-2$_{KO}$* is a functional SPI-2 knock out, it can invade but cannot maintain its presence in SCV. SL1344 *SPI-1$_{NEEDLE}$* has the SPI-1 needle, but does not have the effector proteins that are necessary to invade the host. (C) Verification of invasiveness with gentamycin protection assay of SL1344 T3S mutant strains in HeLa. (D) IFNB levels measured by qRT-PCR 2.5 hours after challenge of HeLa cells. IFN-β levels of different conditions are normalized to wildtype-mcGAS. Filtered supernatant of SL1344 mcGAS and SL1344 mcGAS$_{AA}$ are included as control. Statistics: One-way ANOVA, corrected for multiple comparisons, error bars: SEM **p≤0.005 ****p≤0.0001.

Due to the clinical relevance of SL3261, we continued with SL3261 and determined the IFN-β production on protein level by ELISA. These data confirmed that SL3261-mcGAS induced significantly higher levels of IFN-β than LPS or mcGAS$_{AA}$ (Figure 4B). Next, IRF7 and ISG15 expression levels were measured (Figure 4C, D). A trend was observed for IRF7 between SL3261-mcGAS and SL3261-mcGAS$_{AA}$ and a significant 2-fold higher ISG15 expression is seen in SL3261-mcGAS infected cells. This modest, but significant, difference could possibly be attributed to LPS triggering of TLR4 on primary DCs. Indeed, both LPS and SL3261-mcGAS$_{AA}$ induced a strong but short IFN-β pulse, whereas SL3261-mcGAS induced a stronger and sustained IFN-β expression pattern (Supplemental 5, Figure 4A). Furthermore, SL3261-mcGAS induced significantly higher upregulation of the proinflammatory cytokine IL-1β compared to the catalytically inactive control (Figure 4E). We also determined the expression of the co-stimulatory molecules CD80 and CD86, and maturation marker CD83 by flow cytometry (Figure 4F, G). In this assay, all strains and mutants induced similar levels of CD80 and CD86, which was comparable to the response to LPS. CD83 expression was significantly lower on DCs when infected with either SL3261-mcGAS or SL3261-mcGAS$_{AA}$. Together, these data show that the vaccine strain activates DCs but immunomodulatory properties are further strengthened by mcGAS expression.

SL3261-mcGAS mediated IFN-β production by DCs induces potent cytotoxic T cell responses

Next, we investigated whether DC activation by SL3261-mcGAS is functional with regard to the induction of CTLs. CTLs are crucial players in anti-tumor immunity, which can increase their cytotoxic function when exposed to proinflammatory stimuli such as IFN-β (18). We exposed DCs to LPS, cGAMP, SL3261-mcGAS and SL3261-mcGAS$_{AA}$ and co-cultured these with allogeneic PBLs to analyze their capacity to activate CTLs. After 6 days of co-culture, the cytokine production by CD3^{+}CD8^{+} T cells was determined (Figure 5A-B). LPS or cGAMP-exposed DCs did not significantly increase interferon-γ (IFN-γ) production in CTLs in the co-culture as compared to unstimulated DCs. However, DCs infected with SL3261-mcGAS induced significantly higher IFN-γ levels in CTLs than DCs exposed to SL3261-mcGAS$_{AA}$ (Figure 5C). Interestingly, this difference could be complemented by transfecting cGAMPs into mcGAS$_{AA}$-infected DCs. A similar trend was observed in CTLs for perforin and granzyme B expression levels; incubation of DCs with SL3261-mcGAS led to a slightly higher increase of perforin and granzyme B CTLs as compared to incubation with SL3261-mcGAS$_{AA}$ control (Figure 5D-E). Addition of cGAMP rescued the effect in DCs treated with SL3261-mcGAS$_{AA}$. Interestingly, neither LPS nor CD3/CD28 stimulation induced the expression of perforin or granzyme B as in SL3261-mcGAS, suggesting that DCs infected with SL3261-mcGAS are more efficient in inducing CTL activation. These data suggest that although *S. typhimurium* already induces CTL activation, mcGAS expression further increases the ability of DCs to stimulate the IFN-γ CTL response.

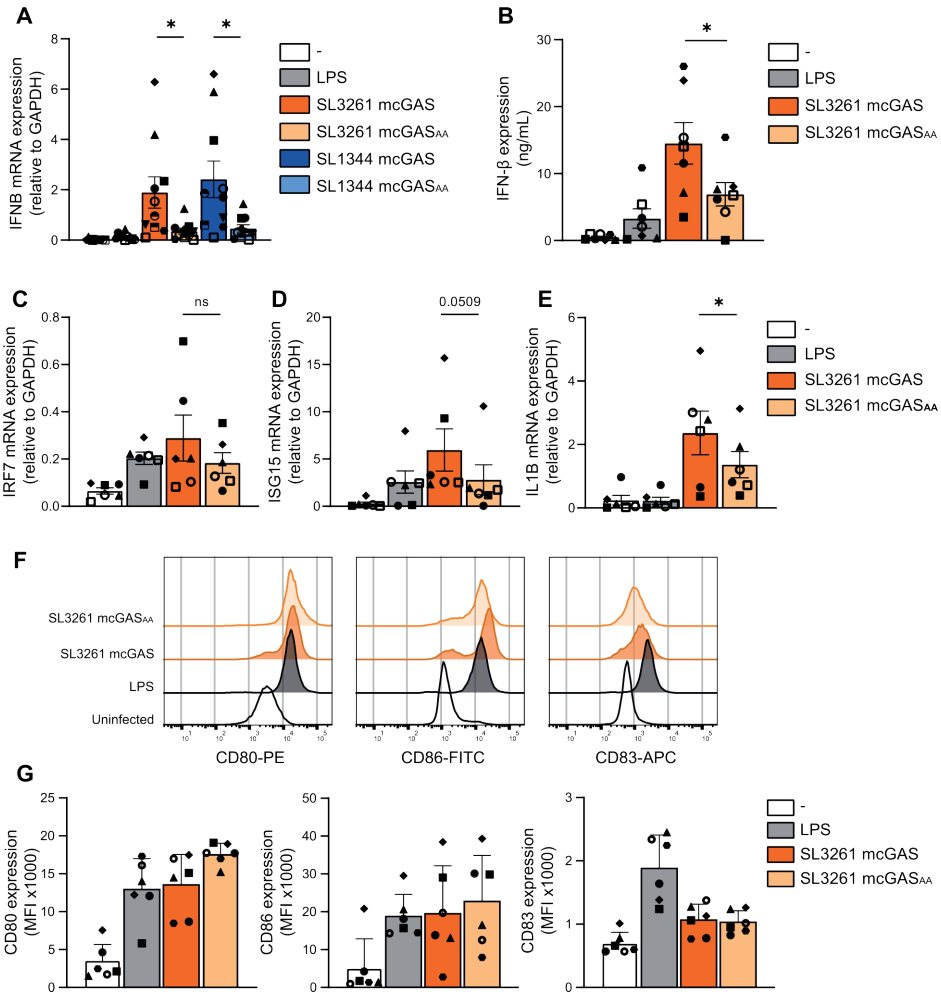

Figure 4: Expression of mcGAS in SL3261 induces IFN-β expression in primary human dendritic cells.

DCs were exposed to LPS, SL1344 mcGAS, SL1344 mcGAS$_{AA}$, SL3261 mcGAS, and SL3261 mcGAS$_{AA}$. Samples were analyzed 5 hours and 18 hours post infection with qRT-PCR, or 24 hours post infection for protein production and maturation. (A-E) Expression levels of IFNB mRNA 5 hours p.i. (A), IFN-β protein 24 hours p.i. (B), IRF7 mRNA 18 hours p.i. (C), ISG15 mRNA 18 hours p.i. (SL3261-mcGAS mean 5.96, SEM 2.23; SL3261-mcGAS$_{AA}$ mean 2.81, SEM 1.58) (D), and pro-IL-1B mRNA 18 hours p.i. (E) were determined. (F) Representative histograms of CD80, CD86 and CD83 expression. (G) Cumulative flow cytometry data of CD80, CD86 and CD83 expression. Data represent 10 donors analyzed in 5 separate experiments (A), 6 donors analyzed in 3 separate experiments (B-E, G), with each symbol representing a different donor. Statistics: 2-way ANOVA, Tukey's multiple comparison test (A+G), paired student's *t*-test (B-E), error bars: SEM *p≤0.05, **p≤0.005, ***p≤0.0005. MFI = mean fluorescence intensity.

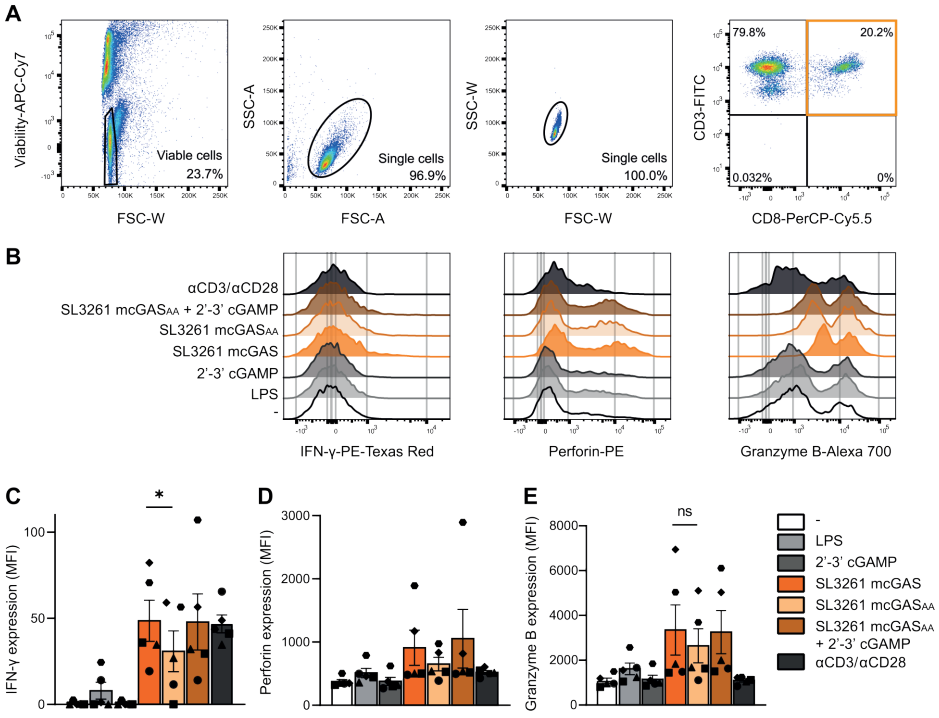

Figure 5: SL3261 mcGAS-mediated IFN-β production by DCs induces cytotoxic T cell responses.

(A-E) DCs were exposed to LPS, cGAMP, SL3261 mcGAS, SL3261 mcGAS$_{AA}$ or SL3261 mcGAS$_{AA}$ supplemented with 2'-3' cGAMP for 16 hours, and subsequently co-cultured with allogeneic human PBLs. (A) After 6 days of co-culture, the CD3$^+$ CD8$^+$ T cells were gated and analyzed for cytokine production by flow cytometry. (B) Representative histograms of IFN-γ, perforin and granzyme B expression. (C-E) Cumulative flow cytometry data of IFN-γ, perforin and granzyme B expression. Data represent 5 donors analyzed in 3 separate experiments, with each symbol representing a different donor. Statistics: Paired student's *t*-test, error bars: SEM. *p≤0.05. MFI = mean fluorescence intensity.

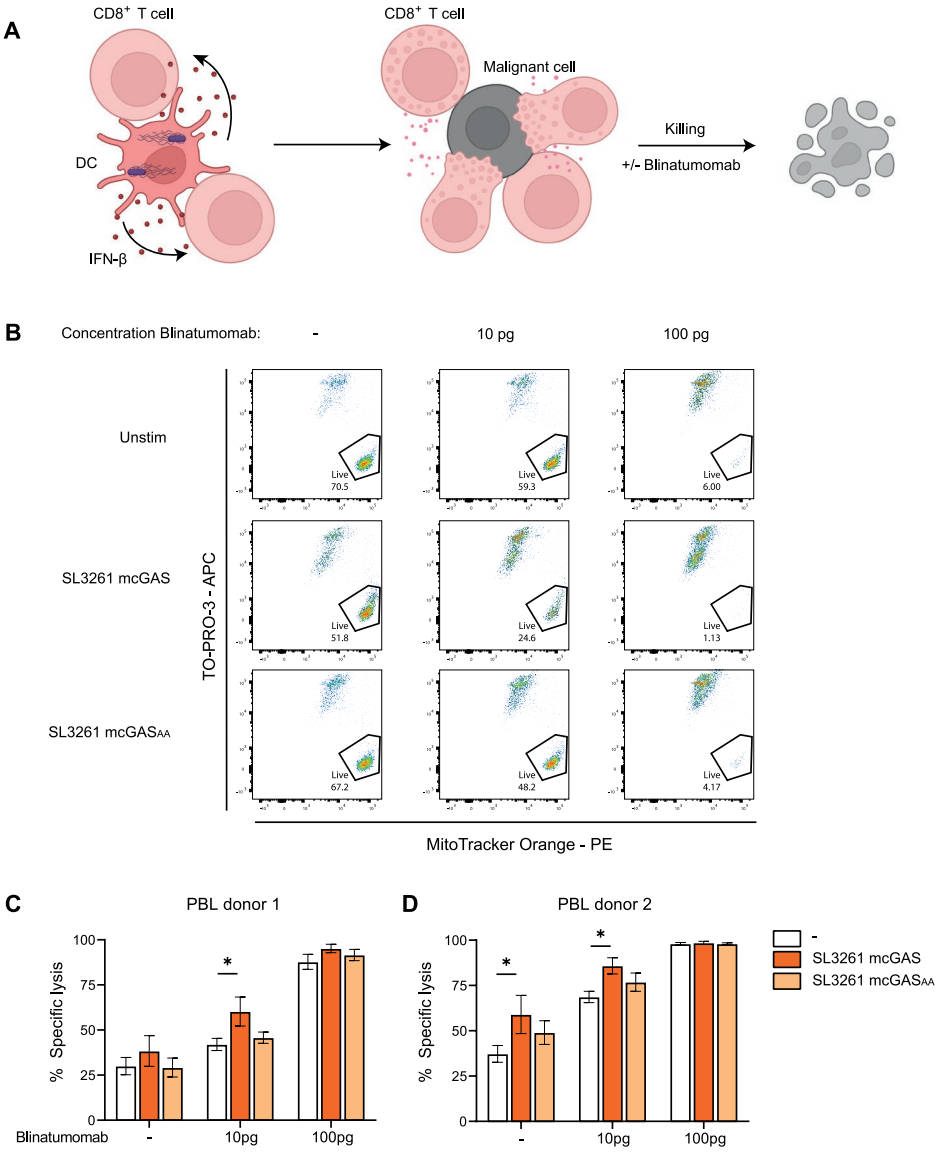

Figure 6: SL3261 mcGAS-mediated IFN-β production by DCs improves anti-tumor T cell responses.

(A) Graphical representation of the assay. DCs were exposed to medium, SL3261-mcGAS, or SL3261-mcGAS$_{AA}$ and subsequently co-cultured with allogeneic human PBLs. After 6 days of co-culture, the PBLs were harvested and counted, and co-cultured with CTV-labelled Jeko-1 B cells in a 4:1 effector to target ratio to assess cytotoxicity by flow cytometry. This figure was created with BioRender.com. (B) Representative dot plots of live/dead staining of CTV$^+$ B cells in co-culture with T cells. (C) Cumulative flow cytometry data of cell specific lysis. For PBL donor 1, data represent 5 DC donors analyzed in 3 separate experiments. For PBL donor 2, data represent 4 DC donors analyzed in 2 separate experiments. Statistics: two-way ANOVA, Tukey's multiple comparison test, error bars: SEM. *p≤0.05.

SL3261-mcGAS mediated IFN-β production by DCs enhances T cell capacity to kill malignant B cells

Next, we investigated whether SL3261-mcGAS activates DCs to enhance allogeneic $CD8^+$ T cell cytotoxicity towards tumor cells by a cytotoxic T cell killing assay (38). Infected DCs were co-cultured with allogeneic T cells, and activated T cells were subsequently co-cultured with CTV-labeled malignant Jeko-1 B cells. To overcome HLA-matching requirements, T and malignant B cells were co-cultured with the CD3-CD19 bispecific antibody (BsAb) Blinatumomab (Figure 6A). The BsAb is used in the clinic to reinvigorate T cell responses against B cell malignancies (34). To bring T and malignant B cells into close proximity without overriding the IFN-β effect mediated by DCs on T cells, we cultured them with low concentrations of activating Blinatumomab and cytotoxicity towards tumor cells was measured (Figure 6B, supplemental 6). Notably, in the absence of Blinatumomab or the presence at a low concentration, SL3261-mcGAS-DC-stimulated T cells were more cytotoxic towards malignant cells than those stimulated by SL3261-mcGAS$_{AA}$-infected or uninfected DCs. SL3261-mcGAS-induced IFN-β production by DCs activated T cells to more efficiently kill malignant tumor cells (Figure 6B-C). As expected, in the presence of a high concentration of Blinatumomab, all T cells became highly cytotoxic towards B cells irrespective of DC activation condition. These results strongly suggest that IFN-β production by DCs leads to the activation of T cells that are more cytotoxic towards malignant tumor cells.

DISCUSSION

The discovery of STING to be a major contributor to IFN-β levels, stimulated research into STING agonists for cancer treatment (39). The proinflammatory cytokine IFN-β has a large and diverse role in shaping the anti-tumor response, for example by promoting DC-antigen cross-presentation, inducing NK cytotoxicity and inhibition of tumor proliferation (16-18, 20). However, important limitations in STING agonists are the rapid enzymatic degradation, membrane impermeability and the insufficient delivery at the tumor site (39). Therefore, this study aimed to engineer *S. typhimurium* with ectopic mcGAS expression that have the potential to migrate to tumor tissues and activate the STING pathway locally. These strains might produce the STING agonist for several days, while synthetic STING agonists diffuse away or end up solely in immune cells.

Our study shows that *S. typhimurium*-mcGAS induce a strong, STING-dependent IFN-β response upon challenge of THP-I macrophages and primary human DCs. We hypothesized that expression of the cGAS enzyme in *S. typhimurium* would lead to constant cGAMP production because of the naked bacterial DNA. This has been

shown previously in an *E. coli* B21 (40). Interestingly, only murine and not human cGAS showed a striking IFN-β increase. Previously, it has been reported that mcGAS produces more cGAMPs and thereby trigger a stronger IFN-β response than hcGAS (8, 35). Activation of hcGAS is highly dependent on dsDNA length, which could explain suboptimal activity in our bacteria (9).

We have investigated the mode of transport of cGAMP from the bacteria into the host. The cGAMP molecule is negatively charged and therefore depends on transporters for cell entry. Several of these transporters have been reported (30, 36, 41). SLC19A1 has been identified as the dominant cyclic dinucleotide transporter in THP-I cells (30, 36). However, using SL1344-mcGAS on single cell THP-I SLC19A1$^{-/-}$ clones did not alter IFN-β induction compared to THP-I wildtype. Interestingly, we could show that cGAMPs are directly transported into the host cell via the via T3S needle. The non-invasive *S. typhimurium* strain with a functional SPI-1 needle, revealed the importance of this T3S system needle in cGAMP transport. Pathogenic Gram-negative bacterial pathogens commonly use the T3S system to modulate the host signaling processes (42-44). To our knowledge, this is the first time it has been shown that a small effector molecule like cGAMP, can be injected into host cells. It seems likely that these results could also be applicable to other small molecules. Indeed, transport of ADP-heptose, the ligand for the innate immune receptor ALPK1, is suggested to be partially mediated by T3S (45). The reverse transport of small molecules in a T3S-like manner, *e.g.* nutrient uptake from the host, has also been documented (46). These data add to the literature that T3S is highly versatile in function for that it can modulate the host not only by protein secretion, but also small molecules. This opens up possibilities for tailoring T3S expressing bacteria to deliver various types of molecules to the host through their secretion needle.

The potential of *S. typhimurium*-mcGAS is further supported by the observation that IFN-β expression is significantly induced in DCs upon challenge. IFN-β target gene expression of IRF7 and ISG15 both show a trend towards induction in the mcGAS samples compared to the inactive site mutant mcGAS$_{AA}$. The expression of the proinflammatory cytokine IL-1β was also increased upon SL3261-mcGAS challenge, this indicates that IL-1β expression is also stimulated upon sustained IFN-β signaling. Overall, a high variability is observed between DC donors which could be due to different responses to LPS. Strong responders can have high IFN-β or IFN-β target gene expression in mcGAS challenge. However, these donor cells tend also to respond more to mcGAS$_{AA}$ challenge than average. In our experiments, CD83 expression showed lower expression levels than the LPS only condition. This suggests active interference of *S. typhimurium* on CD83 activation, a phenomenon which has been described previously (47, 48). Importantly,

we find that SL3261-mcGAS is able to prime human DCs to activate CTL responses in primary human PBLs. Addition of cGAMPs could rescue $mcGAS_{AA}$ while cGAMP alone did not induce CTL responses. This suggests synergistic effect of *Salmonella* and cGAMP-mediated STING activation. In a cytotoxic T cell killing assay, we observed more killing of the B cell-line by $CD8^+$ T cells co-cultured with DCs infected by SL3261-mcGAS, whereas killing by $CD8^+$ T cells activated by DCs infected by SL3261-$mcGAS_{AA}$ was significantly lower and to the same level as $CD8^+$ T cells activated by unstimulated DCs. These data support our other data that indeed type I IFN responses induced by SL3261-mcGAS-infected DCs lead to a more efficient $CD8^+$ T cell activation as well as more cytotoxic capacity towards malignant tumor cells.

A limitation in our study is that we could only show the potential *in vitro* and not in an *in vivo* tumor model. To date, two other groups have used engineered bacteria to activate the STING pathway in a tumor mouse model and have shown promising results (49, 50). These studies indicate the potential of engineered bacterial strains to induce IFN-β as an immunotherapy. An important difference between these reported strains and *S. typhimurium*-mcGAS is that our engineered strains produces cGAMPs, instead of c-di-AMP. cGAMPs are the strongest endogenous STING activator molecules known to date (10, 13, 14). Furthermore, *S. typhimurium*-mcGAS can induce also IFN-β in non-immune cells, such as tumor cells, that could enhance tumor targeting by other immune cells, such as NK cells. Both features might lead to an even stronger anti-tumor immune response than the reported bacterial strains.

In conclusion, our results show that mcGAS expressing *S. typhimurium* are strong IFN-β inducers in human macrophage cell line THP-I and primary human DCs. This effect is STING dependent and relies on the T3S needle. Importantly, our *S. typhimurium*-mcGAS stimulates the CTL response *in vitro*, thereby providing grounds for further study in tumor models.

Acknowledgements:
We thank Jan Rehwinkel (University of Oxford) for donating THP-I cells and David Holden (Imperial College London) provided for providing HeLa cells. THP-I SLC19A1 single knock-out cells were a kind gift from David Raulet (University of California). Also we would like to thank Wolf-Dietrich Hardt (ETH Zürich) for making SL1344 SPI mutants available to us and Matthias Müller (Albert-Ludwigs-Universität Freiburg) for donating and TatB antibody. Maroeska Burggraaf (Amsterdam UMC) kindly provided us the hcGAS construct. We thank Melissa Stunnenberg (AmsterdamUMC) for her expertise of cytotoxic T cell assays. We acknowledge the Microscopy and Cytometry Core Facility at the Amsterdam UMC – Location VUmc for providing assistance in our microscopy and cytometry work.

Author contribution:
LW, LEHvdD, LSA and CK designed experiments; LW, LEHvdD, JM and JLvH performed the experiments; EE, JACvB and JMR contributed materials and scientific discussion; LW, LEHvdD, LSA, TBHG, WB and CK analyzed and interpreted data; LW and LEHvdD wrote the manuscript with input from all listed authors. TBGH, WB and CK supervised all aspects of this study.

Funding:
This work was supported by funding of the Cancer Center Amsterdam to LW. This research was furthermore funded by the European Research Council (Advanced grant 670424 to TBHG). LEHvdD and LSA were supported by the Netherlands Organization for Scientific Research (NWO) (Grant number: 91717305).

Conflicts of interest statement:
The authors have no competing interest to report.

Ethics approval statement:
This study was conducted according to the ethical principles set out in the Declaration of Helsinki and was approved by the institutional review board of the Amsterdam University Medical centers, location University of Amsterdam Medical Ethics Committee and the Ethics Advisory Body of Sanquin Blood Supply Foundation (Amsterdam, Netherlands).

Data availability:
The data generated during this study are available from the corresponding author on reasonable request.

REFERENCES

1. Waldman AD, Fritz JM, Lenardo MJ. A guide to cancer immunotherapy: from T cell basic science to clinical practice. *Nat Rev Immunol* 2020; 20: 651-668.
2. Darvin P, Toor SM, Nair VS *et al*. Immune checkpoint inhibitors : recent progress and potential biomarkers. *Exp Mol Med* 2018; 50: 1-11.
3. Haslam A, Prasad V. Estimation of the percentage of us patients with cancer who are eligible for and respond to checkpoint inhibitor immunotherapy drugs. *JAMA Netw Open* 2019; 2: 1-9.
4. Tang T, Huang X, Zhang G et al. Advantages of targeting the tumor immune microenvironment over blocking immune checkpoint in cancer immunotherapy. *Signal Transduct Target Ther* 2021; 6: 1-12.
5. Chorobik P, Czaplicki D, Ossysek K et al. Salmonella and cancer: From pathogens to therapeutics. *Acta Biochim Pol* 2013; 60: 285-297.
6. Pawalek JM, Low KB, Bermudes D. Tumor-targeted Salmonella as a Novel Anticancer Vector. *Cancer Res* 1997; 57: 4537-4544.
7. Toso JF, Gill VJ, Hwu P *et al*. Phase I study of the intravenous administration of attenuated Salmonella typhimurium to patients with metastatic melanoma. *J Clin Oncol* 2002; 20: 142-152.
8. Sun L, Wu J, Du F *et al*. Cyclic GMP-AMP Synthase is a cytosolic DNA sensor that activates the Type I Interferon Pathway. *Science (80-)* 2013; 339: 786-791.
9. Luecke S, Holleufer A, Christensen MH *et al*. cGAS is activated by DNA in a length-dependent manner. *EMBO Rep* 2017; 18: 1707-1715.
10. Ablasser A, Goldeck M, Cavlar T *et al*. CGAS produces a 2′-5′-linked cyclic dinucleotide second messenger that activates STING. *Nature* 2013; 498: 380-385.
11. Gao P, Ascano M, Zillinger T *et al*. Structure-function analysis of STING activation by c[G(2′,5′) pA(3′,5′)p] and targeting by antiviral DMXAA. *Cell* 2013; 154: 748-762.
12. Diner EJ, Burdette DL, Wilson SC *et al*. The Innate Immune DNA Sensor cGAS Produces a Noncanonical Cyclic Dinucleotide that Activates Human STING. *Cell Rep* 2013; 3: 1355-1361.
13. Zhang X, Shi H, Wu J *et al*. Cyclic GMP-AMP Containing Mixed Phosphodiester Linkages Is An Endogenous High-Affinity Ligand for STING. *Mol Cell* 2013; 51: 226-235.
14. Kranzusch PJ, Lee ASY, Wilson SC *et al*. Structure-guided reprogramming of human cgas dinucleotide linkage specificity. *Cell* 2014; 158: 1011-1021.
15. Ouyang S, Song X, Wang Y *et al*. Structural Analysis of the STING Adaptor Protein Reveals a Hydophobic Dimer Interface and Mode of Cyclic di-GMP Binding. *Immunity* 2012; 36: 1073-1086.
16. Borden EC. Interferons α and β in cancer: therapeutic opportunities from new insights. *Nat Rev Drug Discov* 2019; 18: 219-234.
17. Le Bon A, Durand V, Kamphuis E *et al*. Direct Stimulation of T Cells by Type I IFN Enhances the CD8 + T Cell Response during Cross-Priming. *J Immunol* 2006; 176: 4682-4689.
18. Gutjahr A, Papagno L, Nicoli F *et al*. The STING ligand cGAMP potentiates the efficacy of vaccine-induced CD8+ T cells. *JCI Insight* 2019; 4: 1-11.
19. Fuertes MB, Kacha AK, Kline J *et al*. Host type I IFN signals are required for antitumor CD8+ T cell responses through CD8α+ dendritic cells. *J Exp Med* 2011; 208: 2005-2016.
20. Edwards BS, Hawkins MJ, Borden EC. Correlation between in vitro and systemic effects of native and recombinant interferons-alpha on human natural killer cell cytotoxicity. *J Biol Response Mod* 1983; 2: 409-417.

21. Deng L, Liang H, Xu M *et al*. STING-Dependent Cytosolic DNA Sensing Promotes Radiation-Induced Type I Interferon-Dependent Antitumor Immunity in Immunogenic Tumors. *Immunity* 2014; 41: 843-852.
22. Wan S, Pestka S, Jubin RG *et al*. Chemotherapeutics and Radiation Simulate MHC Class I Expression through Elevated Interferon-beta Signaling in Breast Cancer Cells. *PLoS One* 2012; 7: 1-9.
23. Downey CM, Aghaei M, Schwendener RA *et al*. DMXAA Causes Tumor Site-Specific Vascular Disruption in Murine Non-Small Cell Lung Cancer, and like the Endogenous Non-Canonical Cyclic Dinucleotide STING Repolarization. *PLoS One* 2014; 9: 1-14.
24. Rauca VF, Licarete E, Luput *et al*. Combination therapy of simvastatin and 5, 6-dimethylcanthenone-4-acetic acid synergistically suppresses the aggressiveness of B16.F10 melanoma cells. *PLoS One* 2018; 13: 1-21.
25. Smolarczyk R, Pilny E, Jarosz-biej M *et al*. Combination of anti-vascular agent – DMXAA and HIF-1 α inhibitor – digoxin inhibits the growth of melanoma tumors. *Sci Rep* 2018; 8: 1-9.
26. Curran E, Chen X, Corrales L *et al*. STING Pathway Activation Stimulates Potent Immunity against Acute Myeloid Leukemia. *Cell Rep* 2016; 15: 2357-2366.
27. Primo NLJ, Douillard J, Nakagawa K *et al*. Randomized Phase III Placebo-Controlled Trial of CarboPlatin and Paclitaxel With or Without the Vascular Disrupting Agent Vadimezan (ASA404) in Advanced Non-Small-Cell Lung Cancer. *J Clin Oncol* 2011; 29: 2965-2971.
28. Corrales L, Glickman LH, McWhirter SM *et al*. Direct Activatino of STING in the Tumor Microenvironment Leads to Potent and Systemic Tumor Regression and Immunity. *Cell Rep* 2015; 11: 1018-1030.
29. Conlon J, Burdette DL, Sharma S *et al*. Mouse, but not Human STING, Binds and Signals in Response to the Vascular Disrupting Agent 5,6-Dimethylxanthenone-4-Acetic Acid. *J Immunol* 2013; 190: 5216-5225.
30. Luteijn RD, Zaver SA, Gowen BG *et al*. SLC19A1 transports immunoreactive cyclic dinucleotides. *Nature* 2019; 573: 434-438.
31. Mesman AW, Zijlstra-Willems EM, Kaptein TM *et al*. Measles virus suppresses RIG-I-like receptor activation in dendritic cells via DC-SIGN-mediated inhibition of PP1 phosphatases. *Cell Host Microbe* 2014; 16: 31-42.
32. Hoiseth SK, Stocker BAD. Aromatic-dependent Salmonella typhimurium are non-virulent and effective as live vaccines. *Nature* 1981; 291: 238-239.
33. Hapfelmeier S, Stecher B, Ehrbar K *et al*. Role of the Salmonella Pathogenicity Island 1 Effector Proteins SipA, SopB, SopE, and SopE2 in Salmonella enterica Subspecies 1 Serovar Typhimurium Colitis in Streptomycin-Pretreated Mice. *Infect Immun* 2004; 72: 795-809.
34. Kantarjian H, Stein A, Gökbuget N *et al*. Blinatumomab versus Chemotherapy for Advanced Acute Lymphoblastic Leukemia. *N Engl J Med* 2017; 376: 836-847.
35. Zhou W, Whiteley AT, de Oliveira Mann CC *et al*. Structure of the Human cGAS-DNA Complex Reveals Enhanced Control of Immune Surveillance. *Cell* 2018; 174: 300-311.
36. Ritchie C, Cordova AF, Hess GT *et al*. SLC19A1 Is an Importer of the Immunotransmitter cGAMP. *Mol Cell* 2019; 75: 372-381.
37. Deng W, Marshall NC, Rowland JL *et al*. Assembly, structure, function and regulation of type III secretion systems. *Nat Rev Microbiol* 2017; 15: 323-337.
38. Martens AWJ, Janssen SR, Derks IAM *et al*. CD3xCD19 DART molecule treatment induces non-apoptotic killing and is efficient against high-risk chemotherapy and venetoclax-resistant chronic lymphocytic leukemia cells. *J Immunother Cancer* 2020; 8: 1-13.

39. Amouzegar A, Chelvanambi M, Filderman JN *et al*. Sting agonists as cancer therapeutics. *Cancers (Basel)* 2021; 13: 1-24.
40. Lv Y, Sun Q, Wang X *et al*. Highly Efficient Preparation of Cyclic Dinucleotides via Engineering of Dinucleotide Cyclases in Escherichia coli. *Front Microbiol* 2019; 10: 1-11.
41. Cordova AF, Ritchie C, Volker B *et al*. Human SLC46A2 Is the Dominant cGAMP Importer in Extracellular cGAMP-Sensing Macrophages and Monocytes. *ACS Cent Sci* 2021; 7: 1073-1088.
42. Lou L, Zhang P, Piao R *et al*. Salmonella Pathogenicity Island 1 (SPI-1) and Its Complex Regulatory Network. *Front Cell Infect Microbiol* 2019; 9: 1-15.
43. Figueira R, Holden DW. Functions of the Salmonella pathogenicity island 2 (SPI-2) type III secretion system effectors. *Microbiology* 2012; 158: 1147-1161.
44. Jennings E, Thurston TLM, Holden DW. Salmonella SPI-2 Type III Secretion System Effectors: Molecular Mechanisms And Physiological Consequences. *Cell Host Microbe* 2017; 22: 217-231.
45. Zhou P, She Y, Dong N *et al*. Alpha-kinase 1 is a cytosolic innate immune receptor for bacterial ADP-heptose. *Nature* 2018; 561: 122-126.
46. Pal RR, Baidya AK, Mamou G *et al*. Pathogenic E. coli Extracts Nutrients from Infected Host Cells Utilizing Injectisome Components. *Cell* 2019; 177: 683-696.
47. Aulicino A, Rue-Albrecht KC, Preciado-Llanes L *et al*. Invasive Salmonella exploits divergent immune evasion strategies in infected and bystander dendritic cell subsets. *Nat Commun* 2018; 9: 1-17.
48. Bayer-Santos E, Durkin CH, Rigano LA *et al*. The Salmonella Effector SteD Mediates MARCH8-Dependent Ubiquitination of MHC II Molecules and Inhibits T Cell Activation. *Cell Host Microbe* 2016; 20: 584-595.
49. Leventhal DS, Sokolovska A, Li N *et al*. Immunotherapy with engineered bacteria by targeting the STING pathway for anti-tumor immunity. *Nat Commun* 2020; 11: 1-15.
50. Singh AK, Srikrishna G, Bivalacqua TJ *et al*. Recombinant BCGs for tuberculosis and bladder cancer. *Vaccine* 2021; 39: 7321-7331.

SUPPLEMENTAL INFORMATION
SUPPLEMENT 1

STING (TMEM173) knock out THP-I cell line

The STING knock-out THP-I cell line was made with CRISPR technology using multiguided sgRNA (Synthego Knockout Kit v2) according to Synthego's electroporation protocol. SG Cell Line 4D-nucleofector X kit (Lonza) was used for THP-I electroporation with 4D nucleofector Core Unit (Lonza). DNA of STING$^{-/-}$cells was isolated with DNeasy blood & tissue kit (Qiagen) according to protocol of manufacturer. DNA perturbation was verified using Sanger sequence data (Macrogen, Europe BV) of the STING locus and analyzed using ICE CRISPR Analysis Tool V2 (Synthego, USA). After verification of knockout efficiency, single STING$^{-/-}$ clones were generated.

Plasmid constructs

Sequence of HA-mcGAS with ribosomal binding site was synthesized by IDT technologies:

TACCCGTACGACGTGCCGGACTACGCCGGATCCATGGAAGATCCACGTCGTCGTACAA-
CAGCGCCCCGGGCCAAAAAACCCAGCGCCAAACGCGCACCCACACAGCCATCGCGTA-
CACGTGCTCATGCCGAATCATGTGGTCCTCAGCGCGGTGCACGCAGTCGTCGCGCCGAG-
CGCGACGGCGATACCACTGAAAAGCCCCGTGCCCCTGGGCCACGTGTTCATCCCGCTC-
GTGCTACCGAGTTGACCAAAGACGCGCAGCCATCAGCAATGGATGCGGCTGGTGCTAC-
GGCGCGTCCCGCTGTACGTGTTCCTCAACAACAAGCCATCCTGGACCCCGAGCTGCCT-
GCGGTACGTGAACCACAGCCTCCAGCAGATCCTGAAGCTCGGAAAGTAGTACGCGGGC-
CCTCTCATCGCCGGGGAGCTCGGTCGACTGGGCAGCCGCGTGCGCCCCGTGGCTCTCG-
CAAAGAGCCGGACAAGCTGAAAAAGGTACTTGATAAACTTCGTTTGAAGCGCAAGGA-
CATTTCAGAAGCCGCGGAGACCGTCAACAAAGTCGTGGAGCGCCTTCTTCGTCGTATG-
CAGAAGCGCGAGTCAGAGTTTAAGGGAGTTGAACAATTAAATACGGGATCTTATTATGAA-
CACGTAAAGATCTCTGCGCCCAACGAATTCGACGTCATGTTTAAGCTGGAGGTACCACG-
TATCGAGTTACAGGAGTATTATGAAACGGGTGCGTTTTATTTGGTGAAATTTAAACGTAT-
TCCCCGTGGGAATCCCTTAAGTCACTTTCTGGAGGGGGAGGTACTGAGCGCCACTAAAAT-
GCTGAGTAAATTCCGTAAAATTATTAAAGAAGAGGTCAAGGAAATCAAGGACATCGAT-
GTTTCCGTTGAAAAAGAGAAACCAGGTTCACCCGCGGTCACCTTGTTGATCCGTAACCCG-
GAGGAAATTTCAGTAGATATTATCTTGGCCTTAGAAAGTAAAGGATCGTGGCCCATCTC-
GACCAAGGAGGGCTTACCGATTCAAGGTTGGCTGGGGACAAAGGTCCGCACAAATTTG-
CGCCGCGAGCCGTTTTACCTTGTTCCTAAAAACGCCAAGGATGGGAATAGCTTTCAG-
GGCGAGACATGGCGTCTTTCGTTTTCGCATACTGAAAAATATATTTTGAATAATCACG-
GGATTGAGAAGACATGCTGTGAATCAAGTGGGGCTAAGTGCTGTCGTAAGGAATGTCT-
GAAACTTATGAAGTATCTTTTAGAGCAACTGAAGAAAGAATTCCAGGAGTTGGATGC-

GTTTTGTTCATACCACGTTAAAACAGCTATCTTTCACATGTGGACTCAGGACCCACAAGA-
TAGCCAATGGGACCCGCGTAATTTGAGCTCCTGTTTTGACAAATTATTAGCATTTTTCT-
TAGAATGTTTACGCACTGAGAAACTGGATCATTATTTTATCCCCAAGTTCAATCTTTTCTC-
CCAAGAGCTTATCGACCGCAAGTCAAAGGAATTCCTGTCCAAAAAGATTGAGTACGAGC-
GTAATAATGGCTTCCCCATCTTCGACAAACTTTGAAAGCTTTTTGTTTAACTTTAAGAAG-
GAGAT.

The catalytic inactive mcGAS construct contains a double point mutation at 198G>A and 199S>A and was also synthesized by IDT technologies. Both constructs were amplified by PCR and cloned via Gibson assembly into pMW215 with ssej-promoter, mScarlet fluorescent protein and ampicillin resistance gene. pABCON flag-hcGAS-mCherry with chloramphenicol resistance gene was constructed and donated by Maroeska Burggraaf (Amsterdam UMC). In short, the hcGAS sequence was ordered at IDT technologies:

ATGACTAGTGACTACAAAGACGATGACGACAAGATGCAGCCTTGGCACGGAAAGGCCAT-
GCAGAGAGCTTCCGAGGCCGGAGCCACTGCCCCCAAGGCTTCCGCACGGAATGCCAGGG-
GCGCCCCGATGGATCCCAACGAGTCTCCGGCTGCCCCCGAGGCCGCCCTGCCTAAGGCGG-
GAAAGTTCGGCCCCGCCAGGAAGTCGGGATCCCGGCAGAAAAAGAGCGCCCCGGACAC-
CCAGGAGAGGCCGCCCGTCCGCGCAACTGGGGCCCGCGCCAAAAAGGCCCCTCAGCGC-
GCCCAGGACACGCAGCCGTCTGACGCCACCAGCGCCCCTGGGGCAGAGGGGCTGGAG-
CCTCCTGCGGCTCGGGAGCCGGCTCTTTCCAGGGCTGGTTCTTGCCGCCAGAGGGGCGC-
GCGCTGCTCCACGAAGCCAAGACCCCCGCCCGGGCCCTGGGACGTGCCCAGCCCCGGCCT-
GCCGGTCTCGGCCCCCATTCTCGTACGGAGGGATGCGGCGCCTGGGGCCTCGAAGCTCCG-
GGCGGTTTTGGAGAAGTTGAAGCTCAGCCGCGATGATATCTCCACGGCGGCGGGGATG-
GTGAAAGGGGTTGTGGACCACCTGCTGCTCAGACTGAAGTGCGACTCCGCGTTCAGAG-
GCGTCGGGCTGCTGAACACCGGGAGCTACTATGAGCACGTGAAGATTTCTGCACCTA-
ATGAATTTGATGTCATGTTTAAACTGGAAGTCCCCAGAATTCAACTAGAAGAATATTC-
CAACACTCGTGCATATTACTTTGTGAAATTTAAAAGAAATCCGAAAGAAAATCATCT-
GAGTCAGTTTTTAGAAGGTGAAATATTATCAGCTTCTAAGATGCTGTCAAAGTTTAG-
GAAAATCATTAAGGAAGAAATTAACGACATTAAAGATACAGATGTCATCATGAAGAG-
GAAAAGAGGAGGGAGCCCTGCTGTAACACTTCTTATTAGTGAAAAAATATCTGTG-
GATATAACCCTGGCTTTGGAATCAAAAAGTAGCTGGCCTGCTAGCACCCAAGAAGG-
CCTGCGCATTCAAAACTGGCTTTCAGCAAAAGTTAGGAAGCAACTACGACTAAAGC-
CATTTTACCTTGTACCCAAGCATGCAAAGGAAGGAAATGGTTTCCAAGAAGAAACAT-
GGCGGCTATCCTTCTCTCACATCGAAAAGGAAATTTTGAACAATCATGGAAAATCTA-
AAACGTGCTGTGAAAACAAAGAAGAGAAATGTTGCAGGAAAGATTGTTTAAAACTA-
ATGAAATACCTTTTAGAACAGCTGAAAGAAAGGTTTAAAGACAAAAAACATCTGGA-
TAAATTCTCTTCTTATCATGTGAAAACTGCCTTCTTTCACGTATGTACCCAGAACCCT-

CAAGACAGTCAGTGGGACCGCAAAGACCTGGGCCTCTGCTTTGATAACTGCGTGACAT-ACTTTCTTCAGTGCCTCAGGACAGAAAAACTTGAGAATTATTTTATTCCTGAATTCAAT-CTATTCTCTAGCAACTTAATTGACAAAAGAAGTAAAGAATTTCTGACAAAGCAAATT-GAATATGAAAGAAACAATGAGTTTCCAGTTTTTGATGAATTTTGA.

Construct was amplified with PCR and cloned into pABCON vector with In-Fusion (Takara Bio Europe).

Oligo's	
Human IFN-β (Merck)	FW: 5'- CAACTTGCTTGGATTCCTACAAAG RV: 5'- TATTCAAGCCTCCCATTCAATTG
Human Rpl37a (Merck)	FW: 5'- ATTGAAATCAGCCAGCACGC RV: 5'- AGGAACCACAGTGCCAGATCC
sgRNA TMEM173 KO #1 (Synthego)	5' - GATGGATGGATGCAGGC
sgRNA TMEM173 KO #2 (Synthego)	5' - GCCTGGTGACCCTTTGG
sgRNA TMEM173 KO #3 (Synthego)	5' - ACAGCAGTCCCAGCTGC
TMEM173 sequence primer (Merck)	RV: 5' - GGGAGTGACACACGTTGGAT
Human GAPDH	FW: 5' - CCATGTTCGTCATGGGTGTG RV: 5' - GGTGCTAAGCAGTTGGTGGTG
Human IFNB	FW: 5' - ACAGACTTACAGCTTACCTCCGAAAC RV: 5' - CATCTGCTGGTTGAAGAATGCTT
Human IRF7	FW: 5' - GCTCCCCACGCTATACCATCTAC RV: 5' - GCCAGGGTTCCAGCTTCAC
Human ISG15	FW: 5' - TTTGCCAGTACAGGAGCTTGTG RV: 5' - GGGTGATCTGCGCCTTCA
Human IL-1β	FW: 5' - TTTGAGTCTGCCCAGTTCCC RV: 5' - TCAGTTATATCCTGGCCGCC

SUPPLEMENT 2

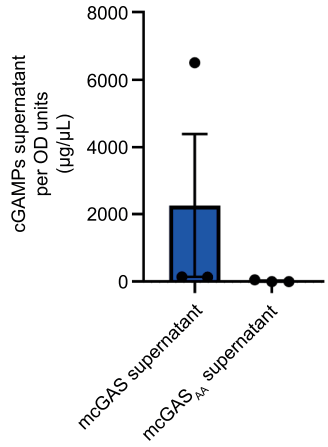

Supplemental Figure 2: Concentration of cGAMPs in supernatant of SL1344 mcGAS and SL1344 mcGAS$_{AA}$ quantified with ELISA. Concentration cGAMPs in bacterial pellets are corrected for OD unit input.

SUPPLEMENT 3

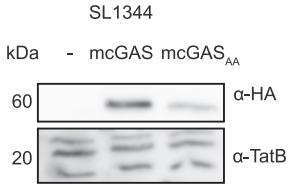

Supplemental Figure 3: Protein expression of mcGAS and mcGAS$_{AA}$ in SL1344 detected by Western blot.

SUPPLEMENT 4

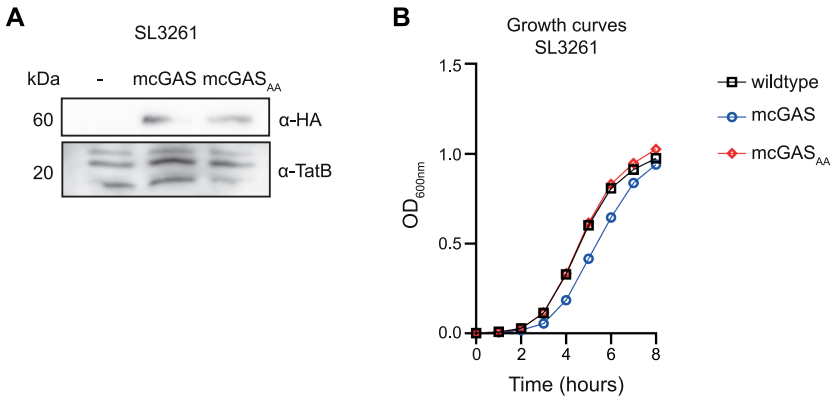

Supplemental Figure 4: (A) Protein expression of mcGAS and mcGAS$_{AA}$ in SL3261 detected by Western blot. (B) Growth curves SL3261 strains in LB.

5

SUPPLEMENT 5

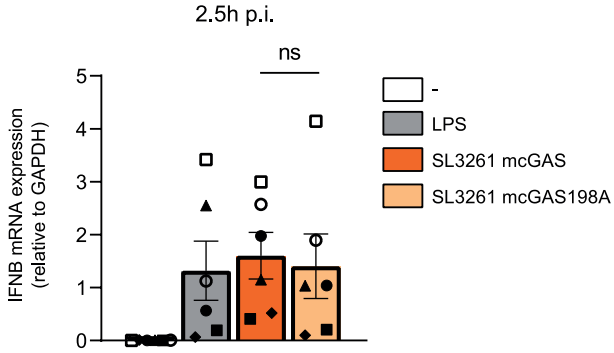

Supplemental Figure 5: IFNB mRNA expression in DCs 2.5 hours after challenge. Each symbol represents a donor. Statistics: paired student's *t*-test, error bars: SEM.

SUPPLEMENT 6

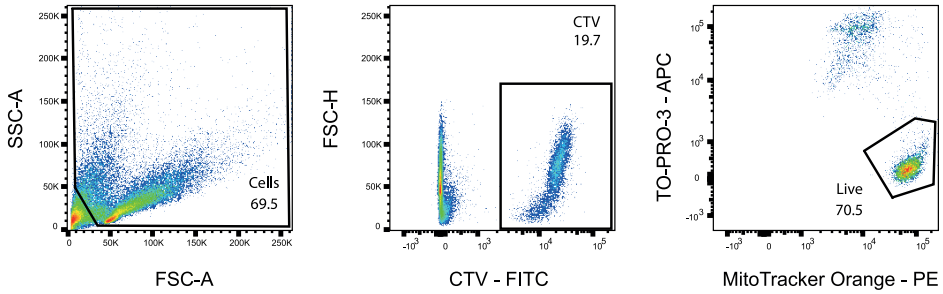

Supplemental Figure 6: Representative dot plots of the gating strategy used in the cytotoxic T cell killing assay. Live cells were gated. CTV-positive B cells were distinguished from T cells. Within the CTV-positive gate, live cells were gated as TO-PRO-3 negative, MitoTracker Orange-positive.

PART 2

MOLECULAR APPROACHES TO STUDY CONTROL OF T CELL RESPONSES

CHAPTER 6

AN OPTIMIZED TOOLBOX FOR OVEREXPRESSION AND GENETIC PERTURBATION OF PRIMARY LYMPHOCYTES

Lieve E.H. van der Donk[1,4], Jet van der Spek[1,4], Tom van Duivenvoorde[1], Marieke S. ten Brink[2], Teunis B.H. Geijtenbeek[1,4], Coenraad P. Kuijl[3,4,5,6], Jeroen W.J. van Heijst[1,7], Louis S. Ates[1,2,3,6]*

[1] Amsterdam UMC location AMC, Department of Experimental Immunology, Meibergdreef 9, Amsterdam, The Netherlands;
[2] Amsterdam UMC location AMC, Division of Infectious Diseases and Center for Experimental and Molecular Medicine, Meibergdreef 9, Amsterdam, The Netherlands;
[3] Amsterdam UMC location VUmc, Department of Medical Microbiology and Infection Control, De Boelelaan 1117, Amsterdam, The Netherlands
[4] Amsterdam institute for Infection and Immunity, Infectious diseases, Amsterdam, The Netherlands;
[5] Cancer Center Amsterdam, Cancer Immunology, Amsterdam, The Netherlands;
[6] Amsterdam institute for Infection and Immunity, Cancer Immunology, Amsterdam, The Netherlands;
[7] Current address: Neogene Therapeutics, Science Park 106, 1096 XG Amsterdam, The Netherlands.

* Address correspondence and reprint requests to L.S. Ates, Amsterdam UMC, Meibergdreef 9, 1105 AZ, Amsterdam.

Biology Open 2022, 11 (2): bio059032.

ABSTRACT

Genetic manipulation of primary lymphocytes is crucial for both clinical purposes and fundamental research. Despite their broad use, we encountered a paucity of data on systematic comparison and optimization of retroviral vectors, the workhorses of genetic modification of primary lymphocytes. Here, we report the construction and validation of a versatile range of retroviral expression vectors. These vectors can be used for the knockdown or overexpression of genes of interest in primary human and murine lymphocytes, in combination with a wide choice of selection and reporter strategies. By streamlining the vector backbone and insert design, these publicly available vectors allow easy interchangeability of the independent building blocks, such as different promoters, fluorescent proteins, surface markers and antibiotic resistance cassettes. We validated these vectors and tested the optimal promoters for *in vitro* and *in vivo* overexpression and knockdown of the murine T cell antigen receptor. By publicly sharing these vectors and the data on their optimization, we aim to facilitate genetic modification of primary lymphocytes for researchers entering this field.

Keywords: Retrovirus, T cell, lymphocytes, overexpression

INTRODUCTION

In a scientific era where high-throughput technologies increasingly dictate immunological research, having tools to characterize individual protein functions is still of great importance. The most fundamental molecular biology tools to achieve this are based on genetic perturbation or overexpression of genes of interest. These tools are often developed and optimized over many years in specialized labs. However, for researchers entering this field it can be daunting to select and obtain the most appropriate vectors for their model. These already difficult decisions are hampered by the paucity of published data on systematic comparisons between components of expression systems. We invested significant effort in developing a versatile vector system and performing quality control and optimization experiments. By sharing these data and systems we aspire to facilitate this process for others.

Genetic perturbation of gene expression by deletion or knockdown in eukaryotic cells has been revolutionized in recent decades by the development of RNAinterference approaches and CRISPR-Cas9-based methods. Similarly, the development of high-resolution fluorescent microscopes and novel fluorescent proteins have revolutionized our knowledge of protein localization and trafficking. However, a limiting factor in the genetic manipulation of primary eukaryotic cells is the efficiency of the transfection or transduction method and the stability of the achieved expression. Especially in primary murine and human T cells, it can be challenging to transduce and express large lentiviral constructs, making CRISPR-Cas9 modification of primary T cells technically challenging beyond specialized labs (1-3). Therefore, genetic perturbation of murine and human T cells is often most readily achieved by expression of optimized microRNAs from gamma-retroviral vectors (3-5). Although gamma-retroviral transduction to achieve gene knockdown or overexpression has been widely used and optimized over recent decades (4-8), we noted a lack in published literature describing a systematic evaluation of which promoters to use for stable *in vitro* and *in vivo* gene silencing of primary lymphocytes. We set out to select the optimal promoter sequences to stably express proteins and microRNAs of interest in primary T cells *in vitro* and *in vivo*. We constructed a publicly available modular set of vectors, which can be used to express any gene of interest and/or microRNA together with a choice of promoters, linkers, and fluorescent, or surface markers. We tested these different components in primary T cells derived from C7 mice, which express a recombinant T cell receptor (TCR) recognizing a MHC-II-peptide fragment called $ESAT6_{1\text{-}20}$, which is derived from *Mycobacterium (M.) tuberculosis* (9-11). We expect that this set of easy-to-use optimized vectors will make molecular biology approaches to study primary T cells more widely accessible and adaptable.

MATERIALS AND METHODS

Molecular cloning

The pMX vector backbone was created by modifying pMXs-IRES-GFP (Cellbiolabs/Bio-connect, NL) by removing the eGFP, IRES and MCS insert by restriction with ClaI and SalI and ligating a synthetic MCS fragment containing PacI, BamHI, NotI, MluI, SphI, SbfI, HindIII and ClaI restriction sites respectively (TTAATTAACTCCGTGGATC-CGGTCGTGCGGCCGCACGGAAACGCGTGGCCTGGCATGCCGCGACCCTGCAGGTTTCT-GAAGCTTGAGTACATCGAT).

Similarly, the original pMY-IRES-GFP vector (Cellbiolabs/Bio-connect, NL) was modified to replace the multiple cloning site. Furthermore, the second SalI site in this vector was removed by restriction with SalI followed by 3'exonuclease digestion and blunt-end ligation, creating pMY-Empty-MCS (Addgene: #163351).

A lentiviral vector suitable for convenient subcloning between these modified pMY and pMX vectors was made by modifying lentiCRISPR v2 (Addgene: #52961) (12). First, the U6 and gRNA scaffold were removed by restriction with KpnI and EcoRI followed by blunt ligation. Next, the Cas9 insert was replaced by eGFP by cloning with AgeI and BamHI. The full GFP-P2A-PuroR including the 3'WPRE and 3'LTR was shuttled to the empty pMY backbone with PacI and ApaI to allow easier modification. Here, the GFP-P2A-PuroR insert was removed by PacI and MluI and replaced with the MCS sequence with PacI and ClaI. This insert was shuttled back into the pLenti backbone with PacI and ApaI replacing the original fragment. Next the endogenous NotI and MluI sites were removed consecutively by restriction followed by 3'exonuclease digestion and blunt-end ligation, creating pLenti-EFS-MCS-WPRE (Addgene: #163362).

The different promoter sequences were obtained by synthesis (GeneArt) and were amplified by PCR before being ligated into the pMX-vector backbone with PacI and BamHI (Supplemental table 2 for primers). The murine surface marker Ly6G was codon optimized and synthesized (GeneArt, supplemental methods 1). The sequence was amplified with primers Ly6Gopt_SalP2A_Fwd and Ly6Gopt_Sbf_Rev and ligated into pMY with SalI and SbfI, creating pMY-MCS-P2A-Ly6G (Addgene: #163353). Similarly, the sequences for CD90.1 and CD90.2 (also known as Thy1.1 and Thy1.2) were amplified from C7, or C57bl/6 cDNA with primers CD90.2_SalP2A_Fwd and CD90.2_Sbf_Rev and ligated into pMY, creating vectors pMY-MCS-P2A-CD90.1 (Addgene: #163354) and pMY-MCS-P2A-CD90.2 (Addgene: #163355). P2A-GFP was amplified from a previously constructed vector (pMX-CAF-Slc7a1-P2A-GFP unpublished) with primers P2A_SalI_Fwd and GFP_Sbf_Rev and was cloned into pMY with SalI and SbfI, creating

vector pMY-MCS-P2A-GFP (Addgene: #163356). Similarly, puromycin and blasticidin resistance genes were amplified from existing vectors and were labeled with an HA-tag and DYK-tag respectively. To this end, the blastR cassette was amplified with primers BlastR_SalP2A_Fwd and BlastR_DYK_Sbf_Rev and the PuroR cassette with primers PuroR_SalP2A_Fwd and PuroR_HA_Sbf_Rev. These products were cloned into the pMY backbone with SalI and SbfI to create pMY-MCS-P2A-PuroHA (Addgene: #163352) and pMY-MCS-P2A-BlastDYK (Addgene: #163357) respectively.

The transmembrane and intracellular components of the CD3 complex CD3γ, CD3δ, CD3ε and TCRζ were codon optimized and synthesized on an expression construct, where the genes were separated by T2A, F2A and E2A peptides, followed by a P2A peptide and the codon optimized Ly6G surface marker (Supplemental methods 1). This construct was cut with NotI and SalI and ligated into pMY-MCS-P2A-CD90.2 to express it in frame with the CD90.2 surface marker instead of Ly6G, creating pMY-CD3-P2A-CD90.2 (Addgene: #163338). The full CD3-CD90.2 insert was further subcloned into the pMX vectors with different promoters using BamHI and HindIII (Addgene #163334-7).

The gene encoding mCherry was amplified with a GSG linker from vector pMSCV-nMCL1GFP-IRES-mCherry (Unpublished, kind gift from Chiara Montironi and Eric Eldering, Amsterdam UMC), which is a derivate of pMSCV-IRES-mCherry (Addgene #52114), with primers mCherry_Sal_GSG_Fw and mCherry_Hind_Rv. This product was cloned into pMY to create the intermediate product pMY-MCS-GSG-mCherry. This was used as a backbone to clone murine *lyz2* into, which was amplified from C57bl/6 mouse cDNA with primers Lyz2_MluI_Fwd and Lyz2_GSG_SalI_Rev, creating vector pMY-Lyz2-GSG-mCherry (Addgene: #163346). This vector was used as a backbone to replace the genes encoding the other fluorescent proteins. mTurquoise2 (Addgene: #163347), mVenus (Addgene: #163348). In parallel, GSG-eGFP was cloned in the pMY empty vector creating pMY-SalI-GSG-eGFP (Addgene: #163350). These GSG-FP fragments were amplified with primers mCherry_Sal_GSG_Fw and mCherry_Hind_Rv. The template for mTurquoise2 was pEGFP-N1-4xmts-mTurquoise2 Addgene #98819 (13), for mVenus it was pEGFP-C1-SYFP1 (unpublished, kind gift from Joachim Goedhart) (14, 15).

The MiR30 fragment was amplified from pGIPZ-miR30-FYN (Horizon discovery) with primers miR30_Hind_Fwd and miR30_Cla_Rev and was cloned into pMY-Ly6G-P2A-PuroHA, pMY-LygG, pMY-CD90.2-Blast-DYK, or pMY-CD90.2 with HindIII and ClaI. Target sequences for antagomirs were selected with help of the genetic perturbation platform and the antagomir fragments were designed according to published

guidelines for miR30 generation (4, 16). Antagomir sequences were synthesized as single stranded oligonucleotides SHC007_shRNAmiR_temp (Rluc) and Cd247A_miR_temp (CD247/TCRζ) and were amplified with primers miRE-Xho-Fwd and miRE-Eco-Rev before being inserted in the miR30 backbone with XhoI and EcoRI.

Isolation, activation and culture of C7 cells

Transgenic C7-TCR.CD90.1 mice were killed by administration of a sublethal dose of 0.1 mL KetMet/10 g of mouse weight (KetMed consists of 12.5 mg/mL ketamine and 30 µg/mL dexmedetomidine), followed by cervical dislocation. Spleens and lymph nodes were collected and homogenized through a 100 µm EASYstrainer cell strainer (Greiner). After washing the cells with PBS, they were resuspended in 900 µl MACS buffer and 100 µL anti-CD4 MACS bead suspension (CD4 L3T4 microbeads Miltenyi) was added and incubated on ice for 15 minutes. The suspension was centrifuged and resuspended in 1 mL MACS buffer, divided over 2 35 µm cell strainers (FALCON 5 mL round bottom tube with cell strainer cap) and spun down (500g). Cells were resuspended in 3 mL MACS buffer and were applied to a prewashed LS MACS column (Miltenyi) on a MACS magnet. The $CD4^-$ fraction was collected by triple washing with 3 mL MACS buffer and collecting flow through. Afterwards, the LS column was removed from the magnet and the remaining cells were collected as $CD4^+$ fraction.
Cells were counted on a CASY cell counter and the $CD4^-$ cells were irradiated by exposure to a Cesium (^{137}C)-source to receive 10gy. C7 cells were activated by adding $1.5*10^6$ irradiated $CD4^-$ cells to $0.5*10^6$ $CD4^+$ cells per mL RPMI+, supplemented with 10 ng/mL IL-12 and 5 µg/mL $ESAT6_{1-20}$ peptide (produced by the Netherlands Cancer Institute (NKI). $CD4^+$ and non-irradiated $CD4^-$ fractions were stained with flow cytometry panel 2 to assess MACS efficiency.

Transfection and transduction

To produce ecotropic retrovirus, platinum-E (PLAT-E) cells were transiently transfected (6). To achieve this, PLAT-E cells were pre-cultured in IMDM medium supplemented with 10% fetal calf serum, penicillin and streptomycin. From an exponentially growing PLAT-E culture, $3*10^6$ cells were inoculated in 45 mL IMDM+ in a T225 culture flask 72 hours before transfection. On the day of transfection, PLAT-E cells were washed with 45 mL of PBS and were dissociated from the culture flask by a 5 minute incubation (37°C) with 9 mL of TrypLE reagent (Gibco), which was inactivated by adding 36 mL PBS. The PLAT-E cells were washed, resuspended in IMDM+ and filtered over a 40 µm cell strainer, after which the cells were counted with a CASY cell counter. $2.5*10^6$ PLAT-E cells were suspended in 1 mL IMDM and these cells were transfected by adding the transfection mix.

The transfection mix was made by dissolving 2 µg of the indicated vectors in combination with 0.4 µg of the helper plasmid pCL-ECO (Addgene plasmid 12371) (17) and for miR30 vectors 0.4 µg DGCR8 siRNA (18) (synthesized by Qiagen) in a total volume of 95.4 µL Opti-MEM (Gibco). After mixing of DNA by flicking tubes and a short spin, 5.6 µL P3000 reagent was added (ThermoFisher). Simultaneously, 5.6 µL P3000 transfection reagent per sample was dissolved in 94.4 µL Opti-MEM, this mix was added to the DNA-containing mix and incubated for 10 minutes. After incubation, 800 µL of IMDM was added and the mix was added to the PLAT-E cells in 6-well culture dish. One day after transfection the IMDM medium was carefully removed from the transfected cells and replaced with 1.5 mL of RPMI medium containing L-glutamine 50 µM β-mercaptoethanol, 10% FBS and 10,000 U/mL penicillin/streptomycin (Referred to as RPMI+ for the rest of the methods section). After overnight incubation, virus-containing supernatant was collected and filtered over a 0.2 µm filter. Activated C7 cells were concentrated and 4 mL of culture was resuspended in 1 mL RPMI+ containing 10 µg/mL $ESAT6_{1-20}$ peptide + 20 ng/mL IL-12 (Peprotech) + 20 ng/mL IL-2 (Peprotech). 1 mL of virus-containing supernatant was added to 1 mL activated C7 cells on retronectin coated 6-well culture plates and centrifuged for 2 hours on 1000x *g*. After further 3 hours of culture, 2 mL of RPMI+ containing 10 ng/mL IL-2 was added to each well. Remaining PLAT-E cells were washed with PBS and stained with flow cytometry panel 2 (below) to assess transfection efficiency.

Similar procedures were performed for the production of amphotropic retrovirus. However, PLAT-A cells (6) were used instead of PLAT-E cells. Since PLAT-A cells tend to dissociate easily from plates once virus production has started, culture plates were pre-treated with Poly-D-Lysine. Finally, the helper plasmid pCL-Ampho (17) (Novus Biologicals NBP2-29541) was used instead of pCL-Eco.

Flow Cytometry

PLAT-E cells were dissociated by TrypLE reagent (Gibco) before FACS staining while C7 cells were stained directly. All cells were first stained for viability with Fixable Viability Dye eFluor™ 780 (1:1000 in PBS) (eBioscience), before cell surface staining with the antibody combination depicted in supplemental table 3, depending on the condition. Antibody cocktails were prepared in FACS buffer (PBS containing 0.5% bovine serum albumin (BSA; Sigma) and 0.1% NaN_3) cells were stained for 10-15 minutes at 4°C before fixation in 2% paraformaldehyde solution for 5 minutes (Electron Microscopy Sciences). In the case of intracellular staining for TCRζ, cells were permeabilized, by incubation with Perm/Wash solution (BD Biosciences) for 5 minutes at 4°C, before intracellular staining and second fixation step. Flow cytometry was performed on Canto flow cytometer (BD Bioscience) and data was analyzed using FlowJo V10 software (TreeStar).

Confocal microscopy

C7 T cells were washed in PBS, fixed in 2% PFA for 5 minutes washed again and mounted on glass slides (ProLong Gold mounting medium without DAPI), two days and five days after transduction. Slides were imaged with a Leica SP8X confocal microscope using a 63x objective (Numerical aperture 1.4) using LasX software (Leica, version 3.5.6). Blue fluorophore mTurquoise2 was excited with a UV laser at 405 nm (Shutter 20%, Laser power 50%, Laser strength 2%) and emission was measured at 488-493 nm (HyD, Gain 100V, Offset -0.2%, Pinhole 0.7 Airy units). Other fluorophores were excited with a white-light laser (Shutter 20%, Laser power 50%, Laser strength 2%) at 488 nm for eGFP, 515 nm for mVenus and 587 nm for mCherry and emission was acquired at 500-535 nm (eGFP), 520-560 nm (mVenus), or 610-650 nm (mCherry) (HyD, Gain 600 V, Offset 0.0%, Pinhole 0.7 Airy units). Images were acquired at 10x zoom, resolution of 512x512 pixels, a line average of 4 images, bidirectional X imaging, speed setting of 600 and a distance between Z-planes of 0.2 nm. Images were deconvolved using Huygens Professional Software suite (Version 19.10) and images were 3D rendered in LasX software (Version 3.5.6).

***In vivo* experiments**

Transduced cells were split 1:2 one day after transduction by adding fresh RPMI+ containing 10 ng/mL IL-2. Two days after transduction, cells were washed and suspended in PBS to reach $1*10^7$ cells/mL. 200 µL of this solution (*i.e.* $2*10^6$ cells) was intravenously injected into the tail vein of healthy C57Bl6 mice (7 weeks old). Recipient mice were randomly distributed over 6 cages by animal caretakers and experimental groups were separated per cage after receiving C7 cells. One mouse belonging to the group transduced with CAG-containing construct did not receive the full 200 µL of C7 cells. Blood aliquots were collected in EDTA containing tubes at the indicated timepoints by tail vein bleed (Maximally 50 µL per bleed) after puncture with a 25G medical needle. EDTA tubes containing blood samples were spun, resuspended in red blood cell lysis buffer and incubated for 2 minutes. After this lysis step, cells were resuspended in FACS buffer and kept at 4°C until staining with flow cytometry panel 3. Please note that the first bleed at 5 days post transduction yielded insufficient cells to perform an intracellular staining and therefore no data on TCRζ-expression are available for this timepoint. Furthermore, not all samples could be analyzed at this timepoint and therefore some error bars are missing from the corresponding figure.

Recipient mice were sacrificed 22 days after T cell activation (*i.e.* 18 days after adoptive transfer) as above. 200 µL of blood was collected in EDTA tubes and analyzed as above. Lungs and spleens were harvested from all mice. Lungs were homogenized by cutting with sterile scissors in the presence of 0.5 mL digestion buffer (HBSS supplemented with 5mM $CaCl_2$ and 200 U/mL collagenase IV). 2 mL digestion buffer was added to the

lung fragments and transferred to 12 mL round bottom tubes, which were incubated for 30 minutes at 37°C while shaking at 225 rotations per minute. Digested lung sample was homogenized by passing 10 times through a 19 G needle fitted to a 2 mL syringe. Homogenized tissue was filtered over a 100 µm EASYstrainer (Greiner) cell strainer, which washed with 10 mL PBS. Spleens were pooled per experimental group and were homogenized by sieving through a 100 µm EASYstrainer. Cells were resuspended in PBS and analyzed by flow cytometry as above.

RESULTS

Development of a versatile vector set for stable gene expression in lymphocytes
We set out to optimize existing (gamma-)retroviral and lentiviral vector backbones for the stable genetic modification of human and murine lymphocytes. We recently reported the systematic comparison of these lentiviral and retroviral backbones for use in human peripheral blood lymphocytes (3). To achieve those comparisons we streamlined multiple cloning sites to achieve shuttling of identical inserts between the vector backbones. First, we introduced the same multiple cloning site into the retroviral vector backbones pMX and pMY and the lentiviral vector pLenti (Figure 1A) (6). In parallel, the endogenous SalI site in pMY and the NotI and MluI sites in pLenti were removed. Therefore, all enzyme sites in the MCS are unique cutters in all vectors with the exception of HindIII and SphI in the pLenti backbone. This harmonization of multiple cloning sites allows simple subcloning of any insert from one vector to another, facilitating direct comparisons to select optimal vector systems for specific model systems. To further optimize this vector set, we selected different promoters, which to our knowledge have not been systematically compared in primary lymphocytes (Figure 1B). Finally, we constructed overexpression constructs, which are organized as modules so that individual building blocks can easily be inserted or interchanged (Figure 1B, C). After the promoter, we inserted a first building block, followed by a choice of linkers and a second building block. Selection of an appropriate linker sequence is important and depends on the goal of the experiments. For direct protein fusion of the two building blocks that can for instance be used in protein localization studies, we used a flexible glycine-serine linker (GSGGSG). For production of separate proteins we included either an internal ribosome entry site (IRES) sequence or a P2A sequence. The IRES sequence is longer and may therefore reduce expression levels of the inserts, but it has the advantage that no remnants of the sequence will be translated (19). In contrast, the short P2A sequence induces efficient ribosome skipping that leads to separate translation of the two building blocks.

However, after this "cleavage" the majority of the 2A amino acids remain on the C terminus of the block 1 protein and the terminal proline becomes part of the block 2 protein (20). These extra amino acids may interfere with the correct localization or function of certain proteins. Please note that while 2A fusion results in equimolar amounts of the two proteins, IRES fusion may result in a 3:1 ratio of the two proteins (21). To select for, or monitor the expression of, the gene-of-interest we selected a wide range of reporter genes. These include genes encoding the fluorescent proteins mTurquoise2, eGFP, mVenus and mCherry, antibiotic selection cassettes against puromycin or blasticidin and non-immunogenic murine cell surface markers Ly6G and CD90.2 (Figure 1C, Supplemental Figure 1) (14, 15, 22, 23).

Promoter selection by overexpression of a large construct in primary murine T cells *in vitro*

Gene expression from retroviral vectors is generally more stable when the insert is limited in size (24). To get a stringent read out of which promoters in our expression system are most stable and efficient in murine T cells, we selected a construct which in our hands was relatively challenging to express at high levels. This construct, consisting of the four intracellular components of the T cell receptor (TCR)/CD3 complex consists of codon optimized murine genes encoding CD3γ, CD3δ, CD3ε, TCRζ (CD247) and the marker CD90.2. These genes were separated by the self-dissociating peptides T2A, F2A, E2A and P2A respectively (20). This insert was expressed from pMX vectors with the promoters hPGK, hFTH1, CAG, or mPGK and from the pMY vector with its native LTR promoter (Addgene vectors #163334-8). We transduced $CD4^+$ T cells isolated from C7 mice, which express a recombinant TCR and therefore all recognize the same epitope derived from *M. tuberculosis* (9). This transduction resulted in high initial transduction efficiencies, ranging from 60% for the constructs under control of the CAG promoter to almost 100% for the pMY based vector (Figure 2A). However, in line with our previous experience regarding the unstable expression of such a large construct, the percentage of $CD90.2^+$ $CD4^+$ T cells diminished markedly over time for all constructs. Where these levels approached 0% for vectors under control of the CAG and hFTH1 promoters, the pMY-LTR and hPGK based vectors seemed most stable (Figure 2A). These trends were confirmed by investigating the expression level of CD90.2 within the $CD90.2^+$ cells (Figure 2B). Quantification of TCR/CD3 subunit overexpression was hampered by expression of the endogenous TCR on these $CD4^+$ T cells. However, a clear overexpression of the different TCR subunits TCRζ, TCRβ and CD3ε could be detected for all vectors 2 days post transduction and was most pronounced with the pMY vector (Figure 2C-E). Overexpression

of individual TCR/CD3 proteins could only be detected when the CD3 construct was expressed in pMY at day 5 post transduction and was undetectable in all conditions beyond that timepoint (Figure 2C-E). Our data therefore suggest that the pMY vector with its native LTR promoter is the most efficient and stable way to overexpress large protein constructs in murine CD4$^+$ T cells *in vitro*.

Vectors for protein localization in T cells by multicolor confocal microscopy

Having established pMY as the most efficient vector to overexpress proteins in murine T cells *in vitro*, we constructed a range of these vectors where any gene of interested can be cloned in frame to a C-terminal GSGGSG linker followed by a choice of fluorescent proteins with different excitation and emission spectra (Figure 1B, C, Supplemental Figure 1). For proof of concept, we selected murine *lyz2*, which is of interest to our ongoing research. *Lyz2* was cloned N-terminally of genes encoding either mTurquoise2, mVenus or mCherry (Addgene vectors #163347-9) (14, 15, 23). It should be noted that mVenus and GFP have partly overlapping fluorescent emission and excitation spectra and it is therefore not advised to use these in combination. We selected mVenus over eGFP for its excellent brightness and monomeric nature (25). We transduced C7 CD4$^+$ T cells with these single vectors, or combinations thereof. Cells were fixed and mounted 2 days after transduction and were analyzed by confocal microscopy (Figure 3A, B). The lyz2-fluorophore combinations localized in cellular compartments that resemble either lysosomes or secretory granules, independently of which fluorophore was used (Figure 3A). Because of the three fluorophores' different spectra, these could be easily imaged without significant background in the other channels (Figure 3A). Double transduction with two viruses simultaneously (Lyz2-mTQ2 + Lyz2-mCherry, or Lyz2-mVenus + Lyz2-mCherry) resulted in a full colocalization of fluorescent compartments, without signal in the remaining channel (Figure 3B). These data suggest that these vectors can be readily used for protein colocalization studies. Therefore, we set out to provide further proof of concept with simultaneous transduction of three different retroviral vectors, Lyz2-mTQ2, GFP-Rab27a and Mpeg1-mCherry (Figure 3C). Different localization of the three fluorophores was observed in the imaged cells, indicating that indeed, triple transduction with our multicolored pMY vectors is a viable approach to study intracellular protein localization in primary murine CD4$^+$ T cells.

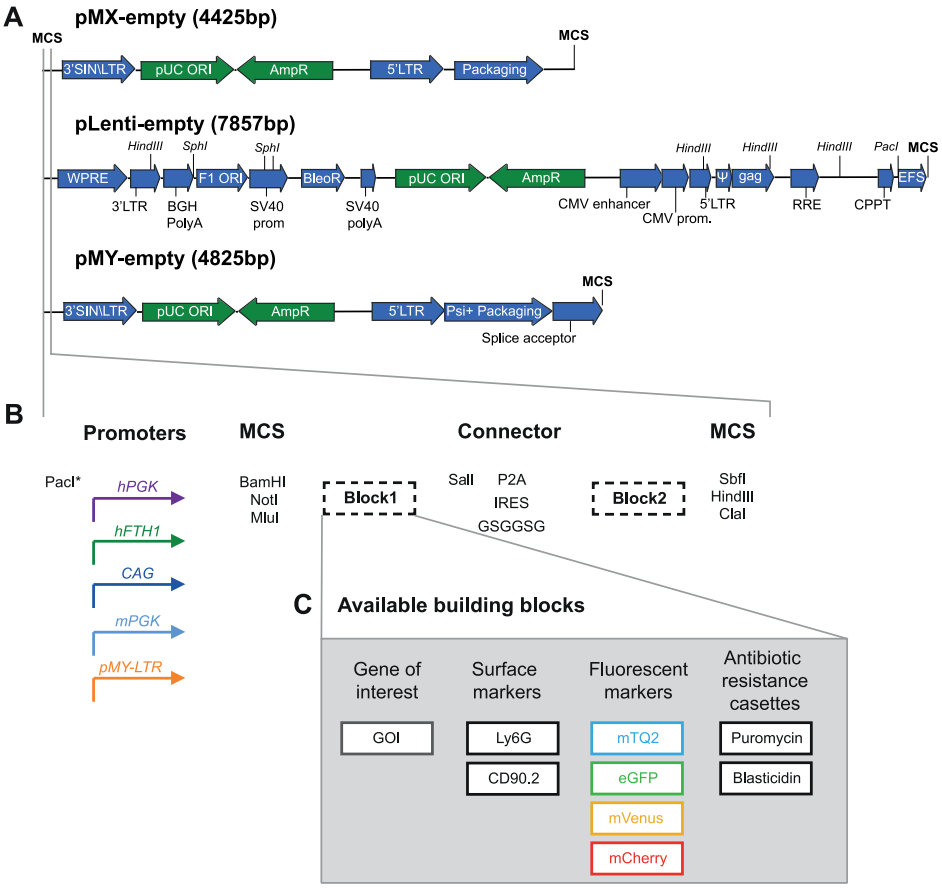

Figure 1: Vector backbones and design.

(A) Vector backbones of pMX, pMY, and pLenti. Green arrows indicate elements needed for bacterial replication; blue arrows are part of the retroviral genome. (B) Organization of the versatile expression cassette used in all three vector backbones. A choice of five different promoter sequences (colored arrows) was assessed for optimal expression *in vitro* and *in vivo*. Note that the lentiviral and pMY backbones already include the EFS/EF1α and LTR promoters respectively and therefore include the PacI site in the MCS after the promoter. Overexpression constructs are designed to express the gene of interest in either block 1 (for C-terminal labelling) or block 2 (for N-terminal labelling). These building blocks are separated by an in frame SalI restriction site and a choice of IRES, P2A peptide, or GSGGSG linker to create a fusion protein or equimolar separately produced proteins. (C) Available building blocks include surface markers of murine Ly6G, CD90.1 (Thy1.1) and CD90.2 (Thy1.2), fluorescent proteins mTurquoise2, eGFP, mVenus and mCherry and the antibiotic resistance cassettes conferring resistance to either puromycin or blasticidin.

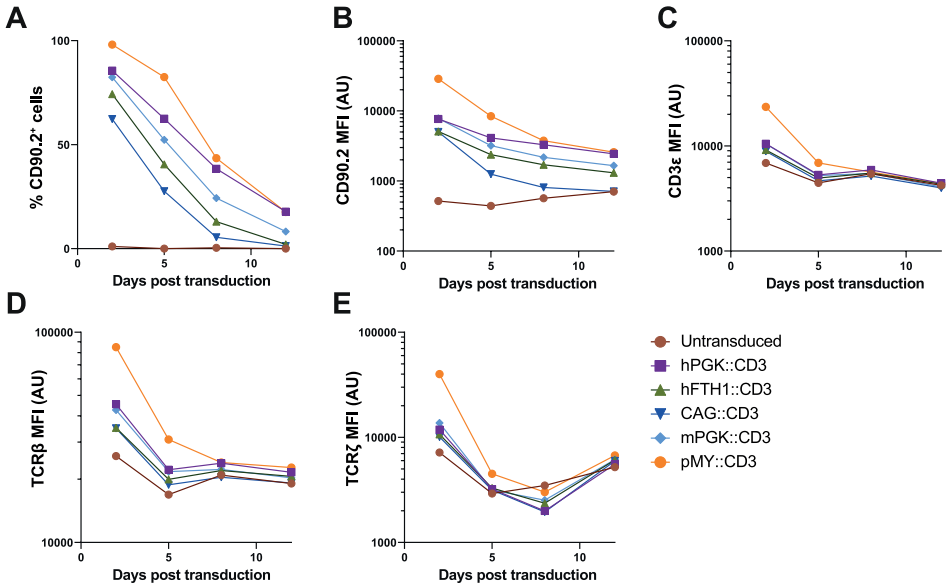

Figure 2: Testing promoter fidelity *in vitro* by overexpression of an oversized construct.

Murine C7 splenocytes were transduced with the indicated constructs 2 days after activation with ESAT-$6_{1\text{-}20}$ peptide in the presence of IL-12. Expression of CD90.2 (A, B), CD3ε (C), TCRβ (D) and TCRζ (E) was measured 2, 5, 8 and 12 days after transduction by flow cytometry within the viable $CD45^+$, $CD90.1^+$, $CD4^+$ cells. Cells were maintained in the presence of IL-2 after transduction, which was replaced with IL-7 at 8-days after transduction.

6

Assessment of optimal promoters for retroviral mediated knockdown in primary murine T cells *in vitro*

Besides creating vectors for overexpression studies, we were also interested in creating a range of retroviral and lentiviral vectors that can be used to knockdown genes of interest by expressing microRNAs (4). To select the optimal constructs for *in vitro* and *in vivo* microRNA-mediated knockdown, we tested the surface marker expression levels and knockdown efficiency of a range of TCRζ microRNA constructs. Since TCRζ is the limiting component for TCR surface expression, knockdown of TCRζ was expected to result in full loss of TCR/CD3 surface expression. First, we selected five target sequences for mouse *Cd247*/TCRζ from the genetic perturbation platform (https://portals.broadinstitute.org/gpp/public/) (Supplemental table 1), cloned corresponding antagomirs into a pMX-based vector, and tested for highest knockdown efficiency. The first target sequence (TRCN0000068158) was found to be most efficient in knockdown of TCRζ and ensuing reduction of surface TCRβ levels (data not shown). The antagomir targeting this sequence was cloned in pMY, or in pMX vectors with four different promoters (hPGK, hFTH1, CAG and mPGK), followed by

the surface marker CD90.2 (Figure 4A, Addgene vectors: 163324-8). As a non-target microRNA control, we selected a specific antagomir targeting the Rluc gene encoding *Renilla* luciferase (Supplemental table 1, Addgene vectors 163329-33).

We compared *in vitro* TCR-knockdown efficiency by transducing activated primary murine C7 CD4$^+$ T-cells with the respective retroviral knockdown constructs. We cultured C7 CD4$^+$ T-cells in the presence of IL-2 until 5 days after transduction, at which point it was replaced with IL-7 to allow long term *in vitro* culture of the T cells. The proportion of C7 cells expressing the retroviral construct was measured by CD90.2 staining and flow cytometry. The highest and most-stable expression of the knockdown construct was achieved by the constructs containing the hPGK and hFTH1 promoters (Figure 4C). However, the expression level of CD90.2 within the CD90.2$^+$ cells was highest in the cells transduced with the pMY vectors (Figure 4D). Expression from the CAG or mPGK promoters seemed to be the least efficient. Although differences in CD90.2 expression levels were pronounced between constructs, the knockdown efficiency of TCRζ (Figure 4E) and surface TCRβ (Figure 4F) were similar between the different constructs. This likely indicates that a plateau is reached for this efficient antagomir. Both the proportion of CD90.2$^+$ cells (Figure 4C) and the CD90.2 expression within those cells (Figure 4D) in the pMY-transduced cells seemed to fall considerably after the addition of IL-7 to the culture medium. Therefore, we repeated the experiment with a culture maintained on IL-2, which was discontinued at 8 days post transduction. Similar to the first experiment, the percentage of cells that expressed the construct was highest under control of the hPGK and hFTH1 promoters (Supplemental Figure 2A). However, these were now closely followed by pMY, which did not exhibit the marked decline of CD90.2$^+$ cells, previously observed after addition of IL-7. Expression levels of CD90.2 and reduction of surface TCRβ were highest in the constructs under control of the pMY-LTR and hPGK promoters and lowest under control of the CAG promoter (Supplemental Figure 2A-D). Together we conclude that for *in vitro* gene-silencing the pMY-LTR, hPGK and hFTH1 promoters are most efficient. Of these, pMY seemed to facilitate slightly higher expression levels leading to the most considerable reduction in surface TCRβ, whereas expression was more stable from hPGK and hFTH1 in the presence of IL-7. Because expression from pMY achieved the highest expression levels, but the expression of this vector was less stable, we also created pMY based knockdown vectors with puromycin and blasticidin resistance cassettes as well as the CD90.2 and Ly6G surface markers (Figure 4A, Addgene vectors 163340-1). These are our vectors of choice when knocking down genes *in vitro* in primary murine or human lymphocytes and can be used for single knockdown as well as for simultaneous knockdown of two genes of interest as we recently demonstrated in van der Donk et al. (3).

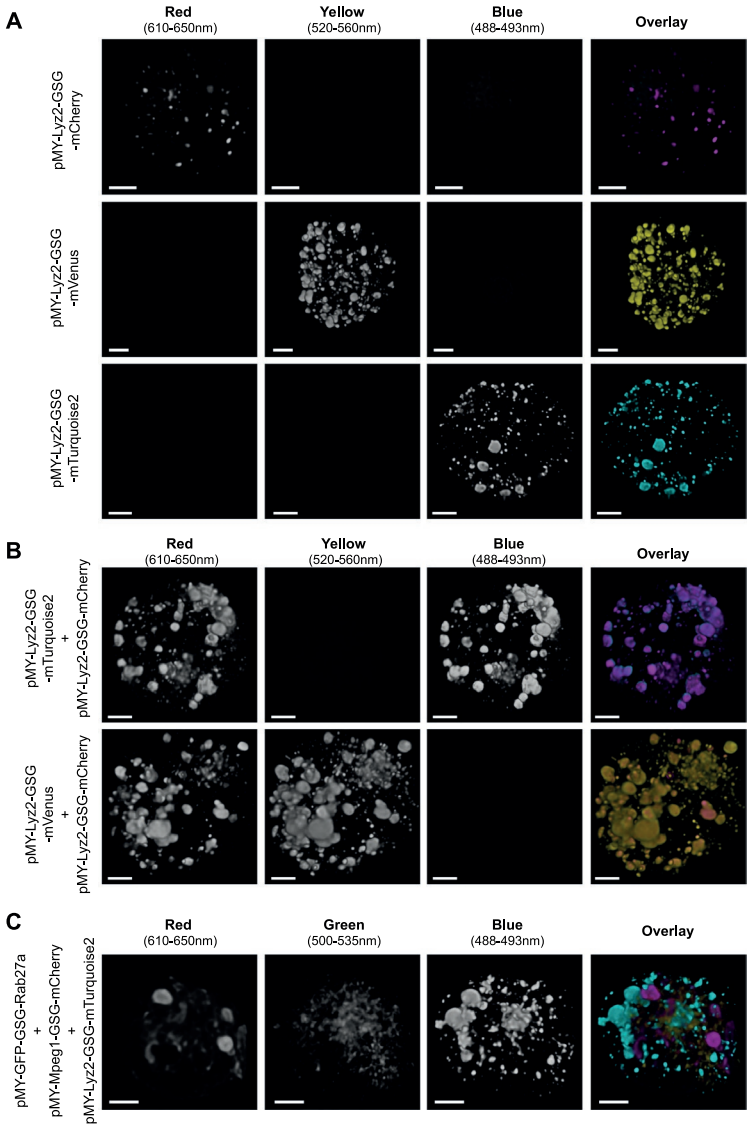

Figure 3: Validation of vectors encoding fluorescent proteins for cellular localization studies.

Murine C7 CD4⁺ T cells were transduced with the indicated vectors 2 days after activation. Cells were fixed and mounted to be imaged by confocal microscopy 2 days after transduction. (A-C) 3D rendering of Z-stacks with single channels depicted in greyscale and overlays of channels in artificial Cyan, Yellow and Magenta. (A) Transduction with single vectors expressing Lyz2, labeled by either mTurquoise2, mVenus, or mCherry shows similar subcellular localization independent of the fluorophore used and minimal spectral overlap in the other channels. (B) Co-transduction of two viral vectors was an effective approach to obtain cells expressing both constructs and led to full colocalization of the differently labeled proteins. (C) An example of triply transduced C7 CD4⁺ T cells co-expressing Lyz2-mTurquoise, GFP-Rab27a and Mpeg1-mCherry. Scale bars represent 2 nm.

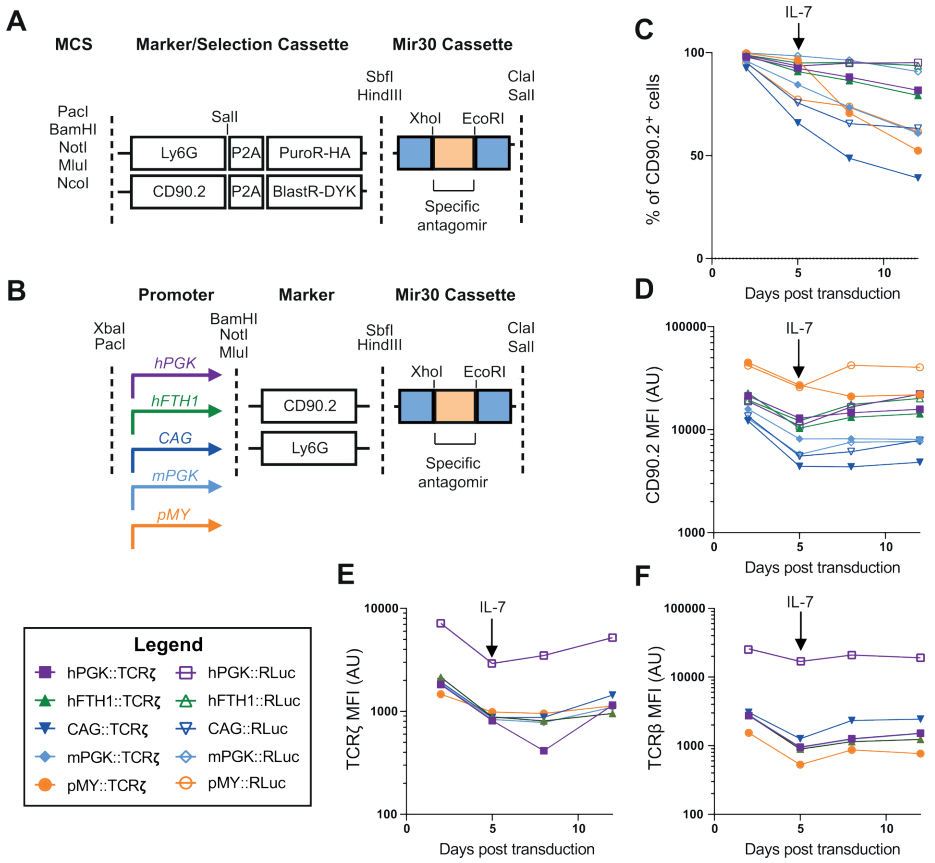

Figure 4: Design and *in vitro* validation of microRNA knockdown vectors.

(A) Design of vector inserts containing resistance cassettes to puromycin (PuroR), or blasticidin (BlastR). The vectors contain surface markers Ly6G or CD90.2, as well as an HA/FLAG epitope tag on the antibiotic resistance genes, to assess the transduction efficiency by flow cytometry. (B) Design of microRNA knockdown vectors suitable for *in vivo* experiments. The microRNA cassette is placed after the surface markers CD90.2 or Ly6G. Four different promoters were assessed in the pMX backbone and compared to the pMY vector with its LTR promoter. (C-F) Murine C7 CD4$^+$ T cells are activated and cultured *in vitro* and transduced with the indicated vectors containing a microRNA targeting *cd247* (TCRζ, filled symbols) or the *renilla* firefly luciferase (Rluc, empty symbols) gene as a non-target control. Transduction efficiency and stability were assessed by measuring the percentage of CD90.2$^+$ cells within the CD45$^+$, CD90.1$^+$, CD4$^+$ cells (C) and the CD90.2 expression levels within CD90.2$^+$ cells (D) at 2, 5, 8 and 12 days after transduction. Knockdown efficiency was assessed by measuring intracellular TCRζ (E) and surface TCRβ (F) within the CD90.2$^+$ population.

Comparison of promoters for retroviral mediated knockdown in CD4⁺ T cells *in vivo*
In parallel with the *in vitro* assessment of expression levels and stability described above, we also assessed these characteristics *in vivo*. The same transduced cells depicted in Figure 4C-F were administered to wild-type C57Bl/6 mice via intravenous injection of $2*10^6$ transduced CD4⁺ T cells 2 days after transduction (*i.e.* 4 days after T cell activation). The number and characteristics of the transferred C7 CD4⁺ T cells was followed over time by tail vain bleeds at the indicated intervals. The percentage of CD90.1⁺ cells (C7 T cells) of total leukocytes (defined here as CD45⁺ cells) was comparable for all promoter constructs except for the pMY vector which was markedly lower from day 10 onwards (Figure 5A). The level of CD90.2 expression was consistently lowest for constructs under control of the CAG and mPGK promoters. For the pMY vector, CD90.2 marker gene expression was initially high, but dropped significantly at 22 days post activation (Figure 5B). In contrast, the construct under control of the hPGK promoter was initially expressed at relatively low levels but this expression level was stable and even increased over time (Figure 5B). The efficiency of TCRζ knockdown was assessed by staining intracellular TCRζ as well as surface TCRβ and CD3ε (Figure 5C-E). Although differences between the constructs were modest, knockdown was clearly impaired at the latest timepoint when under control of the pMY promoter. Trends for the most efficient phenotypic knockdown closely resembled expression levels of CD90.2, with the most efficient and most stable knockdown being achieved under control of the hFTH1 promoter (Figure 5C-E). At the termination of the experiment, 22 days after T cell activation, we collected and homogenized lungs and spleens of recipient mice to assess knockdown efficiency in resident CD4⁺ T cells within these target tissues. Spleen and lung phenotypes closely resembled each other and showed considerably lower percentages of CD90.2⁺ cells when expressed from the pMY vector (Figure 5F, I). CD90.2 expression levels within the CD90.2⁺ cells were highest for constructs under control of hFTH1 and hPGK promoters although the latter was quite variable between individual animals (Figure 5G, J). Surface levels of TCR components did not markedly differ between the constructs expressed from the different pMX vectors, but decreased to control levels (Luciferase antagomir) with the pMY based vector (Figure 5H, K). Taken together, we conclude that the hFTH1 promoter is likely the prime candidate to achieve stable and high expression levels *in vivo*. These combined data indicate that our vectors can be used for efficient gene knockdown in primary murine CD4⁺ T cells and that vector expression and knockdown efficiency can be maintained over relatively long timespans allowing for *in vivo* experiments in the context of for instance *M. tuberculosis* infection (9-11).

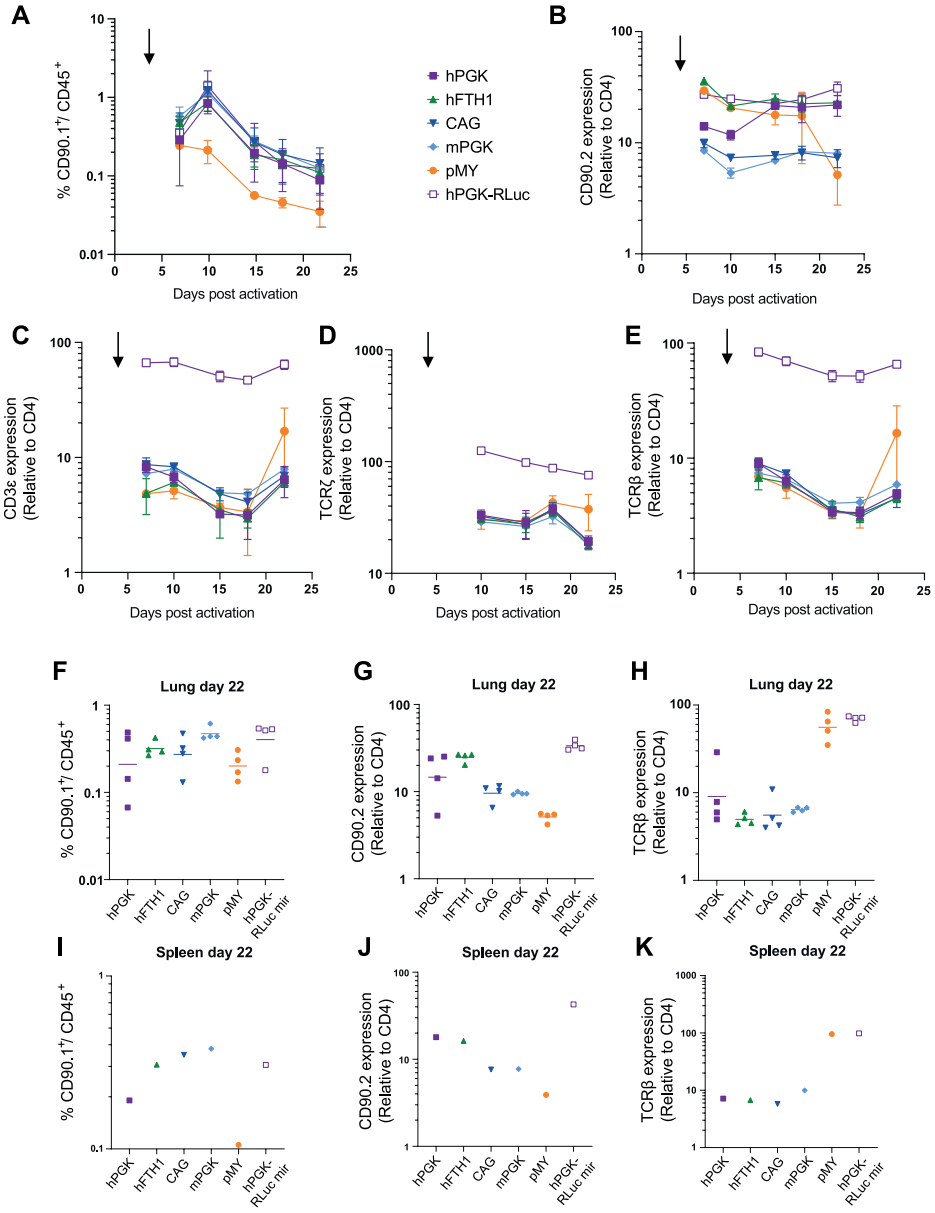
A
% CD90.1+/ CD45+
Days post activation
hPGK
hFTH1
CAG
mPGK
pMY
hPGK-RLuc
B
CD90.2 expression (Relative to CD4)
Days post activation
C
CD3ε expression (Relative to CD4)
Days post activation
D
TCRζ expression (Relative to CD4)
Days post activation
E
TCRβ expression (Relative to CD4)
Days post activation
F
Lung day 22
% CD90.1+/ CD45+
G
Lung day 22
CD90.2 expression (Relative to CD4)
H
Lung day 22
TCRβ expression (Relative to CD4)
I
Spleen day 22
% CD90.1+/ CD45+
J
Spleen day 22
CD90.2 expression (Relative to CD4)
K
Spleen day 22
TCRβ expression (Relative to CD4)
hPGK
hFTH1
CAG
mPGK
pMY
hPGK-RLuc mir

◂ Figure 5: *In vivo* validation of microRNA knockdown vectors.

Murine C7 CD4$^+$ T cells were activated and transduced before being adoptively transferred to wild-type C57Bl/6 mice by tail-vein injection 3 days post transduction (black arrow). (A-E) A maximum of 50 µL of blood was obtained from the mice at the indicated time points by tail-vein bleeds to investigate by flow cytometry. n=4 per group with some exceptions where adoptive transfer was unsuccessful. Individual values are depicted in Supplemental Figure 3. (A) The number of remaining C7 T cells was measured by assessing the percentage of CD90.1$^+$ cells within the CD45$^+$ cells. (B) The level of CD90.2 expression within the CD90.1$^+$ cells was normalized to CD4$^+$ expression and used as a read-out of expression stability of the vector. (C-E) Knockdown efficiency was measured by intracellular staining of TCRζ (D) and surface expression of CD3ε (C) and TCRβ (E). At the end of the experiment, mice were killed and lungs (F-H) and spleens (I-K) were homogenized to assess the percentage of remaining C7 cells (F, I), vector expression stability within the C7 cells (G, J), and knockdown efficiency of the TCR (H, K).

DISCUSSION

Laboratories that specialize in genetic modification of eukaryotic cells accrue and optimize their tools over the years. Although novel tools that push technical boundaries are often well described, tools that are the "workhorses" of genetic modification and especially data on their optimization or limitations, can be hard to find in published literature. We have developed a versatile toolbox of retroviral vectors, which can be readily used to induce or impair the expression of genes of interest in the context of a wide range of markers. We optimized our vectors allowing efficient cloning of building blocks in different vector backbones and we have tested the optimal promoter sequence for overexpression and genetic perturbation in primary murine lymphocytes *in vitro* and *in vivo*. These same vectors have been recently compared and used in primary human lymphocytes, further confirming their versatility (3).

It should be emphasized that these vector backbones, as well as the different promoter sequences, surface and fluorescent markers and shRNA-miR building blocks are not in themselves novel and are the result of decades of research by others (4-7, 13-17, 22, 23, 25). Furthermore, some researchers may prefer other methods to genetic perturbation based on CRISPR-Cas9 approaches (26, 27). However, these approaches have been particularly challenging to implement for primary murine and human lymphocytes. Although these difficulties can be circumvented by advanced methodology such as electroporation with purified Cas9 protein, implementing this requires costly reagents, or a specialized laboratory with a wide range of expertise (1, 2, 27). We were similarly unable to

transduce primary murine or human T cells efficiently with retroviral and lentiviral Cas9 expression vectors and have therefore opted for the optimized shRNA-miR strategy of genetic perturbation instead (3). It should be noted that research efforts to optimize microRNA design have markedly improved this technique over the last decade and knockdown efficiencies of >90% were in our experience often achievable with the system employed here (4, 5, 16).

Since we were unable to find any systematic comparison of the most efficient and stable promoters to express proteins and miRNA's in murine lymphocytes, we decided to perform these comparisons in this work. We find that the pMY vector backbone with its LTR promoter was the strongest promoter for *in vitro* experiments and therefore this is our promoter of choice in short-term *in vitro* experiments. We created versions of the pMY vectors with antibiotic resistance cassettes to further circumvent reduction of expression during *in vitro* culture. The silencing of pMY-based expression is likely due to the presence of IL-7 *in vivo* and in our extended *in vitro* culture conditions (28). Based on our *in vivo* experiments we conclude that the hFTH1 promoter is an excellent candidate to drive stable expression in adoptively transferred murine lymphocytes *in vivo*. The hPGK promoter may be the best choice when a single promoter for high and stable expression is needed for both *in vitro* and *in vivo* experiments (29). Surprisingly, we consistently observed higher expression driven by the hPGK promoter than the mPGK promoter, which could be due to a lack of endogenous repressors. This may similarly explain the efficiency of the hFTH1 promoter. Although the data on promoter performance provided here may be important for other researchers' experimental design, other experimental models may require independent optimization.

When these vectors are used for long-term *in vivo* experiments, such as the adoptive T cell transfer experiment described here, extra care should be taken in their choice and design. The overexpression of heterologous proteins, such as antibiotic selection markers and fluorescent proteins can lead to the development of adaptive immune responses against these components (30). Such immune responses could result in rejection of the adoptively transferred cells and thereby invalidate potential research findings. Therefore, we advise to only use these antibiotic and fluorescent selection markers *in vitro*, or in short-term *in vivo* experiments and opt for the Ly6G and CD90 surface markers for long-term *in vivo* experiments. Similar care should be taken to vector design on a molecular level, especially in the context of overexpression of a gene of interest. Firstly, the gene of interest should be investigated whether N-terminal or C-terminal tagging is expected to interfere with the protein product's

correct localization and function. When a C-terminal tag is not expected to have negative consequences, this may be preferable for reporter constructs, since the protein of interest can be expected to be produced in at least equimolar amounts as the reporter. Therefore, we have focused on C-terminal reporter constructs. In cases where it is expected or experimentally found that both N-terminal and C-terminal tagging interfere with protein function the IRES-sequence can be used to create transcriptional fusion of separate protein products.

Together, the vectors presented here form a versatile "starter set" for researchers with the ambition to apply molecular biology approaches to validate their research. We sincerely hope that sharing these vectors and the data regarding their optimization will aid researchers in immunology to apply these molecular techniques to their research.

Acknowledgements:
The authors would like to thank Joachim Goedhart for providing plasmids, insightful discussion and proofreading of the manuscript. We thank the microscopy twitter community for providing feedback shaping Figure 3. We thank Chiara Montironi and Eric Eldering for sharing plasmid pMSCV-IRES-mCherry. We thank Tom van der Poll for sharing expertise and resources. We thank the imaging core facility of the Amsterdam UMC for use of confocal microscope and technical assistance.

Author contribution:
Conceptualization: LEHvdD, JvdS, CPK, JWJvH, LSA; Methodology: LEHvdD, JvdS, TvD, MStB, JWJvH, LSA; Formal analysis: LEHvdD, JvdS, TBHG, JWJvH, LSA; Investigation: JvdS, MStB, JWJvH, LSA; Resources: MStB, CPK, JWJvH, LSA, TBHG; Data curation: JWJvH, LSA; Writing – original draft: LSA; Writing – review & editing: LEHvdD, TBHG, CPK, JWJvH, LSA; Visualization: LSA; Supervision: TBHG, JWJvH, LSA; Project administration: LEHvdD, TBHG, JWJvH, LSA.; Funding acquisition: TBHG, JWJvH, LSA.

Funding:
Open Access funding provided by Amsterdam UMC, University of Amsterdam, location AMC. Deposited in PMC for immediate release. LEHvdD, JvdS, JWJvH and LSA were supported by NWO-VIDI grant 91717305 to JWJvH). LSA was furthermore supported by a PostDoc stipend of the Amsterdam Infection and Immunity Institute.

Conflicts of interest statement:
All authors declare no commercial or financial conflicts of interest.

Ethics approval statement:
All animal experiments have been approved by the Dutch central committee for registration of animal experiments (CCD: Project DIX298) as well as the local committee of the AmsterdamUMC (formerly AMC, Work protocol DSK298).

Data availability:
The data that support the findings of this study are available from the corresponding author upon reasonable request.

REFERENCES

1. Hultquist JF, Schumann K, Woo JM, Manganaro L, McGregor MJ, Doudna J, et al. A Cas9 Ribonucleoprotein Platform for Functional Genetic Studies of HIV-Host Interactions in Primary Human T Cells. Cell Rep. 2016;17(5):1438-52.
2. Schumann K, Lin S, Boyer E, Simeonov DR, Subramaniam M, Gate RE, et al. Generation of knock-in primary human T cells using Cas9 ribonucleoproteins. Proc Natl Acad Sci U S A. 2015;112(33):10437-42.
3. van der Donk LEH, Ates LS, van der Spek J, Tukker LM, Geijtenbeek TBH, van Heijst JWJ. Separate signaling events control TCR downregulation and T cell activation in primary human T cells. Immun Inflamm Dis. 2021;9(1):223-38.
4. Dow LE, Premsrirut PK, Zuber J, Fellmann C, McJunkin K, Miething C, et al. A pipeline for the generation of shRNA transgenic mice. Nat Protoc. 2012;7(2):374-93.
5. Fellmann C, Hoffmann T, Sridhar V, Hopfgartner B, Muhar M, Roth M, et al. An optimized microRNA backbone for effective single-copy RNAi. Cell Rep. 2013;5(6):1704-13.
6. Kitamura T, Koshino Y, Shibata F, Oki T, Nakajima H, Nosaka T, et al. Retrovirus-mediated gene transfer and expression cloning: powerful tools in functional genomics. Exp Hematol. 2003;31(11):1007-14.
7. Kurachi M, Kurachi J, Chen Z, Johnson J, Khan O, Bengsch B, et al. Optimized retroviral transduction of mouse T cells for in vivo assessment of gene function. Nat Protoc. 2017;12(9):1980-98.
8. Morgan RA, Boyerinas B. Genetic Modification of T Cells. Biomedicines. 2016;4(2).
9. Gallegos AM, Pamer EG, Glickman MS. Delayed protection by ESAT-6-specific effector CD4+ T cells after airborne M. tuberculosis infection. J Exp Med. 2008;205(10):2359-68.
10. Gallegos AM, Xiong H, Leiner IM, Susac B, Glickman MS, Pamer EG, et al. Control of T cell antigen reactivity via programmed TCR downregulation. Nat Immunol. 2016;17(4):379-86.
11. Gallegos AM, van Heijst JW, Samstein M, Su X, Pamer EG, Glickman MS. A gamma interferon independent mechanism of CD4 T cell mediated control of M. tuberculosis infection in vivo. PLoS Pathog. 2011;7(5):e1002052.
12. Sanjana NE, Shalem O, Zhang F. Improved vectors and genome-wide libraries for CRISPR screening. Nat Methods. 2014;11(8):783-4.
13. Chertkova AO, Mastop M, Postma M, van Bommel N, van der Niet S, Batenburg KL, et al. Robust and Bright Genetically Encoded Fluorescent Markers for Highlighting Structures and Compartments in Mammalian Cells. bioRxiv. 2020:160374.
14. Goedhart J, von Stetten D, Noirclerc-Savoye M, Lelimousin M, Joosen L, Hink MA, et al. Structure-guided evolution of cyan fluorescent proteins towards a quantum yield of 93%. Nat Commun. 2012;3:751.
15. Kremers GJ, Goedhart J, van Munster EB, Gadella TW, Jr. Cyan and yellow super fluorescent proteins with improved brightness, protein folding, and FRET Forster radius. Biochemistry. 2006;45(21):6570-80.
16. Chang K, Marran K, Valentine A, Hannon GJ. Creating an miR30-based shRNA vector. Cold Spring Harb Protoc. 2013;2013(7):631-5.
17. Naviaux RK, Costanzi E, Haas M, Verma IM. The pCL vector system: rapid production of helper-free, high-titer, recombinant retroviruses. J Virol. 1996;70(8):5701-5.

18. Chang K, Marran K, Valentine A, Hannon GJ. Packaging shRNA retroviruses. Cold Spring Harb Protoc. 2013;2013(8):734-7.
19. Pestova TV, Hellen CU, Shatsky IN. Canonical eukaryotic initiation factors determine initiation of translation by internal ribosomal entry. Mol Cell Biol. 1996;16(12):6859-69.
20. Liu Z, Chen O, Wall JBJ, Zheng M, Zhou Y, Wang L, et al. Systematic comparison of 2A peptides for cloning multi-genes in a polycistronic vector. Sci Rep. 2017;7(1):2193.
21. Goedhart J, van Weeren L, Adjobo-Hermans MJ, Elzenaar I, Hink MA, Gadella TW, Jr. Quantitative co-expression of proteins at the single cell level--application to a multimeric FRET sensor. PLoS One. 2011;6(11):e27321.
22. Cormack BP, Valdivia RH, Falkow S. FACS-optimized mutants of the green fluorescent protein (GFP). Gene. 1996;173(1 Spec No):33-8.
23. Shaner NC, Campbell RE, Steinbach PA, Giepmans BN, Palmer AE, Tsien RY. Improved monomeric red, orange and yellow fluorescent proteins derived from Discosoma sp. red fluorescent protein. Nat Biotechnol. 2004;22(12):1567-72.
24. Addgene. Plasmids 101: A Desktop Resource.: Addgene.Org2017, 1-125; 2017 [
25. Lambert TJ. FPbase: a community-editable fluorescent protein database. Nat Methods. 2019;16(4):277-8.
26. Jinek M, Chylinski K, Fonfara I, Hauer M, Doudna JA, Charpentier E. A programmable dual-RNA-guided DNA endonuclease in adaptive bacterial immunity. Science. 2012;337(6096):816-21.
27. Roth TL, Puig-Saus C, Yu R, Shifrut E, Carnevale J, Li PJ, et al. Reprogramming human T cell function and specificity with non-viral genome targeting. Nature. 2018;559(7714):405-9.
28. Tsunetsugu-Yokota Y, Kobayahi-Ishihara M, Wada Y, Terahara K, Takeyama H, Kawana-Tachikawa A, et al. Homeostatically Maintained Resting Naive CD4(+) T Cells Resist Latent HIV Reactivation. Front Microbiol. 2016;7:1944.
29. Adra CN, Boer PH, McBurney MW. Cloning and expression of the mouse pgk-1 gene and the nucleotide sequence of its promoter. Gene. 1987;60(1):65-74.
30. Stripecke R, Carmen Villacres M, Skelton D, Satake N, Halene S, Kohn D. Immune response to green fluorescent protein: implications for gene therapy. Gene Ther. 1999;6(7):1305-12.

SUPPLEMENTAL INFORMATION
SUPPLEMENTAL METHODS 1: SYNTHESIZED SEQUENCES.

CD3-complex optimized NotI-gamma-MfeI-T2A-delta-MluI-F2A-epsilon-SphI-E2A-zeta-SalI-P2A-Ly6G-SbfI

GCAGAACCGCGGCCGCGCCACCATGGAACAGAGAAAAGGCCTGGCCGGCCTGTTCCTG-
GTTATCAGTCTGCTGCAGGGCACAGTGGCCCAGACCAACAAGGCTAAGAACCTGGTGCAG-
GTGGACGGCTCTAGAGGCGACGGATCTGTGCTGCTGACATGTGGCCTGACCGACAAGAC-
CATCAAGTGGCTGAAGGACGGCTCCATCATCAGCCCTCTGAACGCCACCAAGAACACCT-
GGAACCTGGGCAACAACGCCAAGGACCCCAGAGGCACCTATCAGTGCCAGGGCGCCAAA-
GAGACAAGCAACCCTCTGCAGGTCTACTACAGAATGTGCGAGAACTGCATCGAGCTGAA-
CATCGGCACCATCAGCGGCTTCATCTTCGCCGAAGTGATCAGCATCTTCTTTCTGGC-
CCTGGGCGTGTACCTGATCGCTGGACAAGATGGCGTGCGGCAGAGCAGAGCCAGCGA-
TAAGCAGACACTGCTGCAGAACGAGCAGCTGTACCAGCCTCTGAAGGACAGAGAGTAC-
GACCAGTACAGCCACCTCCAGGGCAACCAGCTGCGGAAGAAGGGATCTGGCCAATTG-
GAAGGCAGAGGCTCTCTTCTTACATGCGGCGACGTCGAGGAAAACCCAGGACCTATG-
GAACACTCTGGCATCCTGGCTAGCCTGATCCTGATTGCCGTTCTGCCTCAAGGCAGC-
CCCTTCAAGATCCAAGTGACCGAGTACGAGGACAAGGTGTTCGTGACCTGCAACACCAGC-
GTGATGCACCTGGATGGCACCGTGGAAGGATGGTTCGCCAAGAACAAGACCCTGAACCTC-
GGCAAGGGCGTGCTGGACCCTAGAGGCATCTACCTGTGTAACGGCACAGAGCAGCTGG-
CCAAGGTGGTGTCTAGTGTGCAGGTCCACTATCGGATGTGTCAGAACTGCGTGGAACTG-
GACAGCGGCACAATGGCCGGCGTGATCTTCATCGACCTGATCGCTACCCTGCTGCTGG-
CACTGGGAGTGTATTGCTTCGCTGGCCACGAGACAGGCAGACCTAGCGGAGCTGCTGA-
AGTTCAGGCCCTGCTGAAGAATGAACAGCTCTATCAGCCCCTGCGCGACAGAGAGGATAC-
CCAGTACTCTAGACTCGGCGGCAACTGGCCCAGAAACAAGAAATCTGGAAGCGGCACG-
CGTGTCAGACAGACCCTGAACTTCGATCTGCTTAGACTGGCCGGGGACGTCGAGTCTA-
ATCCAGGACCAATGCGGTGGAACACCTTCTGGGGCATCCTGTGTCTGTCTCTGCTGGCT-
GTGGGCACCTGTCAGGATGACGCTGAGAACATCGAGTATAAGGTGTCCATCTCCGGCAC-
CAGCGTCGAGCTGACTTGTCCTCTGGACTCCGACGAGAACCTGAAGTGGGAGAAGAAC-
GGCCAAGAGCTGCCTCAGAAGCACGACAAGCACCTGGTGCTGCAGGACTTCAGCGAG-
GTGGAAGATAGCGGCTACTACGTGTGCTACACCCCTGCCAGCAACAAGAACACATACCT-
GTACCTGAAGGCTCGCGTGTGCGAGTACTGTGTCGAGGTGGACCTGACAGCCGTGGC-
TATCATCATCATCGTGGACATCTGCATCACCCTGGGCCTGCTGATGGTCATCTACTACTG-
GTCCAAGAACCGGAAGGCCAAGGCCAAGCCTGTGACAAGAGGAACCGGCGCTGGAAG-
CAGACCAAGAGGCCAGAACAAAGAAAGACCTCCTCCTGTGCCTAATCCTGACTACGAGC-
CCATCCGGAAGGGCCAGAGAGATCTGTACTCTGGCCTGAACCAGAGGGCCGTGGGTTCTG-
GCGCATGCCAGTGTACCAACTATGCTCTCCTGAGACTCGCAGGCGACGTTGAGAGTAATC-
CAGGGCCTATGAAGTGGAAAGTGTCTGTGCTGGCCTGCATCCTGCATGTTCGATTCCCTGG-

CGCTGAGGCCCAGTCTTTTGGACTGCTGGACCCCAAGCTGTGCTACCTGCTGGACGGCAT-
TCTGTTTATTTATGGCGTGATCATCACCGCTCTGTACCTGCGGGCCAAGTTCAGCAGAAGC-
GCTGAGACAGCTGCCAATCTGCAGGACCCTAACCAGCTGTACAACGAGCTGAATCTGGGG-
CGCAGAGAAGAGTACGATGTGCTGGAAAAGAAGAGAGCCAGAGATCCCGAGATGGGCG-
GCAAACAGCAGAGAAGGCGGAATCCTCAAGAAGGCGTGTACAACGCCCTGCAGAAAGA-
TAAGATGGCCGAGGCCTACAGCGAGATCGGCACAAAGGGCGAACGCAGAAGAGGCAAG-
GGACACGATGGACTGTACCAGGGCCTGTCCACAGCCACAAAGGACACATACGATGCCCT-
GCACATGCAGACACTGGCCCCTAGAGGCAGCGGCGTCGACGCCACAAACTTCAGCCT-
GCTGAGACAGGCTGGCGACGTGGAAGAGAATCCTGGACCTATGGACACCTGTCATATC-
GCCAAGAGCTGCGTGCTGATCCTGCTGGTGGTTCTGCTGTGTGCCGAGCGAGCACAGG-
GACTGGAGTGCTACAACTGTATCGGCGTGCCACCTGAGACAAGCTGCAACACCACCACCT-
GTCCTTTCAGCGACGGCTTCTGTGTGGCCCTGGAAATCGAAGTGATCGTGGACAGCCAC-
CGCAGCAAAGTGAAGTCCAACCTGTGCCTGCCTATCTGCCCCACCACACTGGACAACAC-
CGAGATCACAGGCAACGCCGTGAACGTGAAAACCTACTGCTGCAAAGAGGACCTCTG-
CAACGCCGCTGTTCCAACAGGCGGAAGCTCTTGGACAATGGCTGGCGTGCTGCTGTTCAG-
CCTGGTGTCTGTTCTGCTGCAGACCTTCCTGTGACCTGCAGGGGATGCAT

hPGK:

TTAATTAACGGGGTTGGGGTTGCGCCTTTTCCAAGGCAGCCCTGGGTTTGCGCAGGGACG-
CGGCTGCTCTGGGCGTGGTTCCGGGAAACGCAGCGGCGCCGACCCTGGGTCTCGCACAT-
TCTTCACGTCCGTTCGCAGCGTCACCCGGATCTTCGCCGCTACCCTTGTGGGCCCCCCG-
GCGACGCTTCCTGCTCCGCCCCTAAGTCGGGAAGGTTCCTTGCGGTTCGCGGCGTGCCG-
GACGTGACAAACGGAAGCCGCACGTCTCACTAGTACCCTCGCAGACGGACAGCGCCAGG-
GAGCAATGGCAGCGCGCCGACCGCGATGGGCTGTGGCCAATAGCGGCTGCTCAGCAGGG-
CGCGCCGAGAGCAGCGGCCGGGAAGGGGCGGTGCGGGAGGCGGGGTGTGGGGCGGTAGT-
GTGGGCCCTGTTCCTGCCCGCGCGGTGTTCCGCATTCTGCAAGCCTCCGGAGCGCACGTC-
GGCAGTCGGCTCCCTCGTTGACCGAATCACCGACCTCTCTCCCCAGGGATCC

mPGK:

GCAGAACCTTAATTAAAAATTCTACCGGGTAGGGGAGGCGCTTTTCCCAAGGCAGTCT-
GGAGCATGCGCTTTAGCAGCCCCGCTGGGCACTTGGCGCTACACAAGTGGCCTCTG-
GCCTCGCACACATTCCACATCCACCGGTAGGCGCCAACCGGCTCCGTTCTTTGGTG-
GCCCCTTCGCGCCACCTTCTACTCCTCCCCTAGTCAGGAAGTTCCCCCCCGCCCCG-
CAGCTCGCGTCGTGCAGGACGTGACAAATGGAAGTAGCACGTCTCACTAGTCTCGT-
GCAGATGGACAGCACCGCTGAGCAATGGAAGCGGGTAGGCCTTTGGGGCAGCGGC-
CAATAGCAGCTTTGCTCCTTCGCTTTCTGGGCTCAGAGGCTGGGAAGGGGTGGGTCCGG-
GGGCGGGCTCAGGGGCGGGCTCAGGGGCGGGGCGGGCGCCCGAAGGTCCTCCGGAGGC-
CCGGCATTCTGCACGCTTCAAAAGCGCACGTCTGCCGCGCTGTTCTCCTCTTCCTCATCTC-
CGGGCCTTTCGACGGATCCGGATGCAT

hFTH1:

TTAATTAATCCGCCAGAGCGCGCGAGGGCCTCCACCGGCCGCCCCTCCCCCACAGCAGGG-
GCGGGGTCCCGCGCCCACCGGAAGGAGCGGGCTCGGGGCGGGCGGCGCTGATTGGCCG-
GGGCGGGCCTGACGCCGACGCGGCTATAAGAGACCACAAGCGACCCGCAGGGCCAGAC-
GTTCTTCGCCGAGAGTCGTCGGGGTTTCCTGCTTCAACAGTGCTTGGACGGAACCCGGC-
GCTCGTTCCCCACCCCGGCCGGCCGCCCATAGCCAGCCCTCCGTCACCTCTTCACCGCAC-
CCTCGGACTGCCCCAAGGCCCCCGCCGCCGCTCCAGCGCCGCGCAGCCACCGCCGCCGC-
CGCCGCCTCTCCTTAGTCGCCGCCGGATCC

CAG:

TTAATTAATCGACATTGATTATTGACTAGTTATTAATAGTAATCAATTACGGGGTCAT-
TAGTTCATAGCCCATATATGGAGTTCCGCGTTACATAACTTACGGTAAATGGCCCGCCTG-
GCTGACCGCCCAACGACCCCCGCCCATTGACGTCAATAATGACGTATGTTCCCATAGTA-
ACGCCAATAGGGACTTTCCATTGACGTCAATGGGTGGACTATTTACGGTAAACTGC-
CCACTTGGCAGTACATCAAGTGTATCATATGCCAAGTACGCCCCCTATTGACGTCAATGAC-
GGTAAATGGCCCGCCTGGCATTATGCCCAGTACATGACCTTATGGGACTTTCCTACTTGG-
CAGTACATCTACGTATTAGTCATCGCTATTACCATGGGTCGAGGTGAGCCCCACGTTCT-
GCTTCACTCTCCCCATCTCCCCCCCCTCCCCACCCCCAATTTTGTATTTATTTATTTTTTA-
ATTATTTTGTGCAGCGATGGGGGCGGGGGGGGGGGGGGCGCGCGCCAGGCGGGGCG-
GGGCGGGGCGAGGGGCGGGGCGGGGCGAGGCGGAGAGGTGCGGCGGCAGCCAATCA-
GAGCGGCGCGCTCCGAAAGTTTCCTTTTATGGCGAGGCGGCGGCGGCGGCGGCCCTATA-
AAAAGCGAAGCGCGCGGCGGGCGGGAGTCGCTGCGTTGCCTTCGCCCCGTGCCCCGCTC-
CGCGCCGCCTCGCGCCGCCCGCCCCGGCTCTGACTGACCGCGTTACTCCCACAGGTGAG-
CGGGCGGGACGGCCCTTCTCCTCCGGGCTGTAATTAGCGCTTGGTTTAATGACGGCTC-
GTTTCTTTTCTGTGGCTGCGTGAAAGCCTTAAAGGGCTCCGGGAGGGGGATCC

Ly6Gopt

GCAGAACCCCTGCAGGCCACCATGGACACCTGTCATATCGCCAAGAGCTGCGTGCT-
GATCCTGCTGGTGGTTCTGCTGTGTGCCGAGCGAGCACAGGGACTGGAGTGCTACAACT-
GTATCGGCGTGCCACCTGAGACAAGCTGCAACACCACCACCTGTCCTTTCAGCGAC-
GGCTTCTGTGTGGCCCTGGAAATCGAAGTGATCGTGGACAGCCACCGCAGCAAAGT-
GAAGTCCAACCTGTGCCTGCCTATCTGCCCCACCACACTGGACAACACCGAGATCACAG-
GCAACGCCGTGAACGTGAAAACCTACTGCTGCAAAGAGGACCTCTGCAACGCCGCT-
GTTCCAACAGGCGGAAGCTCTTGGACAATGGCTGGCGTGCTGCTGTTCAGCCTGGTGTCT-
GTTCTGCTGCAGACCTTCCTGTGAGCATGCCAATTCTCATCGATTGCATTGGGTCGACG-
GATGCAT

SUPPLEMENTAL FIGURES

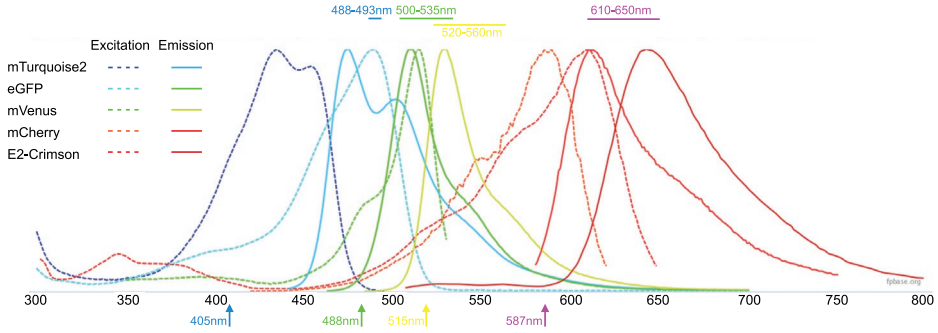

Supplemental Figure 1: Excitation and emission spectra of the used fluorescent proteins.

The X-axis depicts the wavelength in nm; Y-axis depicts relative fluorescent intensity for each fluorophore. Primary investigations with E2-Crimson were not promising and this protein was therefore not included in the vector set. Not that excitation and emission spectra of eGFP and mVenus are quite close and therefore these proteins should only be used together with that knowledge considered. Colored arrows at the bottom indicate used excitation wavelengths. Bars and text at the top indicate acquisition wavelengths used for mTQ2, GFP, mVenus and mCherry respectively. Figure was created with fpbase.org spectra-viewer tool.

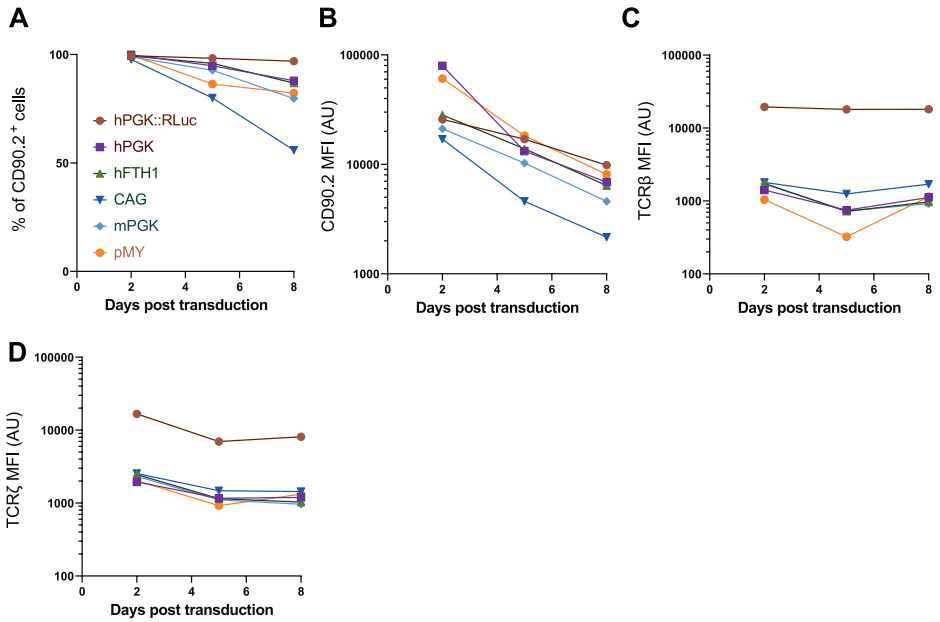

Supplemental Figure 2: Vector stability and expression *in vitro*, without the addition of IL-7.

The experiment in Figure 4C-F was repeated, but cells were maintained constantly on IL-2 instead of changing to IL-7 supplementation 5 days post transduction. Comparable results regarding the proportion of CD90.2⁺ cells (A) and the expression levels of the CD90.2 surface marker (B), TCRβ (C) and TCRζ (D) within the CD90.2⁺ population were obtained, except for the steep decline in the percentage of CD90.2⁺ cells observed for cells transduced with pMY observed before. Note that without the addition of IL-7 the cells stop proliferating strongly after 5 days post-transduction and therefore the experiment was terminated at day 8.

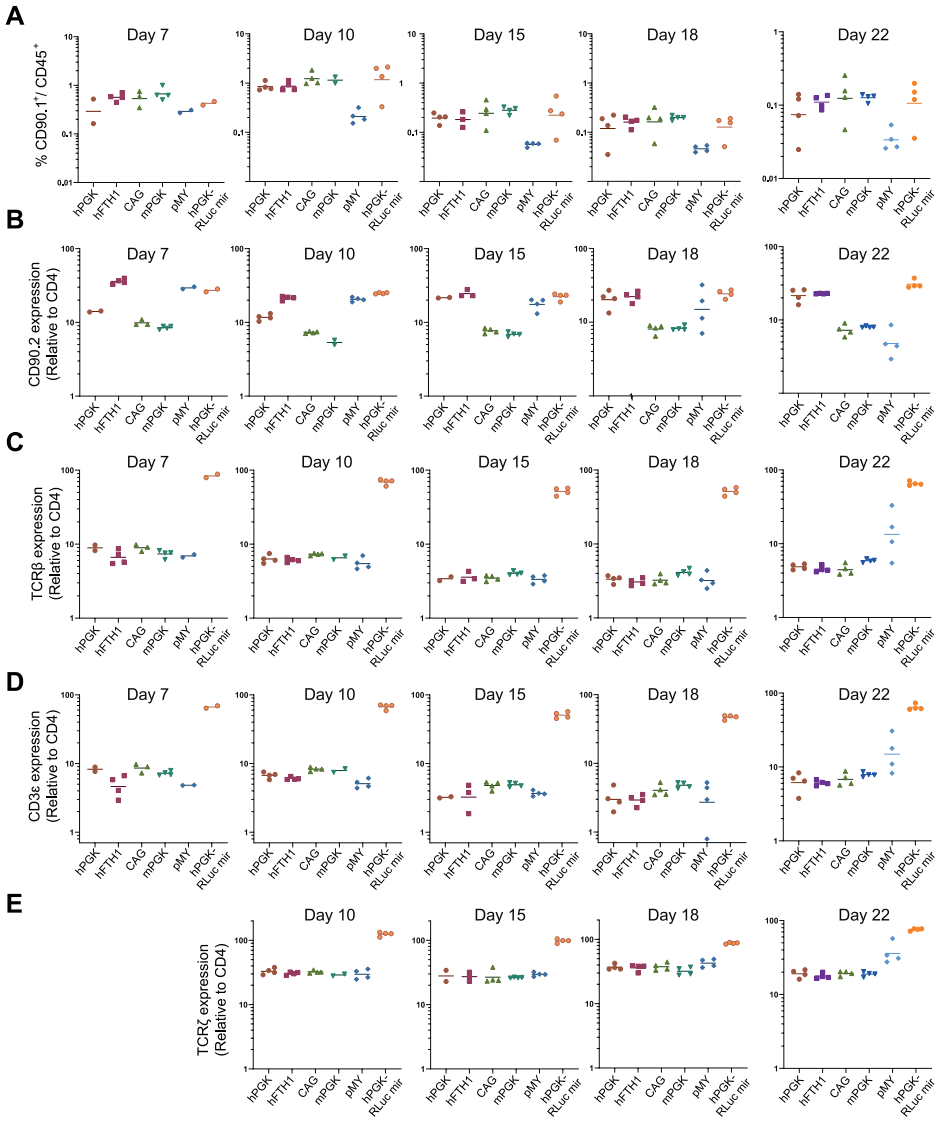

Supplemental Figure 3: Individual values of *in vivo* vector validation in blood.

Individual values corresponding to the data of figure 5A-E. Cells obtained from tail-vein bleeds at the indicated timepoints were assessed by flow cytometry. Bars depict the mean.

Supplemental File 1: Full information on all vectors used in this study and constructed as part of the vector starter set.

SUPPLEMENTAL TABLES

Supplemental table 1: shRNA-miRs used in this study.

Target	shRNA-MiR code	Target Sequence
CD247/TCRζ-A	TRCN0000068158	CCTCTTCATCTACGGAGTCAT
CD247/TCRζ-B	TRCN0000068159	GCTAGATGGAATCCTCTTCAT
CD247/TCRζ-C	TRCN0000068160	CGTATACAATGCACTGCAGAA
CD247/TCRζ-D	TRCN0000068161	CTCTACAATGAGCTCAATCTA
CD247/TCRζ-E	TRCN0000068162	CCAATCCTGTGCCAGCGTCTT
Renilla Firefly luciferase	SHC007	CCGCTGAGTACTTCGAAATGTC

The antagomir target sequences were derived from the genetic perturbation platform of the Broad Institute (https://portals.broadinstitute.org/gpp/public/). Bold sequences were selected and used throughout the manuscript.

Supplemental table 2: Primers used in this study.

Primer name	**Primer sequence 5′ → 3′**
hFTH1prom_Pac_Fwd	GCAGAACCTTAATTAATCCGCCAGAGCGCGCGAG
hFTH1prom_Bam_Rev	ATGCATCCGGATCCGGCGGCGACTAAGGAGAGGC
mPGK_prom_Pac_Fwd	GCAGAACCTTAATTAAAAATTCTACCGGGTAGGGGAGGCGCTTTTC
mPGK_prom_Bam_Rev	ATGCATCCGGATCCGTCGAAAGGCCCGGAGATGAGGAAGA
hPGK_Fwd (PacI)	GCAGAACCTTAATTAACGGGGTTGGGGTTGCGCCTTT
hPGK_Rev (BamHI)	ATGCATCCGGATCCCTGGGGAGAGAGGTCGGTGATTCG
CMV_prom_Pac_Fwd	GCAGAACCTTAATTAAGACATTGATTATTGACTAGTTATTAATAGTA-ATCAATTACGGGGTCAT
CMV_prom_Bam_Rev	ATGCATCCGGATCCAGCTCTGCTTATATAGACCTCCCACCGTA
miR30_Hind_Fwd	GCAGAACCAAGCTTTGTTTGAATGAGGCTTCAGTACTTTACAGAAT
miR30_Cla_Rev	ATGCATCCATCGATAAAGTGATTTAATTTATACCATTTTAAT-TCAGCTTTGT
miRE-Xho-Fwd	TACAAATACTCGAGAAGGTATATTGCTGTTGACAGTGAGCG
miRE-Eco-Rev	ACTTAGAAGAATTCTAGCCCCTTGAAGTCCGAGGCAGTAGGC
Ly6Gopt_SalP2A_Fwd	CAGAACCACGCGTGGCCTGGCATGCCGCGACGTCGACGC-CACAAACTTCAGCCTGCTGAGACAGGCTGGCGACGTGGAA-GAGAATCCTGGACCTATGGACACCTGTCATATCGCCAAGAG
CD90.2_SalP2A_Fwd	GCAGAACCACGCGTGGCCTGGCATGCCGCGACGTCGACGC-CACAAACTTCAGCCTGCTGAGACAGGCTGGCGACGTGGAA-GAGAATCCTGGACCTATGAACCCCGCCATCTCTGTG
Ly6Gopt_Sbf_Rev	ATGCATCCCCTGCAGGTCACAGGAAGGTCTGCAGCAGAA
CD90.2_Sbf_Rev	ATGCATCCCCTGCAGGCTACAGAGAGATGAAGTCCAGGGC

Supplemental table 2: Primers used in this study.

Primer name	Primer sequence 5′ → 3′
P2A_SalI_Fwd	GCAGAACCGTCGACGCCACGAACTTCTCTCTGTTAAGACAA
GFP_Sbf_Rev	ATGCATCCCCTGCAGGTTACTTGTACAGCTCGTCCATGCCG
BlastR_SalP2A_Fwd	CAGAACCGTCGACGCCACAAACTTCAGCCTGCTGAGACAGGCTGGCGACGTGGAAGAGAATCCTGGACCTATGAAAACATTTAACATTTCTCAACAAGATCTAGAATTAGTAGAAGTAGC
BlastR_DYK_Sbf_Rev	ATGCATCCCCTGCAGGTCATTTGTCGTCGTCGTCCTTGTAGTCGCCGCTGCCATTTCGGGTATATTTGAGTGGAATGAGTTCTTCAATCG
PuroR_SalP2A_Fwd	GCAGAACCACGCGTGGCCTGGCATGCCGCGACGTCGACGCCACAAACTTCAGCCTGCTGAGACAGGCTGGCGACGTGGAAGAGAATCCTGGACCTATGACCGAGTACAAGCCCACG
PuroR_HA_Sbf_Rev	ATGCATCCCCTGCAGGTCAGGCGTAATCAGGCACATCGTAAGGGTAGCCGCTGCCGGCACCGGGCTTGCGGG
mCherry_Sal_GSG_Fw	GCAGAACCGTCGACGGATCTGGCATGGTGAGCAAGGGCGAGGA
mCherry_Hind_Rv	ATGCATCCAAGCTTTTACTTGTACAGCTCGTCCATGCC
Lyz2_MluI_Fwd	GCAGAACCACGCGTGCCACCATGAAGACTCTCCTGACTCTGGGACT
Lyz2_GSG_SalI_Rev	ATGCATCCGTCGACGCCAGATCCGACTCCGCAGTTCCGAATATACTGG
EFS_Pac_Fwd	GCAGAACCTTAATTAAGGCTCCGGTGCCCGTCAGT
EFS_Bam_Rv	ATGCATCCGGATCCCCTGTGTTCTGGCGGCAAACC
SHC007_shRNAmiR_temp	TGCTGTTGACAGTGAGCGCCGCTGAGTACTTCGAAATGTCTAGTGAAGCCACAGATGTAGACATTTCGAAGTACTCAGCGTTGCCTACTGCCTCGGA
Cd247A_miR_temp	TGCTGTTGACAGTGAGCGCCCTCTTCATCTACGGAGTCATTAGTGAAGCCACAGATGTAATGACTCCGTAGATGAAGAGGATGCCTACTGCCTCGGA

Supplemental Table 3: Antibody combinations used for flow cytometry staining.

	Transfection (Panel 1)	MACS (Panel 2)	*In vitro*/*vivo* (Panel 3)
FITC	Ly6G#	B220	CD3ε
PE		CD62L	TCRζ*
PE/Dazzle594		CD45	CD45
PerCP/eFluor710		CD11a	CD90.2
PE/Cy7		CD4	CD4
APC	CD90.2#	TCRβ	TCRβ
AlexaFluor700		CD90.1	CD90.1
eFluor 780	Viability	Viability	Viability

Details on the individual antibodies can be found in Supplemental table 4. *: Intracellular stain performed after fixation and permeabilization. #: Marker specific staining was used where opportune.

Supplemental Table 4: Antibody clones, suppliers and dilutions used in this study.

Name	reactivity	Supplier	Isotype	Clone	Catalog #	Dilution
Ly-6G/Ly-6C-FITC	Mouse	eBiosci.	Rat IgG2b, κ	RB6-8C5	11-5931-82	1:400
CD90.2-APC	Mouse	BD Biosci.	Rat IgG2a, κ	53-2.1	553007	1:400
CD90.2- PerCP eFluor710	Mouse	eBiosci.	Rat IgG2b, κ	30-H12	46-0903-80	1:400
CD45R/B220-FITC	Mouse	BD Biosci.	Rat IgG2a, κ	RA3-6B2	553087	1:100
CD62L-PE	Mouse	BD Biosci.	Rat IgG2a, κ	MEL-14	553151	1:100
CD45-PE/Dazzle594	Mouse	Biolegend	Rat IgG2b, κ	30-F11	103146	1:800
CD11a-PerCP eFluor710	Mouse	eBiosci.	Rat IgG2a, κ	M17/4	46-0111-80	1:400
CD4-PE/Cy7	Mouse	Biolegend	Rat IgG2a, κ	RM4-5	100528	1:400
TCRβ- APC	Mouse	Biolegend	Hamster/IgG	H57-597	109212	1:100
TCRζ (CD247)-PE	Human/Mouse	Biolegend	Mouse IgG1κ	6B10.2	644106	1:100
CD90.1-AlexaFluor700	Mouse	Biolegend	Mouse IgG1κ	OX-7	202528	1:400
CD3ε-FITC	Mouse	Biolegend	Hamster IgG	145-2C11	100306	1:100
Fixable viability dye eFLuor780	N/A	eBiosci.	N/A	N/A	N/A	1:1000

CHAPTER 7

SEPARATE SIGNALING EVENTS CONTROL TCR DOWNREGULATION AND T CELL ACTIVATION IN PRIMARY HUMAN T CELLS

Lieve E.H. van der Donk[1,2]*, Louis S. Ates[1,2], Jet van der Spek[1,2], Laura M. Tukker[1,2], Teunis B.H. Geijtenbeek[1,2], Jeroen W.J. van Heijst[1,3]

[1] Amsterdam UMC location AMC, Department of Experimental Immunology, Meibergdreef 9, Amsterdam, The Netherlands;
[2] Amsterdam institute for Infection and Immunity, Infectious diseases, Amsterdam, The Netherlands;
[3] Current address: Neogene Therapeutics, Science Park 106, 1096 XG Amsterdam, The Netherlands.

* Address correspondence and reprint requests to L.E.H. van der Donk, Amsterdam UMC, Meibergdreef 9, 1105 AZ, Amsterdam.

Immunity, Inflammation and Disease 2021;9:223-238.

ABSTRACT

Introduction: T cell antigen receptor (TCR) interaction with cognate peptide:MHC complexes triggers clustering of TCR/CD3 complexes and signal transduction. Triggered TCR/CD3 complexes are rapidly internalized and degraded in a process called ligand-induced TCR downregulation. Classic studies in immortalized T cell lines have revealed a major role for the Src family kinase Lck in TCR downregulation. However, to what extent a similar mechanism operates in primary human T cells remains unclear.

Methods: Here, we developed an anti-CD3-mediated TCR downregulation assay, in which T cell gene expression in primary human T cells can be knocked down by microRNA constructs. In parallel, we used CRISPR/Cas9-mediated knockout in Jurkat cells for validation experiments.

Results: We efficiently knocked down the expression of tyrosine kinases Lck, Fyn and ZAP70, and found that, while this impaired T cell activation and effector function, TCR downregulation was not affected. Although TCR downregulation was marginally inhibited by the simultaneous knockdown of Lck and Fyn, its full abrogation required broad-acting tyrosine kinase inhibitors.

Conclusions: These data suggest that there is substantial redundancy in the contribution of individual tyrosine kinases to TCR downregulation in primary human T cells. Our results highlight that TCR downregulation and T cell activation are controlled by different signaling events and illustrate the need for further research to untangle these processes.

Keywords: $CD4^+$ T cells, protein tyrosine kinases, T-cell activation, T-cell receptor, TCR downregulation

INTRODUCTION

T cells are essential players in the adaptive immune responses that are needed to protect against infections and cancer. T cell receptors (TCRs) on T cells recognize peptide antigens presented on major histocompatibility complex (MHC) by antigen-presenting cells (APCs). This specific recognition, bolstered by co-stimulatory molecule interactions, induces signaling pathways that lead to T cell differentiation, effector functions, and survival (1).

The TCR is comprised of a genetically diverse α and β chain that together confer antigen specificity. To form the fully functional TCR, TCRα/β are noncovalently associated with the invariant CD3γε and CD3δε subunits and the TCRζζ homodimer (2). The cytoplasmic domains of CD3ε, CD3δ, CD3γ and TCRζ all contain immunoreceptor tyrosine-based activation motifs (ITAMs) (3). After the TCR is triggered through recognition of peptide:MHC, intracellular signaling is initiated by phosphorylation of these ITAMs by Src family kinases, of which Lck and Fyn are most abundantly expressed throughout the lifespan of human T cells (4, 5). Lymphocyte-specific protein tyrosine kinase (Lck) is the dominant kinase initiating T cell activation through ITAM phosphorylation (6-8). Lck is non-covalently attached to the co-receptors CD4 and CD8 (9, 10) and is thereby recruited to the TCR after recognition of a peptide:MHC complex. Phosphorylated ITAMs serve as docking sites for the Syk family tyrosine kinase ZAP70, which is activated through phosphorylation by Lck (11, 12). ZAP70 in turn phosphorylates downstream molecules, such as LAT (13) and SLP76 (14), which eventually leads to T cell activation (1, 7, 8, 15).

T cell activation is tightly regulated to induce specific responses, while preventing hyper-reactivity that could lead to damage to healthy tissues and auto-immunity. One such T cell regulation mechanism is the rapid internalization and active degradation of the TCR upon TCR triggering, a process that is called ligand-induced TCR downregulation (16-19). The extent of TCR downregulation is generally proportional to the strength of signaling input, meaning that higher affinity ligands induce greater TCR downregulation (20, 21). In addition, we recently observed that clonally-expanded T cells also display persistent TCR downregulation, the extent of which is programmed by the strength of the initial T cell antigen recognition (22). Such T cells with adjusted TCR expression display an increased threshold for cytokine production and renewed proliferation upon secondary antigen encounter, and therefore presumably are better equipped to execute a balanced immune response. These findings underscore that downregulation of the TCR is an important protective mechanism against hyper-reactive T cell responses that could harm the host (23, 24). Understanding the

molecular mechanisms that underlie TCR downregulation is therefore important to fine-tune immunotherapeutic approaches, either by preventing TCR downregulation in *e.g.* CAR-T cell therapies, or by inducing it in patients with auto-immune disorders.

Because TCR triggering and TCR downregulation are tightly linked (1, 25, 26), it is possible that the upstream molecular pathways of T cell activation and TCR downregulation are similar. Besides the importance of Lck for T cell activation, it has also been described to be involved in TCR downregulation. Specifically, Lck was described to control TCR downregulation through phosphorylation of ITAMs in CD3 and TCRζ (27). Chemical inactivation of Lck in immortalized Jurkat T cells inhibited TCR downregulation (16, 28), and, conversely, a constitutively active form of Lck caused rapid internalization of cell surface TCR/CD3 complexes and their degradation in lysosomes (16). Although the molecular pathways of TCR downregulation have been studied in detail, the majority of these findings have been obtained in mouse models and immortalized T cell lines, instead of human primary T cells (7, 8, 11, 15, 16, 29-31). Importantly, cellular processes such as the dynamics of TCR internalization may differ markedly between primary T cells and Jurkat cells, and between mice and man. For instance, TCR recycling in T cell hybridoma cells is reported to be faster than in naïve $CD4^+$ T cells (17) and the constitutive degradation rate of TCRζ and CD3ε is slower in primary cells than in Jurkat cells (32). Furthermore, human primary T cells and Jurkat cells have distinctive patterns of cytokine release and co-receptor expression, and they induce different phosphorylation levels of target molecules (33). Because of these fundamental differences between human primary T cells and Jurkat cells, we set out to investigate the molecular mechanisms of TCR downregulation in a more physiological setting and developed a model to study this by efficient gene knockdown in human primary T cells.

Our data strongly suggest that Src family kinases as a group are required for TCR downregulation in human primary T cells. However, its members Lck and Fyn as well as the directly downstream kinase ZAP70 are individually redundant in this process, despite having profound impact on T cell activation and effector functions. Thus, this work highlights that TCR downregulation and T cell activation are separable molecular processes and provides the tools to further unravel these pathways in primary human cells.

MATERIALS AND METHODS

Cell lines

Human embryonic kidney cells that contain the mutant version of the SV40 large T cell antigen (HEK293T cells) were used to generate lentiviruses. Platinum A (PLAT-A) cells are retroviral packaging cells, used to generate retroviruses (34). Both the HEK293T and PLAT-A cell lines were maintained in IMDM (Gibco) containing 10% fetal bovine serum (FBS) (Sigma) and 10,000 U/mL penicillin/streptomycin. Jurkat cells are a human acute leukemic T cell line, which was maintained in RPMI 1640 (Gibco) with L-glutamine, 50μM β-mercaptoethanol, 10% FBS and 10,000 U/mL penicillin/streptomycin (complete RPMI).

Primary cells

This study was performed according to the Amsterdam University Medical Centers, location AMC Medical Ethics Committee guidelines and all donors gave written informed consent in accordance with the Declaration of Helsinki. Human peripheral blood lymphocytes (PBLs) were isolated from buffy coats by density gradient centrifugation on Lymphoprep (Nycomed) and Percoll (Pharmacia). PBLs were activated in non-tissue culture treated 6-well plates (Greiner Bio-One) coated with 2.5μg/mL plate-bound anti-CD3 (UCHT-1) and anti-CD28 (CD28.2; both Biolegend) diluted in 0.1M sodium bicarbonate buffer, and cultured in complete RPMI supplemented with 10ng/mL IL-2 (Peprotech). After activation, the PBLs were maintained in complete RPMI supplemented with IL-2.

Construction of retroviral and lentiviral microRNA vectors, and lentiviral CRISPR vectors

For retroviral transductions, 5-6 microRNA oligonucleotide sequences per gene were selected from the Genetic Perturbation Platform (Broad Institute) and ordered from Sigma. A microRNA sequence targeting luciferase (RLuc) was used as control. Using standard molecular cloning techniques, the microRNA was cloned into a modified pMY backbone (Cell Biolabs, San Diego, CA, USA) containing the marker Ly6G or CD90.2 (Van der Donk *et al*. In preparation). To enable lentiviral microRNA transductions, the marker and microRNA cassette were cloned into a modified lentiCRISPR v2 backbone (Addgene #52961; kind gift from Prof. Dr. N. Zelcer). For lentiviral CRISPR/Cas9 transductions, 4 CRISPR gRNAs were selected per gene from the Toronto human knockout pooled library (TKOv3) (35), ordered from Sigma, annealed, and cloned into the lentiCRISPR v2 backbone using standard molecular cloning techniques. A gRNA targeting hAAVS1 was used as control.

Retroviral transfection of PLAT-A and lentiviral transfection of HEK293T, and transduction of T cells

For retroviral transfection of PLAT-A cells (34), $2.5x10^6$ cells per condition were plated in Advanced TC 6-well plates (Greiner Bio-One), coated with poly-D-lysine (Sigma). The cells were incubated overnight at 37°C in the presence of transfection complexes containing 2µg pMY vector, 0.4µg pCL-Ampho (Novus Biologicals (36)), 0.4µg DGCR8 siRNA (Qiagen (37)), P3000 and Lipofectamine 3000 (ThermoFisher), supplemented with Opti-MEM (Gibco). For lentiviral transfection of HEK293T cells, $2.5x10^6$ cells were used per condition in a regular 6-well plate. The cells were incubated overnight at 37°C in the presence of transfection complexes containing 1µg lentiviral vector, 0.6µg pMDLg/pRRE (Addgene #12251), 0.2µg pRSV-Rev (Addgene #12253), 0.3µg pMD2.G (Addgene #12259) (38), 0.4µg DGCR8 siRNA (not required for lentiviral CRISPR experiments), P3000 and Lipofectamine 3000. After overnight incubation, the supernatants of transfected cells were replaced with 1.5mL complete RPMI. 48 hours after transfection, viral supernatants were harvested, filtered over a 0.45µm filter, and used to transduce T cells. The remaining HEK293T or PLAT-A cells were washed with PBS and resuspended for FACS analysis to determine the transfection efficiency. 48 hours prior to transduction, PBLs were stimulated at 37°C on non-tissue culture treated 6-well plates that were coated with 2.5µg/mL anti-human CD3 (UCHT1) and anti-human CD28 (CD28.2). For the transduction, $1x10^6$ Jurkat cells or PBLs were plated on retronectin-coated plates (2.5µg/mL; Takara), before adding 1mL virus-containing supernatant. The cells were then centrifuged for 2 hours at 1000 x g at 32°C, followed by 3 hours incubation at 37°C, after which 2mL fresh complete RPMI was added per well (for PBLs containing IL-2). At 2 days (before antibiotic selection) and 5 days (after antibiotic selection) after transduction, cells were harvested and stained for flow cytometry as described below. Antibiotic selection during 72 hours was performed by adding 5µg/mL puromycin or 10µg/mL blasticidin, depending on the vector.

Flow cytometry staining

All cells were first stained for viability using Fixable Viability Dye eFluor™ 780 (1:1000) (eBioscience). For cell surface staining, cells were incubated in FACS buffer (PBS containing 0.5% bovine serum albumin (BSA; Sigma) and 0.1% NaN_3) containing antibodies for 10 minutes at 4°C. Then, cells were fixed with 2% paraformaldehyde (PFA, Electron Microscopy Sciences) for 5 minutes at 4°C. For intracellular staining, the fixation step was followed by a permeabilization step in Perm/Wash solution (BD Biosciences) for 5 minutes at 4°C, and an intracellular staining step with antibodies diluted in Perm/Wash solution for 10 minutes at 4°C. The antibody clones and manufacturers used are listed in supplemental table 1. Single-cell measurements were performed on a FACS Canto flow cytometer (BD Biosciences) and FlowJo V10 software

(TreeStar) was used to analyze the data. For each flow cytometry experiment, viable single cells were gated, after which Jurkat cells were selected on CD45 expression, and PBLs were selected on CD8 or CD4 expression. For transduction experiments, the Jurkat cells were gated on FLAG, and PBLs on Ly6G or CD90.2 (or both) and then on CD4. Exceptionally, the Ly6G$^+$ Lck-KD, and Ly6G$^+$CD90.2$^+$ Lck/Fyn-KD PBLs were not gated on CD4, but the total T cells were assessed.

FYN antibody conjugation

Since there is no commercial flow cytometry antibody available for Fyn, we conjugated our immunoblot antibody for Fyn (Supplementary Table 1) to a fluorochrome with a Lightning-Link® conjugation kit (Expedeon) according to the manufacturer's instructions.

Optimization of T cell stimulations: testing the steric hindrance of antibodies using a primary and secondary staining

To investigate steric hindrance of antibodies, 1x10^5 Jurkat cells or PBLs were seeded per well in tissue-treated 96-well plates (Greiner Bio-One). Cells were stained in several rounds to test the accessibility of the target protein for the secondary, fluorochrome-labeled antibody after staining with a primary antibody. Firstly, cells were stained with FACS buffer, or 2.5µg/mL of various anti-CD3 antibodies (purified UCHT1, purified OKT3, purified SK7, purified HIT3a, or FITC-labeled UCHT1) for 10 minutes at 4°C. After washing, the cells were stained with an antibody solution to assess different surface markers. For Jurkat, the secondary antibody solution contained 5µg/mL fluorochrome-labeled anti-CD45 and anti-TCRβ. For PBLs, the secondary antibody solution contained 5µg/mL fluorochrome-labeled anti-CD4, anti-CD8α, anti-CD27, anti-CD45RA, and anti-TCRβ. Cells were fixed with 2% PFA, followed by intracellular staining with anti-TCRζ, and analyzed with flow cytometry. The percentage of hindrance by each antibody was determined from the mean fluorescence intensity (MFI), using the buffer control as reference, such that the expression of an indicated molecule in the buffer control was set at 100% (e.g. Expression % TCRβ = MFI condition 1 / MFI buffer control * 100%). Cells were stimulated with the anti-CD3ε clone UCHT1, unless indicated otherwise.

TCR downregulation assay

A TCR downregulation assay was set up and performed to determine the extent of TCR expression of stimulated samples versus unstimulated controls. A non-tissue culture treated 96-wells plate was coated overnight at 4°C with either an isotype control (anti-mouse IgG (-)) or anti-human CD3 (low dose 0.25µg/mL (+); high dose 2.5µg/mL (++)) and anti-human CD28, diluted in 0.1M sodium bicarbonate buffer. Samples are stimulated

with the high dose, unless indicated otherwise. Plates were blocked with 2% BSA in PBS and washed once with PBS. $1x10^5$ T cells were seeded per well and incubated for the indicated duration at 37°C. After incubation ice-cold MACS buffer (PBS supplemented with 0.5% BSA and 2mM EDTA) was added and cells were transferred to a non-coated 96-well plate. The cells were stained for flow cytometry as described above, including antibodies targeting TCRβ, TCRζ and CD69.
This assay was performed in the presence of various inhibitors. The cells were pre-incubated in the presence of 20μM PP2 (Sigma), 100nM Dasatinib (Sigma), 50μM Imatinib Mesylate (Selleckchem), or 1μM Bafilomycin A1 (Invivogen) for 1 hour at 37°C before directly being transferred to the antibody-coated plate. Stimulation and staining is similar as described above.

Immunoblot analysis
After antibiotic selection, the cells were spun down and resuspended in RIPA buffer (Cell Signaling) supplemented with protease and phosphatase inhibitors (Roche). Then, 5x concentrated Laemmli sample buffer was added and the lysates were incubated for 10 minutes at 95°C before separation by SDS-PAGE. Proteins were transferred to nitrocellulose membranes (GE Healthcare Life Science) or Immobilon®-FL PVDF membranes (Sigma) by immunoblot and stained with Ponceau red (Sigma), followed by blocking in 5% milk (Sigma). Blots were incubated O/N at 4°C with indicated primary antibodies diluted in 1% milk in TBST: anti-β-actin, and anti-Fyn. Secondary antibodies, diluted in 1% milk, were IRDye 800CW goat-anti-mouse IgG (H+L) and IRDye 680RD goat-anti-rat IgG (H+L) (Li-Cor). Measurements were performed on the Odyssey, and analyzed with Odyssey V3.0 software (Li-Cor Biosciences).
To assess total phosphorylation by immunoblot, $5x10^6$ Jurkat cells were stimulated with either anti-mouse IgG1 or anti-mouse IgG1 and anti-human CD3 (UCHT1). The cells were stimulated for 2 or 5 minutes at 37°C, followed by direct addition of 10x-excess ice-cold FACS buffer. Cells were lysed and blotted as described above, except that blots were blocked in 5% BSA in PBS, and the primary (anti-mouse/human β-actin, anti-phosphorylated tyrosine) and secondary antibodies were diluted in 1% BSA/TBST.

Cytokine production assay
A non-tissue culture treated 96-well plate was coated with 0.1M sodium bicarbonate buffer or 2.5μg/mL anti-human CD3 and 2.5μg/mL anti-human CD28 diluted in buffer, and incubated overnight at 4°C. Plates were blocked with 2% BSA in PBS, and washed once with PBS. $2x10^5$ T cells were seeded per well and resuspended in either RPMI with Brefeldin-A (eBioscience; unstimulated control and antibody stimulated samples) or with Brefeldin-A, PMA (50ng/mL, Sigma) and ionomycin (1μg/mL, Sigma) (positive control) and incubated for 5h at 37°C. Cells were stained for flow cytometry as described above.

Statistical analysis

Graphpad Prism v8 (GraphPad Software, San Diego, CA) was used to generate all graphs and for statistical analyses. Statistics were performed using a Student's *t*-test for pairwise comparisons (Figure 1, 5-7). Multiple comparisons within groups were performed using an RM one-way ANOVA with a Tukey's multiple comparisons test (Figure 3). P-values < 0.05 were considered statistically significant.

RESULTS

Antigen-experienced human T cells display lower TCR expression levels

First we investigated whether we could detect evidence of persistent TCR downregulation in human T cells, similar to what has been described recently in animal models (22). To this end, we isolated peripheral blood lymphocytes (PBLs) from five healthy donors and compared TCRβ surface levels on antigen-experienced ($CD45RA^-$ $CD27^-$) with those on naïve ($CD45RA^+$ $CD27^+$) $CD4^+$ T cells (Figure 1A, B). Surface TCRβ levels were significantly reduced on antigen-experienced compared to naïve T cells (Figure 1C; $p<0.001$). Similarly, antigen-experienced T cells had lower levels of intracellular TCRζ compared to naïve T cells (Figure 1D; $p<0.001$). These data strongly suggest that human antigen-experienced $CD4^+$ T cells have lower TCR expression compared to their naïve counterparts. Therefore, TCR downregulation appears to form an integral part of human T cell responses.

CD3/CD28 crosslinking induces TCR downregulation in primary human T cells

To investigate the mechanisms underlying TCR downregulation in PBLs, we optimized an antigen-independent TCR downregulation assay using plate-bound antibodies against CD3ε and CD28 (17, 25, 39). Whilst T cell stimulation with anti-CD3ε/CD28 antibodies is a well-known and effective method to study ligand-induced TCR downregulation, it is important to consider that the CD3ε and TCRβ subunits are present in close proximity on the T cell surface. This implies that anti-CD3ε antibodies used to stimulate T cells, could sterically hinder the binding of fluorochrome-labeled anti-TCRβ antibodies used for the flow cytometry-based readout. In previous studies, such a potential blocking effect of anti-CD3 antibodies was not investigated (31, 32, 40). To optimize the T cell stimulation for PBLs and Jurkat cells, we investigated the steric hindrance of five different anti-CD3ε antibodies, by staining PBLs (Supplemental Figure 1A, B) and Jurkat cells (Supplemental Figure 1C, D) at 4°C. Detection of surface TCRβ by flow cytometry was impaired after staining with HIT3a and OKT3, suggesting steric hindrance. The capacity to induce TCR downregulation in PBLs (Supplemental Figure 1E, F) and Jurkat cells (Supplemental Figure 1G, H) was assessed by stimulation

with the different plate-bound anti-CD3ε antibodies. Surface TCRβ and total TCRζ expression were both reduced in response to stimulation with UCHT1 in hPBLs as well as Jurkat cells. Interestingly, FITC-labeled UCHT1 induced the lowest level of steric hindrance of all antibodies in both cell types (Figure 2A, B, Supplemental Figure 1I, J). Thus, UCHT1 induced minimal steric hindrance, while efficiently inducing TCR downregulation and was therefore selected for all subsequent assays.

Transient downregulation of TCR complexes via lysosomal degradation

With the optimized assay, pre-activated PBLs were stimulated and the kinetics of ligand-induced TCR downregulation as well as CD69 upregulation as a marker of T cell activation were determined. Surface TCRβ and total TCRζ expression was quickly downregulated after stimulation, with similar kinetics for $CD4^+$ and $CD8^+$ T cells (Figure 2C, D). TCR downregulation was detected as early as 15 minutes after stimulation and reached its maximum after 2-4 hours, which is in accordance with previous literature on human T cell clones (41). CD69 upregulation was consistently detected between donors and increased further until 16 hours after activation, which was therefore selected as optimal timepoint in this assay (Figure 2E). During continued anti-CD3 stimulation, surface TCRβ and total TCRζ expression remained low, but expression recovered after removal of the stimuli and returned to baseline after 48 hours (Figure 2F, 2G).

It is currently thought that the TCR/CD3 complex is degraded in lysosomes after it is internalized upon T cell stimulation (16, 41). We therefore analyzed the expression of surface as well as total levels of both TCRβ and TCRζ in pre-activated PBLs following anti-CD3/CD28 stimulation using the lysosomal acidification inhibitor Bafilomycin A1 (Figure 2H, I). TCRβ-degradation was completely blocked by Bafilomycin A1, while surface downregulation still occurred. Moreover, approximately two-fold higher levels of TCRζ remained in cells pretreated with Bafilomycin A1. Thus, these data confirm that triggered TCR/CD3 complexes are internalized and subsequently degraded in lysosomes.

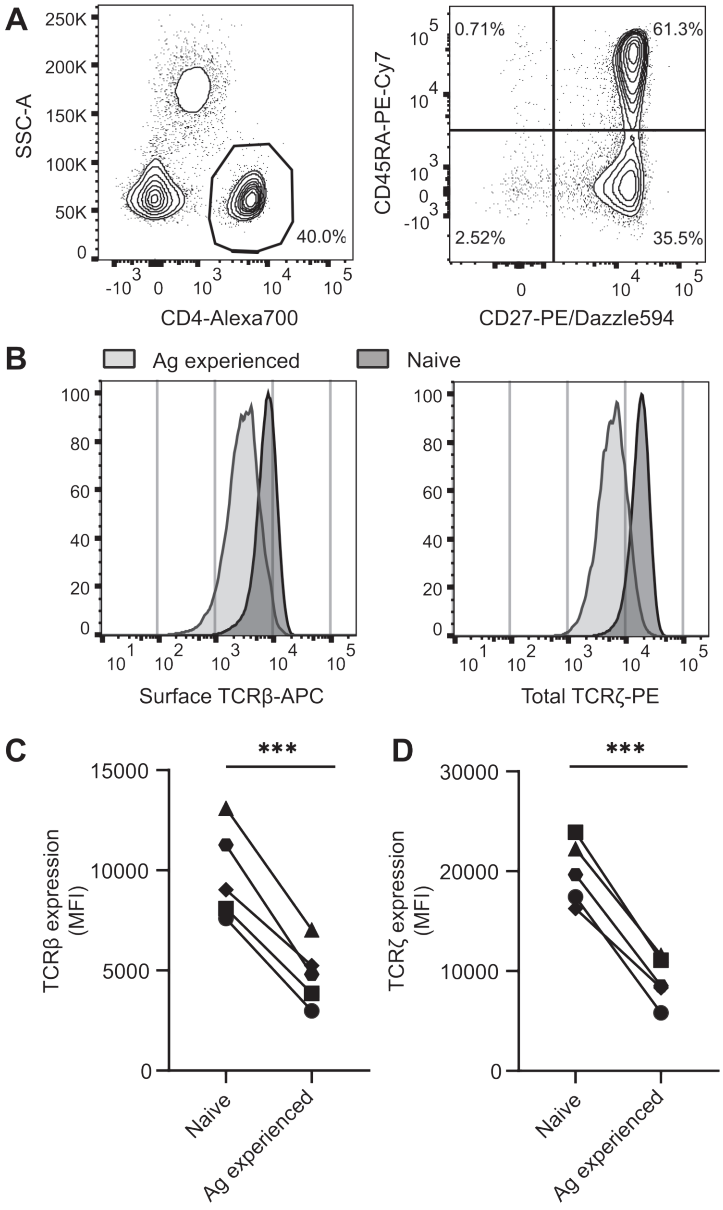

Figure 1: Reduced TCR expression in antigen-experienced primary human CD4⁺ T cells.

Human PBLs from healthy donors were gated (A) to select CD4⁺, CD45RA⁺CD27⁺ naive and CD45RA⁻ CD27⁻ antigen-experienced T cells and measure surface TCRβ and total TCRζ expression within these separate populations (B). Data in A and B are one representative experiment of the five biological replicates depicted in C and D. (C-D) Aggregate MFI data for surface TCRβ (C) and total TCRζ (D) expression for n=5 donors in one experiment, with each symbol representing an individual donor. Paired student's *t*-test, ***p<0.001.

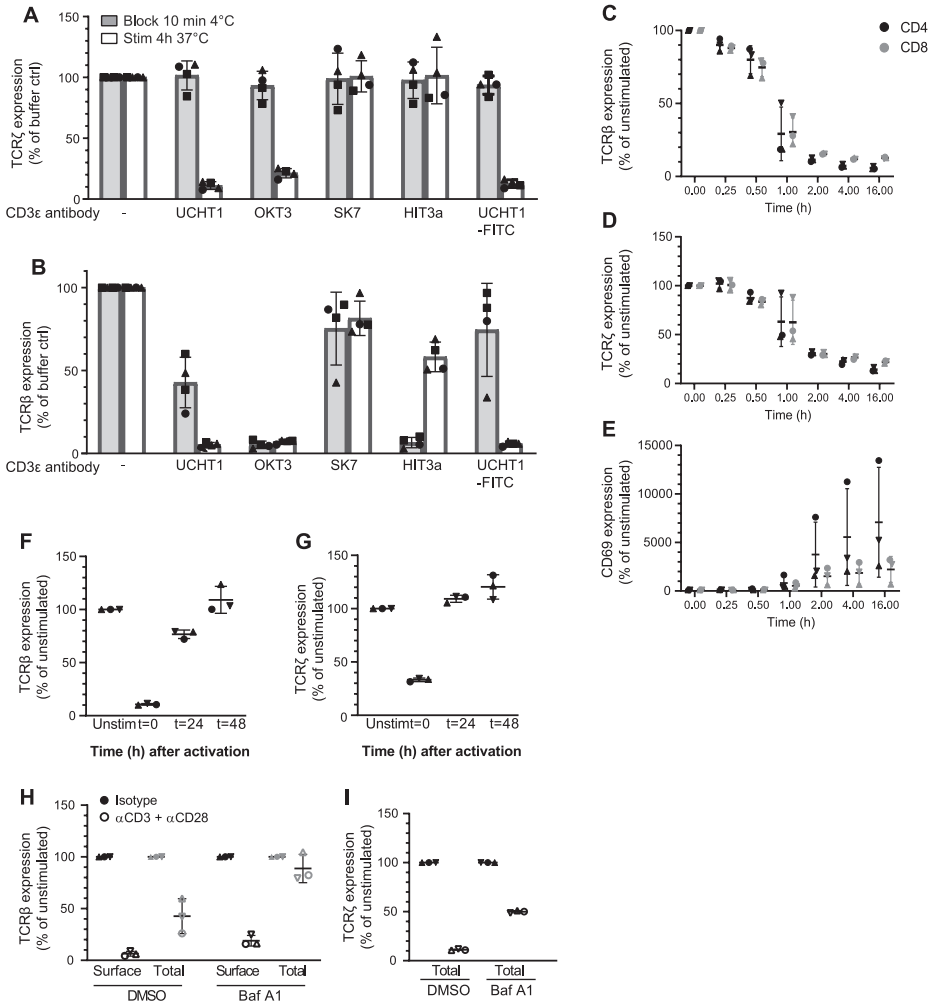

Figure 2: TCR downregulation includes internalization and lysosomal degradation.

(A) Total relative TCRζ expression in human CD4⁺ T cells after stimulation with different anti-CD3ε clones. SK7 and HIT3a did not induce TCR downregulation. (B) Surface TCRβ staining of human CD4⁺ T cells revealed that UCHT1 induced TCR downregulation, without causing steric hindrance. (C-G) Kinetics of relative surface TCRβ (C) and total TCRζ (D) expression, CD69 upregulation (E) in human CD4⁺ and CD8⁺ T cells from healthy donors (n=3) after stimulation with anti-CD3 (UCHT1)/CD28. Relative surface TCRβ (F) and total TCRζ (G) expression before, during, and after TCR triggering of human CD4⁺ T cells. (H-I) Relative surface (black) and total (grey) TCRβ (H) and total TCRζ (I) expression of human CD4⁺ PBLs after 4 hours stimulation with anti-CD3/CD28 in the presence of Bafilomycin A1. (C-I) Data are depicted as normalized MFI. Symbols represent individual donors (n=3) with bars depicting the median and 95% CI. (A, B) Data are from two independent experiments with in total n=3 individual donors. (C-I) Data from one experiment with n=3 individual donors.

TCR downregulation is dependent on tyrosine kinases

The first proteins downstream of TCR triggering and signaling are the protein tyrosine kinases (PTKs) Lck and Fyn (1, 5, 42). To investigate the role of these PTKs in TCR downregulation of primary human T cells, pre-activated PBLs from healthy donors were stimulated with anti-CD3/CD28 in the presence of different tyrosine kinase inhibitors. PP2 and dasatinib are tyrosine kinase inhibitors with a broad range of targets in the Src kinase family (43, 44). In contrast, whilst imatinib is a well-known Abl inhibitor, it is also described as a more specific inhibitor for Lck in T cells (44, 45). PP2 and dasatinib strongly inhibited TCR downregulation (Figure 3A, B, D, E). In addition, T cell activation was fully blocked as the inhibitors prevented CD69 upregulation (Figure 3C, F). Strikingly, imatinib inhibited TCRζ degradation just as efficiently as PP2 and dasatinib, but did not inhibit TCRβ downregulation and only partially inhibited CD69 upregulation. These data suggest that inhibition by imatinib is either weaker, or more specific, leading to an intermediate phenotype, whereas broad-acting inhibitors PP2 or dasatinib blocked complete TCR downregulation. Thus, these data suggest that a certain phosphorylation threshold is required, or that a combination of Src-family kinases, or another (yet unknown) kinase besides Lck is involved, which is inhibited by PP2 and dasatinib, but not by imatinib (44, 45).

Genetic modification to investigate TCR downregulation in T cells

Next, we more precisely investigated the role of the individual kinases in TCR downregulation using different genetic perturbation methods. To select the optimal method for genetic perturbation in our T cell models, we generated lentiviral and retroviral vectors coding for microRNAs and lentiviral CRISPR/Cas9 vectors to knock-down or knock-out PTK genes, respectively. First, we compared the transduction and genetic perturbation efficiency of each vector in PBLs (Figure 3G). After transduction of PBLs with the lentiviral CRISPR/Cas9 vectors, only a minimal level of Cas9-FLAG-staining was detected and no viable cells remained after antibiotic selection (data not shown). These data confirm reports by others (46, 47) that such lentiviral CRISPR vectors are not a viable tool to achieve gene knockouts in primary T cells. As an alternative method for PBLs, we compared lentiviral and retroviral microRNA knockdown. For proof of principle, we used different vectors containing microRNAs that target TCRζ (*CD247*) with different knockdown efficiencies (Supplemental Figure 1K, L). The lentiviral microRNA vectors transduced PBLs very efficiently, as shown by a high percentage of Ly6G positive cells (Supplemental Figure 1M). However, within the transduced population ($Ly6G^+$) it appears that the retroviral vectors induced better knockdown of TCRζ (Supplemental Figure 1N) and further reduced surface expression of TCRβ than the lentiviral vectors (Supplemental Figure 1O) (1, 48). In contrast to the PBLs, the lentiviral CRISPR/Cas9 vectors were efficiently transduced into Jurkat

cells, and the proportion of viable cells remained high after antibiotic selection. Within the FLAG$^+$ population, efficient knockout of TCRζ was achieved, and subsequent reduction of surface TCRβ was observed (Supplemental Figure 1P). Therefore, we used CRISPR-mediated gene knockout as the standard method for Jurkat cells and retroviral microRNA-based gene knockdown for primary T cells.

Lck and Fyn are individually redundant for ligand-induced TCR downregulation

To more precisely investigate the contribution of Lck in TCR downregulation, we transduced PBLs with vectors containing the surface marker CD90.2 and microRNAs targeting Lck (Lck-KD), and assessed the contribution of Lck in TCR downregulation in PBLs. The transduction and knockdown was efficient, as represented by expression of surface CD90.2 (Figure 4A) and total Lck (approximately 70% KD) respectively (Figure 4B, Supplemental Figure 2A). As expected, Lck knockdown also led to CD4 downregulation, confirming effective depletion of Lck (49) (Figure 4C). Knockdown was also confirmed with immunoblot (Figure 4D, $p<0.01$, approximately 92% KD). Next, the Lck-KD cells were stimulated with plate-bound anti-CD3/CD28 antibodies to examine TCR downregulation. No difference in surface TCRβ downregulation and TCRζ degradation between the non-target microRNA and the Lck-KD cells was detected (Figure 4E-H). In contrast, CD69 upregulation was significantly impaired in the Lck-KD cells (Supplemental Figure 2B, C; $p<0.01$). Similarly, gene knockout of Lck in Jurkat cells by CRISPR/Cas9 did not impair TCR downregulation (Supplemental Figure 2D-G) even though Lck knockout was complete according to immunoblotting (Figure 4I). The Lck-KO Jurkat cells had only a 80% lower Lck expression by flow cytometry, which is likely due to background levels of the antibody in flow cytometry (Supplemental Figure 2D). Lck knockout in Jurkat cells strongly impaired tyrosine phosphorylation, both at baseline and after stimulation with anti-CD3 (Supplemental Figure 2H), suggesting successful disruption of Lck. The Lck-KO cells were stimulated with anti-CD3/CD28 to investigate the effect on TCR downregulation and CD69 upregulation. Surprisingly, in contrast to the hPBLs, this did not affect CD69 upregulation; however, similar to the hPBL knockdown TCR downregulation was unaffected (Supplemental Figure 2E-G). To investigate the effect of PTK inhibitors on TCR downregulation of Jurkat cells, non-target gRNA or Lck-KO Jurkat cells were stimulated with anti-CD3/CD28 in the presence of dasatinib or imatinib. In contrast to PBLs, whilst these inhibitors block CD69 upregulation, they did not impair TCR downregulation (Figure 4J-L). These results underscore that signal transduction in Jurkat cells differs from PBLs, and therefore it is important to study TCR downregulation in primary cells. Furthermore, these data suggest that the effect of imatinib on Jurkat cells is not exclusively mediated by its action on Lck but possibly by other Src family kinases. These data could also imply that apart from Src family kinases, another family of

kinases is involved in TCR downregulation. Together, these data confirm that Lck is required for T cell activation of both primary human T cells and Jurkat cells, but is not essential for full TCR downregulation.

Fyn is another important tyrosine kinase in T cells (15), and Fyn and Lck have overlapping functions (6, 15, 50, 51). However, the contribution of Fyn to T cell activation and TCR downregulation in primary human T cells is unclear. Therefore, we transduced PBLs with vectors containing the surface marker Ly6G and microRNAs targeting Fyn (Fyn-KD) (Figure 4M, N; Supplemental Figure 2I, J). Fyn-KD did not inhibit TCR downregulation (Figure 4O-R), despite Fyn knockdown being highly efficient (approximately 90% KD, based on immunoblot). While not significant, a trend of impaired CD69 upregulation was suggested in the Fyn-KD cells (Supplemental Figure 2K, L). However, despite efficient knockdown of Fyn we conclude that its role in T cell activation is less pronounced than Lck, which is in accordance with data obtained in mice (15, 29, 51, 52). Together, these data suggest that Lck and Fyn are individually dispensable for TCR downregulation, but that especially Lck is essential for full T cell activation.

ZAP70 is dispensable for ligand-induced TCR downregulation, but not for T cell activation

Next we investigated the role of ZAP70, as ZAP70 has been suggested to play a non-redundant role in both TCR activation and downregulation (31). ZAP70 was knocked down in PBLs with microRNAs. Expression levels of ZAP70 were strongly reduced in the ZAP70-KD cells (approximately 99% KD) (Figure 5A, B; Supplemental Figure 3A). ZAP70 knockdown reduced CD69 upregulation (Supplemental Figure 3B, C) and impaired the production of IL-2 and IFN-γ upon stimulation with anti-CD3/CD28 (Supplemental Figure 3D). However, analogous to Lck and Fyn, ZAP70 knockdown did not prevent TCR downregulation (Figure 5C-F). Similarly, knockout of ZAP70 in Jurkat cells had no significant effect on TCR downregulation, whereas it impaired CD69 upregulation (Supplemental Figure 3E-H). Thus, these data suggest that ZAP70 is not essential for TCR downregulation.

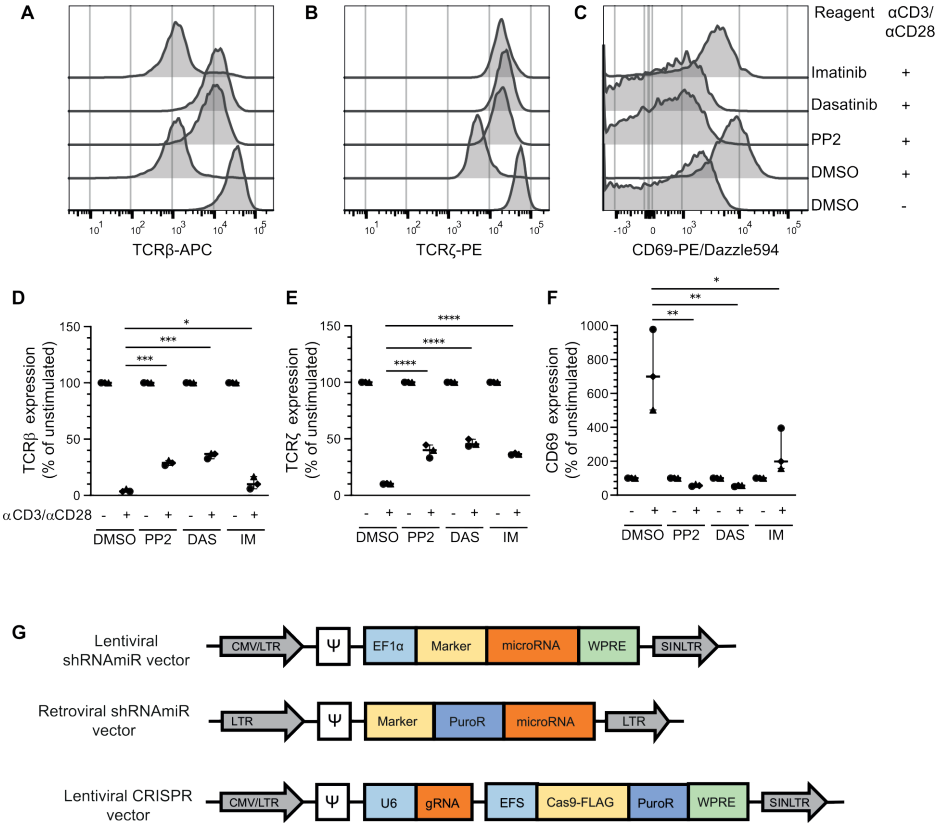

Figure 3: Chemical inhibitors suggest that TCR downregulation is dependent on multiple tyrosine kinases.

Human CD4+ PBLs were stimulated with anti-CD3/CD28 in the presence of protein tyrosine kinase inhibitors PP2, dasatinib, or imatinib. (A-C) Representative histograms of surface TCRβ (A), total TCRζ (B) expression, and surface CD69 (C) expression. (D-F) Aggregate data normalized to the unstimulated control for n=3 individual donors examined in a single experiment, with the median and 95% CI depicted. Statistics were calculated by one-way ANOVA followed by Tukey's test for multiple comparisons, *p<0.05; **p< 0.005; ***p<0.001; ****p<0.0001. (G) Lentiviral and retroviral microRNA vectors and lentiviral CRISPR/Cas9 vectors for knockdown of TCRζ (*CD247*) expression.

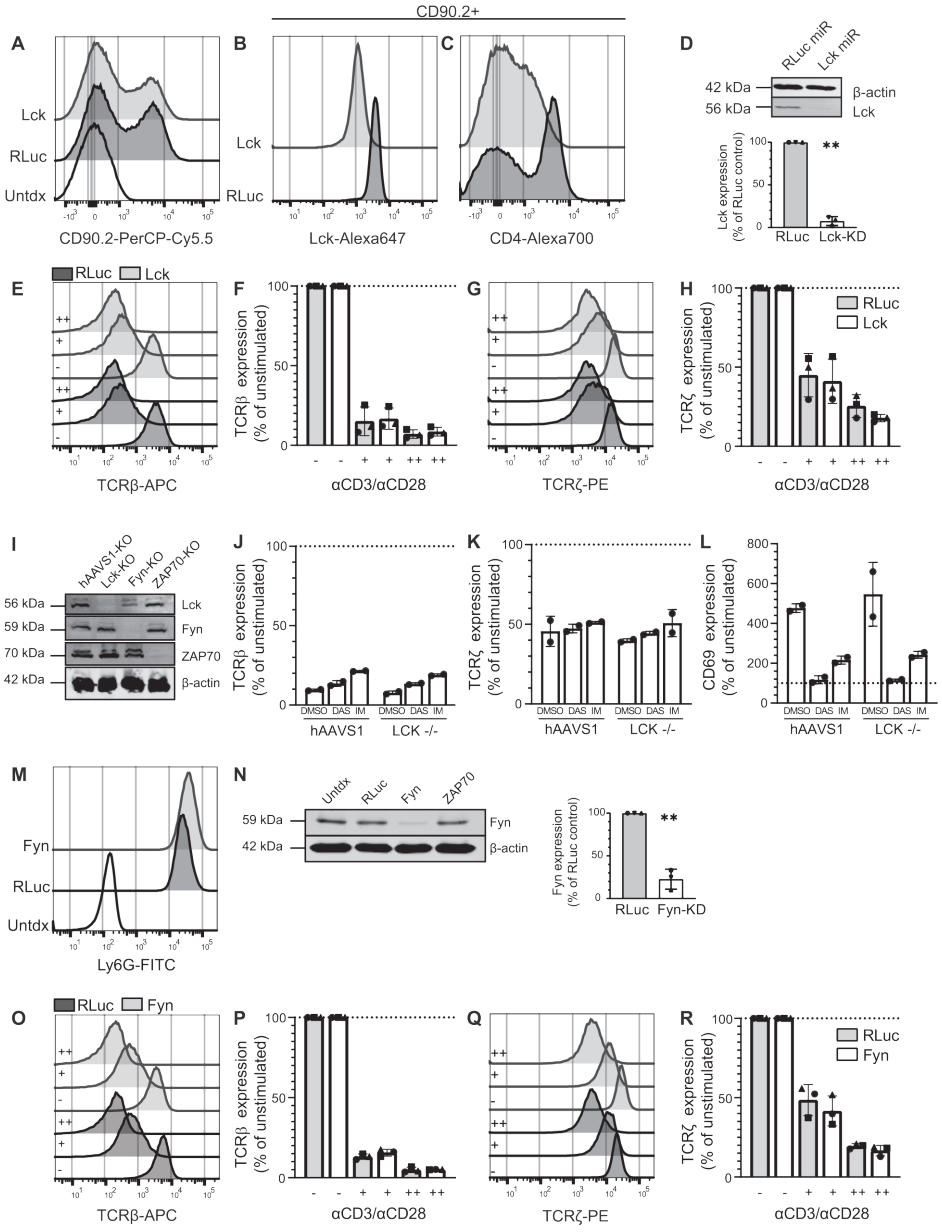
CD90.2+
A
Lck
RLuc
Untdx
CD90.2-PerCP-Cy5.5
B
Lck
RLuc
Lck-Alexa647
C
CD4-Alexa700
D
RLuc miR
Lck miR
42 kDa
56 kDa
β-actin
Lck
Lck expression (% of RLuc control)
RLuc
Lck-KD
E
RLuc
Lck
TCRβ-APC
F
TCRβ expression (% of unstimulated)
αCD3/αCD28
G
TCRζ-PE
H
TCRζ expression (% of unstimulated)
RLuc
Lck
αCD3/αCD28
I
hAAVS1-KO
Lck-KO
Fyn-KO
ZAP70-KO
56 kDa
59 kDa
70 kDa
42 kDa
Lck
Fyn
ZAP70
β-actin
J
TCRβ expression (% of unstimulated)
DMSO DAS IM
hAAVS1
LCK -/-
K
TCRζ expression (% of unstimulated)
L
CD69 expression (% of unstimulated)
M
Fyn
RLuc
Untdx
Ly6G-FITC
N
Untdx
RLuc
Fyn
ZAP70
59 kDa
42 kDa
Fyn
β-actin
Fyn expression (% of RLuc control)
RLuc
Fyn-KD
O
RLuc
Fyn
TCRβ-APC
P
TCRβ expression (% of unstimulated)
αCD3/αCD28
Q
TCRζ-PE
R
TCRζ expression (% of unstimulated)
RLuc
Fyn
αCD3/αCD28

◂ Figure 4: Lck and Fyn are individually redundant for TCR downregulation in human PBLs.
(A-D) Transduction efficiency of non-target microRNA (dark grey) or Lck microRNA vectors (light grey) was measured by CD90.2 (A) expression, and total Lck (B) and surface CD4 (C) expression was measured within the CD90.2$^+$ population of human PBLs. (D) Lck knockdown was confirmed and quantified with immunoblot (representative example of n=3 donors). (E-H) Transduced cells were left unstimulated (-), or stimulated with a low (+) or high (++) dose of anti-CD3/CD28 and surface TCRβ (E, F) and total TCRζ (G, H) was measured. (I) Immunoblots showing the total Lck, Fyn, ZAP70 and β-actin expression in Jurkat cells (representative example of n=2). (J-L) Surface TCRβ (J), total TCRζ (K) and surface CD69 (L) expression in Jurkat cells transduced with hAAVS1 or LCK CRISPR vectors stimulated with DMSO, dasatinib or imatinib. Each symbol represents a separate experiment (n=2). Expression in non-triggered T cells is set at 100%, based on the MFI. (M) Transduction efficiency of non-target microRNA (dark grey) or Fyn microRNA vectors (light grey) was measured by Ly6G. (N) Immunoblots showing the total Fyn and β-actin expression within the Ly6G$^+$ population (representative of n=3 donors). (O-R) Human PBLs transduced with Fyn microRNAs underwent the same stimulation as described for Lck, and surface TCRβ (O, P) and total TCRζ (Q, R) was measured. (F, H, P, R) Each symbol represents an individual donor (n=3) examined in a separate experiment. Significance is calculated with the paired student's *t*-test. **p<0.01.

Concomitant knockdown of Lck and Fyn modestly impairs ligand-induced TCR downregulation in T cells

Based on data obtained in mice, where depleting Lck and Fyn simultaneously strongly impaired T cell function (6, 15, 51), we investigated the effect of simultaneously knocking down Lck and Fyn in PBLs (Figure 6A-D; Supplemental Figure 4A). Lck/Fyn double knockdown (dKD) cells (CD90.2$^+$ Ly6G$^+$) were stimulated with plate-bound anti-CD3/CD28 antibodies, and TCR downregulation as well as cytokine production was assessed. Although Lck/Fyn dKD cells did not show altered TCR downregulation in response to stimulation with a high dose of anti-CD3/CD28 (Figure 6E-F), significantly impaired TCRβ downregulation was observed in cells stimulated with a lower anti-CD3/CD28 dose. Notably, this effect was not observed for TCRζ levels (Figure 6G-H). Lck/Fyn dKD also reduced CD69 upregulation (Supplemental Figure 4B, C) and decreased cytokine production after anti-CD3/CD28 stimulation (Supplementary Figure 4D). Thus, despite effective dKD, TCR downregulation was only modestly affected. Together, these data strongly suggest an important role for Lck and Fyn in T cell activation and effector functions. However, the incomplete abrogation of TCR downregulation and the finding that stronger TCR triggering overrides this phenotype imply that other signaling events are involved.

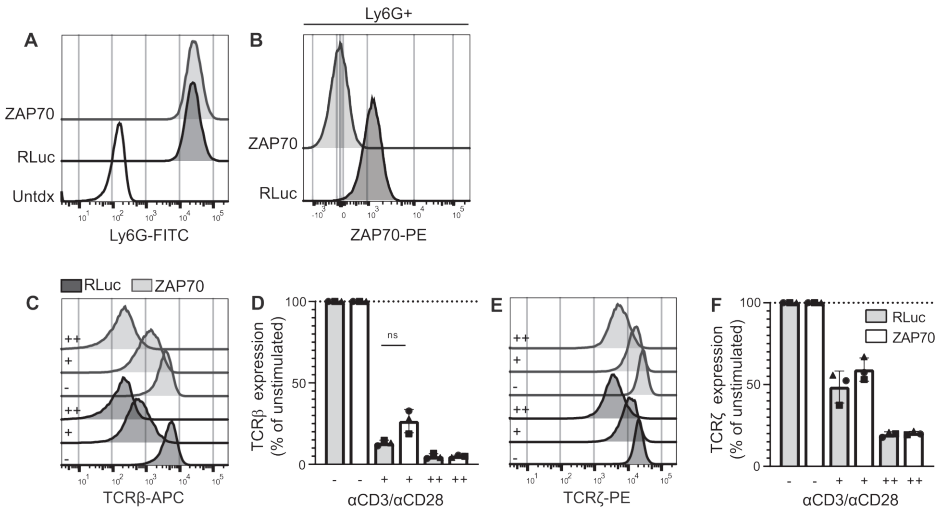

Figure 5: ZAP70 is dispensable for ligand-induced TCR downregulation in human CD4⁺ PBLs.

Human PBLs were transduced with retroviral non-target microRNA (dark grey), or microRNA vectors targeting ZAP70 (light grey). After transduction, Ly6G (A), and total ZAP70 (B) expression was measured; representative histograms are depicted. Transduced cells were left unstimulated (-), or stimulated with a low (+) or high (++) dose of anti-CD3/CD28 and surface TCRβ (C, D) and total TCRζ (E, F) expression was measured. (C-E) Representative histograms where dark grey histograms indicate non-target microRNAs and light grey histograms indicate ZAP70 microRNAs. (D, F) Each symbol represents an individual donor (n=3) examined in a separate experiment, with bars depicting the mean and standard deviations. Significance is calculated with the paired student's *t*-test.

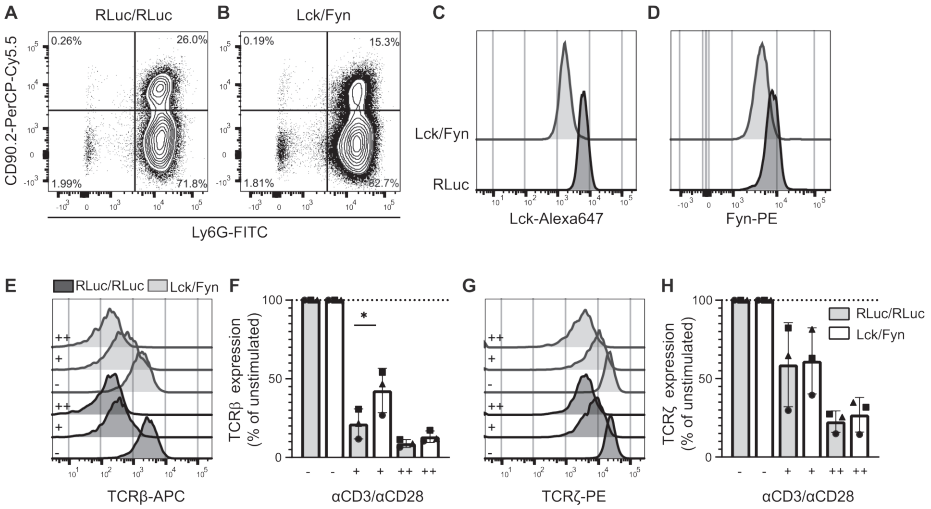

Figure 6: Lck and Fyn double knockdown modestly impairs TCR downregulation in human CD4⁺ PBLs.

Representative histograms of surface CD90.2 (A) and Ly6G (B) expression, and total Lck (C) and Fyn (D) expression human PBLs transduced with retroviral non-target microRNA vectors (dark grey), or microRNA vectors targeting Lck and Fyn (light grey). Representative histograms (E, G) and aggregate data (F, H) of surface TCRβ (E, F) and total TCRζ (G, H) expression in transduced cells left unstimulated (-), or stimulated with a low (+) or high (++) dose of anti-CD3/CD28. (F, H) Each symbol represents an individual donor (n=3) in a separate experiment, with bars depicting the mean and standard deviations. Significance was calculated with the paired student's *t*-test. *p<0.05.

DISCUSSION

Here, we optimized the methods to genetically modify and stimulate human primary T cells and investigate the mechanisms of TCR downregulation. With PTK inhibitors, we strongly inhibited TCR downregulation, and thereby suggest that Src family kinases as a group are involved in TCR downregulation in human PBLs. However, using genetic modification, we found that individual silencing of Lck, Fyn or ZAP70 did not inhibit TCR downregulation. Lck and Fyn dKD partially inhibited TCR downregulation, but did not fully block this process. These data suggest that Lck and Fyn have important yet partially redundant roles in TCR downregulation.

Multiple studies have investigated the role of kinase function in TCR downregulation in murine lymphocytes or cell lines, but the subject has remained unresolved due to conflicting data (23, 53-55). These previous studies were mostly performed with PTK inhibitors such as genistein, herbimycin or tyrphostin. In comparison, the newer generation or optimized PTK inhibitors PP2, dasatinib and imatinib used here, are more efficient and specific. Of these compounds, PP2 and dasatinib are wide-range PTK inhibitors that fully blocked T cell activation and strongly impaired TCR downregulation in our model. In contrast, imatinib is postulated to be more specific in its inhibition, with Lck as the sole predicted target in human T cells (44, 45, 56). Interestingly, we observed significant inhibition of T cell activation and TCRζ degradation with either PP2, dasatinib or imatinib, but the inhibition of T cell activation and TCRβ downregulation was less pronounced with the latter. Based on literature we initially hypothesized that imatinib acts specifically on Lck, while PP2 and dasatinib have a stronger phenotypic effect, because they inhibit other non-redundant kinases besides Lck. However, our findings do not directly support that Lck is the main target of imatinib and dasatinib in our systems. Firstly, dasatinib and imatinib block TCR downregulation to a similar extent in wild-type Jurkat cells compared to Lck-KO cells. Secondly, we did not observe similar phenotypes in Lck-KD/Lck-KO compared to imatinib treated cells in either the Jurkat or PBL experiments. The different phenotypes resulting from imatinib and dasatinib treatment could alternatively be explained by a less potent inhibition of its target by imatinib compared to dasatinib. Concurrently, there could be an even wider network of kinases partially involved in TCR downregulation, which are inhibited by dasatinib and PP2, but not by imatinib. Future research will have to address the validity of these hypotheses.

The importance of Lck in T cell development, T cell activation and TCR downregulation has been extensively studied. It has been established that TCR downregulation is an essential part of thymocyte development (57, 58). Cumulative evidence from data

in murine thymocytes, Jurkat cells and artificial overexpression studies suggested that Lck is an essential kinase in TCR activation and downregulation (16, 30, 59). Contrary to these results, we find no evidence that Lck is individually required for TCR downregulation in either CRISPR/Cas9-modified Jurkat cells or in modified human PBLs. Therefore, we also investigated the kinase Fyn, whose function is similar to Lck. However, also in Fyn-KD cells, we did not observe impaired TCR downregulation, which concurs with the hypothesis of individual redundancy. A contribution of Lck and Fyn together would be in line with data obtained from mouse models investigating T cell development (29, 52). Furthermore, Lck and Fyn also function in concert during T cell activation in mice (15, 51, 60). In concordance with these mouse studies, we found a small but significant inhibition of TCR downregulation and CD69 upregulation in human PBLs with Lck and Fyn knockdown. However, our results simultaneously clearly show that TCR downregulation still occurred to a great extent despite the efficient knockdown of both Lck and Fyn, implying that these kinases are relatively more redundant for ligand-induced TCR downregulation in PBLs than for tonic downregulation in thymocytes. Therefore, we propose that other protein kinases may be involved in TCR downregulation, which could include kinases from other families.

We further hypothesized that inhibition of ZAP70 would interfere with TCR downregulation, since Dumont et al. previously observed a modest phenotype in patients with congenital ZAP70 deficiencies. ZAP70 is generally thought to be essential to relay activating signals from TCR triggering mediated by Lck and Fyn (61, 62) and we expected strong inhibition of T cell activation and TCR downregulation when inhibiting this non-redundant downstream signaling molecule. Indeed, we observed abrogation of T cell effector functions in the form of cytokine production and CD69 upregulation in response to ZAP70 knockdown. Despite the importance of ZAP70 in T cell activation and cytokine production, we found that its role is individually dispensable for TCR downregulation. The discrepancy between our observations and Dumont *et al.* could be explained by the method and moment of ZAP70 depletion. TCR downregulation in T cells from donors with a congenital ZAP70 deficiency may be subject to compensatory mechanisms, while depletion of ZAP70 in circulating PBLs circumvents this issue.

It should be noted that all that our results are obtained with anti-CD3/CD28 antibody-mediated TCR triggering, and more physiologic stimulation with peptide:MHC triggering and native co-stimulation could present alternative results. Our data suggests that TCR downregulation occurs relatively early after stimulation, whilst CD69 upregulation usually takes longer. Therefore, we stimulated the T cells with anti-CD3/CD28 for 16 hours, and measured TCR downregulation and CD69 upregulation

simultaneously. We can hereby exclude the duration of stimulation as a factor that influences the discrepancy between TCR downregulation and CD69 upregulation, suggesting that the differences observed are due to effective knockdown. Finally, our results are obtained in T cells that are activated at least one week before the functional experiments. At the moment of functional assays (7-10 days post-activation), T cells had reverted to their original size and CD69 expression levels, but we cannot exclude that the previous activation of these T cells affects their signaling upon recurrent stimulation. It is possible that a partial inhibition by inhibitors or microRNA knockdown of Lck, Fyn or ZAP70 inhibits T cell activation but allows TCR downregulation, because TCR downregulation would require a lower phosphorylation or signaling threshold. Although we cannot fully exclude this hypothesis, our data showing that low-dose anti-CD3/CD28 stimulation induces less TCR downregulation, but similar CD69 upregulation, argue against this. Together, our data also underscore the profound differences between Jurkat cells and human PBLs, for instance when interpreting the effect of PTK inhibitors on TCR downregulation, or CD69 upregulation in the different models. This illustrates the importance of reinvigorating the mechanistic studies of TCR downregulation in primary cells, now that the genetic toolbox has expanded.

In summary, this work has made clear that TCR downregulation is a process with marked differences between formerly used mouse and cell line models, and human PBLs. Although tremendous progress has been made to understand the molecular pathways of T cell signaling in recent decades, research on the mechanisms of TCR downregulation has lagged behind (1, 63). The importance of a better understanding of TCR downregulation is apparent, since it has direct clinical implications for the understanding of both auto-immune disorders as well as the improvement of immune therapies by increasing the reactivity of T cells. In this light it is important to note that we find clear evidence of lower TCR levels in antigen-experienced PBLs isolated from healthy donors. This observation supports recent findings obtained in mice, which showed that TCR downregulation *in vivo* can persist for long periods of time and is likely a mechanism to fine-tune T cell responses to antigens with varying affinities (22). Together, this work highlights the importance and complexity of studying TCR downregulation in human primary T cells. While we show that Src family kinases drive this process, we emphasize that more research is needed to understand the individual molecules and pathways involved. Our work provides useful tools to answer these questions.

Acknowledgements:
We would like to thank Prof. Dr. Noam Zelcer for the kind gift of plasmids lentiCRISPR v2, pMDLg/pRRE, pRSV-Rev, and pMD2.G, as well as for useful discussion.

Author contribution:
Designed and interpreted experiments: LEHvdD, LSA, JWJvH; performed experiments: LEHvdD, JvdS, LMT; wrote the manuscript: LEHvdD, LSA, TBHG, JWJvH.

Funding:
Lieve E. H. van der Donk, Louis S. Ates, Jet van der Spek, and Jeroen W. J. van Heijst were supported by the Netherlands Organization for Scientific Research (Vidi grant 91717305 to Jeroen W. J. van Heijst). Louis S. Ates is furthermore supported by a PostDoc stipend of the Amsterdam Infection and Immunity Institute and Teunis B. H. Geijtenbeek is funded by the European Research Council (advanced grant 670424).

Conflict of interest statement:
The authors declare no commercial or financial conflict of interest.

Data availability:
The data that support the findings of this study are available upon reasonable request.

REFERENCES

1. Alcover A, Alarcon B, Di Bartolo V. Cell Biology of T Cell Receptor Expression and Regulation. *Annu Rev Immunol*. 2018;36:103-125.
2. Wucherpfennig KW, Gagnon E, Call MJ, Huseby ES, Call ME. Structural biology of the T-cell receptor: insights into receptor assembly, ligand recognition, and initiation of signaling. *Cold Spring Harb Perspect Biol*. 2010;2(4):a005140.
3. Latour S, Veillette A. Proximal protein tyrosine kinases in immunoreceptor signaling. *Curr Opin Immunol*. 2001;13(3):299-306.
4. Chakraborty AK, Weiss A. Insights into the initiation of TCR signaling. *Nature immunology*. 2014;15(9):798-807.
5. Palacios EH, Weiss A. Function of the Src-family kinases, Lck and Fyn, in T-cell development and activation. *Oncogene*. 2004;23(48):7990-8000.
6. Denny MF, Patai B, Straus DB. Differential T-cell antigen receptor signaling mediated by the Src family kinases Lck and Fyn. *Mol Cell Biol*. 2000;20(4):1426-1435.
7. James JR, Vale RD. Biophysical mechanism of T-cell receptor triggering in a reconstituted system. *Nature*. 2012;487(7405):64-69.
8. Su X, Ditlev JA, Hui E, et al. Phase separation of signaling molecules promotes T cell receptor signal transduction. *Science*. 2016;352(6285):595-599.
9. Veillette A, Bookman MA, Horak EM, Bolen JB. The CD4 and CD8 T cell surface antigens are associated with the internal membrane tyrosine-protein kinase p56lck. *Cell*. 1988;55(2):301-308.
10. Artyomov MN, Lis M, Devadas S, Davis MM, Chakraborty AK. CD4 and CD8 binding to MHC molecules primarily acts to enhance Lck delivery. *Proc Natl Acad Sci U S A*. 2010;107(39):16916-16921.
11. van Oers NS, Killeen N, Weiss A. Lck regulates the tyrosine phosphorylation of the T cell receptor subunits and ZAP-70 in murine thymocytes. *J Exp Med*. 1996;183(3):1053-1062.
12. Thill PA, Weiss A, Chakraborty AK. Phosphorylation of a Tyrosine Residue on Zap70 by Lck and Its Subsequent Binding via an SH2 Domain May Be a Key Gatekeeper of T Cell Receptor Signaling In Vivo. *Mol Cell Biol*. 2016;36(18):2396-2402.
13. Zhang W, Sloan-Lancaster J, Kitchen J, Trible RP, Samelson LE. LAT: the ZAP-70 tyrosine kinase substrate that links T cell receptor to cellular activation. *Cell*. 1998;92(1):83-92.
14. Bubeck Wardenburg J, Fu C, Jackman JK, et al. Phosphorylation of SLP-76 by the ZAP-70 protein-tyrosine kinase is required for T-cell receptor function. *The Journal of biological chemistry*. 1996;271(33):19641-19644.
15. Lovatt M, Filby A, Parravicini V, Werlen G, Palmer E, Zamoyska R. Lck regulates the threshold of activation in primary T cells, while both Lck and Fyn contribute to the magnitude of the extracellular signal-related kinase response. *Mol Cell Biol*. 2006;26(22):8655-8665.
16. D'Oro U, Vacchio MS, Weissman AM, Ashwell JD. Activation of the Lck tyrosine kinase targets cell surface T cell antigen receptors for lysosomal degradation. *Immunity*. 1997;7(5):619-628.
17. Liu H, Rhodes M, Wiest DL, Vignali DA. On the dynamics of TCR:CD3 complex cell surface expression and downmodulation. *Immunity*. 2000;13(5):665-675.
18. Cenciarelli C, Hou D, Hsu KC, et al. Activation-induced ubiquitination of the T cell antigen receptor. *Science*. 1992;257(5071):795-797.
19. Rubin B, Llobera R, Gouaillard C, Alcover A, Arnaud J. Dissection of the role of CD3gamma chains in profound but reversible T-cell receptor down-regulation. *Scand J Immunol*. 2000;52(2):173-183.

20. Itoh Y, Hemmer B, Martin R, Germain RN. Serial TCR engagement and down-modulation by peptide:MHC molecule ligands: relationship to the quality of individual TCR signaling events. *Journal of immunology*. 1999;162(4):2073-2080.
21. Valitutti S, Muller S, Cella M, Padovan E, Lanzavecchia A. Serial triggering of many T-cell receptors by a few peptide-MHC complexes. *Nature*. 1995;375(6527):148-151.
22. Gallegos AM, Xiong H, Leiner IM, et al. Control of T cell antigen reactivity via programmed TCR downregulation. *Nature immunology*. 2016;17(4):379-386.
23. Cai Z, Kishimoto H, Brunmark A, Jackson MR, Peterson PA, Sprent J. Requirements for peptide-induced T cell receptor downregulation on naive CD8+ T cells. *J Exp Med*. 1997;185(4):641-651.
24. Schonrich G, Kalinke U, Momburg F, et al. Down-regulation of T cell receptors on self-reactive T cells as a novel mechanism for extrathymic tolerance induction. *Cell*. 1991;65(2):293-304.
25. Valitutti S, Lanzavecchia A. Serial triggering of TCRs: a basis for the sensitivity and specificity of antigen recognition. *Immunology today*. 1997;18(6):299-304.
26. Viola A, Lanzavecchia A. T cell activation determined by T cell receptor number and tunable thresholds. *Science*. 1996;273(5271):104-106.
27. Myers MD, Dragone LL, Weiss A. Src-like adaptor protein down-regulates T cell receptor (TCR)-CD3 expression by targeting TCRzeta for degradation. *J Cell Biol*. 2005;170(2):285-294.
28. Straus DB, Weiss A. Genetic evidence for the involvement of the lck tyrosine kinase in signal transduction through the T cell antigen receptor. *Cell*. 1992;70(4):585-593.
29. van Oers NS, Lowin-Kropf B, Finlay D, Connolly K, Weiss A. alpha beta T cell development is abolished in mice lacking both Lck and Fyn protein tyrosine kinases. *Immunity*. 1996;5(5):429-436.
30. Lauritsen JP, Christensen MD, Dietrich J, Kastrup J, Odum N, Geisler C. Two distinct pathways exist for down-regulation of the TCR. *Journal of immunology*. 1998;161(1):260-267.
31. Dumont C, Blanchard N, Di Bartolo V, et al. TCR/CD3 down-modulation and zeta degradation are regulated by ZAP-70. *Journal of immunology*. 2002;169(4):1705-1712.
32. von Essen M, Bonefeld CM, Siersma V, et al. Constitutive and ligand-induced TCR degradation. *The Journal of Immunology*. 2004;173(1):384-393.
33. Bartelt RR, Cruz-Orcutt N, Collins M, Houtman JC. Comparison of T cell receptor-induced proximal signaling and downstream functions in immortalized and primary T cells. *PLoS One*. 2009;4(5):e5430.
34. Kitamura T, Koshino Y, Shibata F, et al. Retrovirus-mediated gene transfer and expression cloning: powerful tools in functional genomics. *Exp Hematol*. 2003;31(11):1007-1014.
35. Hart T, Tong AHY, Chan K, et al. Evaluation and Design of Genome-Wide CRISPR/SpCas9 Knockout Screens. *G3 (Bethesda)*. 2017;7(8):2719-2727.
36. Naviaux RK, Costanzi E, Haas M, Verma IM. The pCL vector system: rapid production of helper-free, high-titer, recombinant retroviruses. *Journal of virology*. 1996;70(8):5701-5705.
37. Chang K, Marran K, Valentine A, Hannon GJ. Packaging shRNA retroviruses. *Cold Spring Harb Protoc*. 2013;2013(8):734-737.
38. Salmon P, Trono D. Production and titration of lentiviral vectors. *Curr Protoc Hum Genet*. 2007;Chapter 12:Unit 12 10.
39. Luton F, Buferne M, Legendre V, Chauvet E, Boyer C, Schmitt-Verhulst AM. Role of CD3gamma and CD3delta cytoplasmic domains in cytolytic T lymphocyte functions and TCR/CD3 down-modulation. *Journal of immunology*. 1997;158(9):4162-4170.
40. Kishimoto H, Kubo RT, Yorifuji H, Nakayama T, Asano Y, Tada T. Physical dissociation of the TCR-CD3 complex accompanies receptor ligation. *J Exp Med*. 1995;182(6):1997-2006.

41. Valitutti S, Muller S, Salio M, Lanzavecchia A. Degradation of T cell receptor (TCR)-CD3-zeta complexes after antigenic stimulation. *J Exp Med*. 1997;185(10):1859-1864.
42. Salmond RJ, Filby A, Qureshi I, Caserta S, Zamoyska R. T-cell receptor proximal signaling via the Src-family kinases, Lck and Fyn, influences T-cell activation, differentiation, and tolerance. *Immunol Rev*. 2009;228(1):9-22.
43. Hanke JH, Gardner JP, Dow RL, et al. Discovery of a novel, potent, and Src family-selective tyrosine kinase inhibitor. Study of Lck- and FynT-dependent T cell activation. *The Journal of biological chemistry*. 1996;271(2):695-701.
44. Lee KC, Ouwehand I, Giannini AL, Thomas NS, Dibb NJ, Bijlmakers MJ. Lck is a key target of imatinib and dasatinib in T-cell activation. *Leukemia*. 2010;24(4):896-900.
45. Cwynarski K, Laylor R, Macchiarulo E, et al. Imatinib inhibits the activation and proliferation of normal T lymphocytes in vitro. *Leukemia*. 2004;18(8):1332-1339.
46. Wang W, Ye C, Liu J, Zhang D, Kimata JT, Zhou P. CCR5 gene disruption via lentiviral vectors expressing Cas9 and single guided RNA renders cells resistant to HIV-1 infection. *PLoS One*. 2014;9(12):e115987.
47. Seki A, Rutz S. Optimized RNP transfection for highly efficient CRISPR/Cas9-mediated gene knockout in primary T cells. *J Exp Med*. 2018;215(3):985-997.
48. Dietrich J, Geisler C. T cell receptor zeta allows stable expression of receptors containing the CD3gamma leucine-based receptor-sorting motif. *The Journal of biological chemistry*. 1998;273(41):26281-26284.
49. Pelchen-Matthews A, Boulet I, Littman DR, Fagard R, Marsh M. The protein tyrosine kinase p56lck inhibits CD4 endocytosis by preventing entry of CD4 into coated pits. *J Cell Biol*. 1992;117(2):279-290.
50. Chan AC, Dalton M, Johnson R, et al. Activation of ZAP-70 kinase activity by phosphorylation of tyrosine 493 is required for lymphocyte antigen receptor function. *EMBO J*. 1995;14(11):2499-2508.
51. Tsun A, Qureshi I, Stinchcombe JC, et al. Centrosome docking at the immunological synapse is controlled by Lck signaling. *J Cell Biol*. 2011;192(4):663-674.
52. Groves T, Smiley P, Cooke MP, Forbush K, Perlmutter RM, Guidos CJ. Fyn can partially substitute for Lck in T lymphocyte development. *Immunity*. 1996;5(5):417-428.
53. Luton F, Buferne M, Davoust J, Schmitt-Verhulst AM, Boyer C. Evidence for protein tyrosine kinase involvement in ligand-induced TCR/CD3 internalization and surface redistribution. *Journal of immunology*. 1994;153(1):63-72.
54. Salio M, Valitutti S, Lanzavecchia A. Agonist-induced T cell receptor down-regulation: molecular requirements and dissociation from T cell activation. *Eur J Immunol*. 1997;27(7):1769-1773.
55. Martin S, Bevan MJ. Transient alteration of T cell fine specificity by a strong primary stimulus correlates with T cell receptor down-regulation. *Eur J Immunol*. 1998;28(10):2991-3002.
56. Fabian MA, Biggs WH, 3rd, Treiber DK, et al. A small molecule-kinase interaction map for clinical kinase inhibitors. *Nat Biotechnol*. 2005;23(3):329-336.
57. Wang H, Holst J, Woo SR, et al. Tonic ubiquitylation controls T-cell receptor:CD3 complex expression during T-cell development. *EMBO J*. 2010;29(7):1285-1298.
58. Bluestone JA, Pardoll D, Sharrow SO, Fowlkes BJ. Characterization of murine thymocytes with CD3-associated T-cell receptor structures. *Nature*. 1987;326(6108):82-84.
59. Molina TJ, Kishihara K, Siderovski DP, et al. Profound block in thymocyte development in mice lacking p56lck. *Nature*. 1992;357(6374):161-164.

60. Seddon B, Legname G, Tomlinson P, Zamoyska R. Long-term survival but impaired homeostatic proliferation of Naive T cells in the absence of p56lck. *Science*. 2000;290(5489):127-131.
61. Chan AC, Iwashima M, Turck CW, Weiss A. ZAP-70: a 70 kd protein-tyrosine kinase that associates with the TCR zeta chain. *Cell*. 1992;71(4):649-662.
62. Williams BL, Schreiber KL, Zhang W, et al. Genetic evidence for differential coupling of Syk family kinases to the T-cell receptor: reconstitution studies in a ZAP-70-deficient Jurkat T-cell line. *Mol Cell Biol*. 1998;18(3):1388-1399.
63. Baniyash M. TCR zeta-chain downregulation: curtailing an excessive inflammatory immune response. *Nature reviews Immunology*. 2004;4(9):675-687.

SUPPLEMENTAL INFORMATION

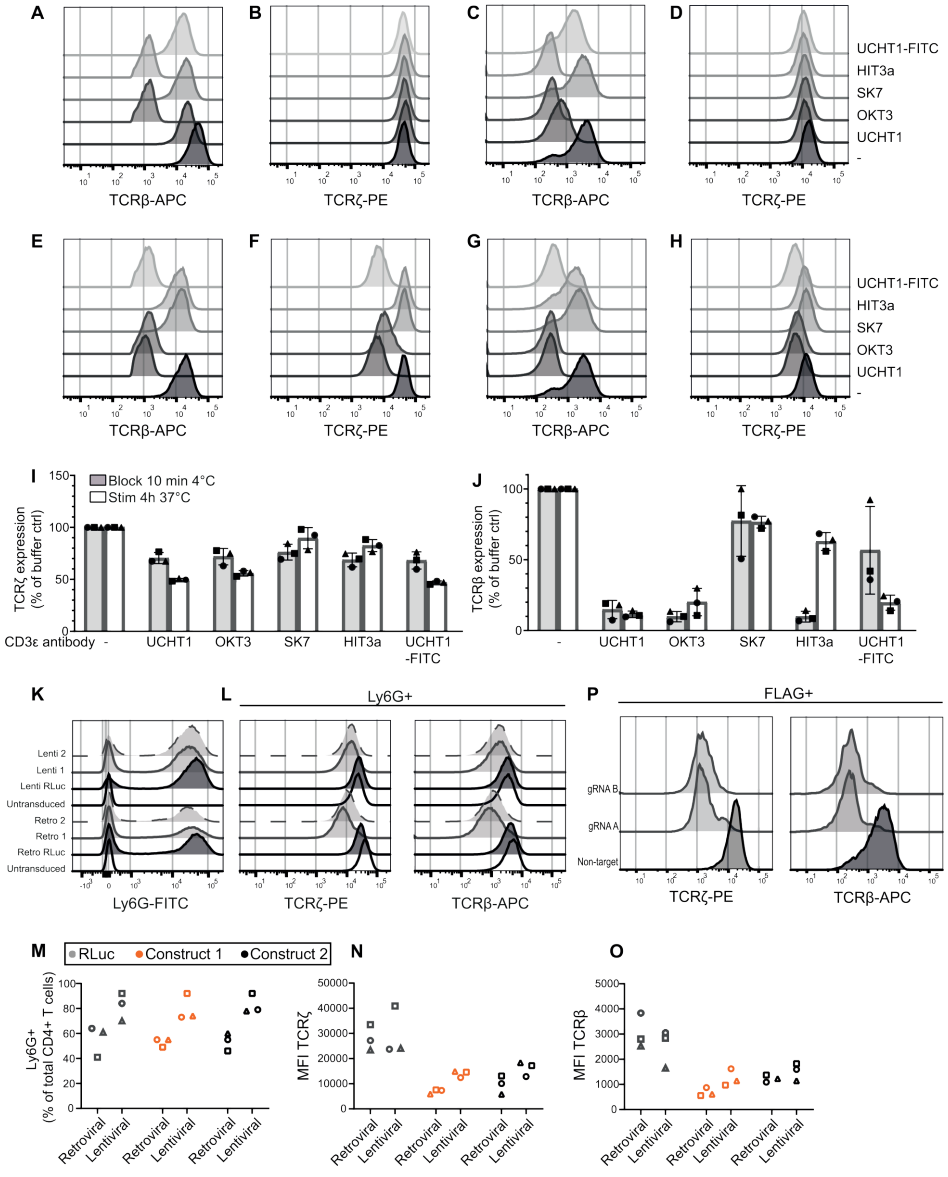

◄ Supplemental Figure 1: Investigation of steric hindrance and stimulation, and genetic modification of human CD4⁺ PBLs and Jurkat cells.

(A-D) Representative histograms showing steric hindrance for human PBLs (A, B) and Jurkat cells (C, D). Surface TCRβ (A) and total TCRζ (B) expression in human PBLs, and surface TCRβ (C) and total TCRζ (D) expression in Jurkat cells were measured after incubation with the indicated anti-CD3 antibodies at 4°C. (E-H) Representative histograms showing the effect of anti-CD3/CD28 stimulation on human PBLs (E, F) and Jurkat cells (G, H). Surface TCRβ (E) and total TCRζ (F) expression in human PBLs, and surface TCRβ (G) and total TCRζ (H) expression in Jurkat after stimulation at 37°C. (I-J) Aggregate data of total TCRζ (I) and surface TCRβ (J) expression of Jurkat cells. For Jurkat cells, each symbol represents an independent experiment (n=3), and the median and 95%CI are shown. Expression in non-triggered T cells is set at 100%, based on the MFI. (K-P) Optimization of genetic modification of hPBL and Jurkat cells. (K-L) Representative histograms showing the surface Ly6G (K), total TCRζ and surface TCRβ (L) expression of human CD4⁺ PBLs after transduction with retroviral/lentiviral microRNA vectors targeting TCRζ in n=3 independent experiments with a different donor. (M-O) Comparison between lentiviral and retroviral microRNA knockdown efficiency of TCRζ in human CD4⁺ PBLs. Percentage of transduced cells (Ly6G⁺; M), total TCRζ (N) and surface TCRβ (O) levels were measured. (P) For the transduction of Jurkat cells with lentiviral CRISPR/Cas9 vectors targeting TCRζ, total TCRζ and surface TCRβ expression in FLAG-positive Jurkat cells were measured. (M-O) Each symbol represents an individual donor, examined in a separate experiment. (P) Representative plots of n=2 independent experiments. MFI = mean fluorescent intensity.

Supplemental Figure 2: Lck and Fyn are individually redundant for TCR downregulation in human PBLs and Jurkat cells.

(A) Aggregate data of total Lck expression of human PBLs after transduction with microRNA vectors targeting Lck, for n=3 healthy donors examined in a separate experiment. (B, C) (B) Representative histogram and (C) aggregate data showing the effect of Lck knockdown on CD69 expression in different donors (n=3) and different experiments that were left unstimulated (-), or stimulated with low (+) or high (++) dose anti-CD3/CD28. Significance is calculated with the paired student's *t*-test, *p<0.05; **p<0.01. (D) Total Lck expression of Jurkat cells after transduction with CRISPR/Cas9 vectors targeting Lck. (E-G) Surface TCRβ (E), total TCRζ (F) and surface CD69 (G) expression of Jurkat cells with Lck knockdown left unstimulated (-), or upon TCR triggering by low (+) or high (++) dose anti-CD3/CD28 for n=3 separate experiments. (H) Immunoblot showing the total tyrosine phosphorylation of cells that were transduced with non-target or Lck CRISPR/Cas9 vectors, and that were left unstimulated (-), anti-CD3 stimulated, or anti-CD3 and pervanadate (PV) stimulated. β-actin was used as loading control. Immunoblot is representative of a single biological replicate. (I) Representative histogram showing the total Fyn expression of human PBLs after transduction with non-target microRNAs or microRNA vectors targeting Fyn. (J) Aggregate data of total Fyn expression of human PBLs after transduction with microRNA vectors targeting Fyn, for n=2 healthy donors examined in a separate experiment. (K, L) Representative histogram (K) and aggregate data (L) showing the effect of Fyn knockdown on CD69 expression in different donors (n=3) that were left unstimulated (-), or stimulated with low (+) or high (++) dose anti-CD3/CD28. Significance is calculated with the paired student's *t*-test, *p<0.05; **p<0.01. ►

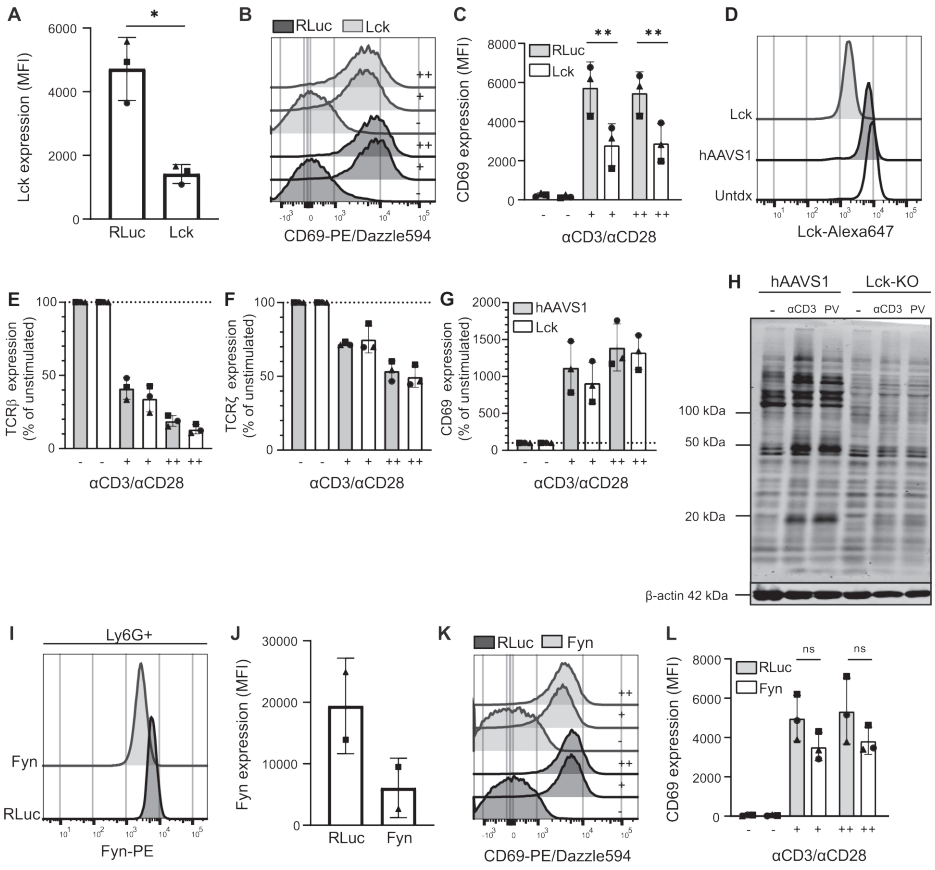
A
Lck expression (MFI)
RLuc
Lck
B
RLuc
Lck
CD69-PE/Dazzle594
C
CD69 expression (MFI)
αCD3/αCD28
D
Lck
hAAVS1
Untdx
Lck-Alexa647
E
TCRβ expression (% of unstimulated)
αCD3/αCD28
F
TCRζ expression (% of unstimulated)
αCD3/αCD28
G
hAAVS1
Lck
CD69 expression (% of unstimulated)
αCD3/αCD28
H
hAAVS1
Lck-KO
αCD3
PV
100 kDa
50 kDa
20 kDa
β-actin 42 kDa
I
Ly6G+
Fyn
RLuc
Fyn-PE
J
Fyn expression (MFI)
RLuc
Fyn
K
RLuc
Fyn
CD69-PE/Dazzle594
L
RLuc
Fyn
ns
CD69 expression (MFI)
αCD3/αCD28

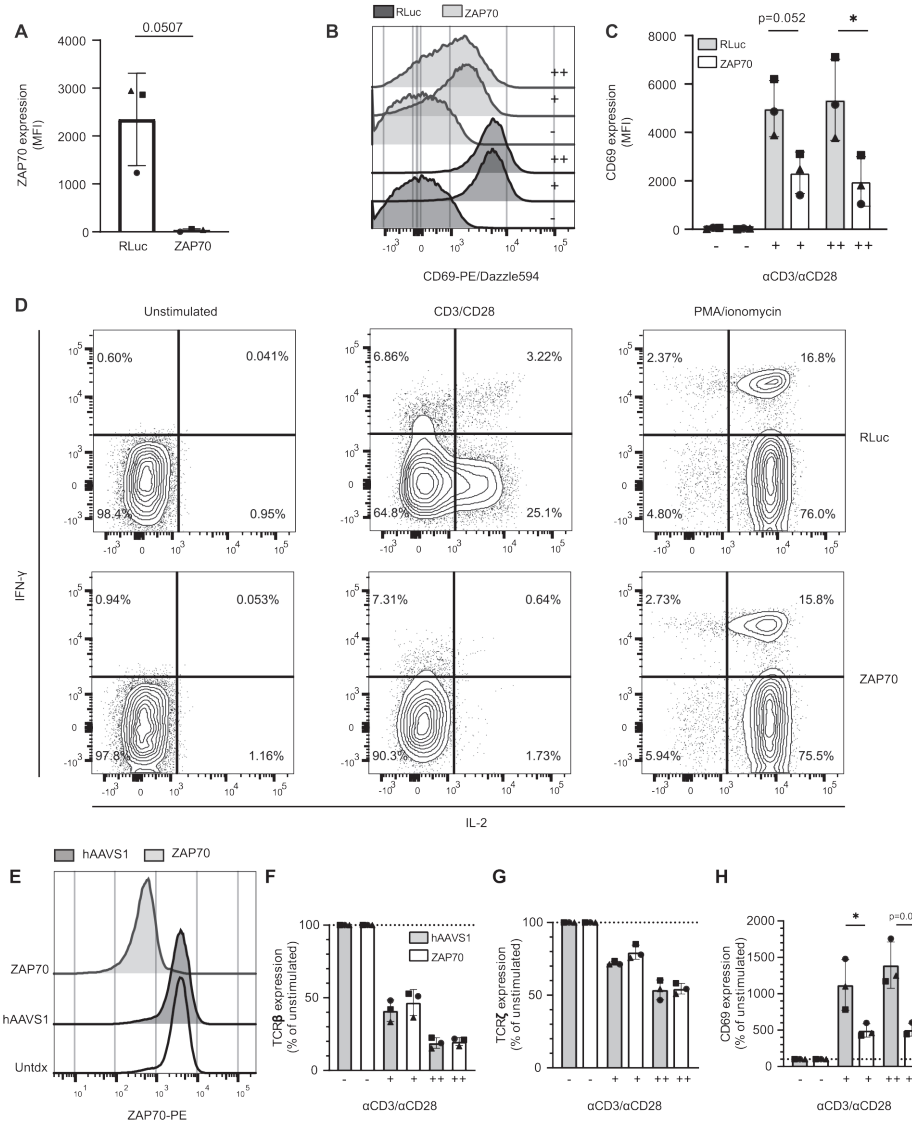
A
0.0507
ZAP70 expression (MFI)
RLuc
ZAP70
B
RLuc
ZAP70
CD69-PE/Dazzle594
C
p=0.052
*
CD69 expression (MFI)
αCD3/αCD28
D
Unstimulated
CD3/CD28
PMA/ionomycin
IFN-γ
IL-2
RLuc
ZAP70
0.60%
0.041%
98.4%
0.95%
6.86%
3.22%
64.8%
25.1%
2.37%
16.8%
4.80%
76.0%
0.94%
0.053%
97.8%
1.16%
7.31%
0.64%
90.3%
1.73%
2.73%
15.8%
5.94%
75.5%
E
hAAVS1
ZAP70
ZAP70
hAAVS1
Untdx
ZAP70-PE
F
TCRβ expression (% of unstimulated)
αCD3/αCD28
G
TCRζ expression (% of unstimulated)
αCD3/αCD28
H
p=0.054
CD69 expression (% of unstimulated)
αCD3/αCD28

◂ Supplemental Figure 3: ZAP70 is required for T cell activation and effector functions in human CD4⁺ PBLs.

(A) Aggregate data of total ZAP70 expression of human PBLs after transduction with microRNA vectors targeting ZAP70. (B, C) Representative histogram (B) and aggregate data (C) of surface CD69 expression in human PBLs with ZAP70 knockdown (dark grey) or non-target microRNA (light grey) without stimulation (-) upon TCR triggering by low (+) or high (++) dose anti-CD3/CD28. (A, C) Each symbol represents an individual donor (n=3) examined in a separate experiment, with bars depicting the mean and standard deviation. Significance was calculated with paired student's *t*-test. *p<0.05. (D) Effect of ZAP70 knockdown on cytokine production by PBLs. Representative plots of 1 donor. (E) Total ZAP70 expression of Jurkat cells after transduction with CRISPR/Cas9 vectors targeting ZAP70 (light grey) or a non-target guide-RNA (dark grey). (F-H) Surface TCRβ (F), total TCRζ (G) and surface CD69 (H) expression of PBLs with ZAP70 knockout left unstimulated (-), or upon TCR triggering by low (+) or high (++) dose anti-CD3/CD28 for n=3 separate experiments.

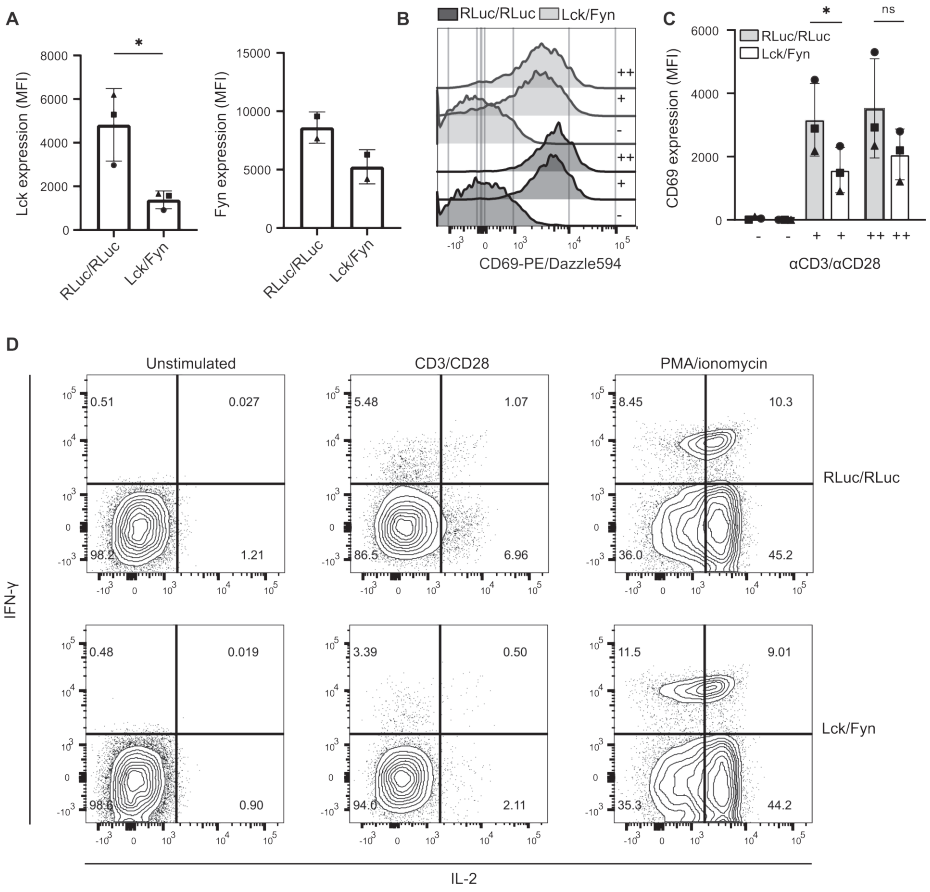

Supplemental Figure 4: Lck and Fyn double knockdown slightly impairs activation of human PBLs.

(A) Aggregate data of total Lck and Fyn expression in human PBLs after transduction with microRNA vectors targeting Lck and Fyn. (B, C) Surface CD69 expression of human PBLs transduced with non-target microRNA vectors (dark grey) or double Lck and Fyn knockdown (light grey) left unstimulated (-), or upon TCR triggering by low (+) or high (++) dose anti-CD3/CD28. (A, C) Each symbol represents an individual donor (n=3) examined in a separate experiment, with bars depicting the mean and standard deviations. (D) Representative plots (n=3) of the effect of Lck and Fyn double knockdown on cytokine production by human PBLs. Significance was calculated with the paired student's *t*-test. *p<0.05.

Supplementary Table 1. Overview of the antibodies used in this study

Antibody	Clone	Manufacturer
Anti-mouse Ly6G/Ly6C	RB6-8C5	eBioscience
Anti-mouse CD90.2	30-H12	Biolegend
Anti-mouse IgG1	RMG1-1	Biolegend
Mouse IgG1, isotype ctrl	MOPC-21	Biolegend
Anti-mouse/human TCRζ	6B10.2	Biolegend
Anti-human CD4	RPA-T4	Biolegend
Anti-human CD8α	RPA-T8	Biolegend
Anti-human CD45	HI100	Biolegend
Anti-human CD45RA	HI100	Biolegend
Anti-human CD27	O323	Biolegend
Anti-human CD69	FN50	Biolegend
DYK/FLAG tag	L5	Biolegend
Anti-human CD3ε	UCHT1	Biolegend
Anti-human CD3ε	OKT3	Biolegend
Anti-human CD3ε	SK7	Biolegend
Anti-human CD3ε	HIT3a	Biolegend
Anti-human CD28	CD28.2	Biolegend
Anti-human TCRβ	IP26	Biolegend
Anti-human Lck	LCK-01	Biolegend
Anti-human ZAP70	1E7.2	Biolegend
Anti-human IL-2	MQ1-17H12	Biolegend
Anti-human IFN-γ	B27	Biolegend
Anti-human Actin (beta)	W16197A	Biolegend
Anti-human phospho-tyrosine	PY20	Biolegend
Anti-human Fyn	FYN-59	Biolegend

CHAPTER 8

GENERAL DISCUSSION

DISCUSSION

In this thesis we have investigated how immune responses mediated by dendritic cells (DCs) and T cells are affected by the host as well as pathogens and whether we can use this knowledge for therapeutic purposes. In **part I**, we focused on immune activation and suppression by SARS-CoV-2. We identified how the virus is able to circumvent induction of antiviral immune recognition by DCs and explored how the immune system utilizes alternative weapons to fight back against the virus. Learning from our experience in studying viral responses, we also investigated whether we can genetically modify bacteria to actively induce such pathways, boosting the immune system's capabilities to kill malignant cells. In **part II**, we focused on the improvement and optimization of methods to study adaptive immune functions in primary T cells, and these methods were used to investigate T cell activation and T cell receptor (TCR) downregulation. Here we will discuss our findings in the field of control of innate immune sensing and T cell activation.

SARS-CoV-2 is invisible to DCs

The role of DCs in SARS-CoV-2 infection remains unclear and conflicting data about the role of DCs in COVID-19 have been published. Several studies suggest that DC function during COVID-19 is affected as their ability to secrete antiviral cytokines, including IFN-β, and antigen presentation capacity is reduced during COVID-19 (1, 2). Even though immune cells express no or very low levels of ACE2, some reports suggest that DCs become infected by SARS-CoV-2, leading to high production of proinflammatory cytokines (3, 4). These studies suggest that infection of DCs might lead to DC activation by SARS-CoV-2. Moreover, during the SARS-CoV-2 pandemic, several reports presented computational analyses to suggest that the Spike (S) protein of SARS-CoV-2 binds to and activates the pattern recognition receptor (PRR) Toll-like receptor (TLR)4, which is highly expressed by DCs. TLR4 triggering by SARS-CoV-2 was thereby suggested to induce DC maturation and secretion of type I interferon (IFN) and cytokine responses. Indeed, several studies show that recombinant SARS-CoV-2 S protein activates macrophages (5-7). In contrast, in **chapter 2** we showed that DCs were neither activated by S protein nor SARS-CoV-2 primary isolate. Since DCs express a wide variety of PPRs besides TLR4, our data suggest that TLR4 and other surface PRRs do not sense SARS-CoV-2. In addition, DCs did not become infected by SARS-CoV-2 as these cells do not express ACE2 (8, 9). Therefore, also the intracellular PRRs are not triggered to instigate type I IFN responses. Notably, ectopic expression of ACE2 on DCs led to infection by SARS-CoV-2 and type I IFN responses, strongly suggesting that upon infection intracellular sensors are able to sense the virus. However, the inability of DCs to sense extracellular SARS-CoV-2

proposes a hiatus in the steps of immune activation; when SARS-CoV-2 is invisible to DCs, the question of how DCs would be able to induce adaptive responses arises. Since antigen-specific T cell responses against SARS-CoV-2 are found in COVID-19 patients (10), our findings suggest that instead of direct DC activation, other mechanisms of indirect DC activation are at play during COVID-19 pathogenesis.

DC activation via the bystander effect

Apart from SARS-CoV-2, other viruses are described to induce immune responses via TLR4 (11). Whilst some of these viruses express surface glycoproteins that directly trigger TLR4, other viruses do not directly trigger PRRs, but induce immune responses via host danger-associated or pathogen-associated molecular patterns (DAMPs or PAMPs). In this so-called bystander effect, infected cells release PAMPs and DAMPs, which in turn trigger PRRs on DCs. We hypothesized that this mechanism could also occur during SARS-CoV-2 infection. ACE2 is highly expressed by epithelial cells in the upper and to a lesser extent in the lower respiratory airways (12). DCs are also present in the airway mucosa and monocyte-derived DCs are attracted to the lungs during infection (13). Thus, infection of epithelial cells might lead to cell death and subsequent activation of DCs. In **chapter 2**, we observed that SARS-CoV-2 infection of epithelial cells and subsequent co-culture with DCs led to upregulation of co-stimulatory molecules and cytokine responses by DCs. Our data suggest that infection of epithelial cells with SARS-CoV-2 leads to the release of PAMPs and DAMPs, which trigger DC activation. These activated DCs might be able to instruct the adaptive immune responses. It would be interesting to further investigate what kind of PAMPs or DAMPs are released by the infected epithelial cells; it remains unknown whether soluble mediators or markers expressed by the epithelial cells induce DC activation, and whether these PAMPs and DAMPs induce the signaling pathways and crosstalk required to fight SARS-CoV-2 infection. It is also unclear whether DCs activated by PAMPs and DAMPs are equipped to induce the appropriate antigen-specific immune responses. It is possible that DC activation by PAMPs or DAMPs leads to different $CD4^+$ T helper cell polarization, which might hamper efficient antiviral immunity. Moreover, since DCs are not directly infected by SARS-CoV-2, DCs would need to cross-present endocytosed SARS-CoV-2 antigens on MHC-I to activate potent $CD8^+$ T cell responses against SARS-CoV-2 (14, 15). However, the ability for cross-presentation is dependent on the DC subset (15, 16). Thus, the ability of specific ACE2-negative DC subsets to cross-present antigens to $CD8^+$ T cells might be important for effective immunity to SARS-CoV-2. Taken together, further research is required to elucidate this bystander mechanism and to investigate whether it contributes to efficient immune responses against SARS-CoV-2, or whether it causes increased damage and disease during COVID-19, and perhaps even long COVID-19.

Complement required for antiviral immunity to SARS-CoV-2

Besides PRRs that directly sense PAMPs, another vital component for sensing pathogens is the complement system. Complement-opsonized viral particles are recognized by immune cells via the complement receptors (CRs), thereby initiating antiviral type I IFN and cytokine responses. Interestingly, the complement system is highly activated during SARS-CoV-2 infection (17, 18). SARS-CoV-2 envelope proteins can trigger the lectin pathway via mannose-binding lectin (MBL), the alternative pathway, or the classical pathway through C1q or SARS-CoV-2-specific antibodies (19-21). In **chapter 3**, we observed that SARS-CoV-2 is rapidly opsonized by complement, and complement-opsonization of SARS-CoV-2 resulted in DC activation via the complement receptors CR3 and CR4. Complement-opsonized SARS-CoV-2 induced efficient type I IFN as well as cytokine responses. These data strongly suggest that complement is required for activation of DCs upon SARS-CoV-2 infection. However, complement might be a double-edged sword: several studies suggest that uncontrolled complement activation might contribute to disease severity of COVID-19 as high circulating C5a and processed C3 levels have been observed in the blood of COVID-19 patients (22, 23). To verify whether serum from COVID-19 patients has different effects on DC activation, we also treated SARS-CoV-2 with serum from convalescent COVID-19 patients. Notably, the serum of convalescent COVID-19 patients attenuated the complement-mediated DC activation via the Fc gamma receptor II (FcγRII; CD32). Similar attenuation of DC activation and type I IFN responses were observed when pre-treating complement-opsonized SARS-CoV-2 with monoclonal antibodies against SARS-CoV-2. These data strongly suggest that once adaptive immune responses against SARS-CoV-2 are induced, complement-induced immune activation is switched off by the antibodies against SARS-CoV-2 to prevent continuous immune activation.

Antibody-mediated effector functions are accomplished by interaction of the antibody's Fc domain with the Fc receptors (FcRs). FcRs are differentially expressed on various immune cell types (24) and for every antibody isotype there is a specific FcR. Thus, different FcR triggering on different immune cells induces tailored immune responses. IgG antibodies bind to the Fc gamma receptors (FcγR) with different affinities. FcγRs with a high affinity only require binding of a monomeric antibody to induce downstream signaling, whilst FcγRs with a lower affinity require binding of antibody-immune complexes such as antibody-opsonized SARS-CoV-2 (25). Furthermore, the family of FcγRs consists of three members, including FcγRI (CD64), FcγRII (CD32) and FcγRIII (CD16), of which we here focused on FcγRII. FcγRII is a low affinity receptor that is triggered by immune-complexes (25). FcγRII can be subdivided into FcγRIIa, FcγRIIb and FcγRIIc. Whilst FcγRIIa signals via the immunoreceptor tyrosine-based activating motif (ITAM) in its cytoplasmic domain, FcγRIIb contains an inhibitory motif (ITIM)

which provides negative feedback to prevent immune overactivation (26). FcγRIIc is only expressed by a small percentage of individuals that express this receptor (24, 27). Our data suggest an inhibitory role for FcγRII in antibody-mediated suppression of cytokine responses, since inhibition of FcγRII using anti-CD32 antibodies restored immune activation by complement-opsonized SARS-CoV-2. Further research is required to investigate the signaling pathways underlying this process. Taken together, our results suggest that COVID-19 illness or vaccination against SARS-CoV-2 leads to induction of antibody responses that not only protect against viruses but also suppress the activation of the immune system during infection, thereby attributing a new role for antibodies during SARS-CoV-2 infection.

The severity of COVID-19 illness varies amongst individuals, ranging from lack of symptoms to mild or severe disease. We observed differences in the individual immune response and composition of the serum of healthy donors. Some of these differences might be due to single nucleotide polymorphisms (SNPs) in genes important for the immune response such as the complement proteins, FcγR expression or virus elimination. We showed that blocking the lectin pathway prevented complement opsonization of SARS-CoV-2, leading to a significantly decreased antiviral response by DCs. These findings indicate that MBL-mediated activation of the complement pathway is an essential step in the immune response against SARS-CoV-2. It is reported that SNPs in the MBL gene influence MBL expression or function, resulting in increased susceptibility to several infections, including HIV-1, SARS-CoV, and SARS-CoV-2 (28-30). Notably, a SNP affecting MBL function had a larger impact on COVID-19 severity than a SNP leading to MBL deficiency (28). Together these data suggest that proper functioning of MBL is essential for proper immune activation and SARS-CoV-2 disease phenotype. Moreover, the genes encoding the FcγRs are highly polymorphic and genetic variations with functional consequences have been described for all low-affinity FcγRs (24). SNPs in FcγRIIa might result in increased immune activation, whilst SNPs in FcγRIIb lead to stronger inhibitory signaling (24). A certain SNP in the FcγRIIa is even associated with increased mortality to COVID-19 (FCGR2A rs1801274) (31). However, the effect of these SNPs on molecular mechanisms involved in DC-induced immunity during SARS-CoV-2 infection needs to be further elucidated. Therefore, further research should address the impact of complement- and FcγR genetics on immune cell responses. In the near future, our research will focus on immune-profiling of COVID-19 patients, which might reveal key features in the development of COVID-19 disease as well as the antiviral effects of the complement system. Understanding the role of complement-cascade polymorphisms and their association with SARS-CoV-2 and other infectious diseases may lead to novel prophylactic or therapeutic strategies for targeting these pathways during disease.

SARS-CoV-2 suppresses TLR4 activation

In chapter 2 we have observed that SARS-CoV-2 escapes immune detection as the virus does not trigger DC activation via extracellular PRRs. Alternatively, dysregulation of DC function might also be caused through active suppression by pathogens. Certain viruses are well known to interfere with DC maturation or antigen presentation (32-35), thereby potentially suppressing DC function towards secondary triggers. Virus-induced DC dysfunction is especially important in the context of bacterial superinfections during COVID-19. Frequently, hospitalized COVID-19 patients contract bacterial superinfections, leading to worse disease progression (36, 37). This led us to investigate whether increased susceptibility of COVID-19 patients to bacterial superinfections is due to SARS-CoV-2 specifically interfering with DC function during defense against bacterial infections. In **chapter 4**, we described that the immune response by DCs against the bacterial component lipopolysaccharide (LPS) was diminished in the presence of S protein and SARS-CoV-2 primary isolate, as DCs produced less type I IFN and cytokine responses upon exposure to LPS in the presence of S protein or SARS-CoV-2. Notably, we observed that S protein blocked TLR4 signaling, but not signaling via other TLRs. We hypothesized that S protein might sterically hinder the binding of LPS to TLR4. However, S protein or SARS-CoV-2 did not compete with LPS signaling in a TLR4-overexpressing cell-line, suggesting that binding of S protein to TLR4 does not sterically hinder LPS signaling. Besides TLRs, viral surface glycoproteins bind C-type lectin receptors (CLRs), including DC-SIGN. DC-SIGN is known to modulate immune responses against various pathogens, including HIV, measles virus, and *Mycobacterium (M.) tuberculosis* (38-41). Therefore, we investigated whether crosstalk between TLR4 and DC-SIGN was involved in the altered immune responses against LPS. We showed that recombinant SARS-CoV-2 S protein bound to DC-SIGN expressed by DCs. Moreover, we observed that blocking DC-SIGN restored LPS-induced DC activation in the presence of S protein and SARS-CoV-2. Furthermore, blocking the downstream kinase Raf-1 by a small molecule inhibitor restored immune responses to LPS. These data suggest that SARS-CoV-2 S protein signals via DC-SIGN, thereby suppressing DC responses against secondary bacterial triggers.

Another study on the activation status of DCs from COVID-19 patients also showed reduced production of type I IFNs and diminished upregulation of maturation markers after stimulation with different TLR ligands (42). This study and our study suggest that COVID-19 affects immunity in multiple ways: DC function might be suppressed during COVID-19 by other mechanisms such as aberrant inflammatory responses, which will not only affect bacterial but also viral or fungal superinfections (42). Therefore, it is important to investigate how superinfections with different bacteria, viruses or fungi might affect DC function during COVID-19.

Triggering of DC-SIGN by mannosylated ligands results in activation of Raf-1 as well as NFκB when triggered by *M. tuberculosis*, but also interference with activation of RIG-I and MDA5 or blocking MAVS induced by measles virus or HIV, respectively (40, 41). Here we have identified a novel mechanism used by SARS-CoV-2 to suppress TLR4-induced type I IFN and cytokine responses via the DC-SIGN/Raf-1 axis. Notably, SARS-CoV-2 binding to DC-SIGN blocked both type I IFN and cytokine responses, whereas previous studies have shown that both HIV and *M. tuberculosis* enhance TLR4-induced signaling via DC-SIGN (43). Taken together, our results indicate that SARS-CoV-2 is not only inadequately sensed by DCs, but the virus also suppresses DC functionality towards secondary bacterial infections. Further studies are required to identify the underlying mechanisms.

Type I IFN: important from early innate signals to strong T cell responses

Viral sensing by DCs is essential for the induction of type I IFN responses. Type I IFNs do not only function as proinflammatory cytokines for innate immune cell activation and direct viral restriction, but are also involved in regulating T cell responses. Regulation of type I IFN responses by DCs is crucial, since it affects the function of antigen-presenting cells and T cell activation directly (44). However, we and others described that SARS-CoV-2 fails to induce potent type I IFN and IFN-stimulated gene (ISG) responses (45). Besides insufficient induction, there are also reports that SARS-CoV-2 suppresses type I IFN responses in patients (46). In the case of SARS-CoV-2, our data suggest that complement-opsonization is important for the induction of type I IFN responses. These type I IFN responses and antigen-specific stimulations by DCs are required for the differentiation and activation of Th1 and cytotoxic $CD8^+$ T cell (CTL) responses against viruses. In COVID-19 patients, virus-specific CTL responses were observed within 7 days of symptom onset and peaked after 14 days. Early CTL responses correlated with effective viral clearance and mild clinical outcome (47, 48). However, excessive CTL responses have proven to be detrimental and are associated with severe COVID-19 disease outcome (49, 50). The imbalance between effective and excessive CTL responses is difficult to determine, but could potentially be explained by our findings that DCs do not directly sense SARS-CoV-2 leading to reduced or absent IFN responses by DCs. The absence of proper IFN responses affects the induction of effective T cell responses against the virus (44, 46). This emphasizes the importance of our findings on alternative (in)direct DC activation or complement-mediated DC activation, and the role of type I IFN responses in steering adaptive immune responses. Although the beneficial effects of type I IFN responses on downstream adaptive immune responses are currently still being researched, its role in anti-tumor immune responses is more established.

Harnessing sensing and type I IFN responses for killing tumor cells

The last decades, DCs have been under investigation as key players in various types of anti-tumor treatments. IFN-β and ISGs recently have become of great interest in the field of oncology because their expression is strongly correlated to an anti-tumor immune response (51). From studying immune responses against viral and fungal infections, it is known that type I IFN responses are important in the development of CTLs (52, 53). Properly functioning CTLs are paramount for anti-tumor responses (54). Whilst recently anti-tumor therapy focuses on the reinvigoration of T cells, we targeted DCs in order to ameliorate anti-tumor T cell responses. In a relatively unknown branch of immunotherapy, the bacterial immunotherapy, genetically modified bacteria are used to activate the host's anti-tumor immunity. Bacterial immunotherapy has attracted a lot of interest in the last decade because of its many advantages (55, 56), including the bacteria's fierce immunogenicity and inherent attraction to hypoxic tumor environments. To date, Bacillus Calmette-Guérin (BCG), an attenuated strain of *M. bovis*, is the only bacterial cancer therapy clinically approved to treat patients with bladder cancer (57). Besides BCG, *Salmonella enterica* serovar *typhimurium* (*S. typhimurium*) is also being investigated for bacterial immunotherapy. According to different studies, *Salmonella*-mediated anti-tumor therapy contributes to tumor growth suppression and increased survival in mouse models (58-61). A phase I clinical trial with *S. typhimurium* pointed out that the vaccine strain alone was not sufficient to cure patients (62). Therefore, in **chapter 5**, we aimed to enhance the type I IFN response by DCs for the generation of cytotoxic T cells, which are instructed to kill malignant cells. To this end, we harnessed the immune-stimulating properties of *S. typhimurium* through ectopic expression of cGAS to induce excessive production of cGAMPs. Stimulator of IFN genes (STING) agonists like cGAMPs are of great interest in tumor immunology to induce type I IFN responses (63). However, many challenges regarding the delivery of STING agonists into the tumor has halted development. Bacterial immunotherapy can overcome these barriers and induce both type I IFN and proinflammatory cytokine responses. In **chapter 5**, we developed an intricate model in which DCs were infected by cGAS-overexpressing *S. typhimurium*. We observed that expression of cGAS in Salmonella led to production of cGAMPs and identified that these cGAMPs were actively transported into host cells by Salmonella's type III secretion (T3S) system. Transport of cGAMPs into the host cell triggered STING signaling, leading to induction of type I IFN responses by DCs. Moreover, the cGAS-Salmonella-infected DCs were co-cultured with T cells to assess T cell activation. We observed that co-culture of T cells with cGAS-Salmonella-infected DCs resulted in increased IFN-γ, perforin and granzyme production by cytotoxic $CD8^+$ T cells. Notably, we found that these IFN-γ-producing CTLs have improved cytotoxic potential towards malignant cells. Interestingly, in this assay we made use of the properties of the bispecific antibody blinatumomab to overcome HLA-

restriction. In higher concentrations, blinatumomab activates T cell to become more cytotoxic towards B cells. However, we used blinatumomab in low concentrations to bring the T and B cells in close proximity, without overriding the effect induced by cGAS-Salmonella-infected DCs. Thus, we developed a novel assay that allows DC-T cell activation without antigen specificity. Although our study showed the potential of cGAS-expressing Salmonella for the generation of potent DC and even CTL responses towards malignant cells, further research with antigen-specific solid tumor cells and *in vivo* models is required to advance our model as bacterial immunotherapy. In addition, combining different aspects of bacterial immunotherapy might eventually be key in the development of a potent anticancer treatment. In another study bacteria were modified to produce tumor antigens and induce potent anti-tumor T cell responses against melanoma (56). When these properties are applied to Salmonella, the bacteria are not only capable to overcome local immune suppression, but could also induce antigen-specific anti-tumor immunity. Moreover, whilst BCG therapy in bladder cancer was shown to enhance effector functions of tumor-specific $CD4^+$ T cells, which were activated to produce IFN-γ (64), Salmonella could use its T3S system to transport the cGAMPs as well as the tumor antigens directly into the DC cytosol, thereby also generating adequate $CD8^+$ T cell responses. Further research with these combined therapies opens a great array of possibilities in the treatment of cancer with bacterial immunotherapy.

TCR downregulation to limit T cell activation

Pathogens such as SARS-CoV-2 and *M. tuberculosis* manipulate DC function and thereby T cell immunity. However, not only pathogens are in control of determining DC or T cell activation outcome. Above we discussed how the host contributes to DC activation by means of complement-opsonization, as well as restriction of immune activation through antibodies against SARS-CoV-2. In addition, the host also actively contributes to triggering or limiting T cell activation. From a pathogen's point of view, limiting T cell activation or altering T cell function is important to evade immune detection and ensure survival in the host. To that end, *M. tuberculosis* hides from detection by T cells (65), whilst *Shigella flexneri* invades T cells to modify their behavior (66). HIV has evolved to prevent downmodulation of TCR expression during infection to bolster T cell activation and viral spread (67). However, the host itself is also able to limit T cell activation in order to prevent harmful overactivation. One of these mechanisms is a process called TCR downregulation. Upon TCR triggering, the TCR/CD3 complex is internalized and actively degraded in the lysosomes. Interestingly, clonally-expanded T cells also display persistent TCR downregulation, the strength of which is programmed by the strength of the initial T-cell antigen recognition (68). These cells with adjusted TCR expression are characterized by an increased threshold

for cytokine production and further proliferation upon renewed antigen encounter. It is presumed that these T cells are better equipped to achieve a balanced immune response. On the other hand, TCR downregulation might be an unwanted process in an oncology setting, when chimeric antigen receptor (CAR) T cells downregulate their CAR and become less functional in their cytolytic capacity.

The mechanism underlying TCR downregulation remains elusive. To unravel this mechanism, we designed a toolbox for retroviral knockdown of genes (**chapter 6**), which we used to assess the relative contribution of several proteins. In **chapter 7**, we investigated whether several Src family kinases known to be involved in T cell activation, are also involved in TCR downregulation as is suggested in classical literature (69-76). Since T cell activation and TCR downregulation are tightly linked, we set out to confirm the dogma that the same Src family kinases might be involved in both processes. Surprisingly, we found that individual knockdown of Lck, Fyn, or ZAP70 did not inhibit TCR downregulation, whilst T cell activation was significantly affected. Simultaneous knockdown of Lck and Fyn slightly but significantly abrogated TCR downregulation, suggesting these kinases have overlapping functions and are involved in TCR downregulation. However, their roles are less absolute in primary human lymphocytes compared to classical mouse and cell-line studies that have shaped the field (71, 77-83). Furthermore, whilst these kinases are essential for T cell activation, they are individually redundant for TCR downregulation, which shows that these processes are not strictly linked mechanistically. Further research on the mechanisms underlying TCR downregulation is required, since understanding this process could be used to optimize T cell activity in for instance CAR T cell therapy (84). Our study emphasizes that investigating the process of TCR downregulation in primary human cells is important because results obtained in primary T cell models are different from mouse models and human cell line models. Further investigation using an unbiased genetic screen that allows knockout or knockdown of multiple genes simultaneously would be required to unravel the mechanism. However, despite various attempts from different research groups using different techniques, the mechanisms underlying TCR downregulation have not yet been fully elucidated, which might be indicative of the complexity of studying this matter in relevant models, and also of the complexity of the TCR downregulation pathway itself.

Sharing is caring

Access to the proper tools is vital to advance research. Although novel tools are gaining popularity and are well described in literature, publications about the work on tools that have existed for longer time and produce robust results is harder to find. To promote the general distribution of knowledge on the design and optimization of

vectors for impairment or overexpression of genes, we aimed to make this information widely accessible. In **chapter 6** we describe the generation of an extensive toolbox to design and produce retroviral vectors for the overexpression, knockdown or knockout of genes of interest. Using building blocks of choice, including a promoter, fluorescent protein or surface marker, and antibiotic resistance marker, the vectors can be designed for any specific experimental model. We also describe the optimization of the transfection and transduction protocols of these vectors in immune cell lines, and primary human and murine lymphocytes in **chapter 6** and **chapter 7**. To advance research in primary immune cells, we also made these vectors available in an online database.

Similarly, sharing methods amongst different research groups in the same department is important for continuity and time-efficiency. Instead of re-inventing the wheel, sharing protocols and experimental setups advances research in the entire department. Apart from the extensive protocols for transfection and transduction of primary human lymphocytes we made widely available, we, in turn, were supported by other research groups with knowledge and materials for the development of a cytotoxic T cell killing assay. The bispecific antibody Blinatumomab has been extensively tested in our department for the treatment of chronic lymphocytic leukemia (CLL) (85) (unpublished data) and is used in the clinic for reinvigoration of T cells. However, by using the bispecific antibody as a tool to overcome HLA-matching instead of a T-cell activation treatment, we were able to repurpose this drug in a different type of assay. Taken together, sharing protocols and negative results sometimes leads to advances in research that are more helpful and even outrun the plain presentation of perfect data. The road to success is paved with failure.

Concluding remarks

Together, the research described in this thesis shows that control of immune cell activation is a delicate balance that host factors or pathogens can use for their own benefit. Pathogens might use strategies to evade immune detection, whilst the host factors contribute to pathogen detection. On the other hand, the host also controls immune activation to prevent hyper-activation and damage to the host. Ultimately, studying how the immune activation is controlled will help to understand how the immune system works in sickness and in health, and future research is warranted to unravel more of the intricate and fascinating immune system. Although the content of this thesis followed a series of unpredicted events, by developing robust methods and studying different aspects of innate and adaptive immunity we have discovered unexpected connections and novel applications of our findings.

REFERENCES

1. Hadjadj J, Yatim N, Barnabei L, Corneau A, Boussier J, Smith N, et al. Impaired type I interferon activity and inflammatory responses in severe COVID-19 patients. Science. 2020;369(6504):718-24.
2. Kvedaraite E, Hertwig L, Sinha I, Ponzetta A, Hed Myrberg I, Lourda M, et al. Major alterations in the mononuclear phagocyte landscape associated with COVID-19 severity. Proc Natl Acad Sci U S A. 2021;118(6).
3. Barreda D, Santiago C, Rodriguez JR, Rodriguez JF, Casasnovas JM, Merida I, et al. SARS-CoV-2 Spike Protein and Its Receptor Binding Domain Promote a Proinflammatory Activation Profile on Human Dendritic Cells. Cells. 2021;10(12).
4. Yang D, Chu H, Hou Y, Chai Y, Shuai H, Lee AC, et al. Attenuated Interferon and Proinflammatory Response in SARS-CoV-2-Infected Human Dendritic Cells Is Associated With Viral Antagonism of STAT1 Phosphorylation. J Infect Dis. 2020;222(5):734-45.
5. Aboudounya MM, Holt MR, Heads RJ. SARS-CoV-2 Spike S1 glycoprotein is a TLR4 agonist, upregulates ACE2 expression and induces pro-inflammatory M₁ macrophage polarisation. bioRxiv. 2021:2021.08.11.455921.
6. Shirato K, Kizaki T. SARS-CoV-2 spike protein S1 subunit induces pro-inflammatory responses via toll-like receptor 4 signaling in murine and human macrophages. Heliyon. 2021;7(2):e06187.
7. Zhao Y, Kuang M, Li J, Zhu L, Jia Z, Guo X, et al. SARS-CoV-2 spike protein interacts with and activates TLR41. Cell Res. 2021;31(7):818-20.
8. Bermejo-Jambrina M, Eder J, Kaptein TM, van Hamme JL, Helgers LC, Vlaming KE, et al. Infection and transmission of SARS-CoV-2 depends on heparan sulfate proteoglycans. bioRxiv. 2021:2020.08.18.255810.
9. van der Donk LEH, Eder J, van Hamme JL, Brouwer PJM, Brinkkemper M, van Nuenen AC, et al. SARS-CoV-2 infection activates dendritic cells via cytosolic receptors rather than extracellular TLRs. Eur J Immunol. 2022;52(4):646-55.
10. Le Bert N, Tan AT, Kunasegaran K, Tham CYL, Hafezi M, Chia A, et al. SARS-CoV-2-specific T cell immunity in cases of COVID-19 and SARS, and uninfected controls. Nature. 2020;584(7821):457-62.
11. Olejnik J, Hume AJ, Muhlberger E. Toll-like receptor 4 in acute viral infection: Too much of a good thing. PLoS Pathog. 2018;14(12):e1007390.
12. Ortiz ME, Thurman A, Pezzulo AA, Leidinger MR, Klesney-Tait JA, Karp PH, et al. Heterogeneous expression of the SARS-Coronavirus-2 receptor ACE2 in the human respiratory tract. EBioMedicine. 2020;60:102976.
13. Coillard A, Segura E. In vivo Differentiation of Human Monocytes. Front Immunol. 2019;10:1907.
14. Hilligan KL, Ronchese F. Antigen presentation by dendritic cells and their instruction of CD4+ T helper cell responses. Cell Mol Immunol. 2020;17(6):587-99.
15. Joffre OP, Segura E, Savina A, Amigorena S. Cross-presentation by dendritic cells. Nat Rev Immunol. 2012;12(8):557-69.
16. Embgenbroich M, Burgdorf S. Current Concepts of Antigen Cross-Presentation. Front Immunol. 2018;9:1643.
17. Java A, Apicelli AJ, Liszewski MK, Coler-Reilly A, Atkinson JP, Kim AH, et al. The complement system in COVID-19: friend and foe? JCI Insight. 2020;5(15).

18. Ma L, Sahu SK, Cano M, Kuppuswamy V, Bajwa J, McPhatter J, et al. Increased complement activation is a distinctive feature of severe SARS-CoV-2 infection. Sci Immunol. 2021;6(59).
19. Ali YM, Ferrari M, Lynch NJ, Yaseen S, Dudler T, Gragerov S, et al. Lectin Pathway Mediates Complement Activation by SARS-CoV-2 Proteins. Front Immunol. 2021;12:714511.
20. Satyam A, Tsokos MG, Brook OR, Hecht JL, Moulton VR, Tsokos GC. Activation of classical and alternative complement pathways in the pathogenesis of lung injury in COVID-19. Clin Immunol. 2021;226:108716.
21. Yu J, Yuan X, Chen H, Chaturvedi S, Braunstein EM, Brodsky RA. Direct activation of the alternative complement pathway by SARS-CoV-2 spike proteins is blocked by factor D inhibition. Blood. 2020;136(18):2080-9.
22. Afzali B, Noris M, Lambrecht BN, Kemper C. The state of complement in COVID-19. Nat Rev Immunol. 2022;22(2):77-84.
23. Mastellos DC, Pires da Silva BGP, Fonseca BAL, Fonseca NP, Auxiliadora-Martins M, Mastaglio S, et al. Complement C3 vs C5 inhibition in severe COVID-19: Early clinical findings reveal differential biological efficacy. Clin Immunol. 2020;220:108598.
24. Nagelkerke SQ, Kuijpers TW. Immunomodulation by IVIg and the Role of Fc-Gamma Receptors: Classic Mechanisms of Action after all? Front Immunol. 2014;5:674.
25. Lu LL, Suscovich TJ, Fortune SM, Alter G. Beyond binding: antibody effector functions in infectious diseases. Nat Rev Immunol. 2018;18(1):46-61.
26. Hunter S, Indik ZK, Kim MK, Cauley MD, Park JG, Schreiber AD. Inhibition of Fcgamma receptor-mediated phagocytosis by a nonphagocytic Fcgamma receptor. Blood. 1998;91(5):1762-8.
27. Metes D, Ernst LK, Chambers WH, Sulica A, Herberman RB, Morel PA. Expression of functional CD32 molecules on human NK cells is determined by an allelic polymorphism of the FcgammaRIIC gene. Blood. 1998;91(7):2369-80.
28. Speletas M, Dadouli K, Syrakouli A, Gatselis N, Germanidis G, Mouchtouri VA, et al. MBL deficiency-causing B allele (rs1800450) as a risk factor for severe COVID-19. Immunobiology. 2021;226(6):152136.
29. Garred P, Madsen HO, Balslev U, Hofmann B, Pedersen C, Gerstoft J, et al. Susceptibility to HIV infection and progression of AIDS in relation to variant alleles of mannose-binding lectin. Lancet. 1997;349(9047):236-40.
30. Zhang H, Zhou G, Zhi L, Yang H, Zhai Y, Dong X, et al. Association between mannose-binding lectin gene polymorphisms and susceptibility to severe acute respiratory syndrome coronavirus infection. J Infect Dis. 2005;192(8):1355-61.
31. Lopez-Martinez R, Albaiceta GM, Amado-Rodriguez L, Cuesta-Llavona E, Gomez J, Garcia-Clemente M, et al. The FCGR2A rs1801274 polymorphism was associated with the risk of death among COVID-19 patients. Clin Immunol. 2022;236:108954.
32. Freer G, Matteucci D. Influence of dendritic cells on viral pathogenicity. PLoS Pathog. 2009;5(7):e1000384.
33. Lubaki NM, Ilinykh P, Pietzsch C, Tigabu B, Freiberg AN, Koup RA, et al. The lack of maturation of Ebola virus-infected dendritic cells results from the cooperative effect of at least two viral domains. J Virol. 2013;87(13):7471-85.
34. Majumder B, Janket ML, Schafer EA, Schaubert K, Huang XL, Kan-Mitchell J, et al. Human immunodeficiency virus type 1 Vpr impairs dendritic cell maturation and T-cell activation: implications for viral immune escape. J Virol. 2005;79(13):7990-8003.
35. Moutaftsi M, Mehl AM, Borysiewicz LK, Tabi Z. Human cytomegalovirus inhibits maturation and impairs function of monocyte-derived dendritic cells. Blood. 2002;99(8):2913-21.

36. Musuuza JS, Watson L, Parmasad V, Putman-Buehler N, Christensen L, Safdar N. Prevalence and outcomes of co-infection and superinfection with SARS-CoV-2 and other pathogens: A systematic review and meta-analysis. PLoS One. 2021;16(5):e0251170.
37. Buehler PK, Zinkernagel AS, Hofmaenner DA, Wendel Garcia PD, Acevedo CT, Gomez-Mejia A, et al. Bacterial pulmonary superinfections are associated with longer duration of ventilation in critically ill COVID-19 patients. Cell Rep Med. 2021;2(4):100229.
38. Geijtenbeek TB, Van Vliet SJ, Koppel EA, Sanchez-Hernandez M, Vandenbroucke-Grauls CM, Appelmelk B, et al. Mycobacteria target DC-SIGN to suppress dendritic cell function. J Exp Med. 2003;197(1):7-17.
39. Gringhuis SI, den Dunnen J, Litjens M, van Het Hof B, van Kooyk Y, Geijtenbeek TB. C-type lectin DC-SIGN modulates Toll-like receptor signaling via Raf-1 kinase-dependent acetylation of transcription factor NF-kappaB. Immunity. 2007;26(5):605-16.
40. Gringhuis SI, Hertoghs N, Kaptein TM, Zijlstra-Willems EM, Sarrami-Forooshani R, Sprokholt JK, et al. HIV-1 blocks the signaling adaptor MAVS to evade antiviral host defense after sensing of abortive HIV-1 RNA by the host helicase DDX3. Nat Immunol. 2017;18(2):225-35.
41. Mesman AW, Zijlstra-Willems EM, Kaptein TM, de Swart RL, Davis ME, Ludlow M, et al. Measles virus suppresses RIG-I-like receptor activation in dendritic cells via DC-SIGN-mediated inhibition of PP1 phosphatases. Cell Host Microbe. 2014;16(1):31-42.
42. Zhou R, To KK, Wong YC, Liu L, Zhou B, Li X, et al. Acute SARS-CoV-2 Infection Impairs Dendritic Cell and T Cell Responses. Immunity. 2020;53(4):864-77 e5.
43. Gringhuis SI, den Dunnen J, Litjens M, van der Vlist M, Geijtenbeek TB. Carbohydrate-specific signaling through the DC-SIGN signalosome tailors immunity to Mycobacterium tuberculosis, HIV-1 and Helicobacter pylori. Nat Immunol. 2009;10(10):1081-8.
44. Crouse J, Kalinke U, Oxenius A. Regulation of antiviral T cell responses by type I interferons. Nat Rev Immunol. 2015;15(4):231-42.
45. Blanco-Melo D, Nilsson-Payant BE, Liu WC, Uhl S, Hoagland D, Moller R, et al. Imbalanced Host Response to SARS-CoV-2 Drives Development of COVID-19. Cell. 2020;181(5):1036-45 e9.
46. Kim YM, Shin EC. Type I and III interferon responses in SARS-CoV-2 infection. Exp Mol Med. 2021;53(5):750-60.
47. Notarbartolo S, Ranzani V, Bandera A, Gruarin P, Bevilacqua V, Putignano AR, et al. Integrated longitudinal immunophenotypic, transcriptional and repertoire analyses delineate immune responses in COVID-19 patients. Science immunology. 2021;6(62).
48. Bergamaschi L, Mescia F, Turner L, Hanson AL, Kotagiri P, Dunmore BJ, et al. Longitudinal analysis reveals that delayed bystander CD8+ T cell activation and early immune pathology distinguish severe COVID-19 from mild disease. Immunity. 2021;54(6):1257-75.e8.
49. Mathew D, Giles JR, Baxter AE, Oldridge DA, Greenplate AR, Wu JE, et al. Deep immune profiling of COVID-19 patients reveals distinct immunotypes with therapeutic implications. Science (New York, NY). 2020;369(6508).
50. Su Y, Chen D, Yuan D, Lausted C, Choi J, Dai CL, et al. Multi-Omics Resolves a Sharp Disease-State Shift between Mild and Moderate COVID-19. Cell. 2020;183(6):1479-95.e20.
51. Borden EC. Interferons alpha and beta in cancer: therapeutic opportunities from new insights. Nat Rev Drug Discov. 2019;18(3):219-34.
52. Stunnenberg M, van Hamme JL, Zijlstra-Willems EM, Gringhuis SI, Geijtenbeek TBH. Crosstalk between R848 and abortive HIV-1 RNA-induced signaling enhances antiviral immunity. J Leukocyte Biol. 2022;112(2):289-98.

53. Welsh RM, Bahl K, Marshall HD, Urban SL. Type 1 Interferons and Antiviral CD8 T-Cell Responses. Plos Pathogens. 2012;8(1).
54. Raskov H, Orhan A, Christensen JP, Gogenur I. Cytotoxic CD8(+) T cells in cancer and cancer immunotherapy. Br J Cancer. 2021;124(2):359-67.
55. Huang X, Pan J, Xu F, Shao B, Wang Y, Guo X, et al. Bacteria-Based Cancer Immunotherapy. Adv Sci (Weinh). 2021;8(7):2003572.
56. Chen YE, Bousbaine D, Veinbachs A, Atabakhsh K, Dimas A, Yu VK, et al. Engineered skin bacteria induce antitumor T cell responses against melanoma. Science. 2023;380(6641):203-10.
57. Morales A, Eidinger D, Bruce AW. Intracavitary Bacillus Calmette-Guerin in the treatment of superficial bladder tumors. J Urol. 1976;116(2):180-3.
58. Rosenberg SA, Spiess PJ, Kleiner DE. Antitumor effects in mice of the intravenous injection of attenuated Salmonella typhimurium. J Immunother. 2002;25(3):218-25.
59. Zhao M, Geller J, Ma H, Yang M, Penman S, Hoffman RM. Monotherapy with a tumor-targeting mutant of Salmonella typhimurium cures orthotopic metastatic mouse models of human prostate cancer. Proc Natl Acad Sci U S A. 2007;104(24):10170-4.
60. Badie F, Ghandali M, Tabatabaei SA, Safari M, Khorshidi A, Shayestehpour M, et al. Use of Salmonella Bacteria in Cancer Therapy: Direct, Drug Delivery and Combination Approaches. Front Oncol. 2021;11:624759.
61. Liang K, Zhang R, Luo H, Zhang J, Tian Z, Zhang X, et al. Optimized Attenuated Salmonella Typhimurium Suppressed Tumor Growth and Improved Survival in Mice. Front Microbiol. 2021;12:774490.
62. Toso JF, Gill VJ, Hwu P, Marincola FM, Restifo NP, Schwartzentruber DJ, et al. Phase I study of the intravenous administration of attenuated Salmonella typhimurium to patients with metastatic melanoma. J Clin Oncol. 2002;20(1):142-52.
63. Amouzegar A, Chelvanambi M, Filderman JN, Storkus WJ, Luke JJ. STING Agonists as Cancer Therapeutics. Cancers (Basel). 2021;13(11).
64. Antonelli AC, Binyamin A, Hohl TM, Glickman MS, Redelman-Sidi G. Bacterial immunotherapy for cancer induces CD4-dependent tumor-specific immunity through tumor-intrinsic interferon-gamma signaling. Proc Natl Acad Sci U S A. 2020;117(31):18627-37.
65. Kerksiek KM, Pamer EG. T cell responses to bacterial infection. Curr Opin Immunol. 1999;11(4):400-5.
66. Salgado-Pabon W, Celli S, Arena ET, Nothelfer K, Roux P, Sellge G, et al. Shigella impairs T lymphocyte dynamics in vivo. Proc Natl Acad Sci U S A. 2013;110(12):4458-63.
67. Mesner D, Hotter D, Kirchhoff F, Jolly C. Loss of Nef-mediated CD3 down-regulation in the HIV-1 lineage increases viral infectivity and spread. Proc Natl Acad Sci U S A. 2020;117(13):7382-91.
68. Gallegos AM, Xiong H, Leiner IM, Susac B, Glickman MS, Pamer EG, et al. Control of T cell antigen reactivity via programmed TCR downregulation. Nat Immunol. 2016;17(4):379-86.
69. Alcover A, Alarcon B, Di Bartolo V. Cell Biology of T Cell Receptor Expression and Regulation. Annu Rev Immunol. 2018;36:103-25.
70. Cai Z, Kishimoto H, Brunmark A, Jackson MR, Peterson PA, Sprent J. Requirements for peptide-induced T cell receptor downregulation on naive CD8+ T cells. J Exp Med. 1997;185(4):641-51.
71. D'Oro U, Vacchio MS, Weissman AM, Ashwell JD. Activation of the Lck tyrosine kinase targets cell surface T cell antigen receptors for lysosomal degradation. Immunity. 1997;7(5):619-28.
72. Luton F, Buferne M, Davoust J, Schmitt-Verhulst AM, Boyer C. Evidence for protein tyrosine kinase involvement in ligand-induced TCR/CD3 internalization and surface redistribution. J Immunol. 1994;153(1):63-72.

73. Myers MD, Dragone LL, Weiss A. Src-like adaptor protein down-regulates T cell receptor (TCR)-CD3 expression by targeting TCRzeta for degradation. J Cell Biol. 2005;170(2):285-94.
74. Salio M, Valitutti S, Lanzavecchia A. Agonist-induced T cell receptor down-regulation: molecular requirements and dissociation from T cell activation. Eur J Immunol. 1997;27(7):1769-73.
75. Valitutti S, Lanzavecchia A. Serial triggering of TCRs: a basis for the sensitivity and specificity of antigen recognition. Immunol Today. 1997;18(6):299-304.
76. Viola A, Lanzavecchia A. T cell activation determined by T cell receptor number and tunable thresholds. Science. 1996;273(5271):104-6.
77. Blanchard N, Lankar D, Faure F, Regnault A, Dumont C, Raposo G, et al. TCR activation of human T cells induces the production of exosomes bearing the TCR/CD3/zeta complex. J Immunol. 2002;168(7):3235-41.
78. Dumont C, Blanchard N, Di Bartolo V, Lezot N, Dufour E, Jauliac S, et al. TCR/CD3 down-modulation and zeta degradation are regulated by ZAP-70. J Immunol. 2002;169(4):1705-12.
79. James JR, Vale RD. Biophysical mechanism of T-cell receptor triggering in a reconstituted system. Nature. 2012;487(7405):64-9.
80. Lauritsen JP, Christensen MD, Dietrich J, Kastrup J, Odum N, Geisler C. Two distinct pathways exist for down-regulation of the TCR. J Immunol. 1998;161(1):260-7.
81. Su X, Ditlev JA, Hui E, Xing W, Banjade S, Okrut J, et al. Phase separation of signaling molecules promotes T cell receptor signal transduction. Science. 2016;352(6285):595-9.
82. van Oers NS, Killeen N, Weiss A. Lck regulates the tyrosine phosphorylation of the T cell receptor subunits and ZAP-70 in murine thymocytes. J Exp Med. 1996;183(3):1053-62.
83. van Oers NS, Lowin-Kropf B, Finlay D, Connolly K, Weiss A. alpha beta T cell development is abolished in mice lacking both Lck and Fyn protein tyrosine kinases. Immunity. 1996;5(5):429-36.
84. Tousley AM, Rotiroti MC, Labanieh L, Rysavy LW, Kim WJ, Lareau C, et al. Co-opting signalling molecules enables logic-gated control of CAR T cells. Nature. 2023;615(7952):507-16.
85. Martens AWJ, Janssen SR, Derks IAM, Adams Iii HC, Izhak L, van Kampen R, et al. CD3xCD19 DART molecule treatment induces non-apoptotic killing and is efficient against high-risk chemotherapy and venetoclax-resistant chronic lymphocytic leukemia cells. J Immunother Cancer. 2020;8(1).

ADDENDUM

ADDENDUM

SUMMARY
SAMENVATTING

SUMMARY

Controlling immunity at dendritic cell and T cell level by host, pathogens, and as therapeutics

To prevent ineffective or excessive immune responses, dendritic cell (DC) and T cell activation is controlled at different levels. Here, we have investigated how immune responses by DCs and T cells are controlled by either the host or pathogens, and whether we can use this knowledge for therapeutic purposes. In this thesis, in part I we have studied how sensing of SARS-CoV-2 by DCs is influenced by viral mediators as well as host factors. Moreover, we have explored the therapeutic potential of DCs and investigated how they can be harnessed for the activation of strong T cell responses against tumors. In part II we have designed and optimized methods to successfully genetically modify primary murine and human T cells to efficiently knockdown, knockout, or overexpress genes of interest. Subsequently we have used this toolbox to study the functional role of several genes during T cell activation and T cell receptor (TCR) downregulation in primary human T cells.

After introducing pathogen sensing and antigen presentation by DCs in **chapter 1**, we described in **chapter 2** how the causative agent of the most recent world-wide pandemic SARS-CoV-2 escapes sensing by DCs. During the SARS-CoV-2 pandemic that emerged in 2019, several reports were published which suggested that the SARS-CoV-2 Spike (S) protein triggers DC activation via Toll-like receptor 4 (TLR4), a pattern recognition receptor (PRR) expressed by DCs. Here we investigated whether S protein and authentic SARS-CoV-2 viral particles trigger TLR4 to induce DC maturation and cytokine responses. Notably, neither S protein nor SARS-CoV-2 triggered DC activation, as we did not observe any induction of type I interferon (IFN) nor cytokine production. These data suggest not only that the virus is not sensed by TLR4, but that SARS-CoV-2 is not sensed by any other extracellular PRR expressed by DCs. Together, these findings suggest that SARS-CoV-2 is not directly sensed by DCs and that most likely other mechanisms are required to activate DCs to subsequently instruct adaptive T cell responses during COVID-19.

One mechanism of alternative DC activation is through a bystander effect. We observed that DCs were activated by SARS-CoV-2-infected epithelial cells. It is likely that danger- or pathogen-associated molecular patterns (DAMPs or PAMPs) released by the infected cells trigger DC activation. However, further research is required to determine whether these immune responses are protective, or induce further inflammation and damage to the host during COVID-19.

Furthermore, we identified another possible mechanism of DC activation by SARS-CoV-2 in **chapter 3**. The complement system is an important innate defense mechanism against viruses that is shown to be highly activated during SARS-CoV-2 infection. We observed that SARS-CoV-2 is rapidly opsonized by complement, and complement-opsonization of SARS-CoV-2 resulted in DC activation through complement receptor (CR)3 and CR4 signaling. Serum of convalescent COVID-19 patients contains complement proteins as well as antibodies against SARS-CoV-2 epitopes. Notably, when DCs were exposed to SARS-CoV-2 opsonized with serum from convalescent COVID-19 patients, the SARS-CoV-2 antibodies attenuated the complement-mediated DC activation. Complement-induced DC activation was restored by blocking the antibody receptor CD32. Taken together, these results suggest that antibodies against SARS-CoV-2 play a role in controlling complement-induced inflammatory responses during COVID-19, which might explain why vaccination against SARS-CoV-2 limits incidence of severe disease.

Although DCs are important for sensing and induction of immune responses, viruses also target DCs to subvert immune responses and even promote viral dissemination. It has been reported that DCs isolated from COVID-19 patients display reduced activation and function. Moreover, severely ill COVID-19 patients are susceptible to bacterial superinfections, leading to worse disease prognosis. In **chapter 4**, we investigated whether SARS-CoV-2 affects DC function towards bacterial ligands. We identified that both S protein and SARS-CoV-2 virus blocked TLR4-induced DC activation and cytokines, but not activation of the other TLR signaling pathways. The TLR4 signaling blockade was not due to steric hindrance of lipopolysaccharides (LPS) by S protein or SARS-CoV-2. We also identified that C-type lectin receptor (CLR) DC-SIGN is a receptor for SARS-CoV-2. It is known that other pathogens including HIV, measles virus but also *Mycobacterium (M.) tuberculosis* deployed DC-SIGN to alter immune responses by DCs. Notably, we observed that SARS-CoV-2 binding to DC-SIGN blocked TLR4 function. Blocking DC-SIGN restored the immune response by DCs against LPS. Together, these data suggest that SARS-CoV-2-induced DC-SIGN triggering interferes with TLR4 signaling, thereby disabling DCs to respond to secondary bacterial triggers. These data might explain why COVID-19 patients are susceptible to secondary bacterial infections. Further research is required to elucidate the mechanisms by which SARS-CoV-2 suppresses DC activation and whether SARS-CoV-2 also affects immune responses to secondary infections with other bacteria, viruses or fungi.

DCs can also be therapeutically employed to boost the activation of T cells in tumor therapy. In **chapter 5**, we explored how bacterial immunotherapy could be used as treatment for malignancies. The immunogenic and metabolic characteristics of some bacteria, including *Salmonella enterica* serovar *typhimurium* (*S. typhimurium*) might

allow local immune activation in otherwise immune-suppressive tumor environments. However, a phase I clinical trial with *S. typhimurium* pointed out that the Salmonella vaccine strain alone was not curative, and requires optimization. In this chapter, we aimed to improve Salmonella-induced immune activation by ectopic expression of cyclic GMP-AMP synthase (cGAS) in *S. typhimurium*. DCs infected with cGAS-expressing Salmonella had significantly upregulated type I IFN and IFN-stimulated gene (ISG) responses compared to DCs infected with Salmonella expressing a catalytically inactive cGAS mutant. We observed that activation of cGAS in *S. typhimurium* resulted in production of cGAMPs. These cGAMPs were subsequently actively transported into the host cells by Salmonella's SPI-1 type III secretion system. Furthermore, we found that inside the host cells, the cGAMPs activated stimulator of IFN genes (STING), leading to induction of type I IFN responses. Notably, co-culture of T cells and cGAS-Salmonella-infected DCs led to increased production of IFN-γ, perforin and granzyme B by $CD8^+$ T cells (CTLs). Strikingly, subsequent co-culture of these T cells with malignant B cells resulted in increased cytotoxicity towards malignant B cells. Our results suggest that ectopic overexpression of cGAS in *S. typhimurium* improves the immunogenicity of these bacteria and induces potent immune responses against malignant cells. Further research is required to advance this treatment and clinical trials will reveal the potential of this treatment to cure cancer.

After focusing on the activation of DCs in part I, we set out to elucidate one of the mechanisms involved in controlling T cell activation in part II.

In **chapter 6**, we designed and optimized a toolbox for the overexpression, knockdown or knockout of genes in primary lymphocytes and aimed to make this knowledge accessible to researchers. With this toolbox, the creation of vectors containing a surface marker or fluorescent protein, antibiotic-resistance cassette and sequences to target a gene of interest will be made easier, and our starting-point plasmids are also made available on the Addgene website. It would be interesting to investigate whether these vectors and methods are also suitable for genetic engineering of primary innate immune cells like DCs.

Subsequently, using the toolbox described in chapter 6, we aimed to unravel the mechanisms underlying TCR downregulation in **chapter 7**. When T cells are triggered by their cognate antigen:MHC complexes, the TCR/CD3 complex is quickly internalized and degraded in an attempt to prevent overactivation and undesired harmful effects on the host. T cell activation and TCR downregulation are tightly linked; therefore, we suggested that the upstream signaling events in both processes might be similar. The group of Src family kinases are known to be important for T cell

activation; therefore, we also investigated the contribution of these kinases in TCR downregulation. Interestingly, whilst the kinases Lck, Fyn and ZAP70 are important for T cell activation, their role in TCR downregulation seems to be individually redundant. Only simultaneous knockdown of Lck and Fyn had an effect on TCR downregulation. Further research on the mechanisms underlying TCR downregulation is required, since it would be interesting to determine if this process can potentially be promoted in autoimmune diseases, or halted for reinvigoration of T cell activity in CAR T cell therapy.

Collectively, the results described in this thesis show that DC and T cell activation is controlled at multiple levels, not only by host factors but also by pathogens. Moreover, we suggest that DC and subsequent T cell activation can be targeted to generate immune responses for our own benefit. A balance between immune activation and inhibition is essential to attack and eliminate pathogens whilst protecting against harmful effects on the host.

SAMENVATTING

Regulatie van de afweer op het niveau van DCs en T cellen door de gastheer, pathogenen, en als therapie

Om te voorkomen dat er ineffectieve of overmatige immuunresponsen plaatsvinden, kan de activatie van dendritische cellen (DCs) en T cellen op verschillende niveaus in toom worden gehouden. In dit proefschrift hebben we onderzocht hoe immuunactivatie van DCs en T cellen onder controle gehouden wordt door de gastheer of door pathogenen en hoe we deze opgedane kennis kunnen gebruiken voor therapeutische doeleinden.

In dit proefschrift hebben we in **deel I** onderzocht hoe DCs SARS-CoV-2 infectie signaleren en hoe dit beïnvloed wordt door zowel virale componenten alsook door factoren van de gastheer zelf. Daarnaast hebben we bestudeerd of we DC activatie in een bepaalde richting kunnen sturen om vervolgens effectieve T-celresponsen tegen tumoren te verkrijgen. Dit zou mogelijk als nieuwe therapie tegen kanker kunnen werken. In **deel II** hebben we methoden ontworpen die genetische modificatie van primaire T cellen van muis- en humane origine mogelijk maken, zoals de knockdown, knockout of overexpressie van bepaalde genen. Vervolgens hebben we deze methoden gebruikt voor het bestuderen van de rol van verscheidene genen tijdens de processen van T-celactivatie en T-celreceptor downregulatie in primaire humane T cellen.

Na een introductie over het herkennen van pathogenen en antigeenpresentatie door DCs in **hoofdstuk 1**, hebben we in **hoofdstuk 2** onderzocht hoe DCs het recent ontdekte virus SARS-CoV-2 kunnen herkennen. Gedurende de in 2019 opgekomen SARS-CoV-2 pandemie, werden verschillende artikelen gepubliceerd die suggereerden dat het Spike (S) eiwit kenmerkend voor SARS-CoV-2, zou binden aan TLR4. TLR4 is een patroonherkenningsreceptor (PRR) die op DCs voorkomt en triggering van TLR4 door het S eiwit zou leiden tot DC activatie. Hier hebben we onderzocht of DCs door zowel het S eiwit als door infectieuze SARS-CoV-2 virusdeeltjes geactiveerd werden. Opvallenderwijs zagen we dat DCs niet geactiveerd werden door S eiwit noch infectieus SARS-CoV-2. Dit betekent niet alleen dat SARS-CoV-2 niet herkend wordt door TLR4, maar ook andere PRRs op het oppervlak van DCs worden niet geactiveerd door SARS-CoV-2. Samengenomen geeft dit aan dat SARS-CoV-2 hoogstwaarschijnlijk niet herkend wordt door DCs via TLR4 of andere PRRs op het celoppervlak van DCs en daarom worden er geen immuunresponsen tegen het virus geïnduceerd door DCs. Deze bevindingen suggereren daarom dat er waarschijnlijk andere immuunmechanismen benodigd zijn om DCs te activeren en vervolgens verworven T-celresponsen te verkrijgen tijdens COVID-19.

Een mogelijke alternatieve manier van DC activatie is door een bijstander effect. We hebben gevonden dat DCs geactiveerd kunnen worden door bepaalde stoffen die vrijkomen uit geïnfecteerde of beschadigde epitheelcellen. Dat wil zeggen dat DCs niet zelf door SARS-CoV-2 geactiveerd worden, maar wel gevaar oppikken omdat cellen in de omgeving gevaarsignalen afgeven. Verder onderzoek is echter nodig om te bepalen of deze immuunresponsen wel beschermend zijn, of dat ze juist meer ontsteking en schade aan de gastheer toebrengen tijdens COVID-19.

Daarnaast hebben we nog een ander mogelijk mechanisme van DC activatie door SARS-CoV-2 geïdentificeerd in **hoofdstuk 3**. Het complementsysteem is een belangrijk deel van het aangeboren immuunsysteem dat is betrokken bij het bestrijden van virusinfecties. Tijdens SARS-CoV-2 infectie is er een hoge mate van complementactivatie. We hebben gezien dat SARS-CoV-2 snel geopsoniseerd wordt door complement en complement-opsonisatie van SARS-CoV-2 resulteerde in DC activatie door signalering via complement receptor (CR)3 en CR4. Serum van herstelde COVID-19 patiënten bevat niet alleen complementeiwitten maar ook antilichamen tegen SARS-CoV-2. Opsonisatie van SARS-CoV-2 met dit serum zwakte DC activatie af, wat suggereert dat de SARS-CoV-2 antilichamen complement-gemedieerde DC activatie remmen. Door de antilichaamreceptor CD32 te blokkeren kon de complement-geïnduceerde DC activatie hersteld worden. Onze bevinden geven aan dat antilichamen tegen SARS-CoV-2 een rol spelen in het afzwakken van de ontstekingsreactie die door complementactivatie in gang wordt gezet tijdens COVID-19. Deze bevindingen kunnen tevens verklaren waarom vaccinatie tegen SARS-CoV-2 het aantal gevallen van ernstige COVID-19 beperkt.

Hoewel DCs belangrijk zijn voor het signaleren van pathogenen en het aanzetten van immuunresponsen, kunnen virussen DCs ook onderdrukken en zorgen dat immuunreacties tegen het virus of andere pathogenen gedempt worden, of zelfs zorgen dat DCs bijdragen aan het verspreiden van virus. In **hoofdstuk 4** hebben we onderzocht of SARS-CoV-2 effect heeft op de functie van DCs om te reageren op bacteriële liganden. Onze resultaten lieten zien dat zowel het S eiwit als SARS-CoV-2 virusdeeltjes de immuunrespons van DCs na TLR4 triggering verminderden. Opmerkelijk was dat alleen de TLR4 signalering beïnvloed werd door SARS-CoV-2, terwijl de andere TLRs onaangedaan bleven. Deze TLR4 signaleringsblokkade werd niet veroorzaakt door sterische hindering van LPS door het S eiwit of door SARS-CoV-2 virusdeeltjes. Wel lieten onze resultaten zien dat C-type lectine receptor (CLR) DC-SIGN een receptor is voor SARS-CoV-2. Het is bekend dat andere pathogenen zoals HIV, het mazelenvirus maar ook *Mycobacterium (M.) tuberculosis* DC-SIGN gebruiken om immuunreacties van DCs te beïnvloeden. Opvallend was dat binding van SARS-

CoV-2 aan DC-SIGN TLR4 functie blokkeerde, aangezien de immuunrespons tegen LPS kon worden hersteld door het blokkeren van DC-SIGN. Al deze data suggereren dat SARS-CoV-2-geïnduceerde DC-SIGN triggering ingrijpt op de TLR4 signalering, waardoor de reactie van DCs op secundaire bacteriële agonisten verminderd is. Onze bevindingen kunnen mogelijkerwijs verklaren waarom COVID-19 patiënten erg vatbaar zijn voor secundaire bacteriële infecties. Toekomstig onderzoek is nodig om mechanismen te ontrafelen die ten grondslag liggen aan de onderdrukking van DC activatie door SARS-CoV-2 en om te ontdekken of SARS-CoV-2 ook immuunresponsen tegen secundaire infecties met andere bacteriën, virussen of schimmels beïnvloedt.

DCs kunnen ook ingezet worden in een therapeutische setting om T-celactivatie een boost te geven, hetgeen wenselijk is bij het genezen van kanker. In **hoofdstuk 5** hebben we onderzocht hoe bacteriële immuuntherapie ingezet kan worden als therapie voor maligniteiten. De werking van *Salmonella enterica* serovar *typhimurium (S. typhimurium)* als bacteriële immunotherapie wordt intensief onderzocht maar is tot op heden nog niet succesvol gebleken. Daarom heeft deze therapie verdere optimalisatie nodig. In dit hoofdstuk hebben we onderzocht of Salmonella-geïnduceerde immuunactivatie verbeterd kan worden door middel van overexpressie van cyclische GMP-AMP synthase (cGAS) in *S. typhimurium*. DCs die geïnfecteerd werden door *S. typhimurium* die cGAS tot expressie brachten, produceerden significant meer type I interferon (IFN) en cytokines in vergelijking met DCs die geïnfecteerd werden door *S. typhimurium* die een katalytisch-inactieve cGAS tot expressie brachten. We vonden dat activatie van cGAS in *S. typhimurium* resulteerde in cGAMP productie. Daarnaast identificeerden we dat deze cGAMPs actief getransporteerd werden van de bacterie naar de gastheercellen door middel van Salmonella's type III secretiesysteem. In de gastheercellen, activeerden de getransporteerde cGAMPs vervolgens het molecuul STING, wat leidde tot de inductie van type I IFN responsen. Opmerkelijk was dat het stimuleren van T cellen met cGAS-Salmonella-geïnfecteerde DCs leidde tot verhoogde productie van IFN-γ, perforine en granzyme B door $CD8^+$ T cellen (CTLs). In het bijzonder, het kweken van deze geïnstrueerde T cellen met maligne B cellen resulteerde in verhoogde cytotoxiciteit tegen deze B cellen. Onze resultaten suggereren dat overexpressie van cGAS in *S. typhimurium* de immunogeniteit van deze bacteriën verhoogt en potente immuunreacties tegen maligne B cellen induceert. Verder onderzoek is benodigd om deze therapie verder te ontwikkelen en klinische trials zullen de potentie van deze therapie om kanker te genezen verder uitwijzen.

Na in deel I gefocust te hebben op DC activatie, zijn we in deel II op zoek gegaan naar manieren om de mechanismen van T-celactivatie te ontrafelen.

In **hoofdstuk 6** hebben we het ontwerp en de optimalisatie van een toolbox beschreven waarmee we de overexpressie, knockdown of knockout van bepaalde genen kunnen bewerkstelligen in primaire lymfocyten, en we hebben deze vectoren en kennis toegankelijk gemaakt voor onderzoekers. Met deze toolbox is het maken van vectoren vergemakkelijkt, en er is voor gebruikers grote keuze uit verschillende oppervlaktemarkers, antibioticumresistentiecassettes en sequenties voor het gen van interesse bij het maken van een vector. Hiervoor zijn onze vectoren openbaar verkrijgbaar gemaakt op de website van Addgene. Het zou ten slotte nog interessant zijn om te onderzoeken of deze vectoren en bijbehorende methodes bruikbaar zijn voor genetische modificatie van primaire immuuncellen van het aangeboren immuunsysteem, zoals DCs.

Vervolgens hebben we de toolbox beschreven in hoofdstuk 6, gebruikt om de mechanismen van T-celreceptor (TCR) downregulatie te onderzoeken zoals beschreven in **hoofdstuk 7**. Wanneer T cellen getriggerd worden door hun specifieke antigen:MHC complexen, wordt het TCR/CD3 complex snel geïnternaliseerd en afgebroken in een poging om overactivatie en ongewenste schade aan de gastheer te voorkomen. De processen van T-celactivatie en TCR downregulatie zijn nauw aan elkaar verbonden, daarom voorspelden we dat het vroege deel van de signaleringsroutes zou kunnen overlappen. Om die reden hebben we onderzocht of de groep Src familie kinases, die bekend staat om zijn essentiële rol in T-celactivatie, ook betrokken is bij TCR downregulatie. Interessant was dat terwijl de kinases Lck, Fyn en ZAP70 belangrijk zijn voor T-celactivatie, hun rol in TCR downregulatie individueel rudimentair lijkt te zijn. Alleen knockdown van zowel Lck als Fyn tegelijkertijd had een effect op TCR downregulatie. Meer onderzoek is benodigd om de mechanismen die ten grondslag liggen aan TCR downregulatie te ontrafelen. Het zou interessant zijn om te bepalen of dit proces wellicht geïnduceerd kan worden in auto-immuunziektes, of juist geremd kan worden om T-celactiviteit een impuls te geven in CAR T-celtherapie.

Kortom, in dit proefschrift beschrijven we onderzoek dat laat zien dat DC en T-celactivatie gecontroleerd wordt op meerdere niveaus, niet alleen door gastheerfactoren maar ook door pathogenen. Daarnaast suggereren we dat DC activatie en vervolgens ook T-celactivatie op een bepaalde manier gestuurd kan worden om zo immuunreacties naar eigen hand te kunnen zetten. Het bewaren van de balans tussen immuunactivatie en -remming is essentieel om enerzijds pathogenen te bestrijden en elimineren en anderzijds de gastheer te beschermen tegen schadelijke effecten.

ADDENDUM

PHD PORTFOLIO
LIST OF PUBLICATIONS
CURRICULUM VITAE

PHD PORTFOLIO

Name: **Lieve Elisabeth Hubertha van der Donk**
PhD period: **2018-2023**
Promotor: **Prof. dr. T.B.H. Geijtenbeek**
Co-promotores: **Dr. L.S. Ates and Dr. M. Bermejo-Jambrina**

Courses	**Year**	**ECTS**
The AMC World of Science	2018	0.7
Laboratory Safety	2018	0.4
Advanced Immunology	2019	2.9
Infectious Diseases	2019	1.3
Training venapunctie	2019	0.4
eBROK	2022	1.5
Research Integrity	2022	2.0
Seminars and retreats		
Weekly EXIM seminars	2018-2023	5.0
Weekly Host Defense marathons	2019-2023	4.0
Bi-weekly Journal club lymphocytes	2018-2020	1.0
Monthly Dutch Young Virologists Seminars (DYVS)	2021-2022	1.0
Monthly SARS-CoV-2 work meetings	2021	0.5
EXIM retreats	2018, 2019, 2022	0.6
All PhD retreats	2018, 2021	1.0
Presentations and posters		
Separate signaling events control TCR downregulation and T cell activation in primary human T cells		
NVVI Scientific meeting, poster	2020	0.5
SARS-CoV-2 infection activates dendritic cells via cytosolic receptors rather than extracellular TLRs		
NVVI Scientific meeting, poster	2022	0.5
Dutch Annual Virology Symposium, poster	2022	0.5
The Great Escape: SARS-CoV-2 evades sensing and suppresses dendritic cell function		
DC2022, poster	2022	0.5

&

SARS-CoV-2-induced immunity depends on cytosolic sensors - infection is required for immunity *European Congress of Immunology (ECI), oral presentation*	2021	1.0
SARS-CoV-2 infection activates dendritic cells via cytosolic receptors rather than extracellular TLRs *Dutch Young Virologists Seminar, oral presentation*	2021	1.0
AII PhD retreat, oral presentation	2021	1.0
(Inter)national conferences		
NVVI Scientific meeting	2020, 2022	1.0
NVVI Annual meeting	2020	0.5
AI&II Annual meeting	2020-2023	2.0
European Congress of Immunology (ECI)	2021	2.0
Dutch Annual Virology Symposium (DAVS)	2022	0.5
DC2022, Cairns, Australia	2022	2.0
Supervising		
Bachelor UvA student, internship	4 months, 2019	1.0
Bachelor Inholland student, internship	9 months, 2020-2021	3.0
Master UvA student, internship	6 months, 2022	2.0
Parameters of esteem		
European Congress of Immunology Bright Spark Award	2021	
NVVI travel grant	2022	
AII travel grant	2022	
Aspasia travel grant	2022	

LIST OF PUBLICATIONS

van der Donk LEH, Bermejo-Jambrina M, van Hamme JL, Volkers MMW, van Nuenen AC, Kootstra NA, Geijtenbeek TBH. "SARS-CoV-2 suppresses TLR4-induced immunity by dendritic cells via C-type lectin receptor DC-SIGN." *Submitted.*

Bermejo-Jambrina M, van der Donk LEH, van Hamme JL, Wilflingseder D, van Gils MJ, Kootstra NA, Geijtenbeek TBH. "Antibodies against SARS-CoV-2 control complement-induced inflammatory responses to SARS-CoV-2." *Submitted.*

van der Donk LEH*, Waanders L*, Ates LS, Maaskant J, van Hamme JL, Eldering E, van Bruggen JAC, Rietveld JM, Bitter W, Geijtenbeek TBH, Kuijl CP. "Ectopic expression of cGAS in Salmonella typhimurium enhances STING-mediated IFN-β response in human macrophages and dendritic cells." *Journal for ImmunoTherapy of Cancer. 2023;11(4).*
*Equal contribution

van der Donk LEH, Eder J, van Hamme JL, Brouwer PJ, Brinkkemper M, van Nuenen AC, van Gils MJ, Sanders RW, Kootstra NA, Bermejo-Jambrina M, Geijtenbeek TBH. "SARS-CoV-2 infection activates dendritic cells via cytosolic receptors rather than extracellular TLRs." *European Journal of Immunology. 2022 Apr;52(4):646-55.*

van der Donk LEH, van der Spek J, van Duivenvoorde T, ten Brink MS, Geijtenbeek TBH, Kuijl CP, van Heijst JWJ, Ates LS. "An optimized retroviral toolbox for overexpression and genetic perturbation of primary lymphocytes." *Biology Open. 2022 Feb 15;11(2):bio059032.*

van der Donk LEH, Ates LS, van der Spek J, Tukker LM, Geijtenbeek TBH, van Heijst JWJ. "Separate signaling events control TCR downregulation and T cell activation in primary human T cells." *Immunity, Inflammation and Disease. 2021 Mar;9(1):223-38.*

de Porto APNA*, Claushuis TAM*, van der Donk LEH, de Beer R, de Boer OJ, Florquin S, Roelofs JJ, Hendriks RW, van Der Poll T, Van 't Veer C, de Vos AF. "Platelet Btk is required for maintaining lung vascular integrity during murine pneumococcal pneumosepsis." *Thrombosis and Haemostasis. 2019 Jun;119(06):930-40.*
*Equal contribution

Claushuis TAM, van der Donk LEH, Luitse AL, van Veen HA, van der Wel NN, van Vught LA, Roelofs JJ, de Boer OJ, Lankelma JM, Boon L, de Vos AF. "Role of peptidylarginine deiminase 4 in neutrophil extracellular trap formation and host defense during Klebsiella pneumoniae–induced pneumonia-derived sepsis." *The Journal of Immunology. 2018 Aug 15;201(4):1241-52.*

CURRICULUM VITAE

Lieve van der Donk was born on February 4th 1995 in 's-Hertogenbosch. She obtained her secondary school diploma for bilingual atheneum in 2013 from ORS Lek en Linge in Culemborg. Following secondary school, she started her bachelor's study Health- and Life Sciences at the Vrije Universiteit in Amsterdam, majoring in Biomedical Sciences, which she successfully concluded in 2016. She started the Biomedical Sciences master program (Experimental Internal Medicine track) at the University of Amsterdam and obtained her Master's degree with distinction in 2018. During this two-year program, she developed a specific interest in the immune system, which determined the focus of her two research internships. In her first internship Lieve focused on the role of platelets and neutrophil extracellular traps in pneumonia-derived sepsis under the supervision of dr. T.A.M. Claushuis and dr. C. van 't Veer at the Center for Experimental and Molecular Medicine (CEMM). For her second internship she joined the newly established T cell Immunology group of dr. J.W.J. van Heijst at the Department of Experimental Immunology (EXIM) at the Amsterdam UMC location AMC to study the process of T cell receptor downregulation in primary human T cells. After obtaining her Master's degree, she stayed with the T cell immunology research group as a PhD candidate. However, after several months, the T cell Immunology group was cancelled and Lieve joined the Host Defense group under supervision of prof. dr. T.B.H. Geijtenbeek, with joint co-supervision of dr. L.S. Ates and dr. M. Bermejo-Jambrina, where she developed a wide interest and skills in the field of microbiology, virology, and innate and adaptive immunology, as described in this thesis. In November 2023, Lieve will start her training to become a clinical chemist in the Deventer Ziekenhuis and Isala Zwolle.

&

ADDENDUM

DANKWOORD

DANKWOORD

Er zijn veel mensen zonder wie dit proefschrift niet tot stand zou zijn gekomen. Aan allen, ook wellicht degenen die ik vergeten ben hier persoonlijk te noemen; ik ben jullie dankbaar voor jullie bijdrage! Ik heb veel gezien, gedaan en geleerd, en ben blij met de inzichten, contacten, en ervaringen die ik hier heb opgedaan.

Beste **Theo**, ik ben heel dankbaar dat je me als adoptiegeit hebt begeleid. Tijdens onze pindakaas-meetings op donderdag was er tijd voor wetenschappelijke maar ook persoonlijke data. Je hebt een gave om me altijd gerust te stellen en problemen rustig en realistisch te bestrijden. Als ik iets aankaartte nam je me serieus en liet je me zelf werkbare oplossingen bedenken. Ook al moest ik heel erg wennen aan je vrije manier van begeleiden, het heeft me ook doen inzien dat ik soms juist zonder strenge begeleiding het beste uit mezelf kon halen. Je zit altijd vol met ideeën voor nieuwe proeven of figuren, en bent gericht op het maken en afronden van een paper. Bedankt voor alles en ik wens je nog veel fijne vakanties toe!

Beste **Louis**, ik weet niet eens waar ik moet beginnen! Wat een ongelooflijk bizarre tijden hebben wij meegemaakt op het AMC, maar ik ben blij en dankbaar dat ik iemand had die in hetzelfde schuitje zat. Ik heb ontzettend veel van je geleerd, niet alleen in het lab, maar ook met het schrijven van ons eerste paper, netwerken, en juist ook dingen buiten het werk. Je enthousiasme voor de wetenschap, immunologie en microbiologie werkten aanstekelijk en hebben me vaak het laatste zetje gegeven om door te gaan. Bedankt dat ik altijd om kennis en feedback kon vragen, en ik ben blij en trots dat je er in oktober als copromotor bij bent!

Dear **Marta**, muchas gracias por todo!! When I just joined the HD group, the COVID-19 pandemic started, and I was completely lost. I am so glad you helped me and took me along with the COVID-19 research. You taught me so many things in a really short time; DCs, complement, working in the ML-III, and much more. Within a year we crafted a paper, only because you took me along in your work mentality and worked with me in the lab 7 days a week. I am also very grateful that even though you are in Austria, we still keep in touch and try to work together to wrap up our amazing projects. Thank you for your support and everything you taught me, and I hope we can visit each other in the future, in Amsterdam, Innsbruck, or Sevilla!

Jeroen, bedankt dat ik als AIO in de T cel groep mocht werken, ik heb in korte tijd veel van je geleerd!

&

Graag wil ik ook de **promotiecommissie** bestaande uit prof. dr. T. van der Poll, prof. dr. R. van Ree, prof. dr. R.E. Mebius, prof. dr N.M. van Sorge, dr. C.M. van der Hoek en dr. A. ten Brinke, bedanken voor jullie tijd een aandacht voor het beoordelen van mijn proefschrift en het deelnemen aan de oppositie.

Lieve **Ana** en **Dorith**, jullie waren geweldige stagebegeleiders! Jullie hebben mij als verlegen en onzeker studentje ervan kunnen overtuigen dat alles mogelijk is, als je er maar hard voor werkt. Ik heb ontzettend veel geleerd van jullie, niet alleen over wetenschap maar ook als mensen. Zonder jullie was ik nooit aan een PhD begonnen, bedankt voor jullie vertrouwen!

Lieve groepsgenoten **Maartje, Melissa, Sonja, John, Esther, Tanja, Leanne, Julia, Tracy, Stefanie, Marleen, Killian**, en **Floor**, wat is werk zonder collega's?! Jemig **John** hoeveel RNA samples hebben we wel niet geïsoleerd! Maar naast hard gewerkt, hebben we ook veel gelachen! Heerlijk hoe jij collega's in de maling kan nemen ☺ Ik ben je heel dankbaar voor je relaxte houding, al je tips en advies en natuurlijk voor al je praktische hulp. **Esther**, als er iemand is die weet hoeveel RNA we geïsoleerd hebben en hoeveel vriezerruimte dat kost ben jij het! Ik vond het geweldig om met je samen te werken, te layeren en koffie te drinken, en het was heel fijn dat we over werkelijk alles konden praten, dankjewel daarvoor! **Tanja**, harde werker, je bent onmisbaar voor het lab en weet alles. Gelukkig eet je langzaam, dus als ik weer eens veel te laat was om te lunchen was jij er ook vaak nog, hoe gezellig! Ik wens jullie drie musketiers nog veel plezier en succes op het lab met alle volgende geiten! **Maartje en Melissa**, jullie zijn alweer een tijdje weg, maar hebben echt veel gedaan, uitgevonden en geregeld, en daar kunnen we nog vaak op terugvallen. **Melissa**, enorm bedankt dat je je over mij hebt ontfermd en me een HD-crashcourse gegeven hebt inclusief onderwerpen zoals Buffy, FACS, ELISA, qPCR, co-cultures, Theo en general PhD life. Ik zal het niet vergeten! **Sonja**, bedankt voor je kennis en kritische vragen tijdens de HD meetings! **Tracy**, ik heb je maar een paar keer gezien, maar wat heb je een zonnig karakter en wat een gezelligheid breng je mee! Ik hoop dat je altijd jezelf zult blijven en wil je veel succes wensen met je verdere carrière! **Marleen**, ik ben zo blij dat jij bij de groep bent gekomen ten tijde van mijn 'adoptie'. Je was de perfecte roommate tijdens tripjes en congressen. We kunnen over alles lachen en klagen, en we hebben dezelfde no-nonsense manier van werken. Maar daarnaast ben ik ook blij dat je me altijd serieus neemt en de lessen uit mijn eigen ervaringen ter harte neemt. Je bent de laatste jaren super gegroeid en je Prevotella projecten gaan als een malle! Jij kunt dit! **Julia** you are such a hard worker and have admirable amounts of knowledge about DC subsets, viruses and ML-III protocols. Besides that I also had a lot of fun with you and Stefanie in our extensive trip to DC2022 and the PhD retreats and I'm glad that also now we can still help each other finishing our theses. You can do it! Be more positive! ;-)

Leanne, dank voor al je kennis over LCs, en dat ik soms wat van je overgebleven cellen mocht gebruiken. Het was heel leuk om in de laatste maanden nog even keihard te werken aan het M-pokkenproject! Als 'postdocproject' voelde het wat meer ontspannen in het lab, maar we hebben toch in korte tijd veel gedaan. En hopelijk volgen er nog veel Hitster avonden! It was great together working. We can this! **Stefanie**, I'm so grateful for having you and your resfreshing personality around! Thank you for your extensive protocols and wonderful creative illustrations. I wish you the best of luck finishing your PhD and finding the job you enjoy! And keep me updated on all your exotic trips and sand collection please. **Killian**, toen jij voor het eerst op het lab kwam heb ik mij best zorgen gemaakt om ieders veiligheid, maar het blijkt dat je best capabel en zelfredzaam bent op het lab ;-). Bedankt voor je hulp bij het halen van het BROK examen, maar ook voor het organiseren van vele borrels en uitjes, en wie weet kunnen we elkaar later nog pesten in de kliniek! **Floor**, de nieuwste geit, ik ben blij dat mijn eindeloze geoptimaliseer en gepipetteer in het ML-II niet verloren gaat maar dat jij daar nog profijt van kan hebben! Ik wens je heel veel succes met je superleuke project en in je verdere carrière.

Graag wil ik ook studenten **Laura, Daisy** en **Mette** bedanken. Buiten het feit dat jullie hard gewerkt hebben en veel interessante data gegenereerd hebben, was het ook erg gezellig en leerzaam om jullie te begeleiden.

Dear ADI members **Alex, Anusca, Athanasios, Carla, Kharishma** and **Renée**, it was great to work with you in the lab and talk about the struggles at work and at home. I wish you all the very best in your careers and life!

Beste collega's van M01, Neeltje, Ad, Karel, Marga, Olga, Brigitte, Irma, Agnes, Lisa, Jade, Shirley, Stefanie, en Pien, ik wil jullie bedanken voor de gezelligheid tijdens de megadrukke lunches op M01, maar vooral ook voor de leerzame tijd in het ML-III. Aan de klanken van de radio was het al af te lezen (of luisteren) wie er hard aan het werk was en in wat voor stemming. Bedankt voor het beantwoorden van al mijn vragen en het tolereren van de mondkapjes tijdens alle uren SARS-CoV-2 onderzoek!

Beste **Coen** en **Lisette**, bedankt voor de leuke samenwerking! Het was erg leuk en leerzaam om twee werelden te verenigen in ons paper!

Roomies **Demi** en **Nienke**, het is een verademing om te zien hoe leuk jullie het werk (nog) vinden en hoe jullie – ondanks de hoge temperaturen van de verwarming – een frisse wind door de kamer laten gaan. Jullie waren een grote steun en we hebben van onze kamer een tweede thuis gemaakt. Heb vertrouwen, jullie kunnen het, en er moeten slechte dagen zijn om de goede te waarderen!

Of course also thanks to all my other roommates from K0-154, **Andy, Anne, Fleur, Melissa N, Jenkau, Willianne & Yanaika!** I had a lot of fun in this office, there was always something going on. I miss all your great laughs! Hopefully someday we will be able to do another BINGO!

Dear **fantastic colleagues from KO**, I'm not going to individually name each and every one of you who has worked here in the last 5 years, but I do want to thank all of you for your conversations in the hallways, culture labs or offices, gezelligheid during the lunches and coffee breaks, and for your help with experiments and sharing protocols. Gedeelde smart is halve smart! Beste analisten, rotsen in de branding, bedankt dat jullie alles weten en iedereen kennen. Ik wens jullie een geweldige toekomst met een prachtig magazijn toe!

Dear colleagues from the **EXIM stress team**, it was fun and fruitful to work with you, keep up with what you're doing!

Beste **Ester, Paul, en alle analisten van G1**, graag wil ik ook jullie bedanken dat jullie de tijd en moeite genomen hebben om de wereld van de diagnostiek te laten zien. Ester, ik wil jou in het bijzonder bedanken omdat je zo'n geweldig mens bent, ik kan altijd bij je langs lopen en je hebt me ontzettend geholpen met realiseren wat ik met mijn verdere carrière kan doen en hoe ik dat moet aanpakken.

Beste **collega's bij het CEMM**, ik heb bij jullie ontzettend veel geleerd en mij tevens kostelijk vermaakt. Ik ben blij dat ik nog steeds bij jullie terecht kan voor vragen en voor gezelligheid, en wil jullie hartelijk danken voor jullie zorg en interesse!

Lieke **Lieke** (want lieve Lieke is natuurlijk te verwarrend), in de derde klas wisten wij al dat we later het medicijn tegen AIDS zouden ontdekken. Niet per se gelukt, maar we zijn nog nooit zo dichtbij geweest! Misschien is het tijd om onze doelen bij te stellen, bijvoorbeeld naar het plannen van een filmavond. Bedankt voor het aanhoren van al mijn gezanik. Ik mag jou wel!

Lieve **Annalien, Jody, Judith, Nina** en **Suzanne**, ooit zijn we met dezelfde studie begonnen maar inmiddels doen we allemaal ons eigen ding! Ik vind het heel leuk dat we nog steeds contact hebben en tof om te zien hoe iedereen z'n eigen pad kiest en goed op z'n pootjes belandt.

Beste **Jorrit en Marijn**, bedankt voor alle weekendjes weg en gezellige avonden, jullie zijn een enorme steun en inspiratie geweest de afgelopen maanden!

Lieve **Willem, Martijntje, Bram en Teun**, een betere schoonfamilie kan ik me niet wensen! Ik heb altijd het idee dat we met jullie op avontuur gaan – zij het cultureel, culinair, of gewoon in jullie enorme achtertuin. Bedankt voor jullie interesse en support de afgelopen jaren!

Lieve **papa, mama en Hidde**, hier een stukje typen over jullie bijdrage doet jullie allemaal tekort. Ik wil jullie bedanken voor jullie interesse, ondersteuning en hulp, voor het beantwoorden van alle belletjes over werk, problemen, irritaties en andere dingen, voor het geven van jullie ongezouten meningen over dingen zoals spelling, mijn boekje en carrière, maar vooral ook voor de opbeurende woorden en stimulatie die ik altijd van jullie heb gekregen en nog steeds krijg. Zonder jullie was dit boekje nooit begonnen, laat staan afgerond. Dus enorm bedankt, en op naar nog vele spelletjesavonden en vakanties samen!

En lieve **Stijn**, misschien wel de grootste en beste ontdekking die ik in het lab heb gedaan, ben jij. We begonnen als twee studentjes op G2, en terwijl ik m'n PhD deed, ben jij uitgegroeid tot een goede, betrouwbare en onmisbare analist. Ik waardeer onze dagelijkse fietstochtjes, waarin we alle mogelijke materie hebben besproken. Ik heb het als heel prettig ervaren dat je precies wist wat ik bedoelde als ik vertelde dat een proef mislukt was, en dat je vaak zelfs advies daarover kon geven. Niets is je te gek en je staat overal voor open. Daar kan ik met mijn starre karakter nog wat van leren. Maar door die combi hebben we wel veel gezien en gedaan. Ik vind dat we het goed voor elkaar hebben en ik kijk uit naar wat de toekomst ons gaat brengen!

Kortom, beste allen, in de woorden van menig Brabander: houdoe en bedankt!

Ervaring is wat je krijgt nét nadat je het nodig had

Omdenken